NOVEL DEPLOYABLE MEMBRANE STRUCTURES: DESIGN AND IMPLEMENTATION

TRAN CHI TRUNG

(*B.Eng. National University of Civil Engineering, Vietnam*)

A THESIS SUBMITTED

FOR THE DEGREE OF DOCTOR OF PHILOSOPHY

DEPARTMENT OF CIVIL ENGINEERING

NATIONAL UNIVERSITY OF SINGAPORE

2007

ACKNOWLEDGEMENT

First and foremost, I would like to express my deep gratitude to my supervisor, A/Professor Richard Liew J.Y., for inspiring me to do this research and patiently guiding me along the process of the project.

Special thanks go to Professor Wang Chien Ming, A/Professor Ang Kok Keng and Dr Krishnapillai Anadasivam, for their suggestions and comments on my research contributions.

Great appreciations go to Mr Sit Beng Chiat, Mr Ang Beng Oon, and Ms Annie Tan and other staffs of Structural Laboratory for their constant helps along the project.

I am greatly indebted to my parents who have made many sacrifices during my study. Thank you my best friends, Kien, Dong, Khoa, An, Hang, Hai, Thanh, Anh, Trung and Myint Aung for sharing joy as well as sadness with me for years in NUS.

Lastly, I would like to dedicate this thesis to my wife, Thuy, who has supported and encouraged me throughout my years of academic pursuit. Your love enables me to overcome any obstacle.

The work has been carried out and supported by the National University of Singapore Research Scholarship. Finally, the author's presentations of six international conference papers were made possible with financial support from CORUS fund, Steel-Concrete-Steel fund and the Lee Foundation.

TABLE OF CONTENTS

SUMMARY

Membrane structures and deployable structures are two modern construction systems of growing interest. The former can provide large span and light-weight enclosures with striking appearance while the latter can facilitate the transportation and shorten the construction time of the structure. This research is aimed at proposing and developing two novel deployable membrane systems, named as Deployable strut-tensioned membrane structures (DSTMS) and Butterfly-wing structures, which exploit the advantages of both membrane and deployable structures.

Structural morphology of the proposed deployable membrane structures consists of the deployable form and the membrane form. Various deployable forms of DSTMS and Butterfly-wing structures are made possible based on their conceptual and generative designs. The membrane curvature forms of the structures are found through both computation modelling and physical modelling. The variety in deployable forms allows a wide range application while the aesthetics of the membrane curvature forms allows a striking appearance of these structures.

An integrated approach of force density method and geometrical nonlinear analysis is employed to perform both form-finding and structural analysis of the proposed structures. The understanding of membrane shape and structural efficiencies are the basis to deduce the optimum design parameters of DSTMS and Butterfly-wing structures. These parameters can be used for preliminary design of the proposed structures in practical applications.

Because of the vulnerability of membrane to damage, the safety of the structures in the event of membrane failure must be considered. Robustness of the optimally designed DSTMS and Butterfly-wing structures against hazards, including vandalism and fire, is studied. In the vandalism scenario, the results show that the structures are safe even in the event of total membrane removal. In the fire scenario, the fire resistance of the structures is determined by a performance-based approach which is proposed for large space membrane structures. This approach can determine the fire resistance of the structures scientifically and cost-effectively since it takes the performance of the structures in real fires into account. This approach also helps to identify key factors of the structural fire resistance which can be optimized to minimize the cost needed for membrane structures against fire.

Reduced scale prototypes are built to verify the conceptual design and the deployability of the proposed structures. The prototypes show that they can be folded into compact bundles as well as deployed rapidly into the functional configurations. The prototypes also demonstrate successfully the concept of integrating the membranes into the deployable supporting structures. The deployment of the supporting structures can deploy and tension the membrane while the tensioned membrane helps the whole structure achieve self-stress equilibrium and achieving improved structural stability in the deployed configurations.

A design guideline are provided for practical implementation of the proposed deployable membrane structures, including the detailed design, erection issue as well as potential applications. The success of this research provides a breakthrough in the development of both membrane structures and deployable structures.

LIST OF FIGURES

LIST OF TABLES

LIST OF SYMBOLS

A_g = gross area

A_{ij} = cross sectional area of element *i-j*

A_0 = cross sectional area in the prestressed state

A_{fi} = fire area

A_m/V = section factor (m^{-1}) of the exposed steel member per unit length

[A] = equilibrium matrix

B = width of module

BC = bottom cable

$\{C\}$ = direction cosines at deformed state

$\{C_0\}$ = direction cosines of the element at the prestressed state

DMS = Deployable membrane structures

DCSMS = Deployable Cable-Strut Membrane Structures

DSTMS = Deployable Strut-Tension Membrane Structures

DTMS = Deployable Tensegrity Membrane Structures

DS = diagonal strut

D = length of scissor-like element

D_{fi} = equivalent fire diameter

$\{\delta D\}$ = vector of nodal virtual displacements

d_i, d_j = nodal displacements

E = modulus of elasticity of material

E_{ij} = material modulus of elasticity of element *i-j*

E_0 = material modulus of elasticity in the prestressed state

E_{fi} = total energy contained in fuel in the fire area

E_1 = energy released in the growing phase

E_2 = energy released in the plateau phase

E_3 = energy released in the decay phase

FDM = Force Density Method

FEM = Finite Element Method

F_f = axial load at the fire limit state

$\{F\}$ = internal force contributions of each element incident

$\{G\}$ = assemblage of the total force contributions from all elements

H = rise of the arch

H = structural depth

H_G = Gross height of module

h = inclination height

h = heat transfer coefficient per unit area [W/m^2K]

h_r = radiant heat transfer coefficient [W/m^2K]

h_c = convective heat transfer coefficient [W/m^2K]

h_u = upper inclination height

h_l = lower inclination height

$[I]$ = unit matrix

i = drainage slope

$[K_{NR}]$ = tangent stiffness matrix for an iterative Newton-Raphson method

$[K_{icr}]$ = tangent stiffness matrix for an incremental method

KDOF = Kinematic Degree of Freedom

L = span of the arch/structure

L_{ij} = deformed length of element *i-j*

L_{0ij} = undeformed length of element *i-j*

M = the equivalent uniform moment factor

M_f = the applied moment at the fire limit state

M_b = the buckling resistance moment (lateral torisonal)

M_c = moment capacity of section

M_{cx} = moment capacity of section about the major axis in the absence of axial load

M_{cy} = moment capacity of section about the minor axis in the absence of axial load

M_{fx} = maximum moment about the major axis at the fire limit state

M_{fy} = maximum moment about the manor axis at the fire limit state

N_{ij} = internal force of element *i-j*

n = the number of modules assembled.

PVC = Polyvinylchloride

PTFE = Polytetraflouroethylen

$\{P\}$ = external force contributions of each element at a node plus the concentrated force at the node

P_{ix}, P_{iy}, P_{iz} = external force components at node *i* in *X, Y, Z* directions

{P} = external load on system

$\{P_c\}$ = concentrated nodal forces

p_c = compressive strength of steel

p_y = design strength of steel

Q = heat release rate

Q_{max} = maximum heat release rate

$\{q\}$ = distributed load per unit length

q_{ij} = force density ratio

q_i, q_j = nodal load increments

$q_{f,k}$ = fire load density per unit floor area

R = radius of the arch

R = load ratio

RHR_f = heat release rate per unit area

SLE = Scissor-like element

s = segment length of the element in the deformed state

s_o = segment length of the element in the prestressed state

{s} = internal stress in system

TS = top strut

T = tension in the deformed state

T_0 = pretension in the prestressed state

$T_{membrane}$ = tension forces in membrane

T_{cable} = tension forces in cable

T_{fi} = fire temperature (°C)

T_s = steel temperature (°C)

T_{max} = maximum temperature in steel member exposed to fire

T_{lim} = limiting temperature of steel member exposed to fire

t_1 = time to reach maximum heat release rate

t_2 = time of horizontal plateau phase

t_3 = time of decay phase

t_{loss} = loss duration of membrane tension forces

t_α = time needed to reach a rate of heat release of 1MW

u = displacement in the current state

u_0 = displacement in prestressed state

$\{u\}$ = added displacement from prestressed state

VS = vertical strut

W = modular width of DSTMS

W = average modular width of deployable arch

W_u = upper modular width of deployable arch

W_l = lower modular width of deployable arch

W_c = crossed modular width of deployable arch

x_i, y_i, z_i, x_j, y_j, z_j = nodal coordinates at node i, j

α = inclination angle of the arch

ΔT_s = increase of temperature in an unprotected steel member [°C]

ΔR = small load increment

ε = strain

ε_r = resultant emissivity

λ_0 = elongation ratio in the prestressed state

λ = current elongation ratio

π = 3.1414

φ = open angle of the arch

σ = Stephan Boltzmann constant [W/m^2K^4]

σ = stress

$\sum X_{ij}$ = sum of forces in X direction

$\sum Y_{ij}$ = sum of forces in Y direction

$\sum Z_{ij}$ = sum of forces in Z direction

CHAPTER 1

INTRODUCTION

1.1. Background

The history of construction is associated with the development of building materials- from stone and timber in ancient times to steel and concrete in modern time. A construction material which has a long history but is considered as a recent material is the woven fabric or "membrane" material (Sheaffer, 1995). Though "fabric-tents" have been built since ancient times, the contemporary membrane structure technology was developed only in the 19th century as a result of the development in mechanical spinning and weaving of fabric (Forster & Mollaert, 2004). This development improved the strength of membrane material and thus enabled the possibility of large span membrane structures. Since then, membrane structures have become an alternative to conventional structures, and thus, they are of great interest to researchers.

The theoretical background of membrane structures was first founded by Otto (1969). The most important principle of membrane structures lies on the inherently attractive curved-surfaces generated by tensile equilibrium in the plane of the membrane. This principle is structurally intelligent as it is close to that of natural structures (e.g. bubbles). It gives designers and architects the possibility of creating dramatic and aesthetic shapes that cannot be found in conventional structures. Apart from their aesthetic shapes, membrane structures have many other advantages such as lightweight, natural lighting and good earthquake resistance. Therefore, they have a

wide range of applications such as sport facilities, amphitheatres, exhibitions and military shelters.

Membrane structure is also a potential solution to the modern trend in construction where structures are becoming changeable to address the demand of rapid erection, easy transportation and convenient relocation. As membrane material is flexible and light, it is possible to make the membrane structures deployable. Deployable membrane structures (DMS) are changeable structures which can be stowed compactly in bundles for the ease of transportation and deployed rapidly for fast-track construction on site (Hanaor, 1993). As they are foldable, they can be retracted and relocated to other places of demand.

Owing to these advantageous features, various DMS have been proposed and developed, but up to now there has not been a satisfactory system for modern construction demands. Deployable pneumatic structures (Walter, 1986) offered extreme light weight and high stowage efficiency but their applications are limited due to architectural inflexibility and deployment complexity. Retractable membrane structures (Ishii, 2000) can be considered as deployable membrane structures but their deployment/retraction was designed for weather adaptation, but not for the ease of transportation and erection. Deployable pantograph membrane structures (Escrig *at al.*, 1996) had a high degree of control on the deployment process and high stowage efficiency but had low structural efficiency due to the lack of flexural stiffness. Deployable tensegrity membrane structures and deployable cable-strut membrane structures were the two DMS classes developed from recently proposed systems which are the tensegrity (Motro, 2003) and the cable-strut structures (Wang, 2004; Liew *et al.*

2002 and Vu, 2007). The former provided the deployment with low technical complexity due to the elimination of mechanical joints, but possessed low structural efficiency due to the isolation of compressive components. The latter improved the former's low structural efficiency by making use of a set of continuous struts and a set of continuous cables. However, both of these kinds of structures had to rely on highly pretensioned cables to achieve self-stress equilibrium for structural stability while the membrane was merely used as a roofing material. None of them offer the use of prestressed membrane as a tension component to achieve self-stress equilibrium for structural stability. The challenge is how to design a deployable membrane structure which can harmonize the sometimes conflicting requirements of high versatility, technical simplicity, deployment/stowage efficiency and structural efficiency.

This challenge has inspired the author to propose, in this thesis, two innovative deployable membrane systems named, as Deployable strut-tensioned membrane structures and Butterfly-wing structures. Although having different designs, they originate from the initial concept of using high strength fabric as a structural tension component to stabilize and restrain the deployable supporting structures. These novel DSTMS and Butterfly-wing structures have high stowage efficiency due to the foldability of the supporting structures and the membrane. They could be erected rapidly on site due to their effective deployment mechanisms. The membrane could be tensioned by the deployment of the structures, thus reducing the need of pretensioning equipment. The prestressed membrane could act as structural tension component to achieve self-stress equilibrium for stabilizing the structures in the deployed configurations. They have high weight/structural efficiencies which are attributed to the double-layer grid arrangement (DSTMS) and the use of deployable cable-strut arch

(Butterfly-wing structures). In summary, the proposed DSTMS and Butterfly-wing structures are capable of providing large span enclosures which are capable of fast-track erection, easy transportation and low-cost construction.

1.2. Objective and Scope

The objectives of this thesis are:

a. To propose two novel systems of deployable membrane structures, the so-called Deployable strut-tensioned membrane structures (DSTMS) and Butterfly-wing structures, for medium and large space enclosures.

   These structures are proposed conceptually by introducing the morphology of each structure. Various deployable membrane forms are figured out together with their deployment mechanisms;

b. To present an integrated approach for form-finding and structural analysis of the proposed structures.

   This approach is aimed at finding the equilibrium shape and performing geometrical nonlinear analysis of these structures;

c. To examine the influence of membrane curvature on membrane stress magnitude through shape effect studies and thereby to determine the optimum parameters which provide effective membrane shapes of DSTMS and Butterfly-wing structures.

   The curvature has a great influence on stiffness and structural stability of the membrane, and thus on the structural behaviour of the structures. In shape effect studies, the minimum membrane stress that is induced by a predetermined applied load is used as a basis for determining the effective membrane shape and thus the optimum parameters of the membrane boundary;

d. To determine the optimum design parameters of DSTMS and Butterfly-wing structures through a series of parametric studies.

   One common way to assess the efficiency of a structure is to compare its weight to strength ratio. In parametric studies, minimum weight of structural elements that is designed to resist predetermined load combinations is adopted as a basis for comparison. The optimum design parameters of DSTMS and Butterfly-wing structures are determined based on the lightest weight among different configurations;

e. To study the structural behaviour, structural safety and identify the influencing factors on the robustness of DSTMS and Butterfly-wing structures in hazards.

   As membrane is a structural component but vulnerable to damage, it is essential to ensure the safety of the supporting structures in the event of membrane failure. Two possible hazards to membrane, which are vandalism and fire, are considered in the robustness study of DSTMS and Butterfly-wing structures.

f. To test physical models for verifying the design concept and to provide the design guidelines for implementation.

   Building physical models is the most common way to verify a design concept. This thesis demonstrates the morphology, deployability and stowage efficiency of the proposed structures through reduced-scale prototypes. In the design guidelines, the detailed designs involving joint design, membrane connections and drainage system are developed. Deployment methods and some potential applications of the proposed structures are also given in the design guidelines.

The scope of this research on Deployable strut-tensioned membrane structures and Butterfly-wing structures includes the morphological study to generate innovative

geometric configurations, the geometrical nonlinear analysis to investigate the structural performance, and the physical prototypes investigation to verify the design concepts and the deployability. Although snow load is one of the critical loads to membrane structures, it is not taken into account for the design of DSTMS and Butterfly-wing structures in this thesis since these structures are aimed at applications in Singapore where snow fall is not an issue.

1.3. Organization of Dissertation

This dissertation consists of eight chapters, each covering an aspect of the research.

Chapter 1 describes the evolution of tensioned membrane structures and the needs leading to the development of deployable membrane structures. The scope and objectives of this research are defined.

In chapter 2, a comprehensive literature review on various deployable membrane structures is reported. Fundamental concepts about form and behaviour of membrane structures are summarized.

Chapter 3 describes the conceptual design of DSTMS and Butterfly-wing structures. The concept of integrating the high strength membrane into the deployable supporting structures implemented in these structures is discussed. Various deployable forms of DSTMS and Butterfly-wing structures are generated. Deployment mechanisms of the structures are explained.

Chapter 4 introduces an integrated analytical approach of force density method and geometrical nonlinear analysis, which is implemented in Forten2000 programme, to

perform the form-finding and structural analysis of DSTMS and Butterfly-wing structures. It also covers the study to investigate the effect of surface curvature on membrane stress so as to provide the optimum parameters for achieving effective membrane shapes of these structures.

Chapter 5 presents the results of parametric studies carried out on DSTMS and Butterfly-wing structures of large and medium spans. The optimum design parameters of each structure are determined based on their weight efficiency.

Chapter 6 presents the robustness studies of DSTMS and Butterfly-wing structures against hazards. Post collapse and dynamical analyses are employed to study the behaviour of the structures in the event of total membrane damage due to vandalism. A procedure of performance-based approach is proposed for determining the fire resistance of the structures through considering their performance in real fire.

Chapter 7 presents the prototype investigation and the design guidelines of DSTMS and Butterfly-wing structures. Physical models are built to verify the proposed concept and the deployability of the structures. A design guidelines package is developed for practical implementation of the proposed structures, including their recommended structural parameters for preliminary design, detailed designs for manufacturing, deployment methods for erection and some potential applications for implementation.

Chapter 8 highlights the significant findings and the corresponding conclusions as well as provides the recommendations for future works of this research.

CHAPTER 2

LITERATURE SURVEY AND BACKGROUND INFORMATION

2.1. Introduction to membrane structures

The concept of membrane structures was derived from the nature of fibers which have little or no bending and shear stiffnesses. Therefore, they must rely on their form and internal prestress alone to perform the same functions. Depending on the prestressing manner, membrane structures can be broadly classified into two classes, viz pneumatic structures and tensioned membrane structures.

2.1.1. Pneumatic structures

Pneumatic structures are "structural forms stabilized wholly or mainly by pressure differences of gases, liquids, foam, or material in bulk" (Otto, 1969). The structures are usually in synclastic shape which has primary curvature at every point in their surface in the same direction (e.g. a dome). The synclastic shape and prestress of membrane are induced by the pneumatic or hydrolic pressure that acts perpendicular to the membrane surface. The membrane prestress is in direct proportion to the membrane's curvature. The smaller radii results in smaller tension and vice versa. Pneumatic principle therefore is able to create many forms since it allows for stable structures having varying membrane stress levels due to changing curvatures (Riches and Gosling, 1998). Swallow spherical dome is a typical pneumatic structure of synclastic shape as it avoids the exposure of large areas to downward pressure.

Such structures were first proposed by Willam Lanchester in 1917 for use as field hospital but it never came true. It was Walter Bird who first constructed a full scale air-supported dome of 15 meters. Since then, his Birdair Company has built many pneumatic domes of span up to 220m (Walter, 1986).

As pneumatic structures do not require rigid supporting structure, they are probably the lightest structures which are theoretically able to accommodate very large span enclosures. However, it was found to be difficult to maintain the pneumatic facilities under bad weather. Most of pneumatic structures more or less have suffered from accidental deflation when the fabric was destroyed due to strong wind or heavy snow (Sheaffer, 1995). The applications of pneumatic structures thus have become limited as compared to tensioned membrane structures presented hereafter.

2.1.2. Tensioned membrane structures

Tensioned membrane structures are the structural forms which are stable and stiffened by mechanically applied prestress in the plane of the membrane, such as edge loads, self weight, etc. (Leonard, 1988). The stability of those structures relies on a structural principle that an element can be held in space by using only tension forces that are not acting in a single plane and are in equilibrium. This condition of tensile equilibrium forces the membrane surface into an anticlastic shape. In an anticlastic surface, the principle curvatures at any point are in opposite directions, and the sum of all positive and all negative curvatures are zero (Forster and Mollaert, 2004).

Anticlastic membrane structures resist external loads by form and not by mass. Downward pressure is carried by a concave curvature while outward suction is carried by convex curvature as illustrated in Fig 2.1. In addition, a load applied to any point will result in increasing tension in one direction and decreasing that in the opposite. The surface will deform until achieving the equilibrium between tensile forces in the membrane and the applied load (Shaeffer, 1995).

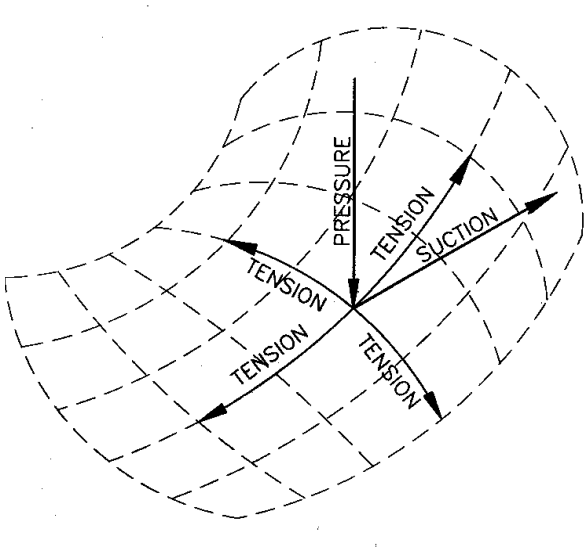

Fig. 2.1. Anticlastic surface of tensile equilibrium (Shaeffer, 1995)

There are two basic anticlastic shapes commonly used in tensioned membrane structures: the saddle form and the cone form.

The saddle surface is formed when a membrane is stretched between non-planar boundaries, defined by alternating high and low points and connected with either straight or curved edges (Sheaffer 1995). A simplest saddle is a hyperbolic paraboloid which is a surface made by two high points and two low points alternately as shown in Fig. 2.2. The principle curvatures following concave and convex directions of the

surface are relatively easy to identify. Many types of saddle were proposed in the work of Otto (1969). The versatile shape of the saddle can be achieved by changing either the shape of the boundary or the relative tension in two principle curvatures of the membrane.

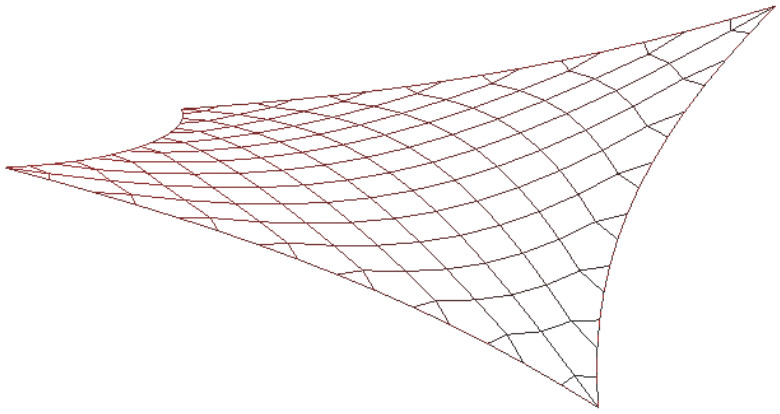

Fig. 2.2. Saddle form

The cone surface is like a volcano shape. It is a hyperboloid surface generated when a membrane is stretched between two vertically displaced concentric boundaries (Sheaffer 1995). The boundaries can be circular, elliptical or rectangular rings. The two boundaries also may be of similar size and shape or they may be significantly different as a radial tent shown in Fig. 2.3. Two sets of opposite principle curvatures follow the circumference and the meridian directions. Several cone-like structures were introduced in the survey of Brian (1994). One of the largest cone-like structures is the Haj Terminal (Huntington, 2004) which consists of 210 identical cone-shaped canopies square in plan, each measuring 45m on a side.

Apart from the two basic anticlastic surfaces, there are a great variety of formal possibilities that comply with the condition of tensile equilibrium within the membrane

surface. A ridge and valley form is a variation of the saddle form where membrane surface is divided by cables into ridge-and-valley patterns and often supported by masts (Berger, 1996). Some other complex anticlastic forms can be defined with different membrane boundary arrangements. They often have unique and distinguished shapes at the expense of difficult installation and membrane patterning (Shaeffer, 1995).

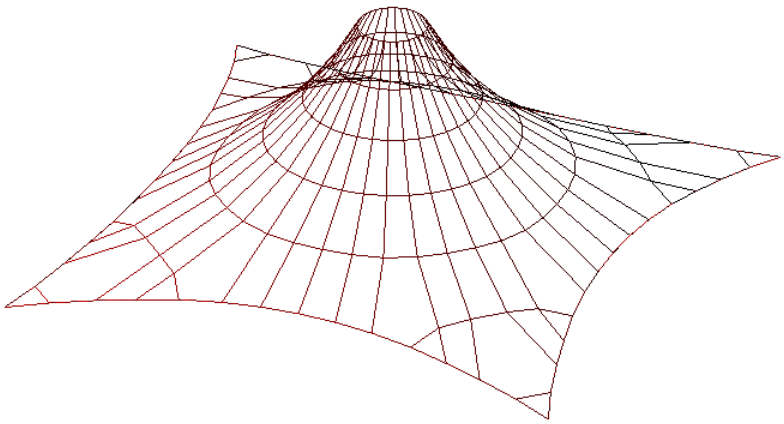

Fig. 2.3. Radial tent

2.2. Deployable membrane structures

As defined by Gantes (2001), deployable structures are those structures that can be transformed from a compact stowed configuration to the final functional form. According to this definition, membrane structure is a type of deployable structures since the membrane itself is deformable and inherently deployable. However, as a deformable component, the membrane has infinite kinematic degree of freedom (KDOF). Therefore, its deployment is difficult to control accurately.

The term of deployable membrane structures in the thesis refers to membrane structures whose kinematics and deployability are governed by the deployability of the supporting elements. As a rule, supporting elements are often in compression to counterbalance with membrane surface tension. In tensioned membrane structures, these compressive elements are constituted of rigid bars, rigid arches or skeletal elements. In pneumatic structures, the compressive element is primarily air pressure. Due to the dependence on the compressive elements of air pressure, the deployment manners of pneumatic structures are limited as compared to that of tensioned membrane structures.

In the subsequent sections, different deployable membrane systems are classified and comparatively evaluated in terms of their:

- Structural efficiency: weight to strength ratio;
- Technical complexity: manufacturing complexity, deployment operation complexity;
- Deployment/stowage efficiencies: reliability of deployment, degree of compactness of stowed components;
- Flexibility: versatility to apply for different applications;

Apart from that, other related issues such as modularity and maintenance may also be taken into account for evaluation.

2.2.1. Deployable pneumatic structures

Pneumatic structures are probably the most efficient deployable structures in terms of stowage efficiency if regardless of auxiliary equipment compressors and anchorage

components. There are two major ways of deploying pneumatic structures according to how air pressure is used to support and prestress the membrane: air-supported membrane and air-inflated membrane (Huntington, 2004).

2.2.1.1. Air-supported membrane structures

Air-supported structures are stabilized by a pressure difference across the membrane surface (Ishii, 1995). The air is pumped into the whole functional space to achieve the pressure difference required to balance the external applied load (such as self weight, wind, snow). Several air-supported domes have been built, for example the U.S.A Pavilion and Kajima Airdome (Shaeffer, 1995).

Since there are no rigid supporting elements required, the structures possess very high stowage efficiency due to the foldability of flexible membrane. In terms of structural efficiency, the structural depth is the full height of the structure, thus structural efficiency is high.

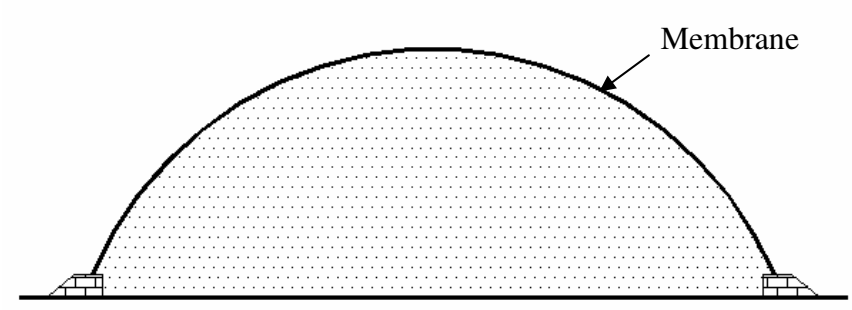

Fig. 2.4. Air-supported membrane structures

However, architectural drawbacks are the obstacle to wide range application of this system. In order to maintain the pressure difference, the enclosed space needs to be

essentially sealed to form an airtight membrane cover and the air must be continuously pumped inside. Safety devices are required against power lost. In addition, due to the uplift pressure acting on the membrane, it must be anchored to the ground or weighted down along the perimeter. Generally, air-supported structures are often designed purposely, thus having low architectural flexibility.

2.2.1.2. Air-inflated membrane structures

Air-inflated membrane structures are those supported by closed tubular cellular spaces, such as tubes, filled with relatively high pressure air (Ishii, 1995). Unlike continuous air-pumping requirement of air-supported structures, the air-pumping is required only at the deployment stage of air-inflated structures. High deployment reliability of the structures is ensured by air compression of individual cells. Each inflated cell is free-standing, hence no anchoring system or special site preparation is required. Versatility of the structures can be achieved by combining inflated tubes and cells to create various architectural forms. Some examples of pneumatic tube structures are introduced by Kroplin & Wagner (1995).

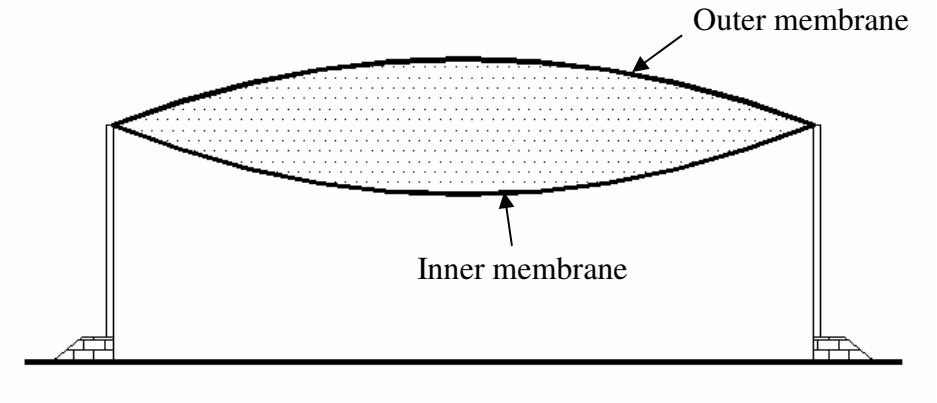

Fig. 2.5. Air-inflated membrane structures

Structural efficiency of air-inflated membrane structures is dependant on the depth and stiffness of individual cells. High pressure therefore is necessary to provide significant stiffness for the structures and as the result, thickness and toughness membrane is required. However, structural stiffness of the structures is low due to the limitation in cells' depth and level of air pressure. In addition, a larger membrane area is required due to the closed section of the cells, resulting in lower stowage efficiency compared to that of air-supported structures.

2.2.2. Deployable tensioned membrane structures

Deployability of tensioned membrane structures is governed by the kinematics and deployability of the supporting elements. Kinematic structure is, by its proper nature, a mechanism. If not, it could not be deployed (Gantes, 2001).

The kinematics is closely related to deployment technology. A kinematic structure is defined as one having a single kinematic degree of freedom, which is the positioning of one node in the structure relative to the others, determines uniquely the geometry of the structure (Kent, 1992). Therefore, the structure has ultimate deployment control where only one point needs to be controlled to determine the configuration at any stage of the deployment process. Such kinematic control is possible only in structures consisting of rigid links such as bars, frames or skeleton. There are two types of releases at the ends of the rigid links to facilitate the kinematic degrees of freedom to make the mechanisms. The "hinge" releases rotational restraint and the "slide" releases translational restraint. While the majority of retractable roof systems employ slides as

frame releases, the majority of kinematically expandable space structures employ hinges as skeleton releases (Gantes, 2000).

Recently, a new possibility of deployable structures without using rigid links is known as tensegrity system (Motro, 2003). The necessary kinematics is provided by the deformable cables. There are no articulated joints, resulting in low mechanical complexity at the expense of low degree of deployment control. Another concept developed from tensegrity system is the cable-strut system that combines rigid links and deformable cables as means of deployment (Wang, 2004). Such mixed rigid-deformable systems provide better deployment control as well as improved structural efficiency.

Based on the kinematic properties of supporting structures, there are four corresponding deployable tensioned membrane groups:

- Retractable membrane systems
- Deployable pantographic membrane systems
- Deployable tensegrity membrane systems
- Deployable cable-strut membrane systems

While retractable membrane systems aims at weather-adaptive roofs, the rest three groups belongs to expandable space structures which aim at rapid construction and relocation on site. The literature review and the pros and cons of each system will be presented in the subsequent sections.

2.2.2.1. Retractable membrane systems

Retractable structures aim at applications which need to be used in both open and closed states as defined by Ishii (2000). The structures are weather adaptive. Natural light can be utilized in the retracted form while the deployed form provides an enclosure to prevent rain or snow.

The crane technology based on slides releases is the most frequently used in retractable membrane roof systems. The roof can be opened/closed by parallel sliding elements as in the case of Ocean Dome (Ishii, 2000) or by rotary sliding elements like the Mukogawa Gakuin School Pool (Ishii, 2000). The sliding of elements can be horizontal or vertical, and either moving or overlapping.

In most retractable roof systems, the supporting frames remain rigid and unfolded while their movements rely on overlap sliding (Gantes, 2000). Therefore the membrane is always in a stressed state regardless of the deployment of the structures. In terms of structural efficiency, it is an advantage of membrane as it can resist loads in both folded and deployed configurations. The membrane is also not subjected to folding frequently, thus avoiding wearing damage. The degree of deployability is relatively high with driving devices. However, the overlapping frames result in heavy supporting structure. Driving mechanism is complicated and costly. Stowed configuration still occupies a relative large area.

Some roofs are made retractable by making use of flexible membrane materials. The opening and closing of the roof are enabled by folding the membrane materials. The

stowage and deployment of membrane are attributed to cable tractors or frame motions. Investigations on various ideas regarding the deployment and retraction of membranes, and the geometry of the folding membranes, have been described in detail in IL5 (1973). Lightweight is the main advantage of such retractable roof systems. Folded configuration is very compact due to high stowage efficiency of membrane. The drawback of such structures lies in the considerable droop of membrane during folding, resulting in the vulnerability of membrane to damage due to abrasion with other structural parts. Deployment is difficult to control but stable at the final state.

2.2.2.2. Deployable pantographic membrane systems

Pantographic system is the most typical kinematic structure. The principle of the pantograph was first introduced and verified experimentally by Pinero (1961). The movement of pantograph makes use of the scissors mechanism. In a pantograph, a pair of bars connected to intermediate node of each other with a pivotal connection forms a scissor-like element (SLE) as shown in Fig. 2.6. Several SLEs are connected together through hinges at ends of bars. The pantograph has only one degree of freedom. The pivotal connection at intermediate node of each SLE allows the two bars to rotate freely about perpendicular axis of pantograph plane but restricts all other degrees of freedom. In deployment process, movement of the bars is theoretically rigid body motion as there is no element deformation. The structure behaves as mechanisms in the sense that all joints of pantograph will move upon the change in position of a joint. Therefore pantographic structure possesses high degree of deployment control.

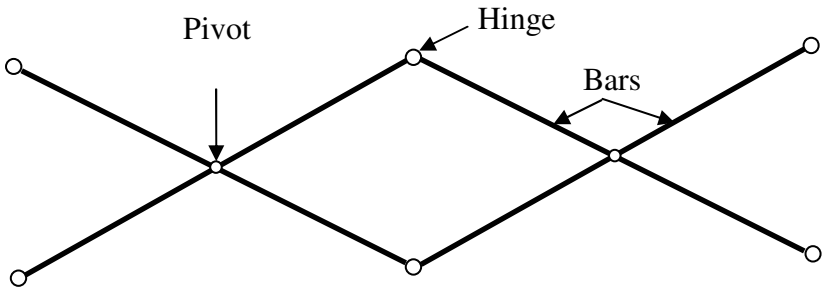

Fig. 2.6. A typical Scissor-like element (SLE)

It is Escrig (1985) who introduced the pantograph principle to his expandable X-frame. The planar pantographic system, however, has very low stiffness due to the lack of chord components. Due to the hinge presented in scissor-like elements, eccentric joint is inevitable when connecting the bars.

One of the simple techniques to improve the low stiffness of planar pantograph is the expandable arch proposed by Sastre (1996). The arch shape is obtained by positioning the pivotal joint out of the middle of the bars as shown in Fig. 2.7. The pluriform shape of expandable arches can be obtained by mixing different but compatible SLEs. The cross stability of the expandable arch can be improved with concept of 3D dome. On the other hand, when expandable arch is used as the rib of membrane structure, the tensioned membrane will restrain lateral and overall buckling of the arch (Sastre, 1996). The compression arch interacts structurally with the membrane, resulting in an efficient and light structure. However, perimeter anchoring system is required, thus limiting the architectural flexibility. Deployment of the membrane is not controlled since it is not associated with the deployment of the arch.

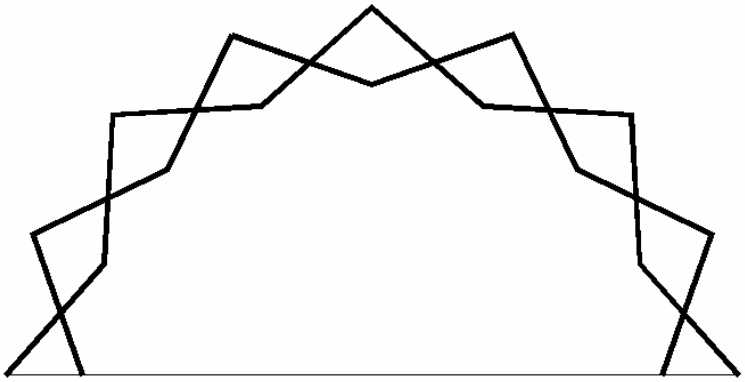

Fig. 2.7. Expandable pantographic arch (Sastre, 1996)

Expandable pantographic arch can be arranged in two directions to make expandable curvature surfaces (vaults, domes). The geometry is simply formed by several pantographic arches with the same properties of folding and deploying connected in two perpendicular directions. Many basic models of expandable grids and their possibility of association were available in the work of Sanchez (1996). However, only the geometrical conditions of expandability are mentioned, neither structural stability conditions nor connection details were investigated. Therefore, the feasibility of expandable grids for large scale structure was not assessed.

To experimentally verify the feasibility of expandable pantographic dome, a deployable pantographic membrane structure for swimming-pool roof was built by Escrig (1996). Two sphere segment of 30x30 sqm. scissor grids were used to cover a plan of approximately 60x30 sqm (Fig. 2.8). Membrane was integrated with the pantographic skeletons as foldable roofing material, thus it could be deployed together with the frame. Construction on site proved the high deployment reliability of pantographic skeletons. The deployment of the selected geometry (dome) was found

satisfactory. However, there were some existing problems such as the difficulty of connection between two perpendicular pantographs and the large deformation of structure at initial stage of deployment process. The size of bars (D120.5mm) was relatively large to accommodate additional moment and torsion force induced by eccentric joints. As the system of expandable grids is not determinate, additional elements and boundary conditions must be provided for overall stability. Membrane was deployed along with the deployment of the skeletons but was not in tension at final deployed state. Diagonal cables were used to control the folding of the fabric and to introduce tension in membrane after the deployment of the structure.

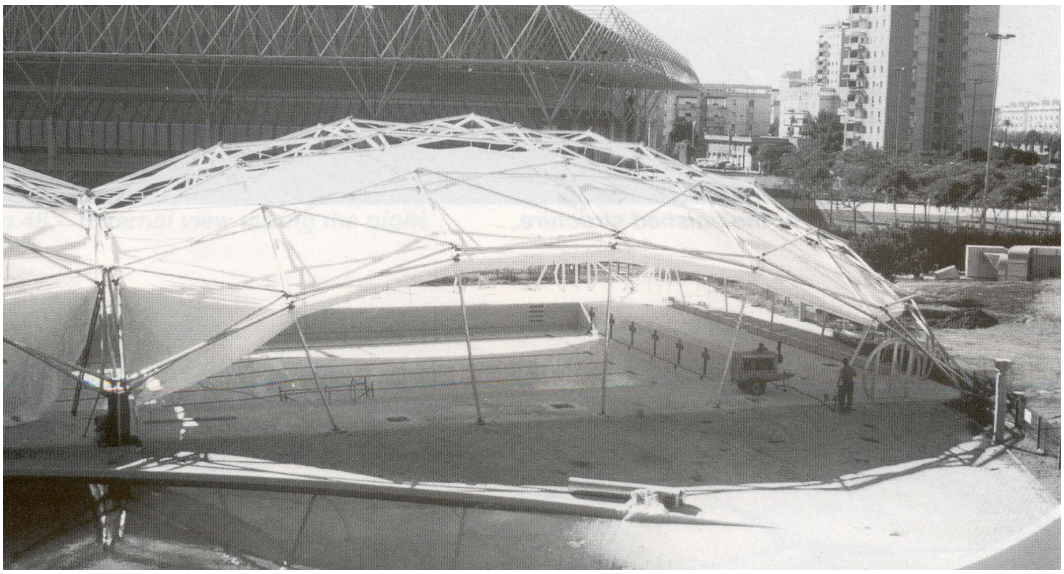

Fig. 2.8. Deployable pantographic membrane structure for swimming-pool roof built by Escrig (1996)

In a pantograph, the bar may not be only straight but also angulated as the *generalized angulated elements* proposed by Pellegrino and You (1996). Furthermore, Pellegrino also discovered the *multi angulated rod* that can replace a series of contiguous angulated rods. These new concepts open up many shapes of 2D pantograph structures. The 2D structures can be also easily extended to 3D dome structures. However, such

mechanisms are quite complicated and the joint solution has not been studied. Thus they are not suitable for practical use.

Recently, Atake (2000) proposed a new kind of pantograph technique that comprises more than two SLEs to form a 3D primary unit. The principle is that at least three components are connected to one another to form a ring. By using a complete pin joint composed by three axes in between scissors, the system is more flexible and able to make almost all kinds of 3D shapes folding into a bundle. However, the joint of ATAKE's structure is designed as door hinge and thus is relatively weak. This drawback may prevent the structure from using for large structures. In addition, the system is also indeterminate and needs additional elements for stabilizing.

In conclusion, the pantograph has been proved as an efficient deployment mechanism. It possesses high deployment control as well as high stowage efficiency. However, the pantograph on its own lacks structural depth, resulting in very low structural efficiency as a planar frame. Therefore, curved forms are preferred in use to provide structural depth as well as to enable axial compression as primary action. However, the low bending stiffness and the need for articulation at joints remain the major reasons that detract from structural efficiency of the pantograph. The inevitable eccentricity of joints introduces a source of additional torsions and imperfections. Additional bars or tendons can be introduced as the chords to improve the stiffness at the expense of complicating the deployment or adding high prestressing cost. Although tensioned membrane can be used as bracing elements, there has not been a deployable pantographic membrane system which uses the membrane as tension component to provide restraint and control member buckling.

2.2.2.3. Deployable tensegrity membrane systems

The term tensegrity was coined from the phase “tensional integrity” by Fuller (1962). As defined by Pugh (1976), tensegrity is a system established when a set of discontinuous compressive components interacts with a set of continuous tensile components to define a stable volume in space. Motro (2003) developed a more comprehensive definition which is a “systems in a stable self equilibrated state comprising a discontinuous set of compressed components inside a continuum of tensioned components”. Membrane element could be combined with this type of structure to create tensegrity membrane structures such as the Georgia Dome (Gerardo and Levy, 1992) and Le Grande Arche de La Defense (Jacob, 2003, Fig. 2.9).

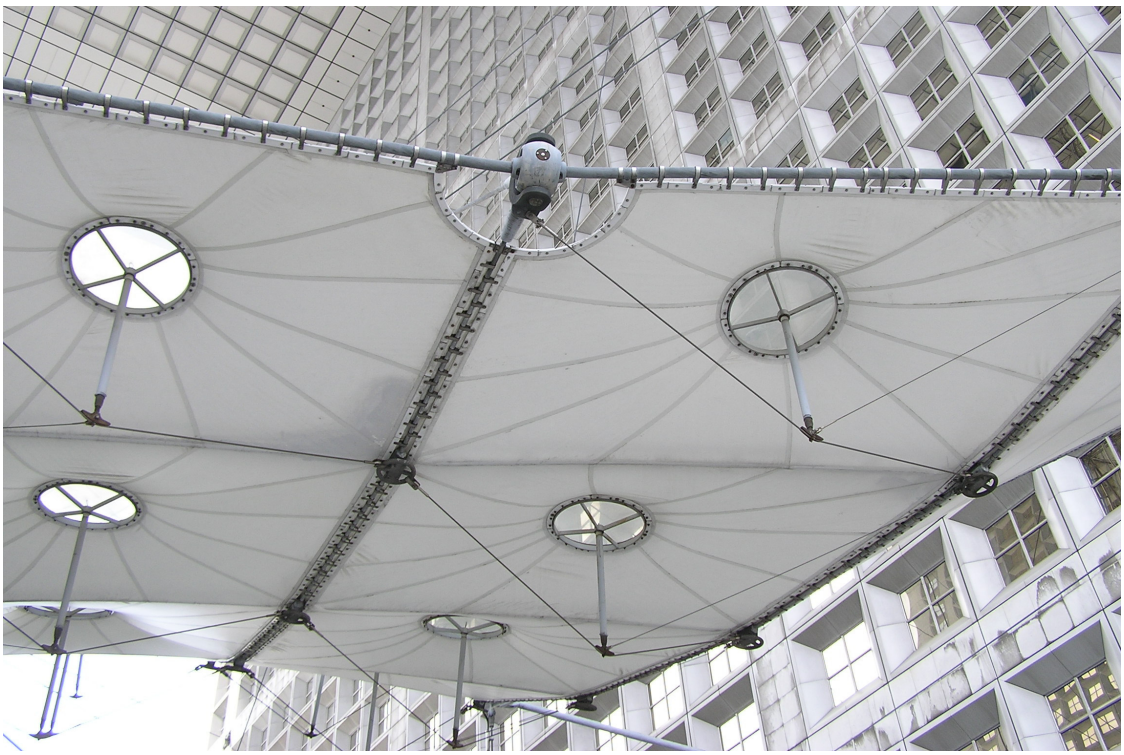

Fig. 2.9. Le Grande Arche de la Defense (Photo taken by author)

The definition of tensegrity structures also opens a new potential for deployable structures because it implies the complete absence of articulated joints (Hanaor and Levy, 2001). Several researchers have proposed different tensegrity structures which are able to be deployed by changing element lengths instead of using articulated joints (Gough, 1998; Bouderbala and Motro, 1998).

As tensegrity structures are constituted of strut and cable elements, there are two possible deployment techniques which either modify the cable length or the strut length. Hanaor (1993) proposed a deployment technique where the strut length can be changed by means of energy supply to the telescoping struts. This technique has high stowage efficiency as the structure is reduced to a bundle of collapsed struts when folded. However, it has low deployment reliability due to the shapeless bundle of struts and cables. Motro and Bouderbala (1996) proposed another technique which involved the change of cable length by pulling or relaxing one or more cables over a system of pulleys attached to the struts. This technique provides better deployment control and seems to be suitable for practical use although the stowage efficiency is less than that of changing strut length.

Both deployment techniques can be used in deployable tensegrity membrane structures (DTMS). Hanaor and Levy (2001) suggested that DTMS may utilize the prestressed membrane to restrain and stabilize the tensegiry system. Shelter System (USA) has built some DTMS in the form of portable membrane shelters which were able to be deployed or folded by the supporting tensegrity system (Fig. 2.10). The main advantage of these DTMS is the technical simplicity since they do not require mechanical joints for the deployment. They also have relatively high deployment

reliability and stowage efficiency due to the deployability of tensegrity system and the foldability of membrane. However, structural efficiency of DTMS is very poor due to the isolation of compressive struts which results in unsmooth force flow. Therefore, they are applicable for small structures or architectural displays only.

Fig. 2.10. Tensegrity shelter by Shelter systems (@ Shelter-systems.com)

2.2.2.4. Deployable cable-strut membrane structures

The low structural efficiency of DTMS can be overcome by avoiding the isolation of compressive element. Hernandez (1996) suggested a deployable vault made of inter-connected struts, cables and membrane but conducted no further investigation into this structure. Wang (1998) proposed a new concept of cable-strut system which was made up of a set of continuous cable and a set of continuous strut. This system allows a smooth internal force flow within the structure, resulting in high structural efficiency. Liew *et al.* (2002) conducted a series of numerical studies and found that the cable-strut systems had higher weight efficiency than the conventional double-layer space truss which is one of the most structurally efficient space structures. These numerical

results have been verified by the experiment carried out on an 8mx8m cable-strut structure (Liew & Lee, 2003). Although Lee (2001) suggested some deployment techniques for cable-strut system, they were neither effective nor verified by prototypes.

An effective deployable cable-strut system using articulated joint was proposed by Vu (2007). Membrane fabric was suggested to be used as a roofing material to create a deployable cable-strut membrane structure (DCSMS). The high structural efficiency and deployment reliability of the structure were verified by numerical studies and prototypes. Several joint designs were proposed to overcome the complicated manufacture of articulated joints. However, this DSCMS requires high prestress introduced in cables for structural stability whereas it does not utilize the prestressed membrane as a tension component to achieve the self-stress equilibrium for structural stability.

2.2.3. Summary of deployable membrane structures

In the previous sections, various deployable membrane structures have been classified by their morphological and kinematic characteristics. They also have been comparatively evaluated in terms of their versatility, deployment reliability, technical complexity, stowage and structural efficiencies. These criteria stem from the demand of modern construction where: versatility is needed to widen the range of applications; deployment reliability is needed to reduce the construction time; stowage efficiency is needed to reduce the cost of transportation; structural efficiency/weight effectiveness is needed to reduce the cost of material; and technical simplicity is needed to reduce the

cost of manufacturing. However, there has not been a satisfactory system which harmonizes these sometimes conflicting criteria. Among those reviewed structures, DCSMS is the one that satisfies almost all requirements. The challenge is how to integrate the membrane into the cable-strut system so as to, on one hand, utilize the membrane as tension component to brace the struts and stabilize the structure while on the other hand, pretension the membrane by the deployment of the cable-strut system. Two novel concepts of deployable membrane structures will be proposed in chapter 3 of this thesis to address this challenge. Before moving on to these new conceptual designs, it is necessary to understand the background information on the form and the behaviour of membrane structures.

2.3. Form and behaviour of membrane structures

The form and physical behaviour of membrane structures are very different from those of conventional stiff linear-elastic structures like steel or concrete structures. The shape of a tensioned membrane cannot be dictated. It has to be found through a process called “form-finding”. As they have little bending and shear stiffnesses, the structures resist loads through changes in surface tensions and very large displacements, resulting in geometrical nonlinear behaviour. Therefore, the design of a membrane structures can be separated into two distinct phases: form-finding and loading analysis.

2.3.1. Form-finding

Fabric membrane has unique shapes under tension. Such shapes are not known in advance and cannot be described by an obvious mathematical function. Hence, the shape/form of the structure must be found before loading analysis can be carried out.

Form-finding is the process of determining the surface geometry in equilibrium of the tensioned membrane spanning a given boundary configuration (Lewis, 2003). The form-finding process should yield optimal structural shapes which satisfy functional requirement at a minimum cost. Hence, it would seem reasonable to aim for uniform stress surfaces, thus the form-found surface would be a minimal surface (Otto, 1969). From an engineering view point, a uniformly stressed membrane would be less likely to undergo slackening or wrinkling due to loading or creeping effects. However, it sometimes needs to vary the surface stress so as to achieve a desired form. A typical case is the conic form where it is frequently not possible to achieve uniform stresses in two opposing main surface curvatures due to the insufficient ring diameter (Day, 1978). The stress therefore is often applied differently in two main curvatures; higher stress in the radial direction and smaller stress in the hoop direction. This principle is applied to the Cone-shaped DSTMS proposed in chapter 3.

Generally, there are two major form-finding methods of membrane structures. The first method involves the construction of small scale physical models using soap film or thin fabric. The other method involves the development of computational models using numerical techniques.

2.3.1.1. Physical modelling

Physical models convey a visual impression instantaneously and truthfully, from any perspective. A great advantage of physical models is the development of a better intuitive understanding about the form of membrane structures. There are two major

physical modeling methods of form-finding corresponding with the use of soap films or high elasticity fabrics.

A soap film spanning between wire supports was first conducted by Otto (1969) with his design of the German Federal Pavilion. The soap film modelling is necessarily constant stress surface which is often the optimal shape of membrane structures. This method is applicable for very small models and requires carefully photographed measurements.

Physical models can be made of high elasticity fabrics, usually stocking material or thin cloth, which can provide more variations of membrane shape other than minimal surface. The models can be used at various design stages for intuitive understanding. As hand-made models, they are expensive, particularly in case of numerous changes or refinements of the surface geometry happen.

Generally, the main drawback of physical modelling method is the limited accuracy. This may cause inaccurate cutting patterns for the full-size structure, resulting in inappropriate membrane shape and surface stress as experienced in the past (Leonhardt and Schlaich, 1972). In addition, measurement of the actual tension field in the surface could be tedious and of limited accuracy.

2.3.1.2. Computational modelling

To improve the accuracy of form-finding of membrane structures, several computational modelling methods have been proposed (Shaeffer, 1995). The

fundamental basis of most computational systems is based on the equilibrium modelling. Iterative process of geometric adjustment of the tensioned surface is needed to reach the static equilibrium. With the rapid development of computer technology, computational modelling methods can generate more accurate and ready forms, thus their applications are increasing in preference to expensive hand-made models.

The most commonly used computational modelling methods, together with their advantages and disadvantages, will be discussed in section 2.3.3.

2.3.1.3. Summary of form-finding

Physical modelling offer better intuitive understanding and more truthful visualization than a computer image. Conversely, computational modelling is able to provide a variety of possible forms and overcome the limited accuracy of physical models.

In this thesis, a combination of computational and physical modellings is employed. Computational modelling is mainly used to generate the forms of the proposed structures. Physical models are built as means of verifying computational results. It is a promising strategy rather than the exclusive use of either methodology (Lewis, 2003).

2.3.2. Geometrical nonlinear behaviour

What makes membrane structures more complicated as compared to conventional rigid structures lies in their highly nonlinear behaviour. The nonlinearity is a result of significant changes in geometry occurring under load due to their low surface stiffness.

Even when working within the elastic limit, their deflections can be so large that the resulting changes of the overall geometry must be taken into account. In addition, the strains developing within membrane materials are much larger than those in common construction materials, steel and concrete for instance. Consequently, membrane structures exhibit much larger deflections and geometric changes under load than conventional structures. This is, however, a desirable property since the structures will increase their capacity to carry load as they deform. The stresses do not rise linearly with the applied loads. The structures are load-adaptive in the sense that the membrane changes its geometry to accommodate the changes in load rather than increases the stress levels (Leonard, 1988).

The geometrical nonlinear behaviour of the structures can be solved by a variety of numerical methods and techniques. In the subsequent section, the most common numerical methods will be discussed.

2.3.3. Numerical methods for form-finding and geometrical nonlinear analysis

The most widely reviewed and applied methods which can be used for both form-finding and geometrical nonlinear analysis of membrane structures are:

- The Transient stiffness method
- The Dynamic relaxation method
- The Force density method

All of these methods idealize the surface as a network of line elements. A brief evaluation of each method will be presented in the following sections.

2.3.3.1. Transient stiffness method

The transient stiffness method relies on a linearization process of the nonlinear system of equilibrium equations and is critically dependant on the assumption of small displacements. Iterative process of geometric adjustment is carried out until the static equilibrium is reached. With the advent of computers, this method is convenient and widely used for analyzing structures exhibiting geometrical nonlinear behaviour as membrane structures. Several nonlinear analyses for membrane structures based on transient stiffness method were proposed (Argyris and Scharpf, 1972; Li and Chan, 2004). They are effective in solving static analysis problems of membrane structures exhibiting large displacement under load, once the initial equilibrium geometry is known.

Although the method can be applied to the form-finding of membrane structures (Tabarrok and Qin, 1991), it has the problem of the dependency on assumed initial surface geometry. Large changes of surface geometry may happen in the initial stages of computational form-finding due to poor predicting shape, resulting in incorrect relation between nodal forces and nodal displacements. This would lead to a non-convergence solution or a wrong solution. Therefore, the size of iterative step needs to be scaled down to ensure the small displacement assumption, but at the expense of slowing down the rate of convergence of the solution.

2.3.3.2. Dynamic relaxation method

The dynamic relaxation method solves geometric nonlinear problem by equating it to a pseudo-dynamic problem which does not require matrix manipulation. By using established principles of dynamic analysis, the problem could be solved by hand calculation. The method was originated from relaxation method proposed by Southwell (1946). However, it is Day (1965) who proposed dynamic relaxation method for solving geometric nonlinear problem of tensioned structures. Later on, Barnes (1988) developed an approach for form-finding and analysis of prestressed membrane based on the dynamic relaxation method with kinetic damping.

Since the method of dynamic relaxation relies on successive relaxation of the out of balance forces at the nodes of the structure, it is extremely tolerant of poor initial form prediction. Nodes can move out of a configuration which will cause non-convergence or wrong solution in transient stiffness method. The main challenge in implementing this method lies in the selecting appropriate mass, damping and time step increments. If these dynamic properties are not appropriately defined, the dynamic analysis will converge very slowly, or may be unstable or not converge.

2.3.3.3. Force density method

The force density method uses a linear system of equations to model the static equilibrium of prestressed network of line elements under prescribed force/length ratio. By ingeniously defining the ratio of tension force to length of each cable to be constant, a system of nonlinear equations are transformed to a set of linear equations

that could be solved directly. However, due to the large number of equations, iterative methods of solution would be required. The method was first proposed by Linkwitz and Schek (1971) for the design of Munich Olympic complex, and then developed and completed by Schek (1973).

The force density method can be used to generate effectively the initial shape in equilibrium of membrane structures with a given of boundary configuration and a set of force density ratio. A variety of geometries in equilibrium can be obtained with different force density ratios. Although the method can be developed to nonlinear force density method for applying in loading analysis, its primary use is in identifying the equilibrium membrane surface associated with a specific prestress (Grundig *et* a, 2000).

2.3.3.4. Summary of numerical methods for form-finding and geometrical nonlinear analysis

Transient stiffness method offers an effective computational approach for solving geometrical nonlinear problem of membrane under load. However, its application to form-finding has the limitation of dependency on estimated initial surface geometry. This drawback is overcome in the Dynamic relaxation method and the Force density method. Dynamic relaxation method can be used quite effectively in form-finding and loading analysis of membrane structure with the condition of appropriately selected dynamic properties. On the other hand, Force density method is numerically robust and effective in finding the initial shapes of membrane structures by specifying only boundary configuration and force density values.

In this thesis, an integrated approach of force density method and transient stiffness method is employed for form-finding and analyzing the geometrical nonlinear behaviour of the proposed deployable membrane structures. Details of the integrated approach will be presented in chapter 4 of the thesis.

2.4. Summary

Fundamental background of membrane structures as well as their distinct form and behaviour are provided in this chapter. Different form-finding and nonlinear analysis approaches are reviewed and evaluated to seek the most suitable methodology for adoption in the present research work.

Also in this chapter, a literature survey of different deployable membrane structures is carried out. There has not been a satisfactory structure which can address the requirements of versatility, deployability, stowage and structural efficiencies. This inspires the author to propose two novel deployable membrane structures which are expected to fulfill these requirements. In chapter 3, the concepts of Deployable strut-tensioned membrane structures and Butterfly-wing structures will be proposed and explained.

CHAPTER 3

NOVEL CONCEPTS ON DEPLOYABLE MEMBRANE STRUCTURES

The literature review in chapter 2 showed that a membrane structure supported by a deployable supporting system could be a smart integration. The deployment of the supporting system can help to deploy and tension the membrane while the tensioned membrane in turn can help to stabilize the supporting system. Two novel deployable membrane structures of different structural designs but originating from the same concept of this smart integration are proposed in this chapter. The morphology and deployability of each system are presented and explained in detail.

3.1. Deployable strut-tensioned membrane structures

The concept of deployable strut-tensioned membrane lies on the idea of combining a system of deployable strut skeleton with high strength membrane to span over large space in a short erection time. This combination makes use of high strength membrane as a tension component to stabilize the deployable skeleton. On the other hand, the membrane can be deployed and tensioned by the deployment of the supporting skeleton.

Based on the concept of deployable strut-tensioned membrane, two novel deployable strut-tensioned membrane structures (DSTMS) which are the Umbrella DSTMS and the Cone-shaped DSTMS are proposed. The proposed structures are constructed from modules which are formed by short struts, cables and membrane. The struts are interconnected to form a continuous kinematic skeleton. Cables and membranes are

designed as tensioned components to achieve the self-stress equilibrium in the deployed configuration of DSTMS. After manufacturing, DSTMS can be stowed in a compact form, which is attributed to the kinematic strut skeleton and the flexible cables and membrane, for the ease of transportation. On site, DSTMS can be deployed rapidly to the functional form. Membrane tensioned by the deployment of the strut skeleton stabilizes and provides restraint to the structural system for load bearing purpose. The appropriate arrangement of struts-cables and the smart integration of membrane lead to the structural efficiency while the pin-connections of struts allow for easy deployment of DSTMS.

There are two aspects that define the geometry of a DSTMS:

1. Deployable strut-tensioned membrane simplex configuration – the way individual elements are arranged to form a basic module.
2. Deployable strut-tensioned membrane grid configuration – the way individual deployable strut-tensioned membrane modules are arranged to form a grid.

In the subsequent sections, novel forms of deployable strut-tensioned membrane simplexes are presented. This will be followed by the presentation of novel deployable strut-tensioned membrane grid configurations. Finally, the deployment mechanism of each DSTMS will be explained.

3.1.1. Novel deployable strut-tensioned membrane simplexes

3.1.1.1. Umbrella simplex

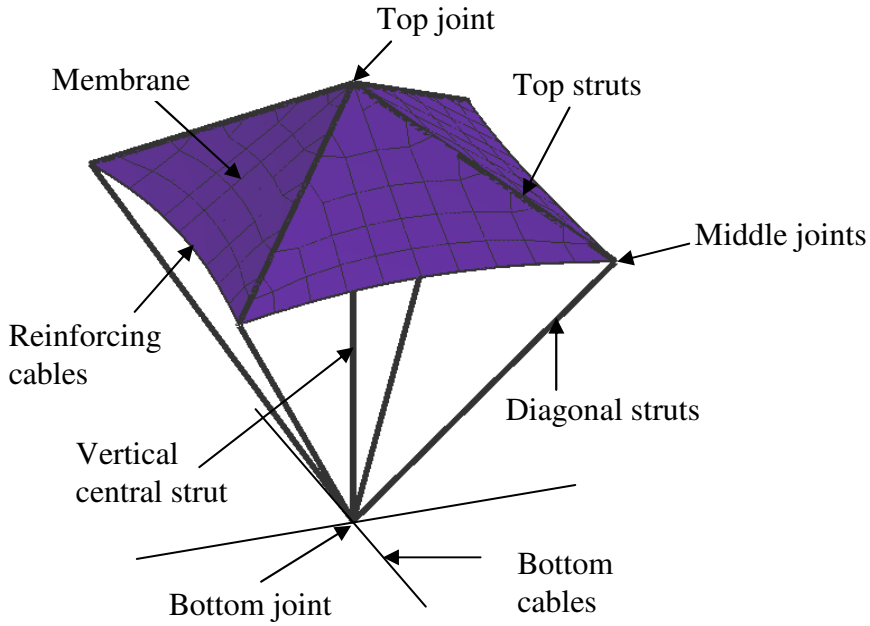

Fig. 3.1. Geometry of an Umbrella module in the deployed configuration

The arrangement of structural members of the Umbrella simplex derives from the structural efficiency of double layer space truss where the chord elements resist the global internal moment and the web elements resist the global internal shear force. The Umbrella simplex consists of four top struts forming a top pyramid, four diagonal struts forming a bottom upside-down pyramid, a vertical strut and a membrane attached to top and middle joints and placed over the top struts (Fig. 3.1). A layer of bottom cables is used to connect the simplexes together. The layer of top struts is acting as the top chord to resist compression forces while a layer of bottom cables forms the bottom chord to resist tension forces. The web elements consist of the vertical struts and diagonal struts that span the distance between the top and bottom chord elements. The tensioned membrane on top provides lateral restraint to the compressive top struts as well as the shading to the below area like that of an umbrella.

3.1.1.2. Cone-shaped simplex

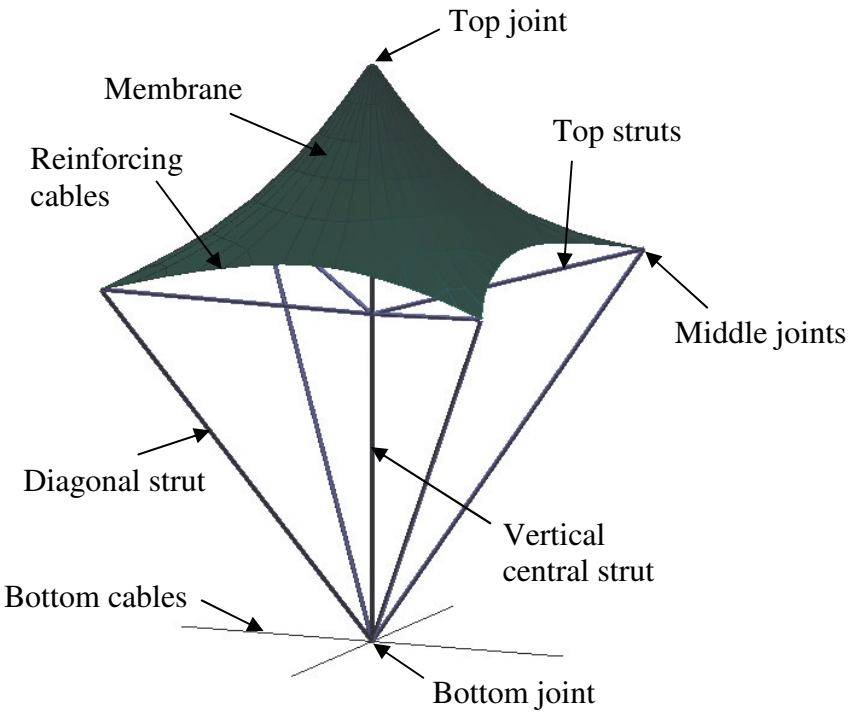

Fig. 3.2. Geometry of a Cone-shaped module in the deployed configuration

Similarly, the structural members of the Cone-shaped simplex are arranged to provide a large moment arm of the chord elements, thus reducing the bending stress induced within the system. Each Cone-shaped module comprises four top struts forming an upside-down inner pyramid, four diagonal struts forming an upside-down outer pyramid and a vertical strut braced by a tensioned membrane. The membrane is propped up at the center, forming a cone-like surface (Fig. 3.2). A layer of bottom cables is used to connect the simplexes together. The top and bottom chord elements are the top struts and bottom cables respectively. The web elements are the diagonal and vertical struts. Cone-shaped simplex attempts to improve the buckling capacity of the long vertical strut by providing bracing of four connected struts at its mid-length.

3.1.1.3. Different forms of deployable strut-tensioned membrane simplex

The Umbrella simplex and the Cone-shaped simplex are the two basic classes of deployable strut-tensioned membrane modules. For the family of each class, there exist numerous modular configurations that can be defined by the shape of the pyramids formed by the struts. Some of the possible configurations are triangular simplex, square simplex and pentagonal simplex (Figs. 3.3 & 3.4).

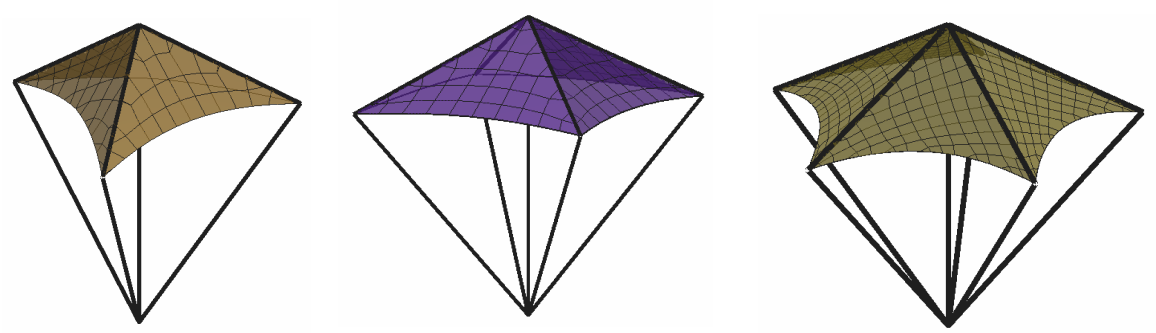

a. Triangular Umbrella simplex

b. Square Umbrella simplex

c. Pentagonal Umbrella simplex

Fig 3.3. Three different forms of Umbrella simplex

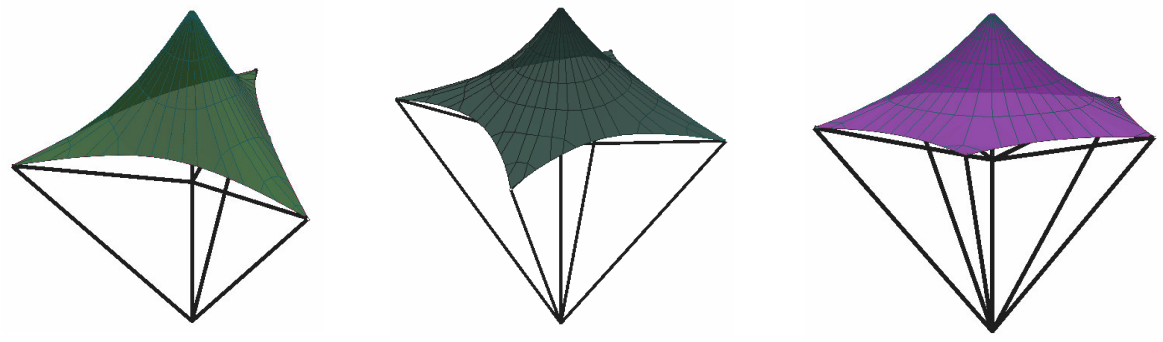

a. Triangular Cone-shaped simplex

b. Square Cone-shaped simplex

c. Pentagonal Cone-shaped simplex

Fig 3.4. Three different forms of Cone-shaped simplex

For this thesis, the terms Umbrella or Cone-shaped simplex in the absence of a noun to describe its geometry will be used exclusively to refer to a Square simplex.

3.1.2. Investigation of deployable strut-tensioned membrane grid

When deployable strut-tensioned membrane modules are connected together, a double layer grid is formed. The double layer grid comprises an upper grid of top struts and a lower grid of bottom cables. The pattern of the grid is defined by the choice of deployable strut-tensioned membrane module and its arrangement. On the other hand, by adjusting the size of bottom cable grid with respect to the module size, different forms of deployable strut-tensioned membrane structures can be created.

3.1.2.1. Different patterns of deployable strut-tensioned membrane grid

The pattern of the grid affects the way of load transfer and thus the length of load path that the load has to travel to reach the support. It also decides the length and quantity of elements needed and their unbraced length.

The choice of deployable strut-tensioned membrane simplex defines the load transfer manner. For a square simplex, the load transfer is two-way while for a triangle simplex we have a three-way load transfer. Furthermore, depending on the arrangement of the modules, the square simplex can be assembled to form either a square or diagonal grid pattern while the triangular simplex can be assembled to form either a triangular or hexagonal grid pattern. Figs. 3.5 - 3.8 show the square and diagonal patterns of the Umbrella and Cone-shaped grids.

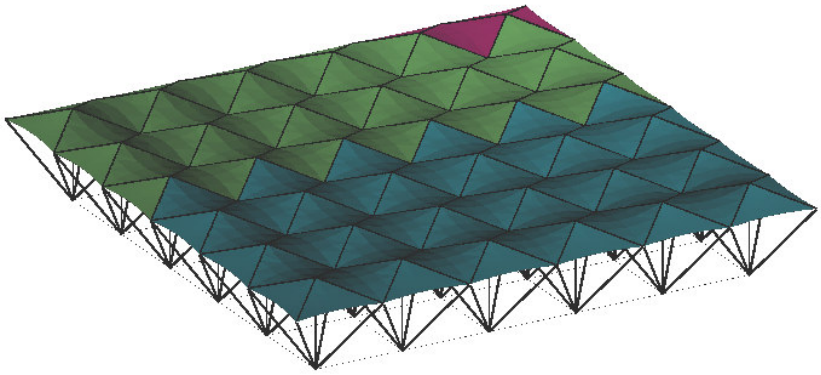

Fig. 3.5. Square pattern of Umbrella grid

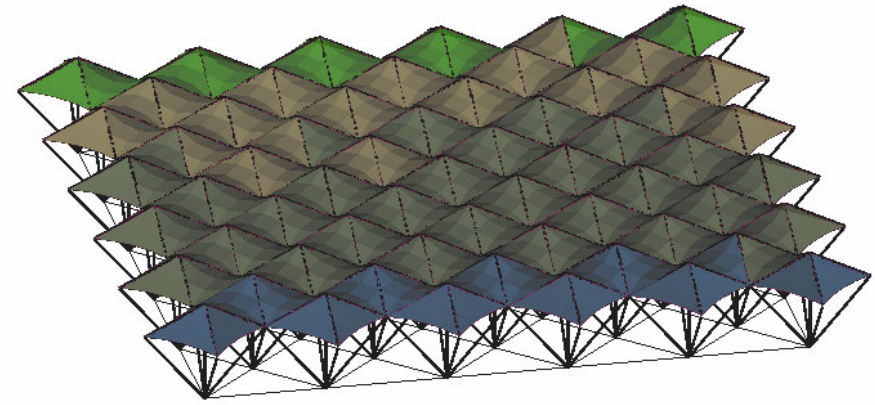

Fig. 3.6. Diagonal pattern of Umbrella grid

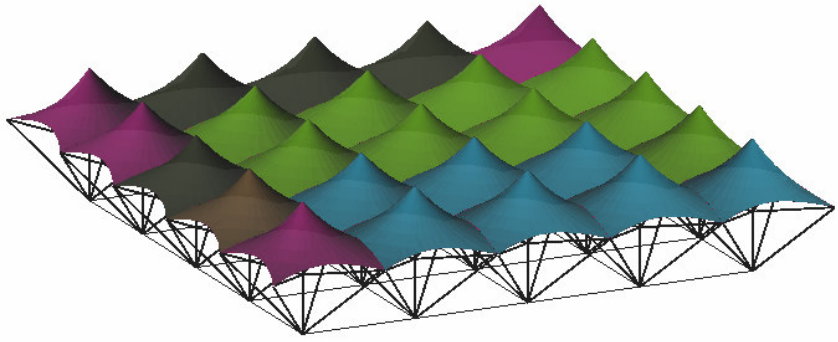

Fig. 3.7. Square pattern of Cone-shaped grid

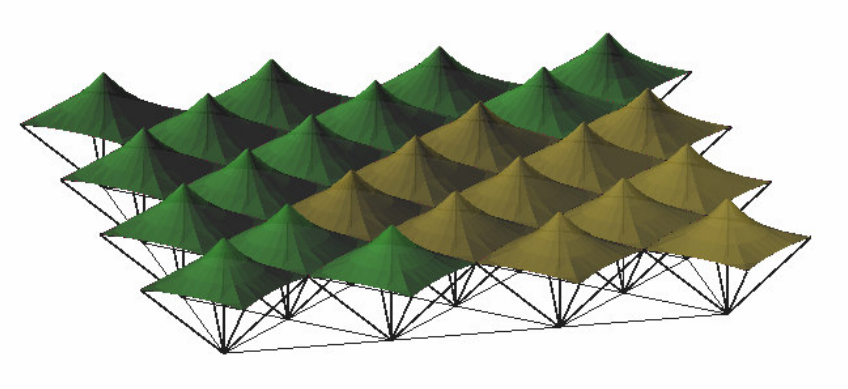

Fig. 3.8. Diagonal pattern of Cone-shaped grid

3.1.2.2. Different forms of deployable strut-tensioned membrane structures

In deployable strut-tensioned membrane grid, the modules are interconnected at their middle nodes while there bottom nodes are linked together by the layer of bottom cables. If the grid sizes of the bottom cable layer in both directions are equal to the width of the module, a flat form of deployable strut-tensioned membrane structures (DSTMS) is generated as illustrated in Figs. 3.5 – 3.8. On the other hand, if the grid size of the bottom cable layer in one direction is smaller than the module width, a curved form of DSTMS in that direction is created (Figs. 3.9 & 3.10).

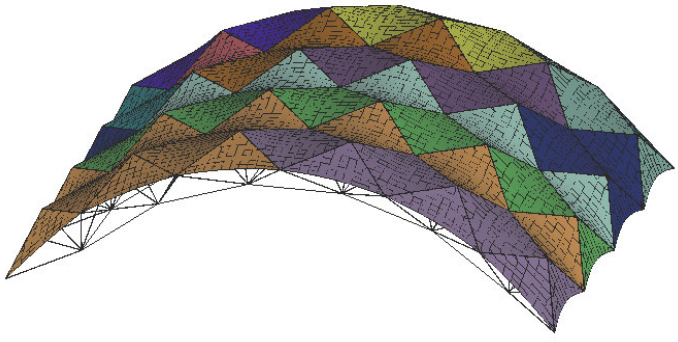

Fig. 3.9. Curved form of Umbrella DSTMS

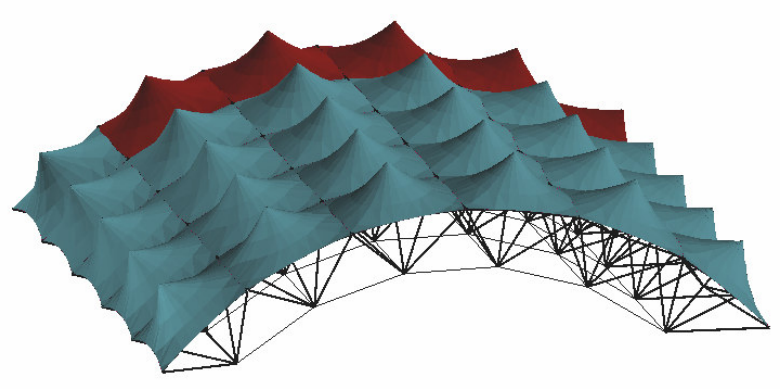

Fig. 3.10. Curved form of Cone-shaped DSTMS

The geometry formulations of a curved DSTMS are given as follows:

$$R = \frac{4H^2 + L^2}{8H} \tag{3.1}$$

$$\sin\frac{\varphi}{2} = \frac{L}{2R} \tag{3.2}$$

$$\sin\frac{\varphi}{2n} = \frac{B}{2R} \tag{3.3}$$

where B is the width of module, L is the span of the structure, H is the rise of the arch, R is the radius of the arch, φ is the open angle of the arch, n is the number of modules assembled. These geometry parameters are illustrated in Fig. 3.11.

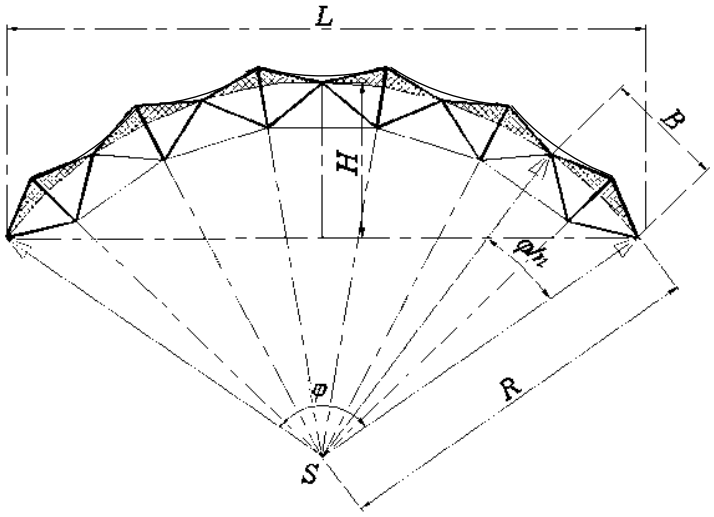

Fig. 3.11. Cross-section of a curved Umbrella DSTMS

3.1.2.3. Self-stress equilibrium

A structure possesses self-stress equilibrium if it is stable without the presence of external load. In mathematical form, it can be expressed as (Lee, 2001):

$$[A]\{s\} = \{P\} = \{0\} \tag{3.4}$$

where [A] is the equilibrium matrix, {s} is the internal stress in system, {P} is the external load on system

In the deployable strut-tensioned membrane grid, the membrane is laid continuously from module to module, forming a series of saddle surface patterns (Umbrella DSTMS) or cone-shaped surface patterns (Cone-shaped DSTMS). The tensile stress in the membrane cause bending moment which is balanced by the tension forces in bottom cables. Therefore, the bottom cables are self-pretensioned due to the tensioned membrane, resulting in a self-stress equilibrium state of the structure (Fig. 3.12).

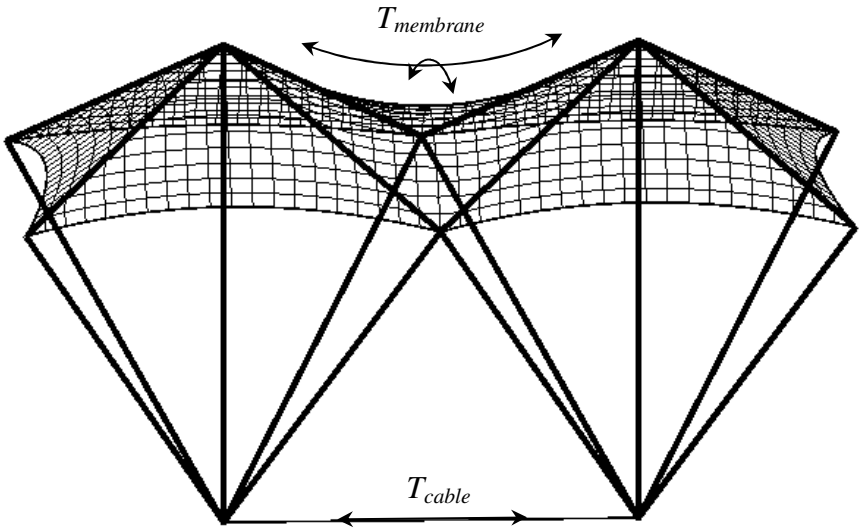

Fig. 3.12. Self-stress equilibrium mechanism of Umbrella DSTMS

Since DSTMS possess self-stress equilibrium, they do not need bulky anchorage systems, a necessity for conventional membrane structures, for stability.

3.1.3. Deployment mechanism of deployable strut-tensioned membrane structures

Deployable strut-tensioned membrane structures belong to the group of kinematic structures which employ the “hinge” release (mentioned in chapter 2) to facilitate the deployment of the structures. In the following sections, deployment of the simplex and the gird of each DSTMS will be presented.

3.1.3.1. Deployment of Umbrella simplex

Deployment of Umbrella simplex is managed by providing a pin connection at the ends of the top and diagonal struts. The joints are designed as a hub so that each strut

connected to them is allowed to rotate freely in a prescribed plane. In square simplex, each pair of connected top and diagonal struts is able to rotate in their corresponding plane. The vertical strut can be lengthened or shortened like a telescope to accommodate the change in geometry of the module during its deployment (Fig. 3.13).

In Umbrella simplex, the vertical strut is acting as the deployment control while the membrane is acting as the deployment restraint. During the deployment process, the vertical strut is shortened to make the module open up like the opening of an umbrella. The membrane attached to top struts is deployed accordingly. When the module is deployed to its final configuration, the membrane will be in tension and thus it restrains the module from opening further. The locking of Umbrella simplex is simply done by providing translational restraint to the vertical strut. In the final deployed configuration, the tensioned membrane tends to collapse the module back to its stowage state, causing the vertical strut subjected to tension.

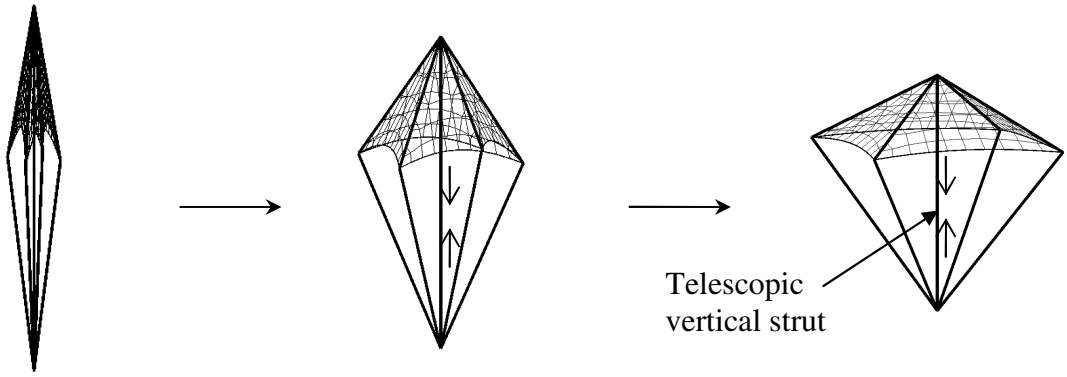

Fig. 3.13. Deployment process of an Umbrella module

The folding process is done by releasing the locking of vertical strut. The vertical strut then is lengthened and the module is stowed back to its compact folded configuration.

3.1.3.2. Deployment of Cone-shaped simplex

Deployment mechanism of Cone-shaped simplex is similar to that of Umbrella simplex. Each pair of connected top strut and diagonal strut hinges on the joints so that they are able to rotate freely in their corresponding plane. To accommodate the change in geometry of the module during its deployment, either a sliding center joint is employed or a telescopic vertical strut is used. Fig. 3.14 shows a center joint sliding along the vertical strut to control the deployment of the Cone-shaped simplex. In the deployment process, the center joint moves upward to open up the module. The membrane is pulled out at four corners while propping at the center, forming a cone-like shape. Another way is to make the lower part of the vertical strut telescopical so that it can be lengthened during the deployment process and shortened during the folding process.

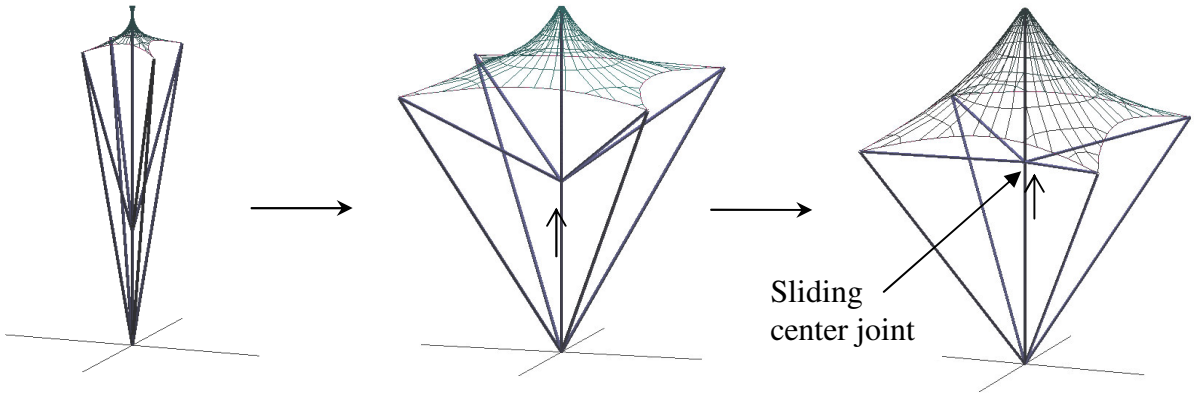

Fig. 3.14. Deployment process of a Cone-shaped module

To lock the deployment of Cone-shaped simplex, either the center joint is fixed or the telescopic vertical strut is translationally restrained. Unlike that of Umbrella simplex, the vertical strut of Cone-shaped simplex is acting as a mast, and thus it is subject to

compression. However, the arrangement of four top struts connected to the vertical strut provides an effective restraining point at its intermediate length, and thus enhancing its buckling resistance.

3.1.3.3. Deployment of deployable strut-tensioned membrane grid

In the deployable strut-tensioned membrane grid, the modules are interconnected at their sharing middle joints to form a continuous kinematic chain. The details of joint designs will be presented in chapter 7. The flexibility of the bottom cables and the membrane facilitates the stowage into a compact configuration of the grid. Deployment of the grid is relied on the deployment of the modules. When the structure is deployed, all modules will be deployed simultaneously due to the constraint of their sharing joints. Figs. 3.15 & 3.16 illustrate the deployment of flat and curved DSTMS from a bundle to the functional configuration.

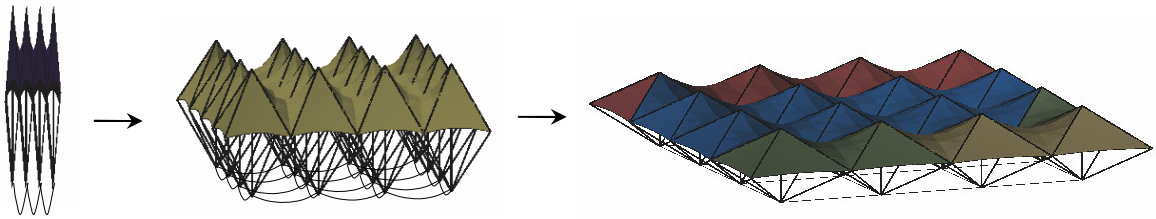

Fig. 3.15. Deployment process of flat Umbrella DSTMS

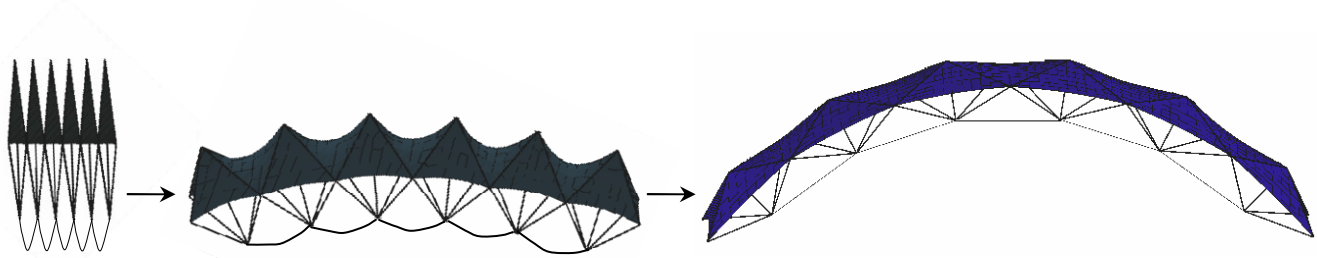

Fig. 3.16. Deployment process of curved Umbrella DSTMS

3.1.4. Advantages and disadvantages of deployable strut-tensioned membrane structures

The key advantages of DSTMS can be summarized as follows:

1. Weight efficiency through
    - The choice of lightweight materials such as membrane and cable.
    - The use of membrane as roofing material and high tensile strength structural element as well.
    - Structurally efficient arrangement of structural members in double layer grid.
2. Efficient load transfer mechanism
    - Elements interconnected in the form of a grid allow for multiple load paths and localized loads to be shared by members through the grid.
3. Aesthetic
    - The natural curved and lightweight forms of membrane create an unexplainable attraction.
    - Regular layout of elements within the grid makes it visually pleasing to the users.
    - The use of membrane provides natural lighting while small-diameter bottom cables minimize the obstruction of light.
4. Efficient deployability
    - The kinematic skeleton and the foldability of membrane fabric and cable minimize the amount of mechanisms needed for the collapse and deployment of the strut system.

- Simultaneous deployment of modules allows the structure to be deployed at once before locking, thus saving construction time and efforts.

5. Self-stress equilibrium
    - Self-stress equilibrium removes the need of any anchoring system and allows more options for the supports.
6. Modularity
    - The modular nature of the system provides a wider scale and variety of applications.
7. Effective prestressing
    - The membrane can be conveniently tensioned owing to the deployment of strut system, thus reducing the need of pretensioning equipment.
    - Self-stress equilibrium results in pretensioning the bottom cables which may help to prevent the cables from slackening under load reversal and reduce vertical displacement of structures.
8. Ease of storage/transportation and rapid erection
    - Owing to the deployability, on one hand DSTMS can be very compact in folded configuration to facilitate the storage and transportation, on the other hand, they can be rapidly deployed to the functional configuration on site, thus reducing erection time and labour forces.
9. Reusability
    - As the structures are deployable, they can be reused or relocated.

One of the existing problems of DSTMS which is also the general problem of tensioned membrane structures is the vulnerability to damage of membrane. However, as the strut skeleton is itself determinate and stable, the damage in membrane should

not create problem to structural integrity and can be patched or replaced simply. The robustness of DSTMS in case of membrane removal will be addressed in chapter 6.

Apart from that, unlike the well-known “scissor” deployment mechanism proposed by Pinero (1962), Escrig (1985) or Sastre (1996) in their deployable pantographic structures mentioned in chapter 2, the deployment of DSTMS is primarily relied on the joint design. Therefore it may be less efficient as compared to pantographic deployment. However, it avoids the problem of eccentric joints existing in pantographic structures, and thus the structural members and joints can be designed in smaller sizes. This contributes to the weight efficiency of DSTMS which will be investigated in chapter 5.

Another disadvantage of DSTMS lies in the need of drainage system for flat roof. The drainage system can be solved with a simple detachable gutters running underneath the middle joints to drain off the rain water to the eaves. Detail of the proposed drainage system will be presented in chapter 7.

3.2. Butterfly-wing structures

Apart from DSTMS, the proposed Butterfly-wing structure is another novel deployable membrane system proposed in this thesis based on the concept of smart integration of tensioned membrane into the rotatable supporting arches.

3.2.1. Background

The essential elements of a membrane structure consist of flexible fabric held under tension to generate stiffness in the surface, boundary cables and rigid support members sustaining compression/bending. Rigid supporting arches thus are widely used in membrane structures due to their inherent curved form, which results in effective membrane surface, and due to their structural efficiency in resisting compression. Most of the arch supported membrane structures are in the form of barrel vault shelter with membrane stretched between a series of vertical parallel arches (Fig. 3.17). This form is widely used in industrial and military applications (Rubb building, American Spaceframe, Sprung structures, etc.) due to its natural modularity. Tensioning devices like hydraulic jacks or turn-buckle systems are often required to apply high tensile stress in membrane. Bracing system is necessary for stability of the structure.

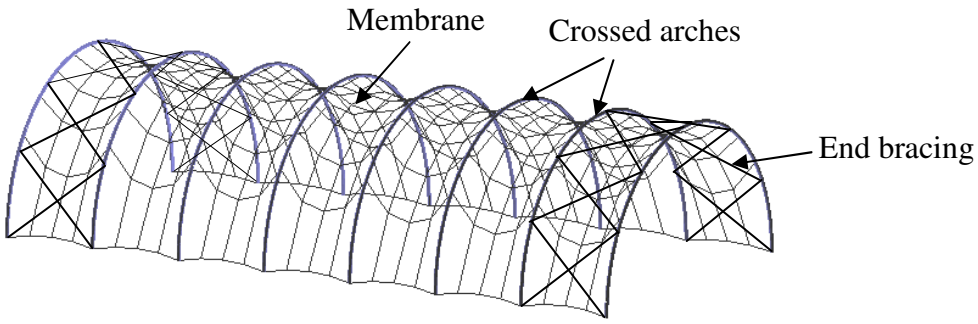

Fig. 3.17. Conventional shelter

This thesis proposed an alternative idea of using rigid arch, which is restrained in inclination position by tensioned membrane and tensioned cables, to generate various distinguished “butterfly wing” forms of membrane structures. The inclined supporting arches make the membrane shape more curved and thus more effective in resisting loads. Many attractive shapes can be created rather than the regular barrel vault form

as in conventional crossed-arch shelters. Generative design provides a variety of deployable structural forms to suit different shapes and sizes for applications. In addition, deployment feature of the structures facilitates fast-tract installation of the structures on site.

Apart from that, the self-weight of inclined arches helps to tension the membrane during erection. Membranes of large area can be pre-tensioned efficiently by sloping down the arches under their self-weight. It helps to avoid the difficulty and costliness in installing and prestressing the membrane.

3.2.2. Butterfly-wing concept

Butterfly-wing structure is constituted from three major elements which are the rigid supporting arches, the fans of anchor cables and the membrane. They are assembled in a mechanism that the arches are not fixed but pin-connected to the hinge-supports and kept stable in inclination position by the tensioned membrane in the middle and the fans of anchor cables radiated from outside.

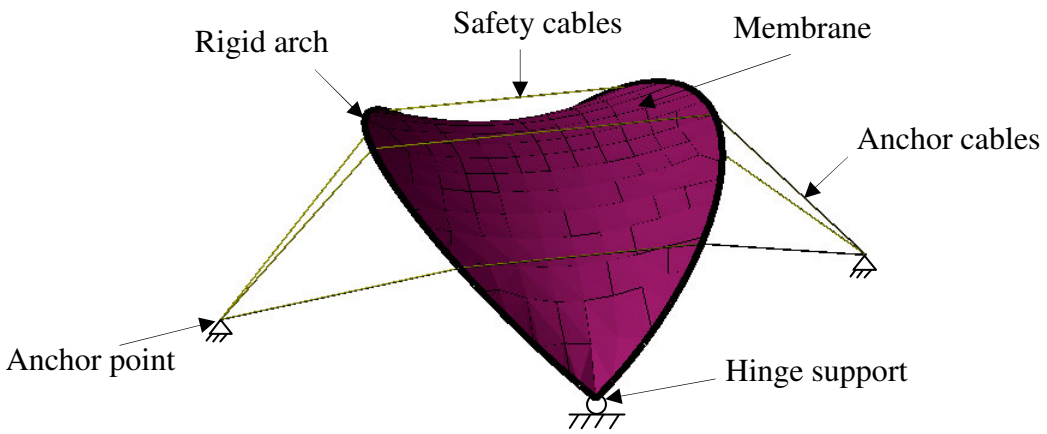

Fig. 3.18. Typical butterfly-wing structure

The key concept of butterfly-wing structure is the use of the inclined arches as the boundary of the membrane. Each inclined arch is the so-called “butterfly wing”. Fig. 3.18 shows a typical butterfly-wing structure. The inclined arches are hinged to the supports so that they are able to rotate perpendicular to their plane. Membrane is attached along these arches, spreading between them to provide space enclosure. A fan of cables radiates from the outside anchor point to the connecting joints on each arch. In the final configuration, membrane is stretched between the inclined arches while cables are tensioned against the anchor points. Hence, the arches are kept inclined in space by the balance of forces including the arches’ self-weight, the tension forces in anchor cables and the prestressing forces in the membrane. The structure therefore achieves self-stress equilibrium state. Self-weight of inclined arches helps to reduce the tensioning forces applied on the anchor cables to stretch the membrane. It also minimizes the requirements for anchor point and foundation to prevent significant loss of prestress. In addition, the tensioned membrane provides lateral restraint to the compressive arches.

To prevent the structure from collapse in case of accidental damage happening to the membrane, either safety cables connecting the two arches (Fig. 3.18) or safety struts are provided. The use of safety struts in Butterfly-wing structures will be presented in section 3.2.7.

3.2.3. Different forms of butterfly-wing structures

Depending on the arrangement of the inclined arches, there exist different forms of butterfly-wing structures. The inclined arches are arranged in a regular polygon to

create a boundary for stretching the membrane in the middle. Theoretically, the more the inclined arches are used, the larger the enclosure is created. However, too many inclined arches may result in fairly low profile in elevation and flat surface at center of the structures. Each inclined arch is called a wing of the structure. Figure 3.19 shows some possible forms of Butterfly-wing structures. They are named as two-wing, three-wing and four-wing butterfly structures as they have two, three and four inclined arches respectively. Butterfly-wing structures having more than two wings may need valley cables to increase the clear height and provide greater articulation form for the membrane (Fig. 3.19).

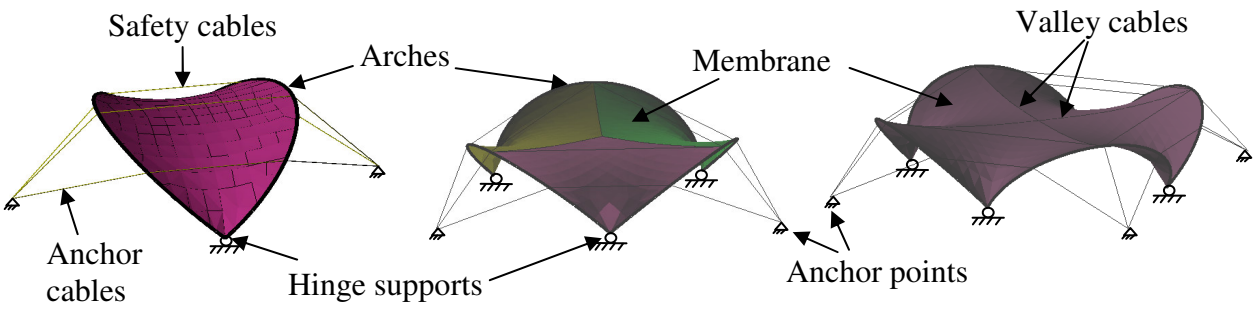

a. Two-wing butterfly structure

b. Three-wing butterfly structure

c. Four-wing butterfly structure

Fig. 3.19. Different forms of butterfly-wing structures

3.2.4. Deployment mechanism of Butterfly-wing structures

Deployment of butterfly-wing structures is made possible by providing the hinge support at the arches' feet so that the arches are able to rotate freely perpendicular to their plane. In folded configuration, all arches are raised up vertically. During the deployment process, the arches are rotated outward gradually by using temporary masts so as to open the membrane. When the membrane is stretched, it will restrain the

rotation of the arches. The tensioned membrane thus is acting as the deployment restraint of the butterfly-wing structures. Anchor cables then are used to pull the arches to tension the membrane further. When the arches are rotated to their designed inclination angle, the membrane will also achieve its designed prestress. Anchor cables are secured to the anchor points to lock the deployment of the structure. Figure 3.20 illustrates the deployment process of different butterfly-wing structures.

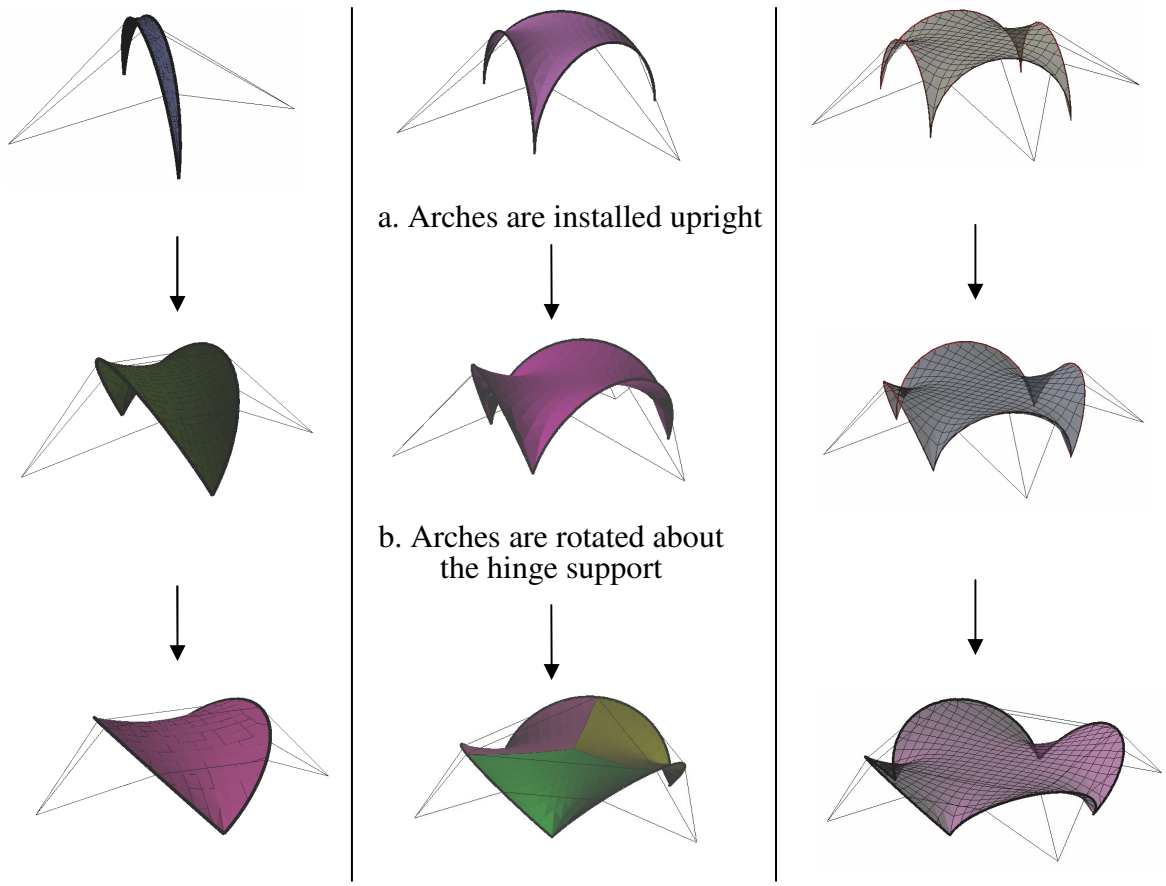

Fig. 3.20. Deployment process of different butterfly-wing structures

3.2.5. Multiple butterfly-wing structures

The three butterfly-wing forms proposed above are the basic single forms. A variety of multiple butterfly-wing forms can be generated by assembling these basic single forms

in a reciprocal manner. In the multiple forms, the peaks of the inclined arches of the single butterfly-wing structures are hinge-connected together at a tangent. Owing to the hinge constraint, the movements of the connected single butterfly-wing structures are dependant on each other, resulting in a simultaneous deployment. Sliding of the arches is attributed to the ground beams acting as a guide-track. The directions of the ground beams for tracking the deployment are shown by the arrows in table 3.1. The deployment of multiple butterfly-wing structures will be illustrated in the next section.

Table 3.1. Generative design of multiple butterfly-wing structures (plan view)

	Two-wing butterfly structure	Three-wing butterfly structure	Four-wing butterfly structure
Single form	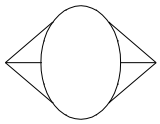	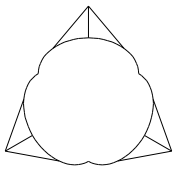	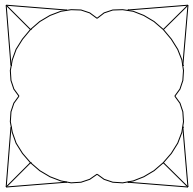
Multiple form	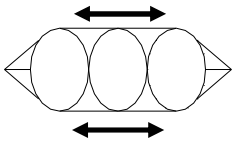	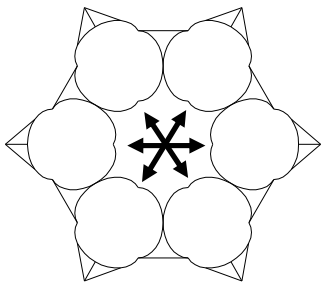	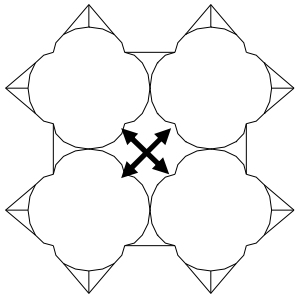

Table 3.1 illustrates the reciprocal assembly of single forms to generate multiple forms of different butterfly-wing structures. The shapes of the multiple butterfly-wing forms are dependant on geometry of the single butterfly-wing forms. For two-wing structure, the single forms are assembled longitudinally while for three-wing and four-wing structures, they are assembled circumferentially. Therefore, multiple two-wing

butterfly structure is suitable for enclosing 1-D plan while multiple three-wing and four-wing butterfly structures are suitable for enclosing hexagonal and square plans respectively. Furthermore, many other forms of multiple butterfly-wing structures can be made possible by assembling different single forms instead of assembling identical single forms.

3.2.6. Deployment of multiple butterfly-wing structures

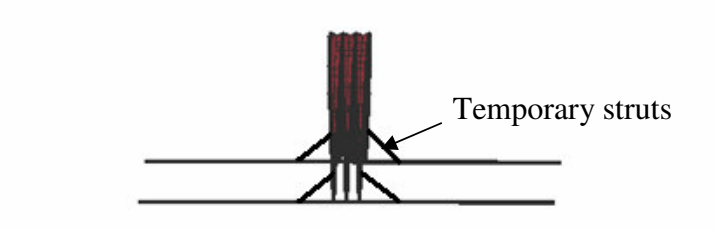

a. Arches are installed upright

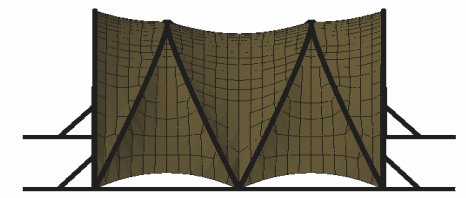

b. Arches are slided along ground beam

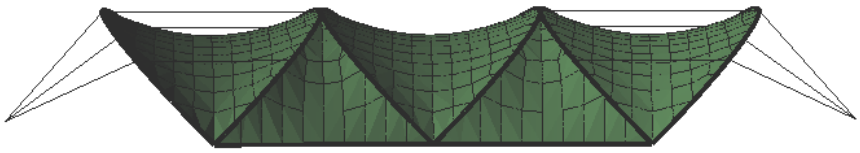

c. Membrane is stretched to final configuration

Fig 3.21. Deployment process of multiple two-wing butterfly structure

Multiple butterfly-wing structures belong to the group of kinematic structures which employ both the “hinge” and the “slide” releases. The deployment of the structures is made possible by providing the ground beam as a guide-track for the sliding of the arches, and by designing the hinge connections at the peaks and the feet of the arches.

With the hinge constraint at the arches' peaks, the whole structures is deployed simultaneously.

Deployment of the multiple two-wing butterfly structures is similar to that of an accordion as illustrated in Fig. 3.21. In folded configuration, all arches are gathered vertically. The two center arches are translationally restrained while the rest are able to slide along the ground beams. During the deployment process, the two end arches are pushed outwards while being kept vertically by temporary struts. The whole structure will open up simultaneously and the membrane between the arches is stretched accordingly. When the structure is deployed to its final position, all supporting arches are locked to the ground beams. The two end arches then are gradually sloped down. After that, anchor cables are tensioned against the anchor points to achieve the design prestress in the membrane.

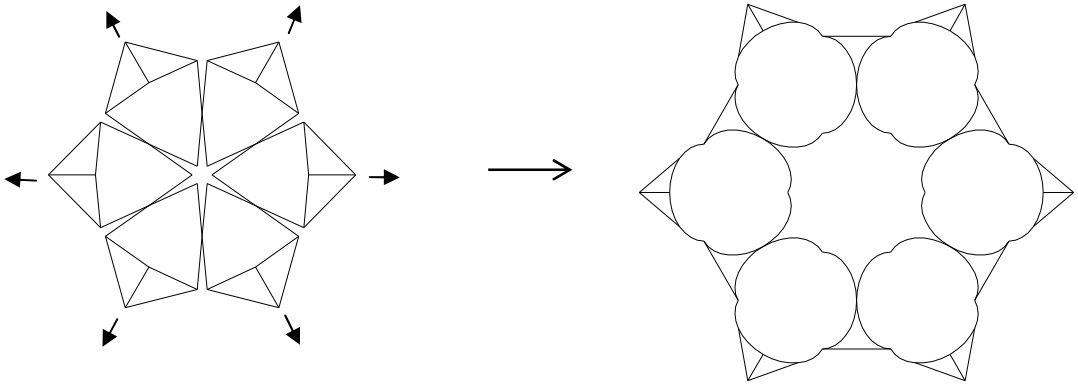

a. Plan view

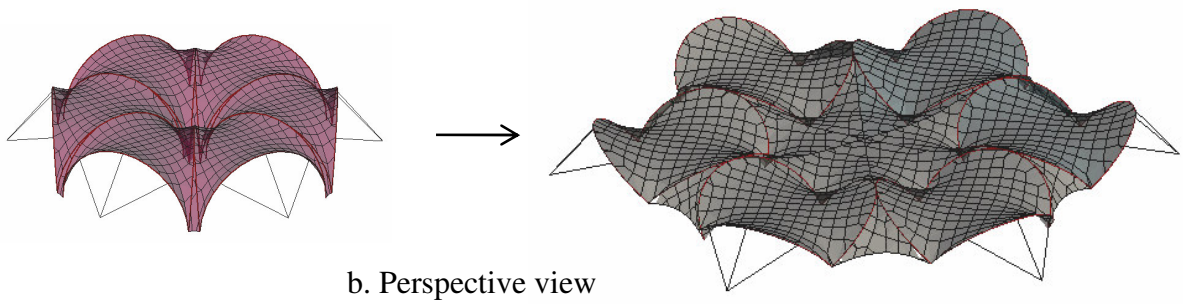

b. Perspective view

Fig. 3.22. Deployment process of multiple three-wing butterfly structure

Similarly, Figs. 3.22 & 3.23 show the deployments of the multiple three-wing and four-wing butterfly structures blossoming from center and expanding to the final configurations. The arches' feet are able to slide along the guide-track ground beams which are placed in the arrow directions. Owing to the hinge connections at their peaks, the movements of the arches are dependent on each other. Therefore, during the deployment process, all arches slide outwards simultaneously along the guide-track to open up and induce tension in the membrane. When the structure is deployed to its final position, all arches are locked to the ground beams and anchor cables are tensioned against anchor points to achieve the design prestress in the membrane.

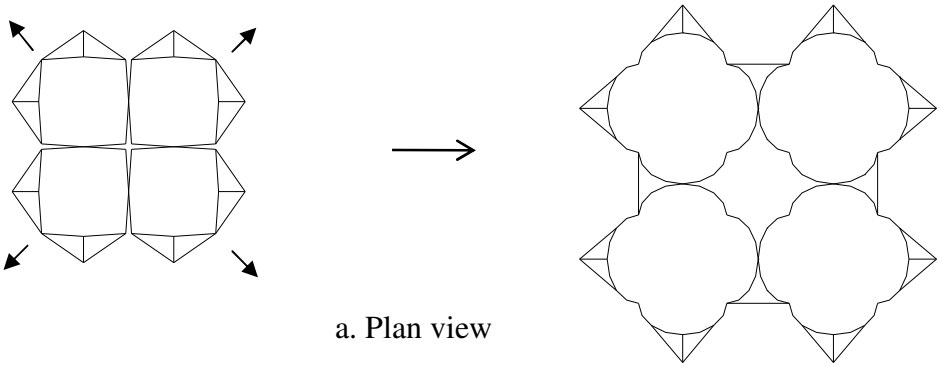

a. Plan view

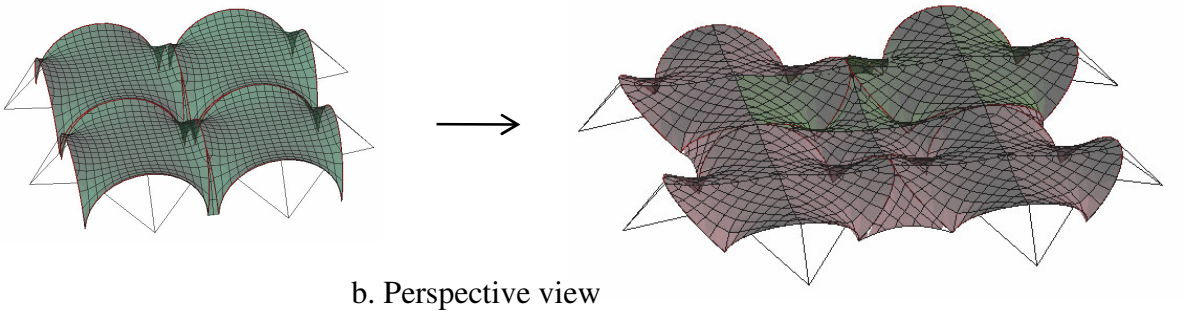

b. Perspective view

Fig. 3.23**.** Deployment process of multiple four-wing butterfly structure

3.2.6. Solution to large span Butterfly-wing structures

For the arch with span over 20m, space truss is an effective option to improve the low buckling resistance of single section. However, assembly of conventional space truss is

a time consuming process and thus increasing the cost of site labour for construction. In this thesis, a deployable cable-strut structure developed by Vu *et al.* (2006) is proposed for medium and large span arch of butterfly-wing structure. It attempts to provide a structurally effective space truss to improve the buckling resistance of the arch of medium and large span. Its deployability enables butterfly-wing structure to be easily transported and rapidly erected.

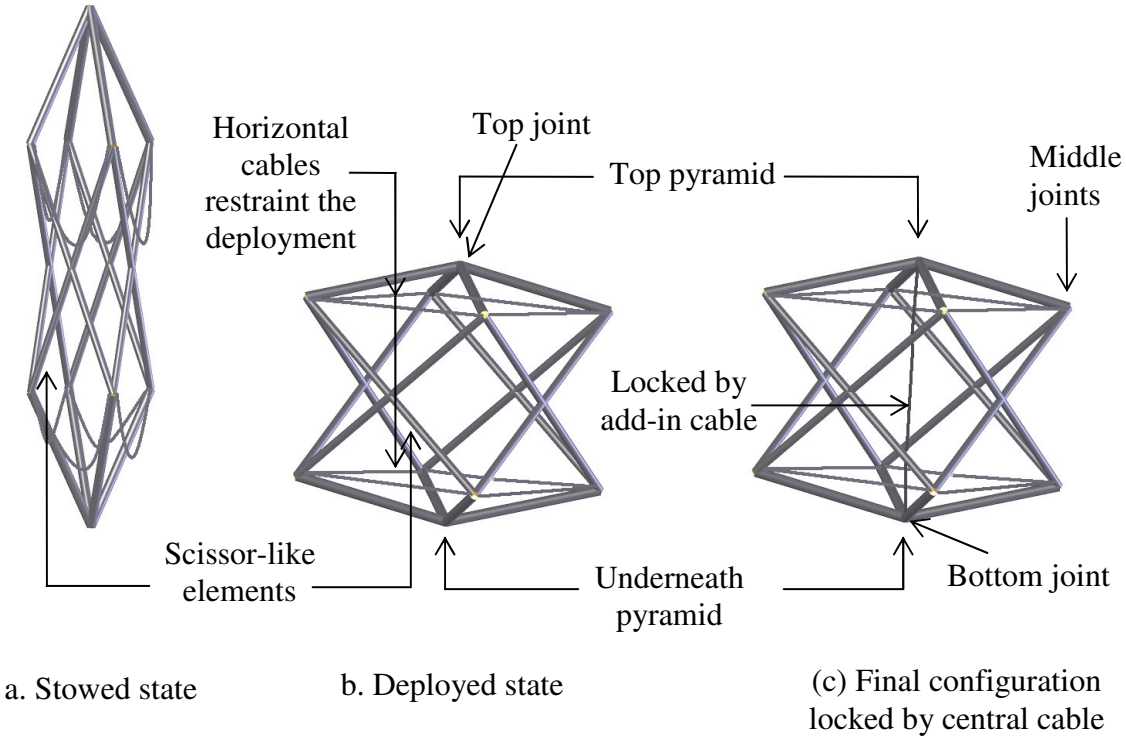

Fig. 3.24. Module configuration and deployment (Vu *et al.*, 2006)

The arch is formed by a series of identical cable-strut modules connected together. Each module is constructed from two strut-pyramids and four scissor-like elements as shown in Fig 3.24. The joints are designed so that they allow each strut connected to them to rotate freely in a prescribed plane. Therefore, the module can be folded into a compact form and deployed to a functional form (Fig. 3.24). The deployment of each module is constraint by the top and bottom layers of cables. The final configuration of

the module after deployment is stabilized by attaching and pre-stressing the central add-in cable.

Deployment of the arch is relied on deployment of the modules. When the arch is deployed, all modules are deployed simultaneously due to joint constraint. The deployment process of the cable-strut arch is illustrated in Fig. 3.25.

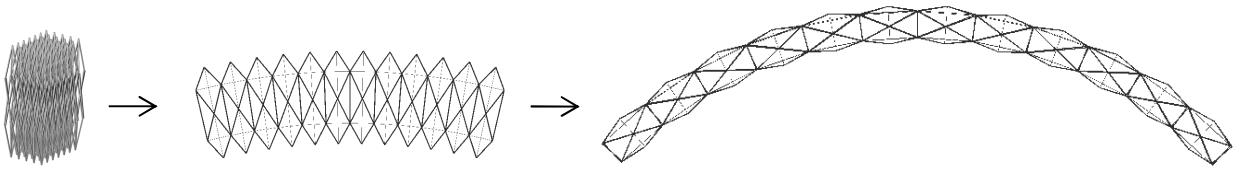

Fig. 3.25. Deployment of a cable-strut arch

Fig. 3.26 shows the configuration of a two-wing butterfly structure using deployable cable-strut arch. The membrane is attached to upper-middle joints of the modules of the arches. With the membrane being continuously attached, the arches are laterally braced along their length.

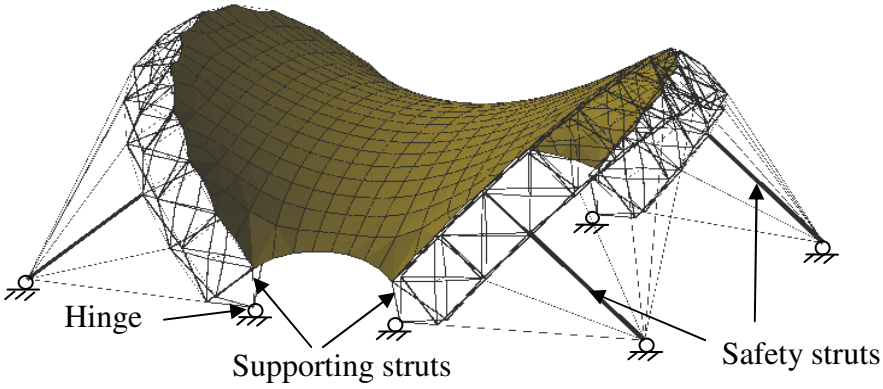

Fig. 3.26. Two-wing butterfly structure using deployable cable-strut arch

In order to avoid the obstruction to the entrances of structure, the center cable-fan is replaced by two side cable-fans. Each cable-fan, including a safety strut, is radiated from the anchor point to the upper middle joints of the arch's modules. Although the safety struts are subjected to tension forces, they are designed to resist the self-weight of the arch to prevent catastrophic collapse if accidental damage happens to the membrane. The ends of the arches are assembled with a group of four supporting struts which forms an upside-down pyramid. The vertex of strut-pyramid is pinned to the ground supports so that the arches are able to rotate about the supports.

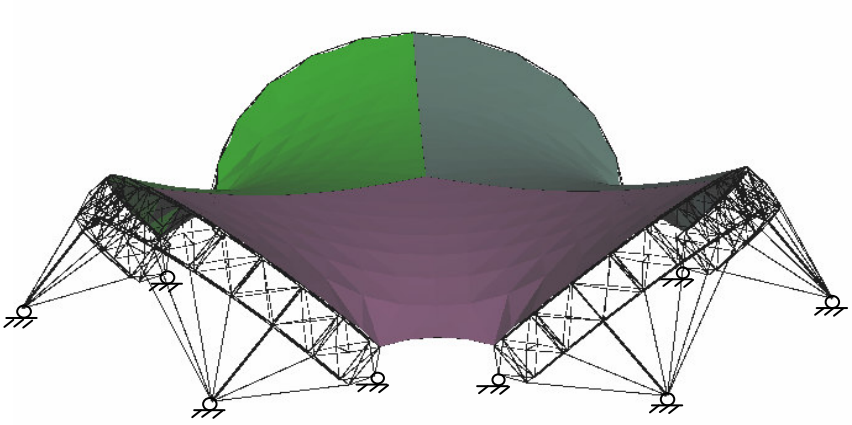

Fig. 3.27. Three-wing butterfly structure using deployable cable-strut arch

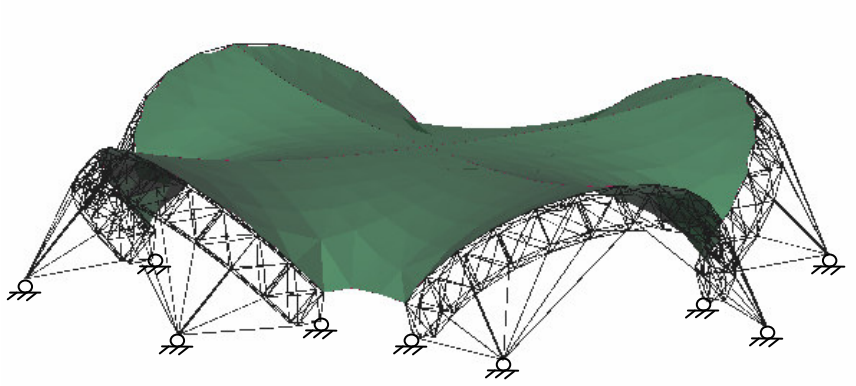

Fig. 3.28. Four-wing butterfly structure using deployable cable-strut arch

Figs. 3.27 & 3.28 show the configuration of three-wing and four-wing butterfly structure using deployable cable-strut arch. The structural efficiency of butterfly-wing structure using deployable cable-strut arch will be investigated in chapter 5.

3.2.6. Advantages and disadvantages of Butterfly-wing structures

Although arch supported membrane structures are not new, the innovative use of inclined arches in deployable forms provides butterfly-wing structures with the following advantages:

1. Effective membrane shape
    - Due to the curved form of the arches and their inclined position, the structures possess effective anticlastic membrane surfaces.
2. Weight efficiency
    - Effective membrane shape results in smaller resultant forces induced by applied loads, and thus leading to lighter structures.
    - Tension forces in membrane are balanced by the arches' self-weight and tension forces in cables, thus resulting in lighter supporting arches.
3. Versatility
    - By making different inclined-arch arrangements, different forms of butterfly-wing structures are made possible.
    - By combining either identical of different butterfly structures in a reciprocal manner, various deployable forms can be generated to suit any shape and size of applications.
4. Efficient deployability

- The hinge supports allow the arches to rotate to deploy the membrane during erection.
- The reciprocal arrangement of the arches and the use of ground beam allow the structures to deploy simultaneously.
- The arch is made deployable by using a kinematic cable-strut system. Deployment and folding processes of the cable-strut arch are facilitated by the hinge joints, flexible cables and special strut arrangement.

5. Effective membrane tensioning
    - Membrane tensioning is attributed to the deployment and the self-weight of the supporting arches, reducing the pretensioning work and equipments.
6. Rapid erection
    - The deployment of the supporting arches enables a fast-track erection of butterfly-wing structures.
7. Aesthetic
    - The double curvature surfaces and the light-weight form of membrane make a striking appearance for butterfly-wing structures.
8. Reusability
    - As a deployable membrane structure, butterfly-wing structure can be reused and relocated.

One of the main disadvantages of the butterfly-wing structures is the loss of stability when membrane is damaged. The design must ensure the safety of the structure in the event of membrane failure. This issue is solved by either using safety cables on top of the arches (Figs. 3.18 & 3.19) or using safety struts to support the arches (Figs. 3.26 – 3.28). In chapter 6, the robustness of butterfly-wing structures subjected to membrane

removal will be addressed.

Apart from that, shipment of the arches in their original form is cumbersome. The arches can therefore be segmented for the ease of shipping and assembling on site. Another possible solution is to the use of deployable cable-strut arch presented in section 3.2.7. The detail design for implementation will be presented in chapter 7.

3.3. Summary

This chapter presented the proposed concepts of two novel deployable membrane structures: the Deployable strut-tensioned membrane structures and the Butterfly-wing structures. These structures make use of the smart integration of tensioned membrane into deployable supporting structures. These structures were designed to achieve the advantages of both membrane structures and deployable structures in terms of versatility, lightweight, structural efficiency and construction speed. The structural morphology and deployability of these structures were studied to describe the major relations among their geometry, deployment mechanism, functionality and structural stability.

CHAPTER 4

STRUCTURAL ANALYSIS METHOD AND SHAPE EFFECT STUDIES

4.1. Introduction

In chapter 3, the conceptual design of two new deployable membrane systems – Deployable strut-tensioned membrane structures and Butterfly-wing structures – were proposed and explained. This chapter will provide background information on how to find the equilibrium form of the membrane and to investigate the structural behaviour of the proposed deployable membrane structures (DMS) through numerical modelling. A proposed integrated approach of force density method and geometrical nonlinear analysis is used for form-finding and for structural analysis of these structures and this approach is presented in this chapter.

Since the membrane relies mainly on its form to resist load, the membrane shape has a great effect on the structural stiffness and the stability of the structures. A series of shape effect studies employing the above integrated approach are carried out to investigate the influence of membrane curvature on the membrane stress magnitude of DSTMS and Butterfly-wing structures. Based on the shape effect study results, the optimum parameters for achieving effective membrane shapes of DSTMS and Butterfly-wing structures are determined.

4.2. Physical characteristics

Deployable membrane structures can be considered as load adaptive structures in the manner that membrane tends to change its geometry to accommodate changes in load rather than increases the stress level. The stiffness of the structures is achieved by the virtue of special geometric shapes with initial prestress in the membrane. Prestressing forces (edge loads, self-weight, etc.) help to stabilize the structure and provide stiffness against further deflection. The response of the structures to prestressing forces is always nonlinear in that the equilibrium configuration of membrane and state of stress in membrane are dependent on those forces. Therefore, the structures respond in a nonlinear fashion to both prestressing forces and applied loads regardless of linearity of materials.

The behaviour of deployable membrane structures can be divided into three stages. The first stage is the deployment stage, in which the membrane and the supporting structure unfold from their compact configurations. The second stage is the prestressing stage, in which the supporting structure deploys to its final configurations and the membrane deforms into a predominant equilibrium configuration under prestressing forces. The final stage is the stage, in which the fully prestressed system is subjected to variable external loads.

The first stage is associated with the deployment process which has been introduced in chapter 3. The behaviour of the structures in this stage is often studied through physical modelling and will be discussed in chapter 7. This chapter will focus on analyzing the behaviour of the proposed deployable membrane structures in the

remaining two stages which are the prestressing or form-finding stage and the fully functional or in-service stage.

4.3. Selection of the method of analysis

Theoretically, structural analysis of membrane structure can be performed by analytical method or numerical method. The choice of the method of analysis is dependent on the physical characteristics and the expected behaviour of the structure, the required accuracy of the analysis and the computational need of the method.

4.3.1. Analytical method

Membrane theory is often used in analytical method to analyze the structure. Although the geometric descriptions of a tensioned membrane surface may be complex, all must conform to the rules of static equilibrium. Analytical method can be used to analyze the statically determinate supporting structure. The determinate structure can be one part or one module of the whole structure.

There are few nonlinear solution techniques for membrane structures that do not require numerical solutions. Leonard (1988) derived a bulk of formulations that could be used for hand calculations of membranes. Analytical, of course, will provide the highest accuracy. However, its formulations are very tedious and not easy to apply. Moreover, it is very time consuming to analyze structures of high complexity.

4.3.2. Numerical method

There are several numerical methods to model and analyze a structure such as the finite different method, the finite element method and the boundary element method. However, with the rapid development of computer technology, the Finite Element Method (FEM) has become powerful and suitable for analyzing nonlinear systems like membrane structures. FEM developed for membrane structure is a numerical analysis technique that assumes it is possible to approximate the behaviour of a smooth surface by defining the geometry, material characteristics and applied loads at a discrete number of locations. The structural elements such as membrane, cable, strut and beam are divided into a discrete number of finite-sized elements which retain their materials properties. The elements may correspond to a structural component or a portion of a component. The elements are interconnected at a discrete number of points, called nodes, on the boundary of the elements. The nodes are used to define the spatial configuration of the structure. Some nodes may be restrained, others will be free to translate and rotate. The elements may be defined with specific material properties, defined to preserve a specified length or defined to preserve a specified force. A set of algebraic equations is derived relating the various nodal displacements and equivalent external nodal loads. As computational capability has become more readily accessible, considerable refinement in the assumption used has been possible.

As membrane is modelled as cable net system which will be discussed in the subsequent section, membrane structure is actually a highly redundant cable system. FEM is proved to be a useful method for structural analysis of highly redundant system (Bathe, 1996) and has following advantages as compared with analytical method:

- Physically interpreted by numerical modelling;
- Flexible to approximate particular problems;
- Feasible to accommodate refined elements in regions of particular interest;
- Easy to generate and change variable mesh sizes;
- Less problem dependent, can include other structural elements, such as beams, in the model.

Therefore, FEM is more widely used than analytical methods. In this research, FEM is employed to analyze the structural behaviour of the proposed DMS.

4.4. Structural modelling

Membrane or shell is often modelled by using 2D membrane elements. However, as membrane materials are made of woven fabric, their characteristics are featured by the properties of warp and weft threads. Therefore, the membrane of the DMS can be conveniently modeled as a network of cables with different cable properties corresponding to warp and weft directions of the fabric (Otto, 1969; Shaeffer, 1995; D'Anza, 2002). Cable is uniaxial element and thus is simpler to formulate and analyze than 2D elements. Therefore it will be very efficient for applying in computer techniques.

If the design mesh is set with nodes on the principal surface curvatures and the element properties are adjusted to reflect the effective tributary area and stress, the behaviour of membrane generally can be adequately examined with cable elements. For that reason, it is important to place the warp and weft directions of the fabric so that they follow the

geodesic paths of membrane surface. In form finding of the DMS, the prescribed stresses in warp and weft directions will be referenced parallel and perpendicular to geodesic paths. Therefore, the geodesic paths must be established during form finding process. These geodesic may be determined by using soap film as introduced by Barnes (1994). A fabric thread floating over the soap film will be stretched to follow the geodesic paths. Another simplified approach that uses the principal membrane stresses can be used to determine the geodesic paths for preliminary design (D'Anza, 2002).

Apart from the membrane, the proposed DMS consist of beams, struts and cables. The beams and struts can be modelled as beam elements. Therefore, analysis of the structures requires two types of elements: cable element and beam element. However, unlike cable and membrane, the beam or strut undergoes small deflection due to its relative large rigidity. Thus, it is appropriate to adopt linear beam element with small deflections for modelling the beams and struts. The beam element for modelling the beams and struts of the DMS is a straight beam of uniform cross section which is capable of resisting axial force, bending moments about two principle axes of its cross section and a twisting moment. The FE formulation of such beam is available in many references (Bathe, 1996; Zienkiewicz and Taylor 2000). In subsequent section, the nonlinear solution for cable element will be discussed.

4.5. Integrated approach for structural analysis

There are several computational approaches that can be used to analyze the structural behaviour of the DMS. They can be summarized into two basic approaches: the matrix

method (transient stiffness method and force density method) and the vector method (dynamic relaxation method) as reviewed in chapter 2. Based on the pros and cons of each method, an integrated approach of force density method and geometrical nonlinear analysis (using transient stiffness method) is employed for structural analysis of DMS. First, the initial equilibrium shape and membrane-cable pre-stresses are determined by using the force density method (prestressing or form-finding stage). After that, geometrical nonlinear analysis will be performed to find the deformed shape and stresses in structural members of the structures subjected to the external applied loads (in-service stage).

4.5.1. Basic principle of Force Density Method

The Force Density Method (FDM) is described originally by Scheck (1973). The advantage of the method is that it provides a linearized solution to the equilibrium form-finding equations for a tension net. The method is independent of the initial location of the joints.

In FDM, the membrane nodes at supports are fixed in order to find the equilibrium shape. The linear system of equations of force equilibrium for an unconstrained node *i* in a net of element *i-j* are:

$$\begin{cases} \sum X_{ij} = 0 \rightarrow \sum_j N_{ij} \dfrac{\left|x_i - x_j\right|}{L_{ij}} + P_{ix} = 0 \\ \sum Y_{ij} = 0 \rightarrow \sum_j N_{ij} \dfrac{\left|y_i - y_j\right|}{L_{ij}} + P_{iy} = 0 \\ \sum Z_{ij} = 0 \rightarrow \sum_j N_{ij} \dfrac{\left|z_i - z_j\right|}{L_{ij}} + P_{iz} = 0 \end{cases} \tag{4.1}$$

where $\sum X_{ij}$, $\sum Y_{ij}$, $\sum Z_{ij}$ are the sum of forces in *X, Y* and *Z* directions; x_i, y_i, z_i, x_j, y_j, z_j are the nodal coordinates at node *i, j*; N_{ij} is internal force of element *i-j*; P_{ix}, P_{iy}, P_{iz} are the external force at node *i*; L_{ij} is deformed length of element *i-j*

The value N_{ij}/L_{ij} in equations (4.1) can be replaced by q_{ij} named as the Force density ratio. When the force densities for all elements at a joint are equal and uniformly distributed around the joint, minimal surfaces are generated (Sheaffer, 1995).

The linear system of equations (4.1) can be solved in a single step, the coordinates of unconstrained nodes are determined. Initial equilibrium shape is obtained. Internal forces N_{ij} and the deformed length L_{ij} can be calculated. The undeformed length L_{0ij} of element *i-j*, used for patterning, can be determined based on the deformed length L_{ij}, material modulus E_{ij} and cross sectional area A_{ij} as follows:

$$L_{0ij} = \frac{L_{ij}}{\left(1 - \frac{N_{ij}}{A_{ij}E_{ij}}\right)} \tag{4.2}$$

4.5.2. Geometrical nonlinear analysis

After the prestress and initial equilibrium configuration of the structure are found by the force density method, geometrical nonlinear analysis is then employed for analyzing the structure under external applied loads. As mentioned in the behaviour of DMS, the membranes undergo large deflection. Thus the finite element formulation of the cable element, which is employed for modelling the membrane as a cable net as mentioned earlier, should be able to capture the large displacements of the membranes.

4.5.2.1. Cable element formulation

The detail of modelling the cable element can be referred to the work of Tabarrok and Qin. (1992) or Li and Chan. (2004). In this research, the virtual work displacement developed by Leonard (1988) is employed to give the basic description of cable element.

The relationship between stresses, strains, and displacements of cable elements are formulated to obtain the stiffness equations for the cable net of membrane. Approximating finite element functions then will be introduced into the principle of virtual work to form matrix representation.

The nonlinear strain-displacement relationship (Bathe, 1996) is given by equation (4.3) below.

$$\varepsilon = \frac{ds^2 - ds_0^2}{2ds_0^2} = \{C_0\}\frac{\partial\{u\}}{\partial s_0} + \frac{1}{2}\left\{\frac{\partial u}{\partial s_0}\right\}^T \left\{\frac{\partial u}{\partial s_0}\right\} \tag{4.3}$$

in which $\{u\}$ is the added displacement from the prestressed state (after form finding), s_0 and $\{C_0\}$ are the segment length and direction cosines of the element at prestressed state, s is the segment length of the element in the deformed state.

Though the structural behaviour of membrane is nonlinear, its stress-strain relation can be considered as piecewise linear within the allowable stress range. Therefore, the tension T in deformed state and strain ε can be related by a piecewise relationship as:

$$T = T_0 + E_0 A(\lambda - \lambda_0) = T_0 + E_0 A_0 \lambda_0 (\sqrt{1+2\varepsilon} - 1) \tag{4.4}$$

with T_0, E_0, A_0 and λ_0 are the pretension, material modulus, cross sectional area and elongation ratio in the prestressed state (after form-finding); λ is the current elongation ratio and

$$\lambda = \lambda_0 \sqrt{1+2\varepsilon} \tag{4.5}$$

The principle of virtual work states that the work done by the internal and external forces during an arbitrary small displacement $\{\partial u\}$ consistent with the kinematic boundary conditions must be zero. The principle furnishes the equilibrium state as:

$$\int_V \left(\{\delta\varepsilon\}^T \{\sigma\} - \{\delta u\}^T \{f\} \right) dv - \{\delta D\}^T \{P_c\} = 0 \tag{4.6}$$

or it can be transformed and re-written as

$$\int_{s_0} \left[\frac{\partial \{\delta u\}^T}{\partial s_0} \{C\}(T) - \frac{1}{\lambda_0} \{\delta u\}^T \{q\} \right] ds_0 - \{\delta D\}^T \{P_c\} = 0 \tag{4.7}$$

where $\{P_c\}$ are concentrated nodal forces, $\{q\}$ are the distributed load per unit length, $\{\delta D\}$ is the vector of nodal virtual displacements; $\{C\}$ are the direction cosines at deformed state which can be determined as:

$$\{C\} = \frac{\{C_0\} + \dfrac{\partial \{u\}}{\partial s_0}}{\sqrt{1+2\varepsilon}} \tag{4.8}$$

The virtual work displacement equation (4.7) can be used for determining the large displacement response u due to applied loads q and P_c.

In the finite element approximation, the cable net can be simply considered as a system of interconnected straight line elements. Each element has uniform material, stress, and geometric properties over its length. A typical cable element is shown in Fig. 4.1 spanning between two nodes *i* and *j* with six degrees of freedom.

The direction cosines $\{C_0\}$ of the element in the prestressed state can be determined from the nodal coordinates as:

$$C_{0i} = \frac{x_i - x_j}{L_{ij}} \qquad \text{(i=1,2,3 corresponding to the global axes)}$$

The straight element approximating functions used for displacements and distributed loads are adopted as:

$$\{u\} = \begin{bmatrix} N_i & N_j \end{bmatrix} \begin{Bmatrix} d_i \\ d_j \end{Bmatrix} \tag{4.9}$$

$$\{q\} = \begin{bmatrix} N_i & N_j \end{bmatrix} \begin{Bmatrix} q_i \\ q_j \end{Bmatrix} \tag{4.10}$$

with $N_j = \xi[I]$ and $N_i = (1-\xi)[I]$; d_i, d_j and q_i, q_j are nodal displacements and nodal load increments respectively; $[I]$ is the unit matrix.

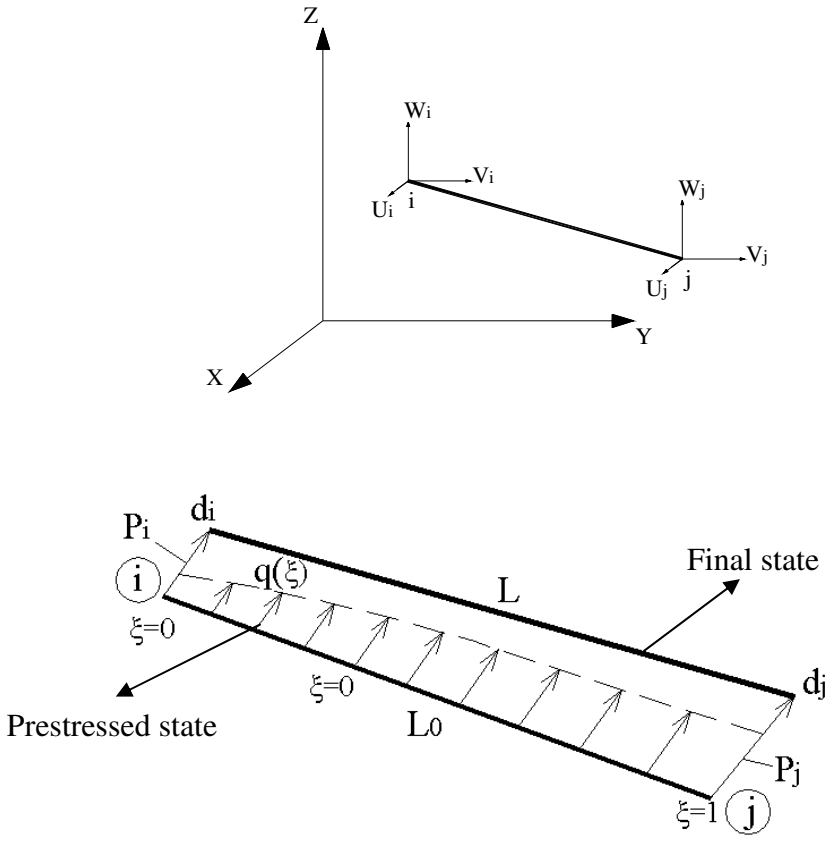

Fig. 4.1. Straight cable element definition

Similarly, the virtual work displacements are:

$$\{\delta u\} = \begin{bmatrix} N_i & N_j \end{bmatrix} \begin{Bmatrix} \delta d_i \\ \delta d_j \end{Bmatrix} \tag{4.11}$$

Substituting the approximating functions in equations (4.10) and (4.11) into equation (4.7), the virtual work displacement can be written as:

$$\sum \left[\begin{pmatrix} \delta d_i^T & \delta d_j^T \end{pmatrix} \left(T\{C\} - \frac{L}{6\lambda_0} \begin{Bmatrix} 2q_i + q_j \\ q_i + 2q_j \end{Bmatrix} \right) \right] - [\delta D]^T \{P_c\} = 0 \tag{4.12}$$

Since the virtual displacements δD are not zero, the assemblage of the total force contributions from all elements should vanish:

$$\{G\} = \{F\} - \{P\} \tag{4.13}$$

where $\{F\}$ is the internal force contributions of each element incident at a node

$$F = \sum T\{C\} \tag{4.14}$$

and $\{P\}$ is the external force contribution of each element at a node plus the concentrated force at the node

$$\{P\} = \sum \left(\frac{L}{6\lambda_0} \begin{Bmatrix} 2q_i + q_j \\ q_i + 2_j \end{Bmatrix} \right) + \{P_c\} \tag{4.15}$$

The tangent stiffness matrix for an iterative Newton-Raphson method can be determined as:

$$[K_{NR}] = \frac{\partial\{G\}}{\partial\{D\}} \tag{4.16}$$

The tangent stiffness matrix for an incremental method has the form:

$$[K_{icr}] = \frac{\partial\{F\}}{\partial\{D\}} \tag{4.17}$$

With the tangent stiffness matrices obtained in equations (4.16) and (4.17), an incremental-iterative strategy is ready to solve the large deflection problem of the structure.

4.5.2.2. Incremental-iterative procedure

Based on the starting geometry (u_0) in equilibrium with pretension (T_0) found in the form-finding state by FDM, nonlinear finite element analysis is performed to analyze the structure with applied external loads (R). Firstly, with a small load increment ($P_1 = \Delta R$), a new shape (u_1) and a new tension state (T_1) are searched by using incremental method. This phase is called the predictor to provide an initial trial solution.

Secondly, Newton-Raphson method is employed to perform a series of iterations until a certain convergence criterion is achieved. This phase is called the corrector to provide a better geometry (u_1) and tension state (T_1) in equilibrium.

A new increment load is then calculated ($P_2 = P_1 + \Delta R$). The above incremental-iterative procedure is repeated to find a new shape (u_2) and new tension state (T_2) in equilibrium.

After a number of increments, the external loads (R) will be fully applied. The final shape and tension state in equilibrium obtained will be the deformed configuration and the tension state of the structure under applied external loads.

4.6. Shape effect studies

As mentioned earlier, surface curvature provides structural stability and stiffness for the tensioned membrane. Larger radii result in larger membrane stresses, which also holds true for the forces in the boundary edge cables and thus the supporting structure.

The larger curvature the smaller the stresses induced in membrane as the result of the applied loads. As explained in the form-finding section presented in chapter 2, the membrane curvature is defined by the membrane boundary and prestress. Since prestress tends to be applied uniformly on the membrane to achieve minimal surface (Lewis, 2003), the change in prestress magnitude does not help to change the membrane curvature. Therefore, the common way to change the membrane curvature is to adjust the membrane boundary.

In the subsequent sections, shape effect study is carried out to investigate the influence of the change in the membrane boundary on the magnitude of stress induced in membrane of DSTMS and Butterfly-wing structures. The objective of the shape effect study is to determine the optimum parameters of the membrane boundary which provides effective membrane shapes of these structures. The basis to determine an effective membrane shape is the minimum membrane stresses induced by a predetermined applied load. The rationale of this basis is that smaller membrane stresses will result in lighter structure which is clearly a benefit.

4.6.1. Shape effects on Deployable strut-tensioned membrane structures

DSTMS possess two basic anticlastic shapes of membrane structures which are the saddle form between those modules of Umbrella DSTMS (except the triangular membrane shape along the boundary) and the conic form of Cone-shaped DSTMS as shown in Figs. 4.2 & 4.3. The membrane shapes of DSTMS are dependent on the ratio between the inclination height h and the modular width W which are defined in Figs. 4.2 & 4.3.

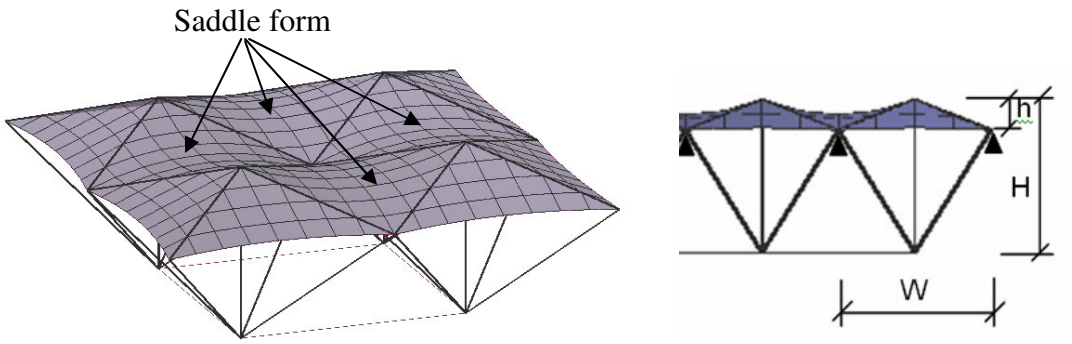

Fig. 4.2. Saddle form of membrane surface between Umbrella DSTMS modules

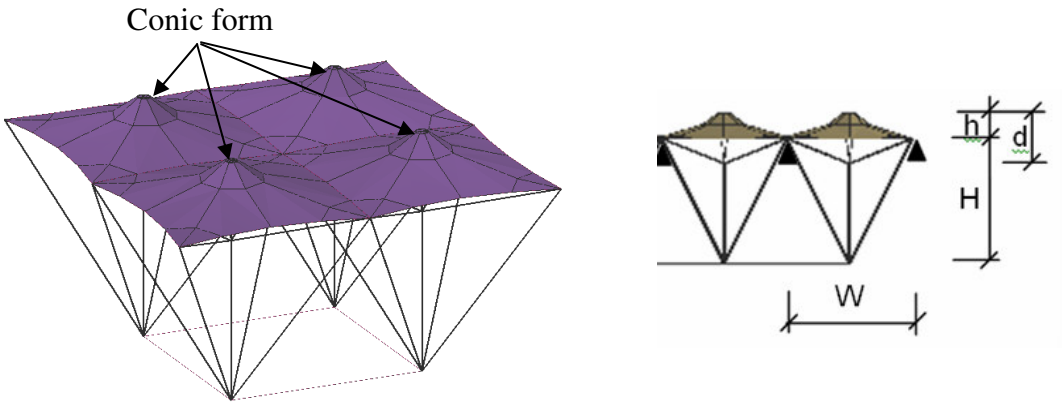

Fig. 4.3. Conic form of Umbrella DSTMS modules

Shape effect studies are carried out to investigate the influence of *h/W* ratio on the membrane stress of both Umbrella and Cone-shaped DSTMS. The objective is to determine the most optimum *h/W* ratio which results in minimum membrane stress. Considering the case in which the two DSTMS (module size 8m x 8m) are subjected to wind uplift pressure of 0.45kN/m^2. It was found that maximum membrane stress occurred at the corners of membrane areas while maximum displacement occurred at the center of membrane areas. Table 4.1 shows the results of maximum membrane stress, maximum membrane displacement and the covering ratio, which is defined as the ratio of membrane area to covering area, of Umbrella and Cone-shaped DSTMS. These results are plotted in Figs. 4.4, 4.5 & 4.6 respectively.

Table 4.1. Maximum membrane stress, maximum membrane displacement and covering ratio of Umbrella and Cone-shaped DSMTS

h/W	Umbrella DSTMS			Cone-shaped DSTMS		
	Max stress (kN/m)	Max displacement (cm)	Covering ratio	Max stress (kN/m)	Max displacement (cm)	Covering ratio
0.1	6.34	27.5	1.013	19.23	51.7	1.013
0.2	5.48	20.7	1.051	5.59	20.2	1.05
0.3	4.43	21.9	1.11	4.5	17.5	1.107
0.4	4.38	23.3	1.187	4.51	15.2	1.179

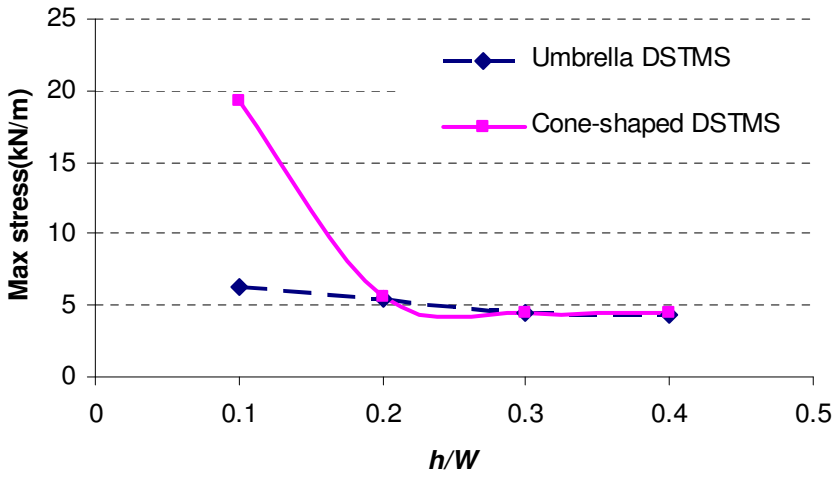

Fig. 4.4. Maximum membrane stress vs. *h/W*

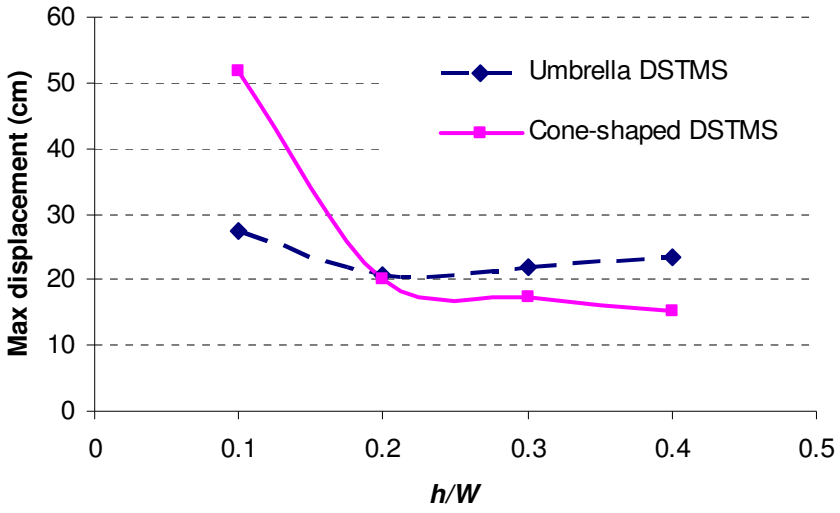

Fig. 4.5 Maximum membrane displacement vs. *h/W* ratio

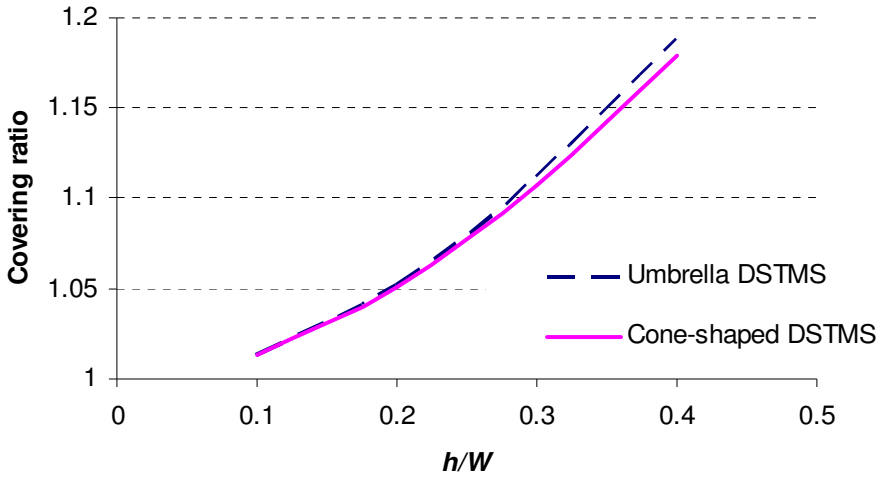

Fig. 4.6. Covering ratio vs. *h/W* ratio

It can be seen from Figs. 4.4 & 4.5 that the maximum membrane stress and maximum membrane displacement decreased when the *h/W* ratio increased. The reason is that the higher *h/W* ratio will provide more curvature for the saddle and the conic shape of DSTMS. The more curvature the smaller the forces that will develop as the result of wind forces. However, when the *h/W* ratio is larger than 0.2, the maximum membrane stress and displacement do not reduce much or start increasing due to significant increase in the membrane area exposed to wind forces. In addition, the higher *h/W* ratio results in the larger membrane area required for covering a given plan area (Fig. 4.6) and thus a higher cost. Therefore, it can be concluded that optimum *h/W* ratio is around 0.2. The *h/W* ratio of 0.2 will be chosen in the parametric studies of DSTMS carried out in chapter 5.

4.6.2. Shape effects on Butterfly-wing structures

The membrane shape of butterfly-wing structures is characterized by the anticlastic surface formed by the boundary inclined arches. There are two major parameters

which control the membrane shape of butterfly-wing structure: the rise/span ratio (*H/L*) and the inclination angle α of the arch. The inclination angle α, the rise *H*, the span *L* and the radius *R* of the arch are illustrated in Fig. 4.7.

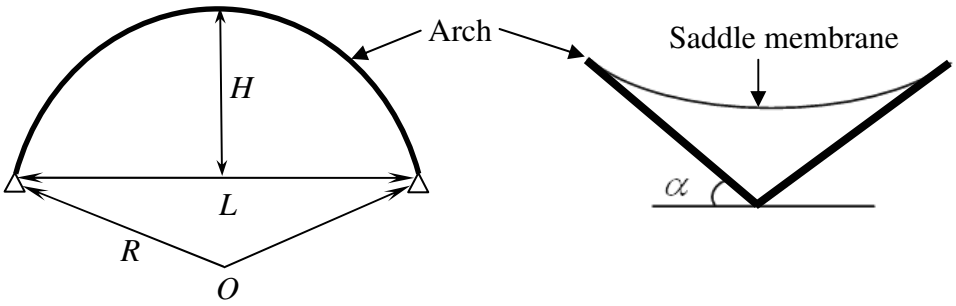

a. Front view b. Elevation view

Fig.4.7. Front view (a) and elevation view (b) of the arch

The relationship between *H*, *L* and *R* can be defined as:

$$R = \frac{4H^2 + L^2}{8H} \tag{4.18}$$

Shape effect studies are carried out to investigate the influence of surface curvature on membrane stress of the two-wing and three-wing butterfly structures of 15m span. The objective is to determine the most optimum rise/span ratio (*H/L*) and inclination angle α of the arch which result in minimum membrane stress induced by a predetermined applied load. Both structures are subjected to a uniform distributed wind uplift of 0.45kN/m^2 and wind downward of 0.1kN/m^2. It is assumed that supporting arches are rigid and prestress in membrane is set at level of 1.5kN/m in both warp and weft directions. The results of maximum membrane stresses of two-wing and three-wing butterfly structures with varying rise/span ratio (*H/L*) and inclination angle (α) are shown in tables 4.2, 4.3 and 4.4. These results are plotted in Figs. 4.8, 4.9 & 4.10 respectively.

Table 4.2. Maximum membrane stress when $H/L = 0.25$

α	H/L	Maximum membrane stress (kN/m)	
		Two-wing butterfly structure	Three-wing butterfly structure
30°	0.25	29.51	55.30
45°	0.25	20.54	41.02
60°	0.25	19.26	40.31

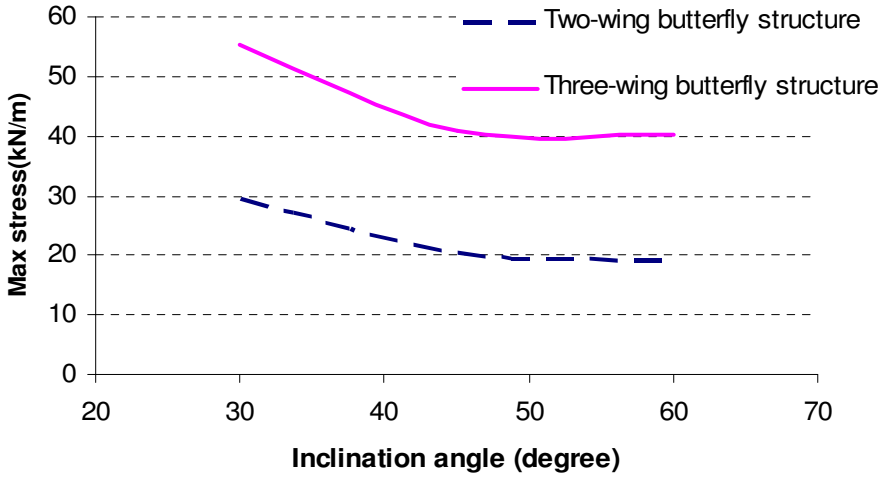

Fig. 4.8. Maximum membrane stress vs. α when $H/L = 0.25$

Table 4.3. Maximum membrane stress when $H/L = 0.375$

α	H/L	Maximum membrane stress (kN/m)	
		Two-wing butterfly structure	Three-wing butterfly structure
30°	0.375	19.88	31.12
45°	0.375	17.34	26.99
60°	0.375	16.16	27.65

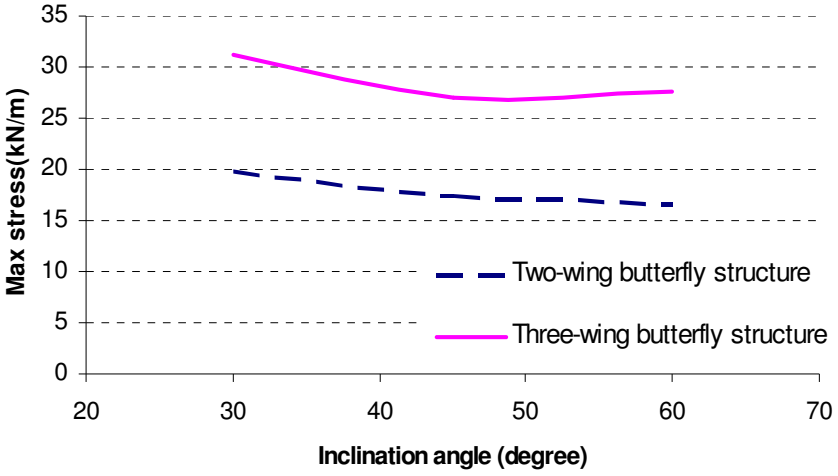

Fig. 4.9. Maximum membrane stress vs. α when $H/L = 0.375$

Table 4.4. Maximum membrane stress when $H/L = 0.5$

α	H/L	Maximum membrane stress (kN/m)	
		Two-wing butterfly structure	Three-wing butterfly structure
30°	0.5	19.02	29.62
45°	0.5	16.63	26.53
60°	0.5	16.36	27.02

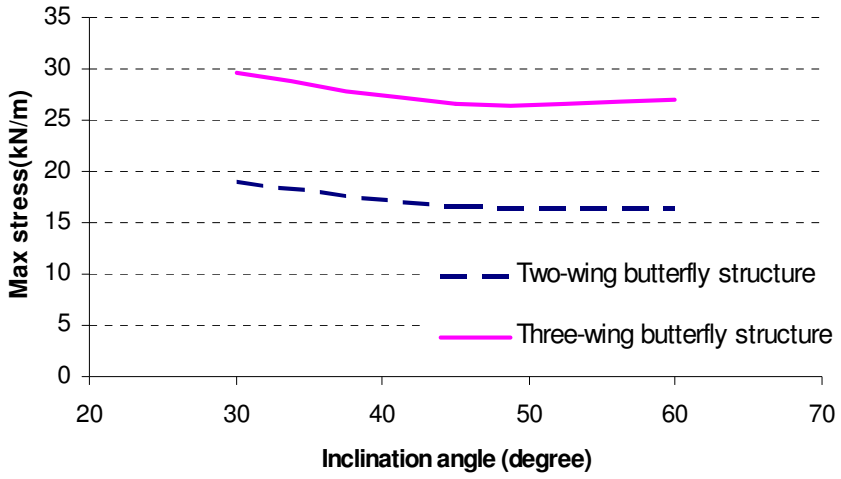

Fig. 4.10. Maximum membrane stress vs. α when $H/L = 0.5$

It can be observed that maximum membrane stress decreased when the inclination angle or the rise/span ratio increased. The reason is that the increase in inclination angle or rise/span ratio will provide larger altitude difference between higher and lower points of the saddle membrane, resulting in more curvature for membrane surface. The more curvature the smaller the forces that will develop as the result of applied loads. However, when the inclination angle is too large, the angle between two inclined arches become too small, causing difficulties in tensioning membrane in the convex curvature. In addition, since maximum membrane stress is located at lower point of the saddle membrane, the smaller angle between two inclined arch results in higher concentrated membrane stress at this location. Thus maximum membrane stress did not change much or started increasing when inclination angles increased from 45°

to 60° though the overall membrane stress decreased. Hence, optimal inclination angle α is in range of 45° to 60°. Similarly, the maximum membrane stress decreased with the increase of rise/span ratio due to the larger curvature. The membrane stress decrease is not significant when rise/span ratio is larger than 0.375. Generally, rise/span ratios of 0.375 to 0.5 will ensure both effective curvature membrane surface as well as the clear height of the structures. Rise/span ratio larger than 0.5 is not considered in the study because the arch is beyond semi-circular shape.

4.7. Summary

The objective of this chapter was to provide the background information of the numerical modelling of the two newly proposed deployable membrane structures. An advanced analysis method which was integrated from the force density method and geometrical nonlinear analysis was proposed to be used for form-finding and structural analysis of these structures. This chapter summarized the basic numerical procedure of the method and explained how it was able to capture the highly nonlinear response of these structures to prestressing forces and applied loads.

Apart from that, shape effect studies were carried out to investigate the influence of membrane curvature on the membrane stress and thereby determining the optimum parameters which provide effective membrane shapes of DSTMS and Butterfly-wing structures. It was found that the optimum inclination height/modular width of DSTMS was about 0.2 while the optimum rise/span ratio and optimum inclination angle of the arch of Butterfly-wing structures were 0.375 to 0.5 and 45º to 60º respectively.

CHAPTER 5

PARAMETRIC STUDIES AND OPTIMUM DESIGN PARAMETERS

5.1. Introduction

In chapter 3, the concept and morphology of DSTMS and Butterfly-wing structures were proposed and explained. An integrated approach for form-finding and structural analysis of the structures was presented in chapter 4. Also in chapter 4, the optimum membrane boundary parameters of the structures were determined through the shape effect studies. This chapter presents a series of parametric studies on both DSTMS and Butterfly-wing structures with the view to determine their optimum design parameters. The integrated approach and optimum membrane boundary parameters presented in chapter 4 will be employed for the parametric studies. The results of these studies serve as the design guidelines for practical applications of DSTMS and Butterfly-wing structures.

5.1.1. Basis of comparison

The common way to measure the efficiency of a structure is to study its weight to strength ratio. In this chapter, the minimum weight of structural elements that is designed to resist predetermined load combinations is used as a basis for comparison. The optimum design parameters of DSTMS and Butterfly-wing structures are determined based on the lightest weight among different configurations.

5.1.2. Design algorithm

As optimization of deployable membrane structures is not the main objective of this thesis, a simplified algorithm is adopted to obtain a rational design weight of the studied structures. The structural redundancy is conservatively assumed as low and thus ultimate collapse load of the structures is assumed to be close to the load causing first member failure. The design procedure is carried out as follows:

1. The structure is modelled with one section for each type of struts, one for cables and one for membrane.
2. Form-finding is performed using the force density method to find the initial equilibrium shape of structure.
3. Geometrical nonlinear analysis is performed with predetermined load combinations.
4. Member capacities are checked against their ultimate limit state. Membrane stress is checked to ensure that the membrane is not under compression or exceeding its allowable stress. Maximum deflection of the supporting structure is checked against serviceability requirement (L/200) specified in BS 5950: Part 1 (2000)
5. The members are resized and the design procedure is repeated from step 2. Member resizing is toward the sections of lightest weight satisfying both ultimate limit state of members and serviceability limit state of structures.

5.1.3. Design parameters

As the design of DSTMS and Butterfly-wing structures aims at large and medium applications (span up to 50m), DSTMS of 48m span (flat roof) and Butterfly-wing structures of 30m arch-span (using deployable cable-strut arch) are chosen as the case

studies. For a given particular span and structural configuration, there are two main factors influencing the efficiency of these structures to resist load. They are the span to depth ratio and the number of modules. For a flat DSTMS, the span to depth ratio is the ratio of structural span to modular depth while the number of modules is actually the ratio of structural span to modular width. In Butterfly-wing structures, the span to depth ratio is the ratio of arch-span to modular depth while the number of modules refers to the number of modules of an arch.

5.2. Parameter investigation of Deployable strut-tensioned membrane structures

Before the parametric studies can proceed, the following design parameters have to be determined:

- Structural configuration
- Support condition
- Structural elements and materials properties
- Prestressing and loading

5.2.1. Structural configurations

To study the relative merit of different DSTMS, the weight efficiency of different structural configurations of Umbrella DSTMS and Cone-shaped DSTMS will be studied. Both structures are in the form of flat square roof with span of 48m x 48m in two dimensions. The configurations of 48m x 48m square grid Umbrella and Cone-shaped DSTMS after form-finding are as shown in Figs. 5.1 & 5.2.

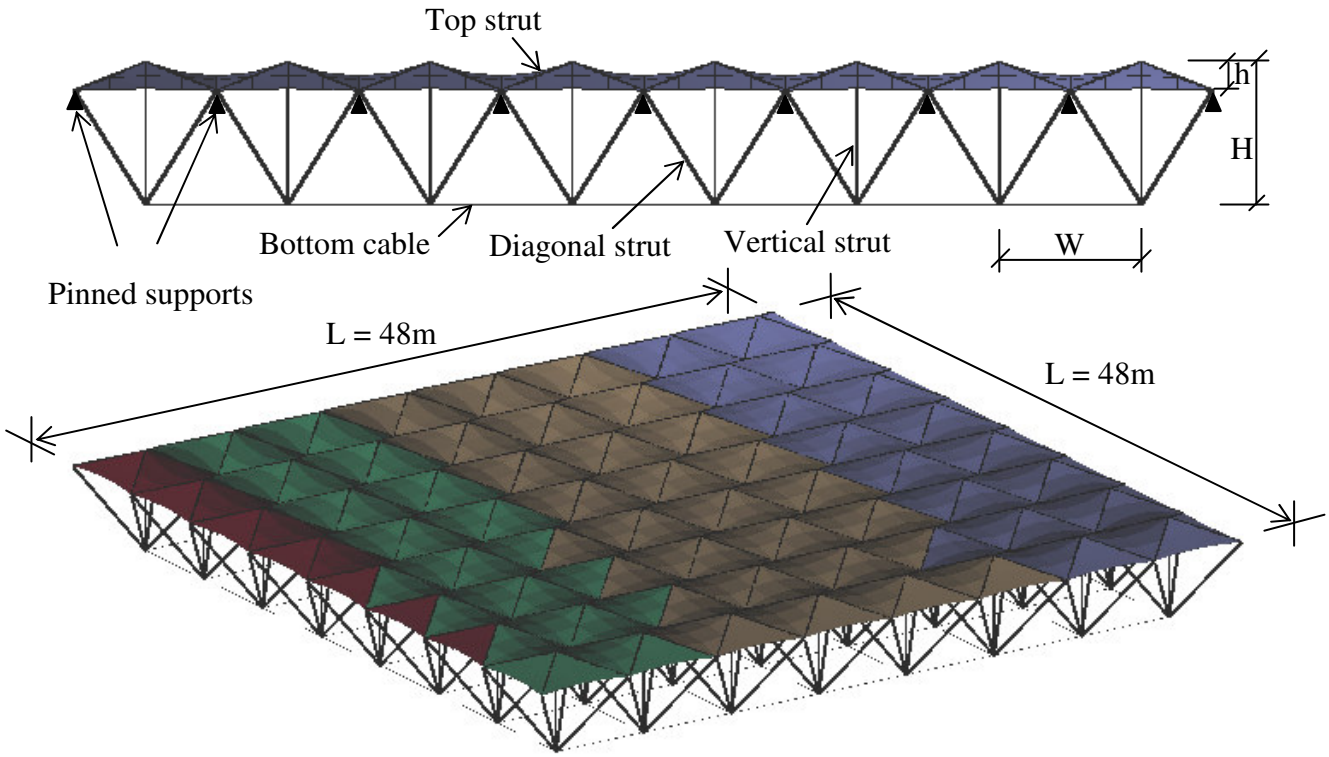

Fig. 5.1. Configuration of UmbrellaDSMTS, span of 48m x 48m

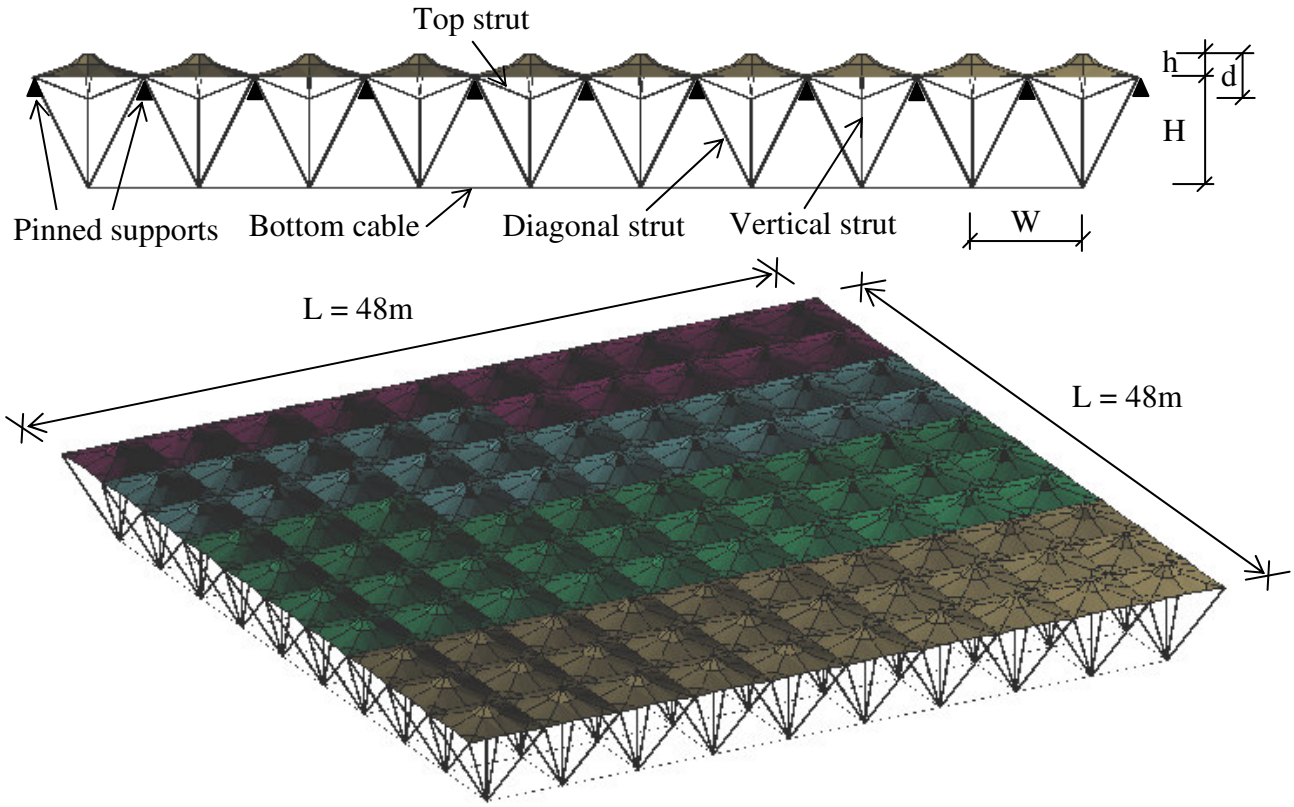

Fig. 5.2. Configuration of Cone-shaped DSMTS, span of 48m x 48m

Based on the shape effect studies in chapter 4, the ratio of inclination height to modular width (*h/W*) of DSTMS is chosen as 0.2 which results in the smallest membrane stress. The inclination height *h*, the depth *H*, the span *L*, the modular width *W* are illustrated in Figs. 5.1 & 5.2.

5.2.2. Support condition

Depending on the application, different support configurations may be provided for space structures. For a flat roof, common support conditions are all surround simple support (factories or other enclosed space), point supports (open-air amphitheatre) and three edge simple support with one edge free (aircraft hangar). For this study, pin supported around the boundary nodes of the roof will be provided.

5.2.3. Structural elements and material properties

There are three main classes of structural elements in DSTMS. They are the strut element, the cable element and the membrane element.

For the strut element, steel circular hollow section with yield strength of 275 MPa and modulus of elasticity of 210000 MPa is used (BS 5950, Part 1, 2000). The main advantage of circular hollow section is that it has a higher compression resistance compared with other sections of the same area since it does not have a weaker axis. Hence, the weight efficiency of the element is improved.

For cable elements, 7-wire high strand tendon with breaking stress of 1089 N/mm^2 and modulus of elasticity of 145000 N/mm^2 is used (AISI, 1973).

For membrane element, there are two commonly used membrane fabrics: PVC coated polyester fabric and PTFE coated fiberglass fabric. PVC coated polyester fabric has relatively high strength and great flexibility. The fabric is soft and easily handled at the expense of large elongation under load. It is the most cost-effective fabric with design life of 15-20 years (Seaman and Venkataraman, 1976). PTFE coated fiberglass fabric has a superior strength (1.5 - 2 times higher than PVC fabric) and a long lifetime of 25-30 years (Sheaffer, 1995). Its high modulus of elasticity makes it stiff with small elongation under load but also makes it brittle. Therefore, PTFE fabric is susceptible to damage if subjected to folding. Since folding is required for deployable membrane structures, PVC coated polyester fabric is used for this study due to its high flexibility. The fabric has a breaking tensile strength of 84000N/m and modulus of elasticity of 420000 N/m in both warp and weft directions (Fibertech Co.).

5.2.4. Prestress level

Prestress forces are introduced to the membrane fabric to stabilize it, pull out wrinkles, and prevent the fabric from slackening when loaded. Prestress level in the membrane should not be lower than the minimum requirement while ensuring that the stresses induced in membrane by applied loads should not exceed allowable stress which is 1/4 to 1/8 of breaking strength. Commonly, membrane prestress ranges from 10-20% of allowable stress. In this study, prestress level of 2 kN/m is applied in both warp and weft directions of the fabric.

5.2.5. Loading conditions

In this study, two major load combinations are used for designing DSTMS. The first load combination includes gravity loadings which are the self-weight of the structure and an imposed live load of 0.75kN/m^2. The load is distributed at the bottom nodes of the structures. The factored gravity load combination is (1.4 x self-weight of structure + 1.6 x imposed load) in accordance with BS 5950, Part 1 (2000).

The second load combination includes wind uplift loading. Wind is often the predominant loading on membrane fabric roof. A typical wind speed of Singapore of 35m/s (Arup, 2003) which is equivalent with a design wind suction load of 0.45kN/m^2 (Foster and Mollaert, 2004) is adopted. The wind uplift force is applied uniformly on the membrane. The factored uplift load combination is (1.0 x self-weight of structure + 1.4 x wind uplift load) in accordance with BS5950, Part 1 (2000).

5.2.6. Parametric studies

The main purposes of the present studies are to investigate the effect of span-depth ratio and span-modular width ratio on the design weight of Umbrella DSTMS and Cone-shaped DSTMS to obtain the most efficiency configuration for each structural system. To achieve this, the weight efficiency for each of the DSTMS studied will be obtained for each of the following parameters:

- Span/depth ratio (*L/H*): 6, 8, 10, 12
- Number of modules or number of modules (*L/W*): 6, 8, 10

The integrated approach of the force density method and geometrical nonlinear analysis is used to find the equilibrium form and to structurally analyze the studied DSTMS. The details of numerical modelling can be referred to chapter 4 of this thesis and will not be presented here.

Under the prescribed load combinations, the global internal force induced in DSTMS is in the form of a combination of moment and shear force. The global internal moment is mainly resisted by the chord constituted of top struts (top chord) and bottom cables (bottom chord). The global internal shear force is transferred by the web made up of diagonal struts and vertical struts. Such arrangement is similar to that of space truss where top chord and bottom chord are spaced at a distance defined by the web. Therefore the large moment arm of the chords of DSTMS reduces significantly the bending stress induced within the system. On the other hand, tensioned membrane on top is acting as the bracing elements improving buckling resistance of top struts.

The weight of DSTMS is contributed mainly from the weight of the chord and the web since the membrane weight is negligible. The effect of span/depth ratio and number of modules on the design weight of DSTMS is a combination of changes in the design weight of the chord and the web. The optimum design parameters will be determined based on the optimum design weight of the structures.

5.2.6.1. Parametric studies of the web

The web consists of the diagonal strut and the vertical strut. Therefore the effect of the span/depth ratio and the number of modules on the web is the combination effect of the two components.

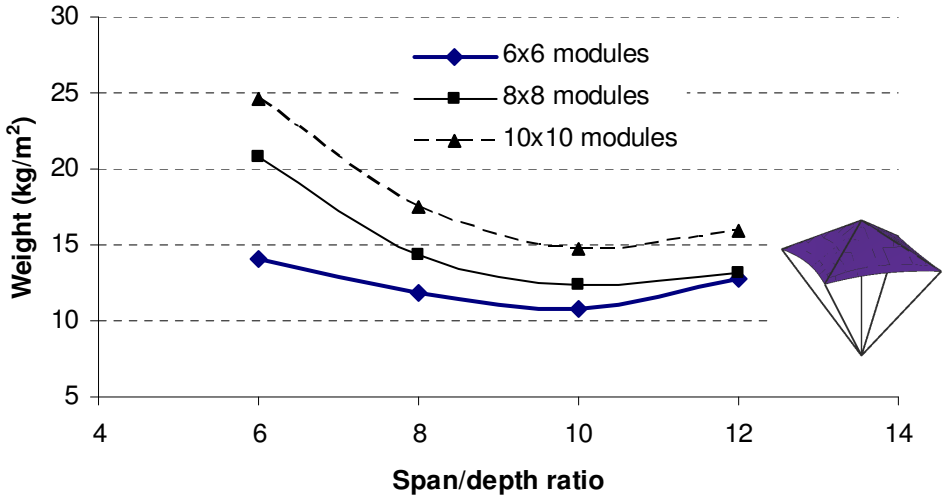

Fig. 5.3. Weight (kg/m^2) of diagonal strut vs. span/depth ratio for different span/modular width of Umbrella DSTMS

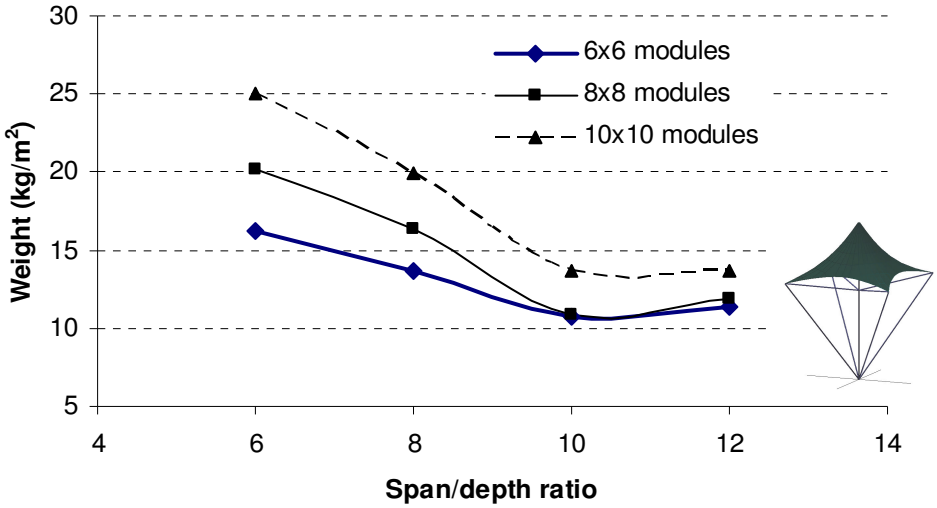

Fig. 5.4. Weight (kg/m^2) of diagonal strut vs. span/depth ratio for different span/modular width of Cone-shaped DSTMS

a. Weight of diagonal struts

Figures 5.3 and 5.4 show the weight of the diagonal struts for different span/depth and number of modules of Umbrella and Cone-shaped DSTMS.

As observed, the weight of the diagonal struts increased with the increase in the number of modules. This can be attributed to the increase in number of the diagonal

struts. Although the weight of each diagonal strut may decrease due to the reduction of member length and internal force, the total weight appears to increase since the increase in number of the diagonal struts is the dominant effect. It is worth noting that an increase in number of modules results in square increase in number of the diagonal struts. It can be deduced from the results that the total weight of the diagonal struts is smallest at number of modules of 6.

The other factor that affects the design weight of diagonal struts is the span/depth ratio. As seen in Figs. 5.3 and 5.4, the weight of the diagonal struts decreased when the span/depth ratio increased from 6 to 10 while it increased when span/depth ratio increased from 10 to 12. One possible explanation is that the increase in span/depth ratio may result in two opposite effects on the weight of the diagonal struts. One is the decrease of member length which probably results in the enhancement of buckling strength and thus the decrease of member weight. The other is the increase in the internal member force which may require a larger section size and thus a higher weight of the diagonal strut. For span/depth ratio from 6 to 10, the diagonal struts are considerably long so that their design weight is dominated by the buckling strength. Hence the decrease of diagonal struts' weight in this range of span/depth ratio can be adequately explained by the significant enhancement of the buckling strength due to the shortening of the member length. For span/depth ratio larger than 10, member length of the diagonal struts is relatively short, thus the gain in strength due to the decrease of member length is not significant. Hence the increase of diagonal struts' weight in this range of span/depth ratio can be accounted for by the increase of the internal member force. In general, it can be deduced from the results that the weight of the diagonal struts is smallest at the span/depth ratio of 10.

b. Weight of the vertical struts

Apart from the diagonal strut, the vertical strut is another component contributing to the total weight of the web. Figures 5.5 and 5.6 show the weight of the vertical struts for different span/depth and number of modules.

It can be seen that the weight of the vertical struts increased with the increase in the number of modules. This effect resembles that on the diagonal struts. It is possible to speculate that, when span/depth ratio increases, the grid density and thus the number of member increases while the internal member force decreases. The increase of the grid density may account for the weight increase of the vertical struts. In addition, at low grid density, the large internal force probably requires large member size, thus resulting in high buckling strength. At high grid density, the opposite is expected. The lower buckling strength of members in the denser grid may account for the higher weight of the vertical strut than that in the coarser grid. It can be deduced from the results that the weight of vertical strut is lowest at number of modules of 6.

The effect of the span/depth ratio on the weight of the vertical struts seems opposed to that of the number of modules. As seen in Figs. 5.5 & 5.6, the weight of the vertical struts decreased with the increase of the span/depth ratio. This effect can be attributed to the length decrease of the vertical struts when the span/depth ratio increases. Since the internal force induced in members remains unchanged, the length decrease may enhance the buckling resistance of the vertical struts. Therefore the required member size and thus the design weight may be smaller. Figures 5.5 and 5.6 also show that the effect of the span/depth ratio on the weight of the vertical struts was significantly pronounced when it is smaller than 8. This can be accounted for by the significant

reduction of member length at low span/depth ratio. The result suggests that the weight of the vertical struts is optimum when the span/depth ratio is larger than 8.

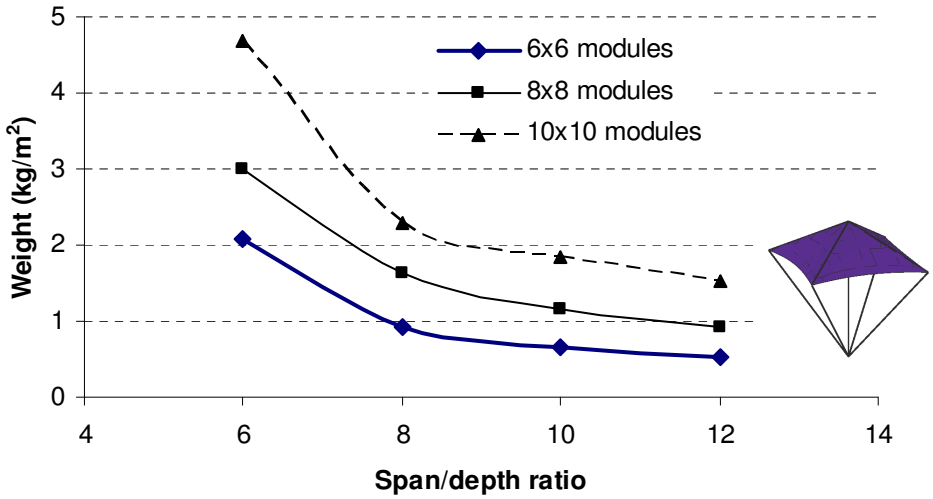

Fig. 5.5. Weight (kg/m^2) of vertical strut vs. span/depth ratio for different span/modular width of Umbrella DSTMS

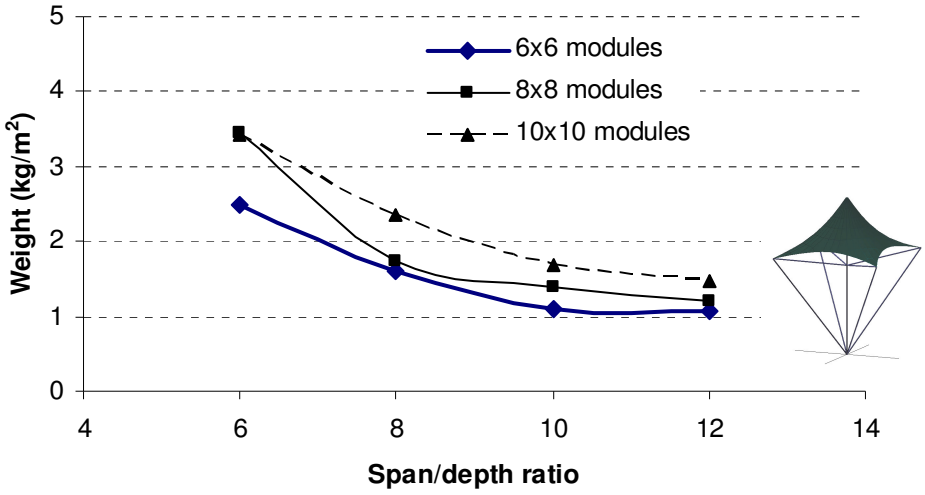

Fig. 5.6. Weight (kg/m^2) of vertical strut vs. span/depth ratio for different span/modular width of Cone-shaped DSTMS

c. Weight of the web

As mentioned earlier, the weight of the web is contributed from the weight of diagonal struts and vertical struts. Figures 5.7 & 5.8 show that the weight of the web increased with the increase in number of modules. The reason is that the weight of both diagonal struts and vertical struts increases with the increase in number of modules, therefore the weight of the web should have the same effect. From the results it can be deduced that the optimum weight of the web is at number of modules of 6.

Unlike the number of modules, the span/depth ratio has different effect on the weight of the web. At span/depth ratio lower than 10, the weight of the web decreased with the increase of span/depth ratio as seen in Figs. 5.7 & 5.8. This can be explained by the decrease of the weight of both diagonal struts and vertical struts in this range of span/depth ratio. However, the weight of the web started increasing when span/depth ratio increased larger than 10. This can be attributed to the increase of diagonal struts' weight with span/depth ratio larger than 10. Although weight of vertical struts still decreased, the weight of the web decreased because the weight contribution of diagonal struts dominated the weight of the web. It can be seen in Table 5.1 that the weight of vertical struts was less than 20% weight of diagonal struts. From the results it can be deduced that the weight of the web is optimum at span/depth ratio of 10.

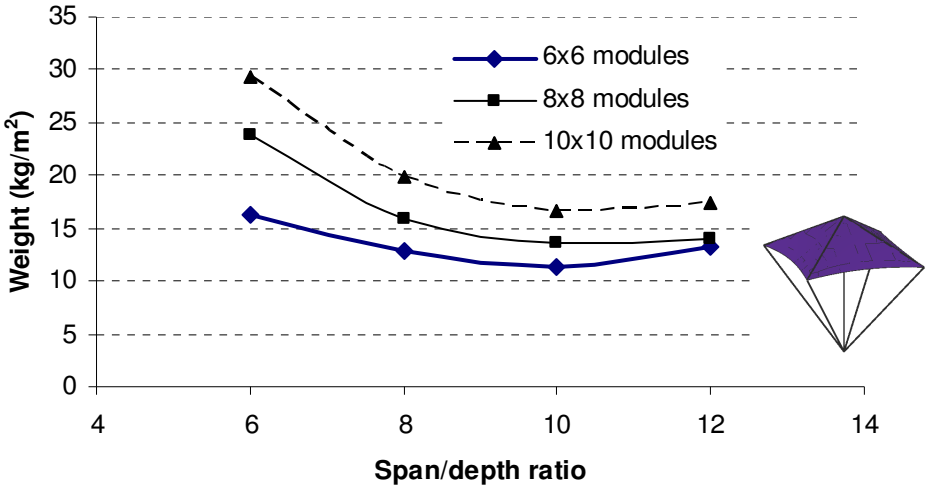

Fig. 5.7. Weight (kg/m^2) of web components vs. span/depth ratio for different span/modular width of Umbrella DSTMS

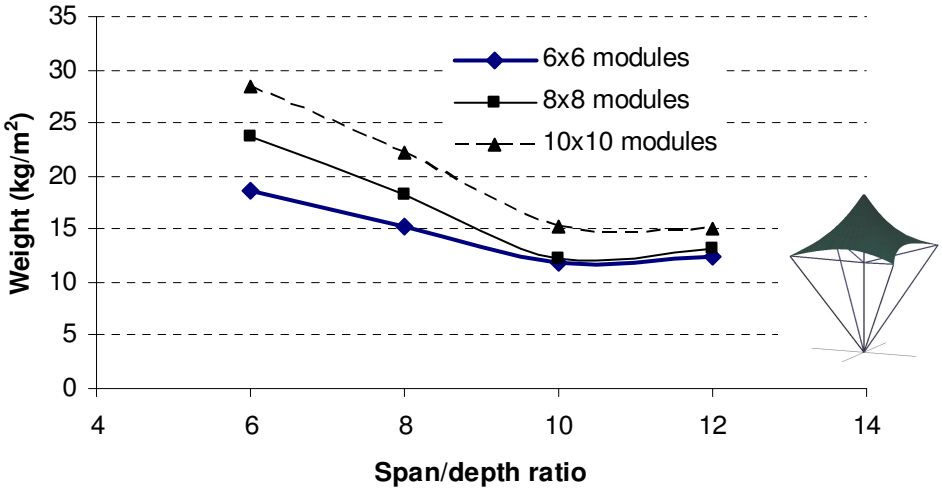

Fig. 5.8. Weight (kg/m^2) of web components vs. span/depth ratio for different span/modular width of Cone-shaped DSTMS

5.2.6.2. Parametric studies of the chord

The chord consists of the top struts and the bottom cables. Therefore, the effect of the change in design parameters on the chord is contributed by a combination of these two components.

a. Weight of top struts

Figures 5.9 and 5.10 show the weight of the top struts for different span/depth and number of modules.

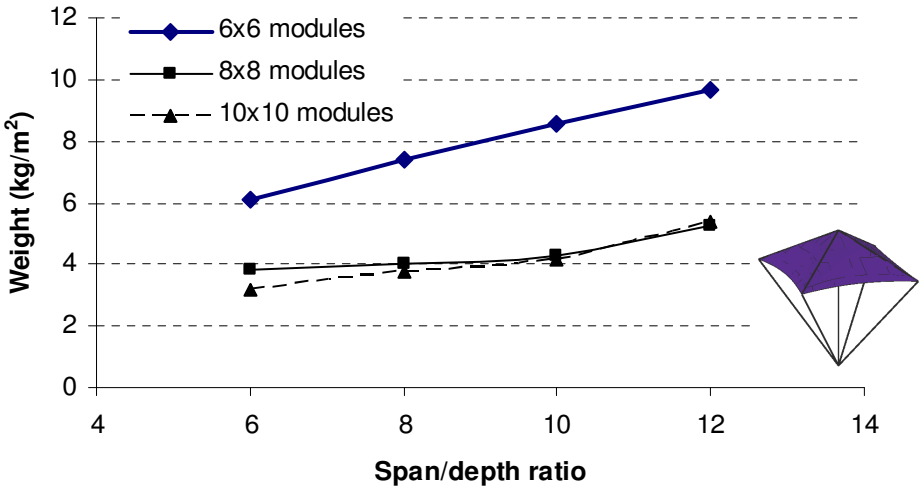

Fig. 5.9. Weight (kg/m^2) of top strut vs. span/depth ratio for different span/modular width of Umbrella DSTMS

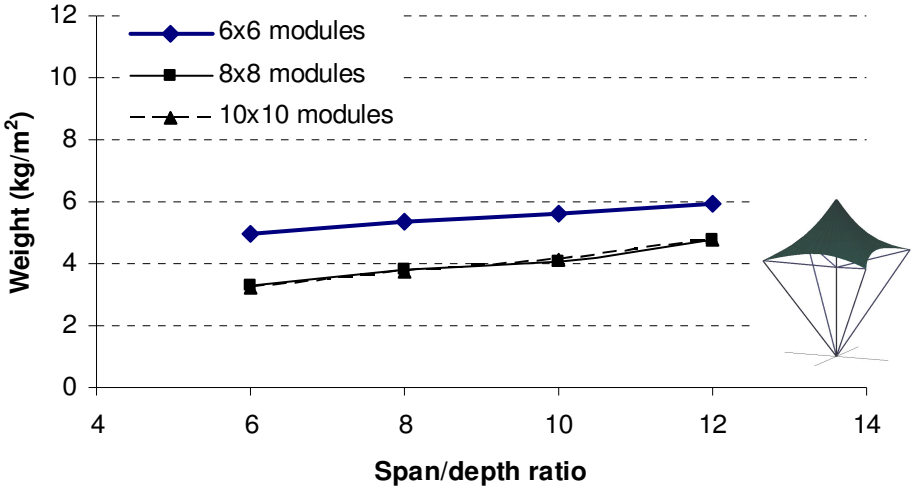

Fig. 5.10. Weight (kg/m^2) of top strut vs. span/depth ratio for different span/modular width of Cone-shaped DSTMS

It can be seen that the weight of top struts increased with the increase of span/depth ratio. This is because of the increase of internal force induced in top struts when the span/depth ratio increased. Since the length of the top struts was unchanged, the

increase of internal force results in larger member size and thus higher weight of top struts. Hence, the minimum weight of top struts is at span/depth ratio of 6.

The other factor affecting the weight of top struts is the number of modules. It can be seen from Figs. 5.9 & 5.10 that the weight of top struts decreased significantly when number of modules increased from 6 to 8 while it was almost unchanged when number of modules increased from 8 to 10. One possible explanation is that the increase in number of modules may result in two opposite effects on the weight of the top struts. One is the increase of grid density increases which results in weight increase and another is the decrease of member length which results in the enhancement of buckling strength and thus the weight decrease. When number of modules increases from 6 to 8, the length of top struts is reduced significantly. The strength gained by the enhancement of buckling strength is the dominant effect, leading to the decrease of top struts' weight. When number of modules increases larger than 8, member length of the top struts is relatively short, thus the gain in strength due to the decrease of member length become less significant. Hence the weight decrease due to member length decrease and the weight increase due to grid density increase are almost equal. Therefore, the increase in number of modules from 8 to 10 has little effect on the weight of top struts. It can be deduced that optimum weight of top struts is at number of modules of 8.

b. Weight of bottom cables

Figs. 5.11 & 5.12 show the weight of bottom cables for different span/depth and number of modules. It is observed that the span/depth and the number of modules had the same effect on the weight of bottom cables

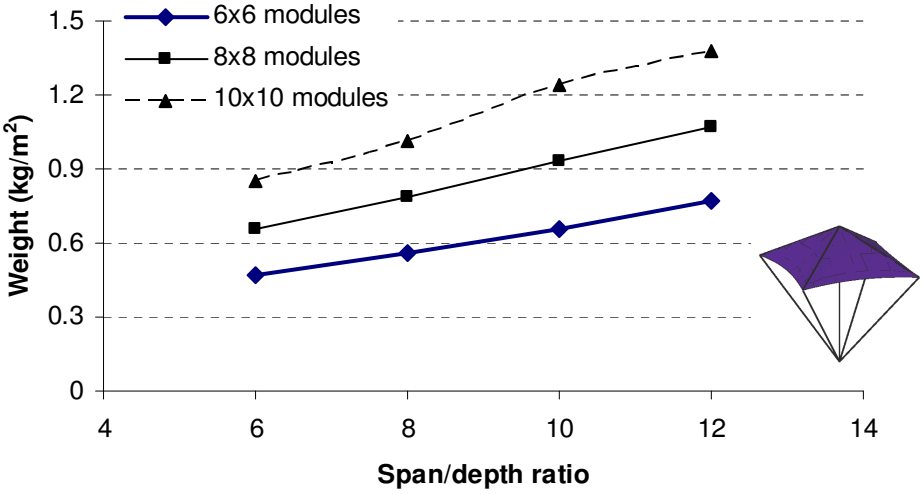

Fig. 5.11. Weight (kg/m^2) of bottom cable vs. span/depth ratio for different span/modular width of Umbrella DSTMS

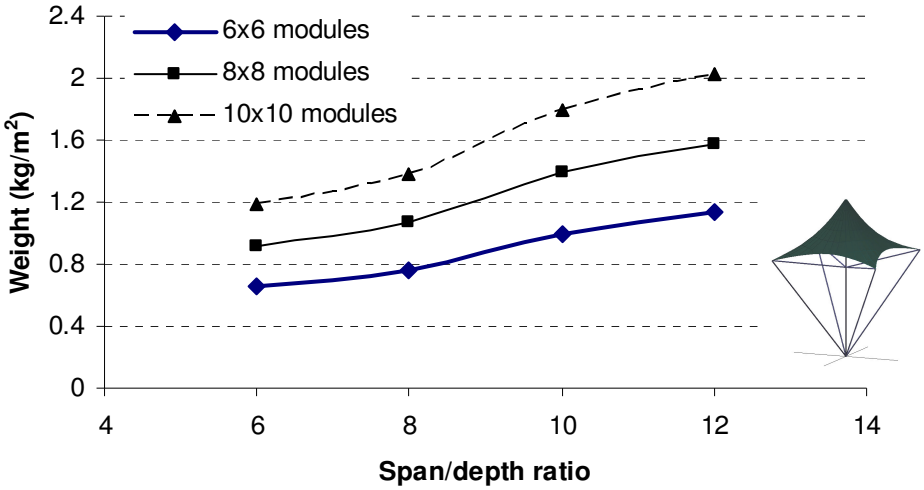

Fig. 5.12. Weight (kg/m^2) of bottom cable vs. span/depth ratio for different span/modular width of Cone-shaped DSTMS

When number of modules increased, the weight of bottom cables increased. This can be attributed to the increase in number of bottom cables. Though the member length is reduced, it does not help to improve the strength of cables since they are under tension. Therefore it can be deduced that the weight of bottom cables is lowest at number of modules of 6.

Similarly, when span/depth ratio increased, the weight of bottom cables increased. This can be explained by the decrease of the structural depth of the structure which results in the increase of internal force induced in bottom cables. Therefore it may require larger member size and thus higher weight of bottom cables. From the results, it can be deduced that the minimum weight of bottom cables is at span/depth ratio of 6.

c. Weight of the chord

The effects of span/depth ratio and number of modules on weight of chord components are as shown in Figs. 5.13 & 5.14.

It is observed that the weight of the chord increased with the increase of span/depth ratio. This is because the increase of span/depth ratio increases the weight of both top struts and bottom cables, thus it should have the same effect on the weight of chord components. The weight of the chord therefore is optimum at span/depth ratio of 6.

However, the effect of number of modules on the weight of the chord is different from that of span/depth ratio. The weight of the chord decreased when number of modules increased from 6 to 8 and increased when span/depth ratio increased from 8 to 10. This may be due to the opposite effect of number of modules on the weight of top struts and bottom cables. At number of modules lesser than 8, the weight of the chord is dominated by the top struts as the weight of bottom cables to top struts is small (less than 20%). Hence, similar to the top struts, the weight of chord components decreases with the increase in number of modules. At number of modules higher than 8, the weight of bottom cables increases and contributes significantly to weight of the chord while the weight top struts is almost unchanged with the increase of span/modular

width. Hence the weight of the chord does not decrease but start increasing when span/depth ratio increases higher than 8. It can be deduced from the results that the weight of the chord is optimum at number of modules of 8.

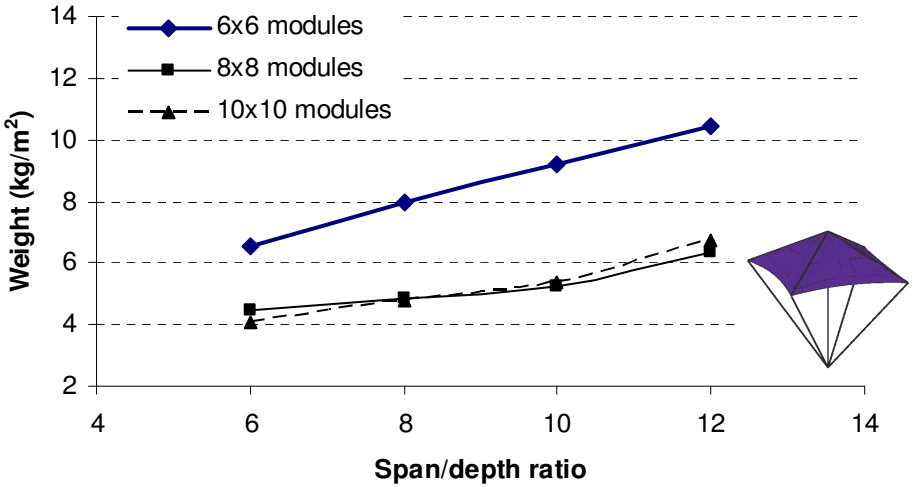

Fig. 5.13. Weight (kg/m^2) of chord component vs. span/depth ratio for different span/modular width of Umbrella DSTMS

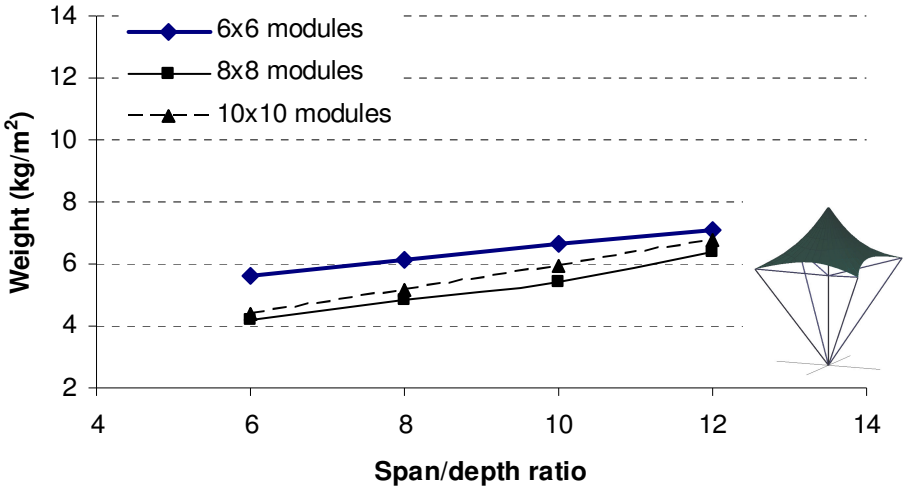

Fig. 5.14. Weight (kg/m^2) of chord component vs. span/depth ratio for different span/modular width of Cone-shaped DSTMS

5.2.6.3. Optimum design parameters

The main purpose of the present parametric studies is to determine the optimum span/depth ratio and number of modules for minimum design weight of DSTMS. The optimum span/depth ratio and number of modules are influenced by their effect on the weight of the web and the chord.

From the discussions in sections 5.2.6.1 and 5.2.6.2, it is seen that the change in span/depth ratio and number of modules have different effects on weight of the web and the chord. Therefore, the effects of span/depth ratio and number of modules on the design weight of DSTMS depend on the weight contribution of web and chord components.

Table 5.1. Weight of different components of Umbrella DSTMS for different span/depth ratio and number of modules

Span/ Modular width	Span/ Depth	Weight of Web Components (kg/m^2)		Weight of Chord Components (kg/m^2)		VS/ DS	BC/ TS	Chord/ Web	Total Weight (kg/m^2)
		DS	VS	TS	BC				
6	6	14.12	2.09	6.10	0.47	0.15	0.08	0.41	22.78
	8	11.85	0.93	7.39	0.56	0.08	0.08	0.62	20.73
	10	10.74	0.66	8.57	0.66	0.06	0.08	0.81	20.63
	12	12.71	0.52	9.69	0.77	0.04	0.08	0.79	23.69
8	6	20.75	3.01	3.80	0.66	0.15	0.17	0.19	28.22
	8	14.30	1.64	4.04	0.79	0.11	0.20	0.30	20.77
	10	12.43	1.16	4.29	0.93	0.09	0.22	0.38	18.81
	12	13.16	0.97	5.26	1.07	0.07	0.20	0.45	20.46
10	6	24.67	4.69	3.21	0.85	0.19	0.26	0.14	33.42
	8	17.51	2.28	3.77	1.01	0.13	0.27	0.24	24.57
	10	14.77	1.83	4.14	1.24	0.12	0.30	0.32	21.98
	12	15.89	1.52	5.37	1.38	0.10	0.26	0.39	24.16

Tables 5.1 & 5.2 show that the weight of chord to web ratio increased with the increase of span/depth ratio and decreased with the increase in number of modules. This is

because at higher span/depth ratio, the internal force induced in chord components due to bending moment increases, resulting in higher weight of chord components, while the weight of web components decrease due to the significant reduction of buckling length. On the other hand, at higher number of modules, the buckling length of top struts is reduced remarkably, resulting in lower weight of chord components, whereas the weight of web components increases at higher grid density due to the increase in number of members.

Table 5.2. Weight of different components of Cone-shaped DSTMS for different span/depth ratio and number of modules

Span/ Modular width	Span/ Depth	Weight of Web Components (kg/m^2)		Weight of Chord Components (kg/m^2)		VS/ DS	BC/ TS	Chord/ Web	Total Weight (kg/m^2)
		DS	VS	TS	BC				
6	6	16.17	2.48	4.96	0.66	0.15	0.13	0.30	24.27
	8	13.61	1.60	5.38	0.76	0.12	0.14	0.40	21.35
	10	10.80	1.09	5.62	1.00	0.10	0.18	0.56	18.51
	12	11.43	1.06	5.96	1.13	0.09	0.19	0.57	19.58
8	6	20.22	3.45	3.30	0.92	0.17	0.28	0.18	27.89
	8	16.41	1.75	3.80	1.07	0.11	0.28	0.27	23.03
	10	10.88	1.38	4.05	1.40	0.13	0.35	0.44	17.71
	12	11.91	1.19	4.78	1.58	0.10	0.33	0.49	19.46
10	6	25.04	3.41	3.21	1.19	0.14	0.37	0.15	32.85
	8	19.87	2.35	3.77	1.38	0.12	0.37	0.23	27.37
	10	13.61	1.69	4.14	1.80	0.12	0.43	0.39	21.24
	12	13.66	1.46	4.76	2.03	0.11	0.43	0.45	21.91

The curvatures of total weight of DSTMS versus span/depth ratio for different number of modules are illustrated in Figs. 5.15 & 5.16. For lower span/depth ratio (below 8-10), the weight contribution of web components is dominant. Thus the total weight is seen to decrease with the increase of span/depth ratio or with the decrease of number of modules. For higher span/depth ratio (above 10-12), the weight contribution of web components decreases while that of chord components increases. Therefore, the total weight is seen to increase with the increase of span/depth ratio. However, the number

of modules has significant effect on chord components when it is smaller than 8 while having little effect when it is higher than 8. Hence, total weight is seen to increase with number of modules smaller than 8 while it decreases when number of modules is higher than 8.

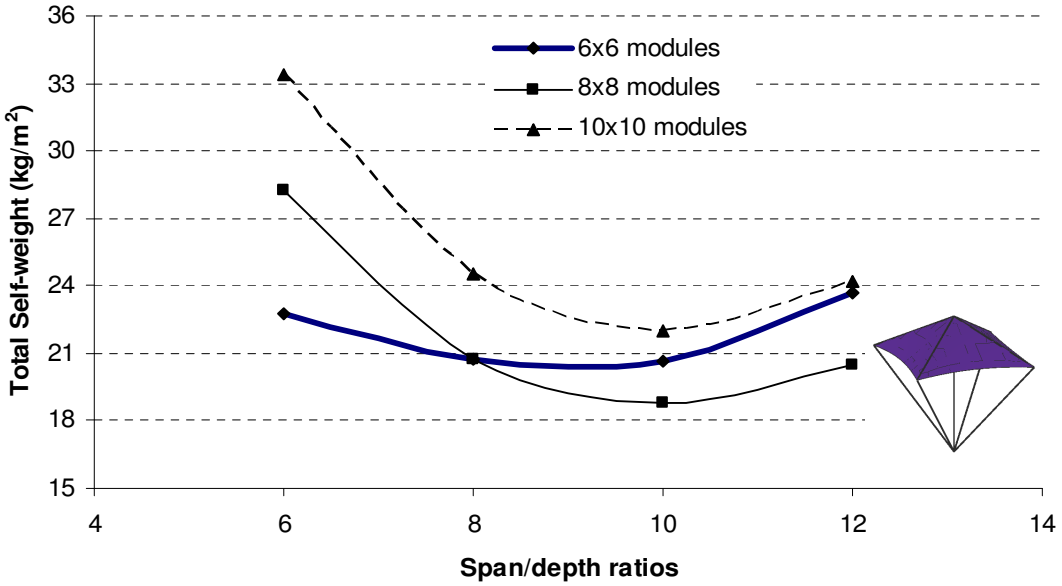

Fig. 5.15. Total weight (kg/m^2) versus span/depth ratio for different number of modules of Umbrella DSTMS

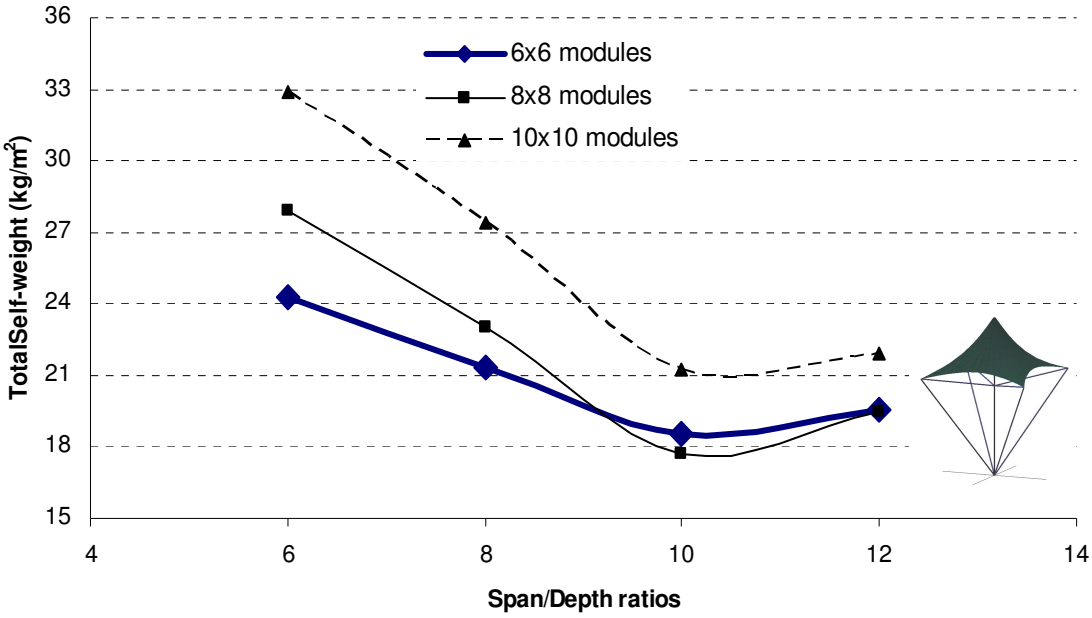

Fig. 5.16. Total weight (kg/m^2) versus span/depth ratio for different number of modules of Cone-shaped DSTMS

It can be concluded from the above results that the optimum weight of each system occurs around a span-depth ratio of 9 to 11 and a number of modules of 6 to 8.

Based on optimal range of span/depth and number of moduless, the relationship between the depth and the modular width of DSTMS can be deduced as shown in Fig. 5.17. It can be observed that optimum depth/modular width ratio is around 0.8. This ratio can be used as a reference to determine the optimum span/depth and number of moduless for curved DSTMS.

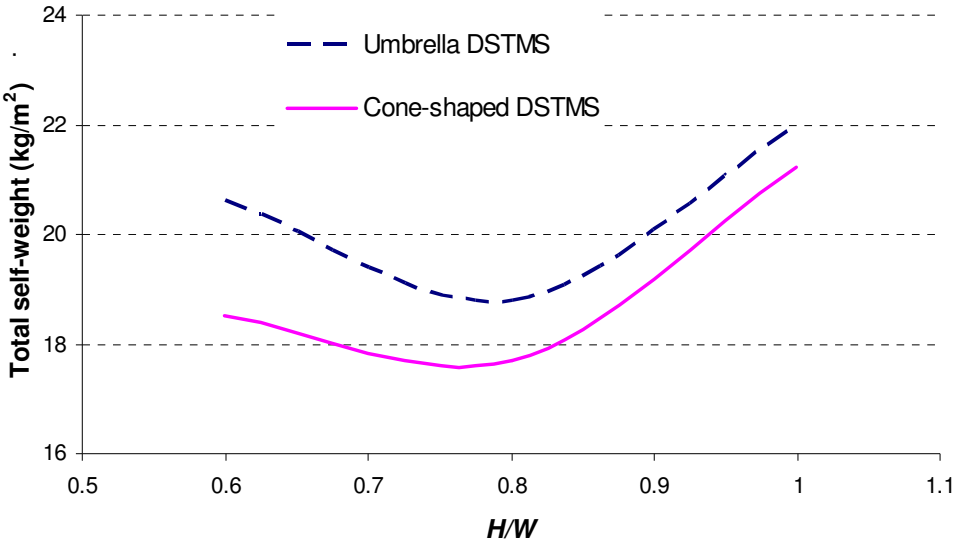

Fig. 5.17. Total self-weight (kg/m^2) vs. *H/W* ratio of Umbrella and Cone-shaped DSTMS

5.2.6.4. Weight efficiency of DSTMS

A summary of the optimum span/depth ratio and number of modules for minimum design weight of DSTMS is given in Table 5.3. The lowest weight of Umbrella DSTMS was 18.81 kg/m^2 while the lightest weight of Cone-shaped DSTMS was 17.71 kg/m^2. They are likely comparable with the self-weight of similar layout

double-layer space trusses of equivalent loading condition excluding roofing material and fabric support framing (in case of using membrane roof, Makowski 1981). It is worth noting that the double-layer space trusses are known as one of the most structurally efficient space systems. One interpretation of this would be that the DSTMS possess high structural efficiency which overcomes the main drawback of low stiffness of existing deployable structures.

Table 5.3. Optimum design parameters and weight of DSTMS (span 48m x 48m)

Type of DSTMS	Optimum *L/H* ratio	Optimum *L/W* ratio	Optimum *H/W* ratio	Optimum total self-weight (kg/m^2)
Umbrella DSTMS	10	8	0.8	18.81
Cone-shaped DSTMS	10	8	0.8	17.71

5.3. Parameter investigation of Butterfly-wing structures

The main objective of the parameter investigation is to study the effect of span/depth ratio and the number of module of the deployable cable-strut arch on the design weight of Butterfly-wing structures. Similar to DSTMS, before the parametric studies can proceed, the following design parameters of Butterfly-wing structures have to be determined:

- Structural configuration
- Support condition
- Structural elements and materials properties
- Prestressing and loading

5.3.1. Structural configuration

Two typical Butterfly-wing structures which are the two-wing and the three-wing butterfly structures will be studied. As aiming at large and medium applications, the arches' span of both structures is chosen to be 30m. With this span, deployable cable-strut arch proposed in section 3.2.6 is chosen to be used. Based on the shape effect studies in chapter 4, the inclination angle α and the rise/span ratio *(H/L)* of the arch are chosen to be 45° and 0.5 respectively which result in the smallest membrane stress. Distance between the supports of two adjacent arches is 10m. The configurations of the two structures after form-finding are illustrated in Figs. 5.18 & 5.19.

The ratios of upper & lower inclination heights (h_u , h_l) to upper & lower modular widths (W_u, W_l) are kept unchanged at 0.1, i.e. $h_u/W_u = h_l/W_l = 0.1$. The upper modular width W_u, lower modular width W_l and modular depth h are determined directly from the parameters of span/depth ratio and number of module. Due to the deployment constraint of the module, the length D of scissor-like elements in two perpendicular plane of the module should be equal (see Figs. 5.18 & 5.19). Therefore, the crossed-width W_c of the module is also dependant on the parameters of span/depth ratio and number of module. The arch-span L, upper & lower inclination heights (h_u , h_l), upper & lower modular widths (W_u, W_l), modular depth h, length D of scissor-like element and crossed-width W_c are defined as shown in Figs. 5.18 & 5.19.

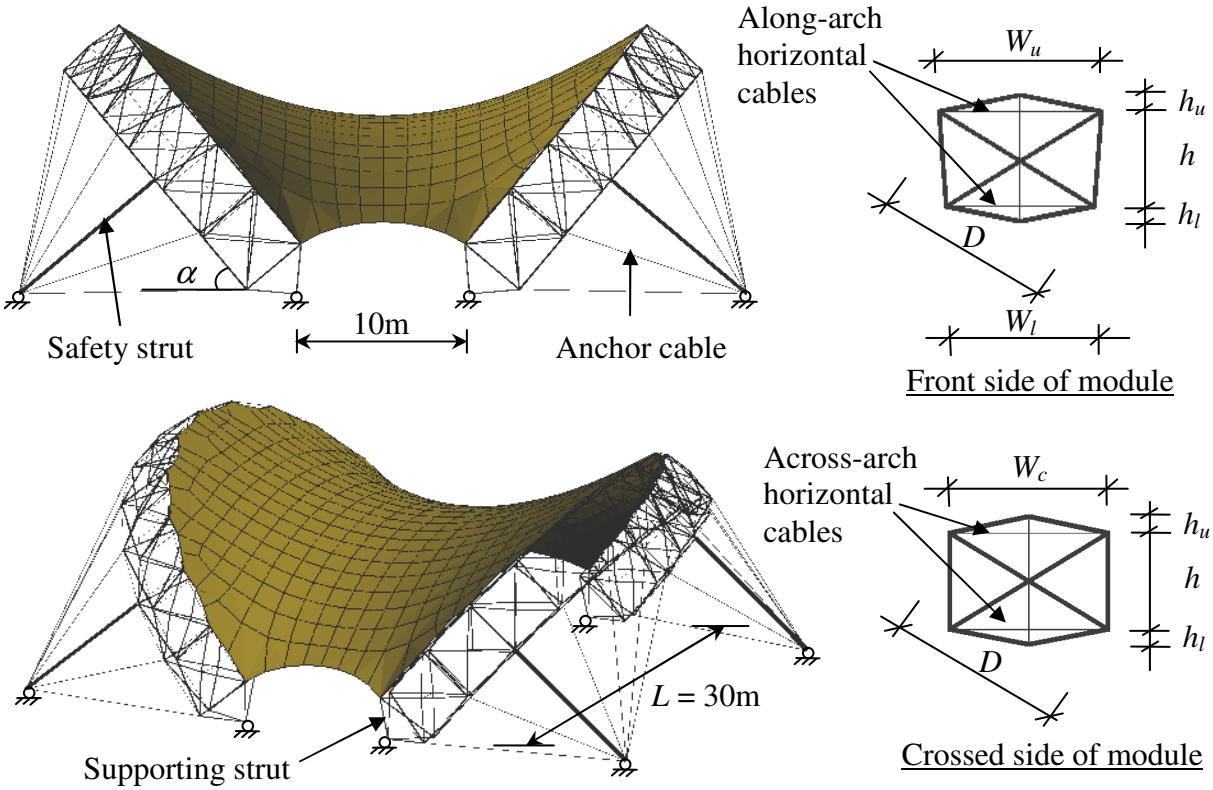

Fig. 5.18. Configuration of two-wing butterfly structure, span of 30m

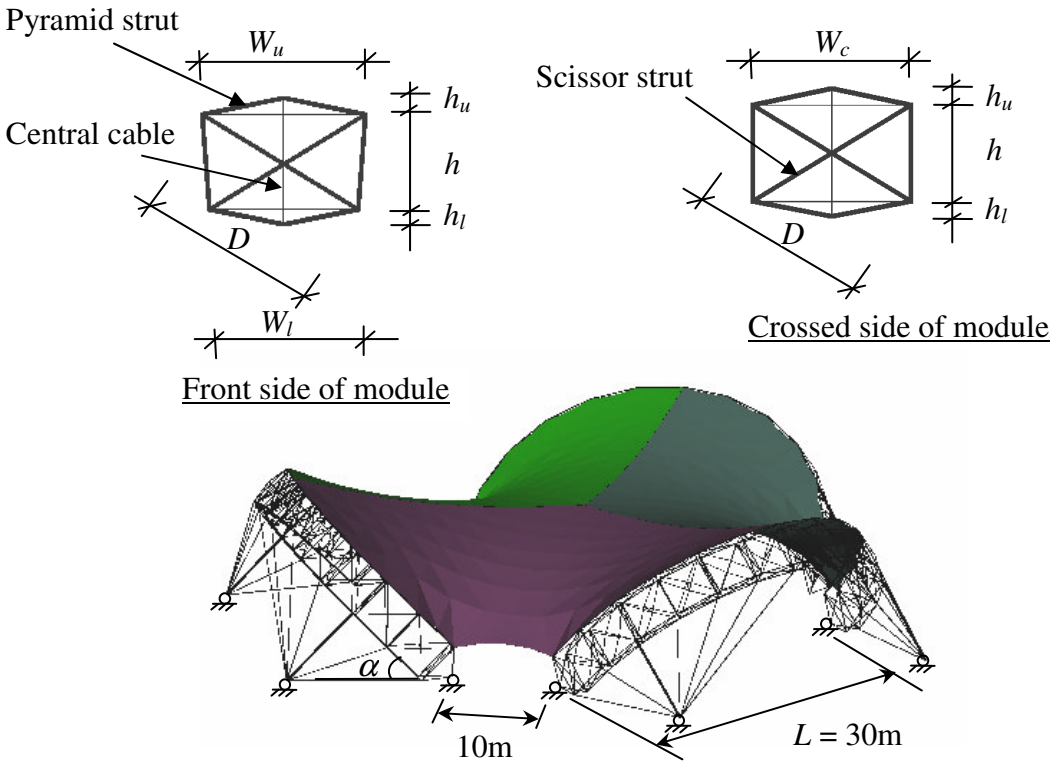

Fig. 5.19. Configuration of three-wing butterfly structure, span of 30m

5.3.2. Support condition

As explained in chapter 3, the arches of Butterfly-wing structures are not fixed but allowed to rotate freely about the supports. In this study, hinge connection will be used at the arches' feet to allow for the in plane rotation of the arches. The safety strut has one end pin-connected to the second modules of the arch and the other end pin-supported to the ground (Figs. 5.18 & 5.19).

5.3.3. Structural elements and material properties

Similar to DSTMS, there are three main classes of structural elements which are the strut element, the cable element and the membrane element.

Owing to the eccentricity of scissor-like elements meeting at the central joint, square hollow section is chosen for all struts to simplify the joint design. Square hollow section also has relatively high resistance to torsion/moment arising from joint eccentricity. Struts are made of steel of design strength 275 MPa and modulus of elasticity 210000 Mpa (BS 5950: Part 1, 2000). Cables made of 7-wire high strand tendon with breaking stress 1089 MPa and modulus of elasticity 145000 Mpa (AISI, 1973).

Material used for membrane element is the same as that used for DSTMS. PVC coated polyester fabric is chosen for this study due to its high flexibility. The fabric has a breaking tensile strength of 84000N/m and modulus of elasticity of 420000 N/m in both warp and weft directions (Fibertech Co.).

5.3.4. Prestress level and loading condition

As mentioned earlier, prestress introduced to membrane is 10% to 20% of allowable stress of the fabric. For PVC coated polyester fabric, it ranges from 1kN/m to 2kN/m. Since Butterfly-wing structures possess anticlastic surfaces with significant curvatures, medium prestress level of 1.5kN/m is applied in two major curvatures of the membrane surface.

For Butterfly-wing structures, wind force is the predominant loading on membrane. Based on the saddle shape of the membrane surface and wind speed of 35m/s which is commonly used in Singapore (Arup, 2003), wind uplift force of 0.45kN/m^2 and wind downward pressure of 0.15kN/m^2 are calculated and adopted for the design of Butterfly-wing structures (Forster and Mollaert, 2004). The wind forces are applied perpendicular to the membrane surface. Accordingly, there are two load combinations of wind uplift pressure and wind downward pressure.

5.3.5. Parametric studies

The weight of Butterfly-wing structures is mainly contributed by the weight of the supporting arches since the weight of membrane fabric is negligible. The weight of the deployable cable-strut arch is heavily influenced by their span/depth ratio and number of modules. The main purposes of the present studies are to investigate the effect of span/depth ratio and number of modules of the arch on the design weight of two-wing and three-wing butterfly structures with the view to obtain the optimum design

parameters for each structural system. To achieve this, the weight efficiency of each Butterfly-wing structures will be obtained for each of the following parameters:

- Arch-span/modular depth ratio (*L/h*): 15, 20, 25
- Number of modules of the arch: 8, 10, 12, 14

The integrated approach of force density method and geometrical nonlinear analysis proposed in chapter 4 is used to find the equilibrium form and to analyze the structural behaviour of the two Butterfly-wing structures.

5.3.5.1. Optimum design parameter

Figures 5.20 & 5.21 show the total weight of the two-wing and three-wing butterfly structures for different arch-span/modular depth ratio and different number of module of the arch.

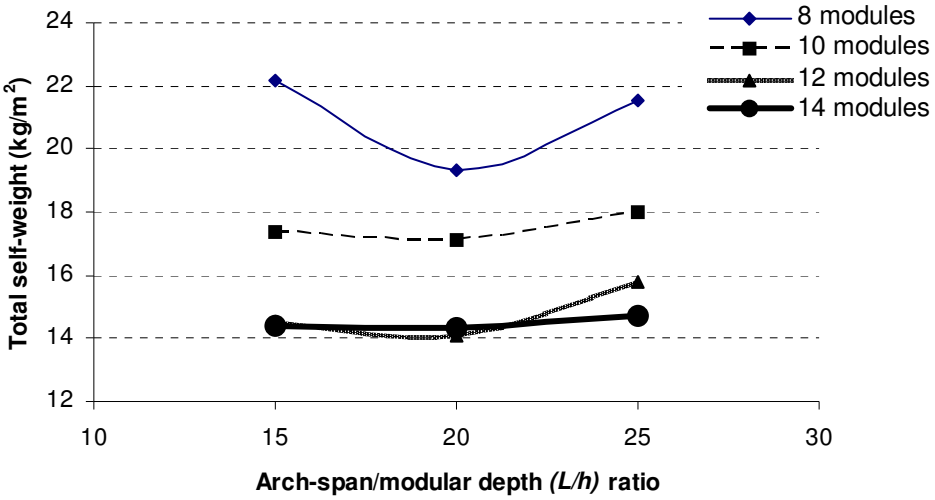

Fig. 5.20. Total weight (kg/m^2) versus arch-span/modular depth ratio for different number of module of two-wing butterfly structure

It is seen that the weight of both structures decreased when arch-span/modular depth ratio increased from 15 to 20 and increased when arch-span/modular depth ratio increased from 20 to 25. As the major action in the arch is compression force, the length of struts has significant effect on their buckling strength. For the same number of module, the increase of arch-span/modular depth ratio reduces the buckling length of the struts in the arch, resulting in small member size required and thus lower self-weight of the structures. When the arch-span/modular depth ratio is larger than 20, the arch becomes slender in plane and the serviceability limit state will govern the design. Hence larger member sizes are required, resulting in higher self-weight. It can be deduced from the results that the minimum weight of both structures occurs at arch-span/modular depth ratio of 19 to 21.

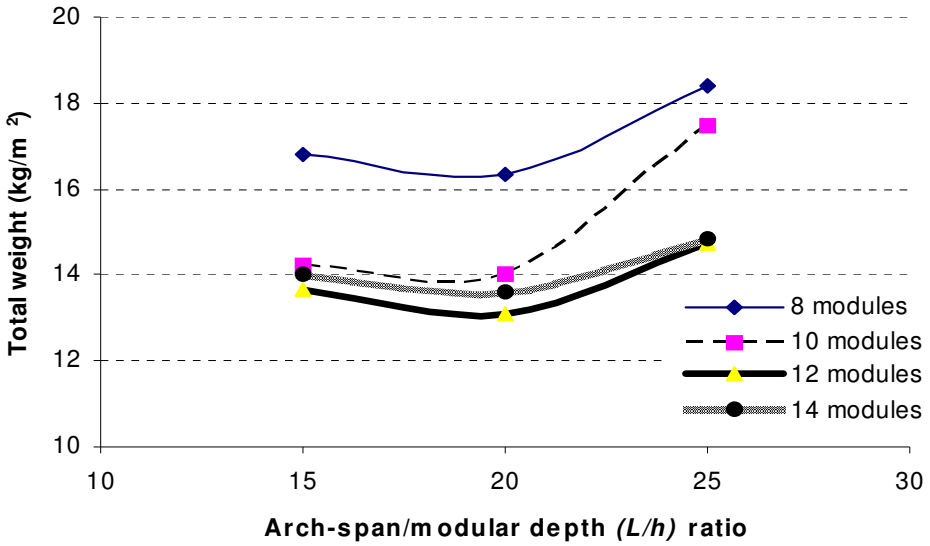

Fig. 5.21. Total weight (kg/m^2) versus arch-span/modular depth ratio for different number of module of three-wing butterfly structure

The change in number of module also has significant influence on the self-weight of the structures. Figures 5.20 and 5.21 show that the weight of the structures decreased when number of module increased from 8 to 12 while it did not decrease much or started increasing when number of module increased from 12 to 14. The possible

reason is that the increase in number of module has two opposite effects on the weight of the structures. On one hand, it reduces the length of the struts which results in the enhancement of buckling strength and thus the decrease of weight. On the other hand, it increases the number of structural members and reduces the crossed width W_c of module. Consequently, it makes the structures become slender out of plane and thus a higher weight is expected. For number of modules from 8 to 12, the struts are considerably long, thus the weight of the structures is dominated by the member buckling length. Hence the weight decrease of the structures in this range can be explained by the enhancement of the buckling strength. For number of module from 12 to 14, the struts are relatively short, thus the gain in buckling strength is not so significant. The structures become slender due to small crossed width W_c of module, thus larger member sizes are required to satisfy the serviceability limit state. In addition, the increase in number of structural members results in the higher weight of structures. It is also worth noting that larger number of module will create more connections and thus inverse the fabrication cost. Therefore, it can be concluded from the results that the optimum number of module of both structures is around 12 to 14.

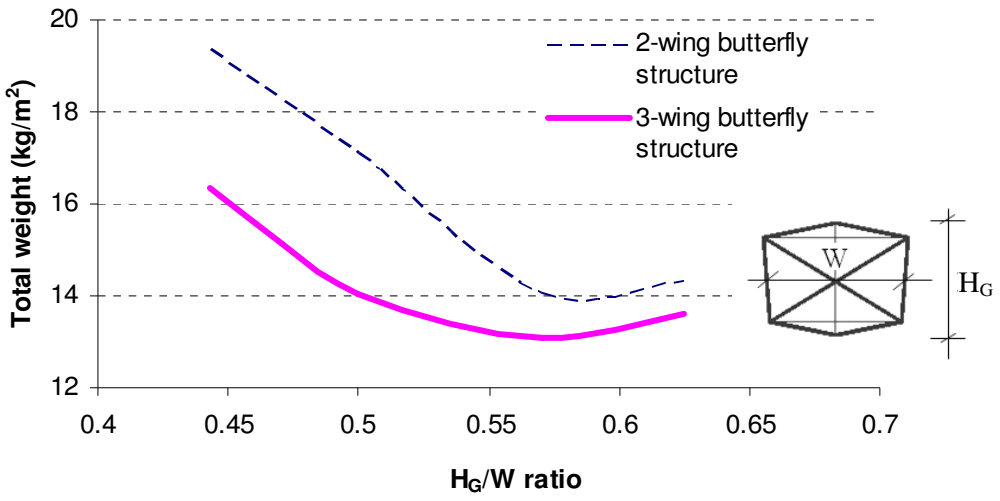

Fig. 5.22. Total weight (kg/m^2) versus H_G/W ratio of two-wing and three-wing butterfly structures

Based on the results of optimum arch-span/modular depth ratio and number of module, the relationship between gross height/average width ratio (H_G/W) of module and self-weight of the structures can be deduced as shown in Fig. 5.22. The gross height H_G and average width W are defined as $H_G = h_u + h + h_l$ and $W = (W_u + W_l)/2$ respectively (Fig. 5.22). It can be seen that optimum H_G/W ratio of both Butterfly-wing structures is about 0.58. This ratio can be used as reference to determine the optimum number of module and arch-span/modular depth ratio for other butterfly-wing structures.

A summary of the optimum arch-span/modular depth ratio and number of module for minimum design weight of two-wing and three-wing butterfly structures is given in Table 5.4. The lowest weight of two-wing butterfly structure is 14.06 kg/m^2 while the lightest weight of three-wing butterfly structure is 13.1 kg/m^2.

Table 5.4. Optimum design parameters and weight of Butterfly-wing structures, span of 30m

Type of Butterfly-wing structure	Optimum arch-span/modular depth	Optimum number of module	Optimum H_G/W ratio	Optimum total self-weight (kg/m^2)
Two-wing butterfly structure	20	12	0.58	14.06
Three-wing butterfly structure	20	12	0.8	13.10

5.3.5.2. Efficiency study of modified arch

The structural inefficiency of the deployable cable-strut arch lies in the two middle horizontal cable layers running along the arch (see Figs. 5.18 & 5.19). The middle horizontal cable layers are designed to restrain the deployment of the arch. They are

under tension when the arch is deployed to its final configuration. When Butterfly-wing structures are subjected to external load, the major resultant force induced is the compression force along the arch. Thus the middle horizontal cable layers running along the arch are subjected to compression, resulting in a number of slackened cables. Tables 5.5 and 5.6 show that the amount of slackened along-arch cables of the two-wing and three-wing butterfly structures (with optimal number of module of 12) were about 40% and 50% respectively.

Table 5.5. Amount of slackened along-arch cables of two-wing butterfly structure

Number of module	Arch-span/modular depth ratio	Total along-arch cables	Slackened along-arch cables	$\frac{\text{Slackened}}{\text{Total}}$
12	15	96	46	0.48
	20	96	44	0.46
	25	96	40	0.42

Table 5.6. Amount of slackened along-arch cables of three-wing butterfly structure

Number of module	Arch-span/modular depth ratio	Total along-arch cables	Slackened along-arch cables	$\frac{\text{Slackened}}{\text{Total}}$
12	15	144	66	0.46
	20	144	60	0.42
	25	144	60	0.42

Structural efficiency of the system can be improved by using struts to replace those along-arch cables at the expense of more time consumed for strut assembling. Figures 5.23 & 5.24 show the weight of two-wing and three-wing butterfly structures with arch modified and unmodified. This modification resulted in a weight reduction of about 10% and 20% for two-wing and three-wing butterfly structures respectively as shown in Table 5.7 & 5.8. In this case, the existing across-arch cable layers are acting as the deployment restraint of the arch. The assemblage of the replacing struts to along-arch

cables can be simply done by bolt connection after the arch is in fully deployed configuration.

Table 5.7. Weight reduction of two-wing butterfly structure with arch modified

Number of module	Arch-span/modular depth ratio	Weight of two-wing butterfly structure (kg/m^2)		Modified / Unmodified
		Unmodified arch	Modified arch	
12	15	14.53	14.02	0.96
	20	14.06	13.17	0.93
	25	15.76	14.11	0.89

Table 5.8. Weight reduction of three-wing butterfly structure with arch modified

Number of module	Arch-span/modular depth ratio	Weight of two-wing butterfly structure (kg/m^2)		Modified / Unmodified
		Unmodified arch	Modified arch	
12	15	13.67	11.23	0.82
	20	13.10	10.84	0.83
	25	14.73	11.65	0.79

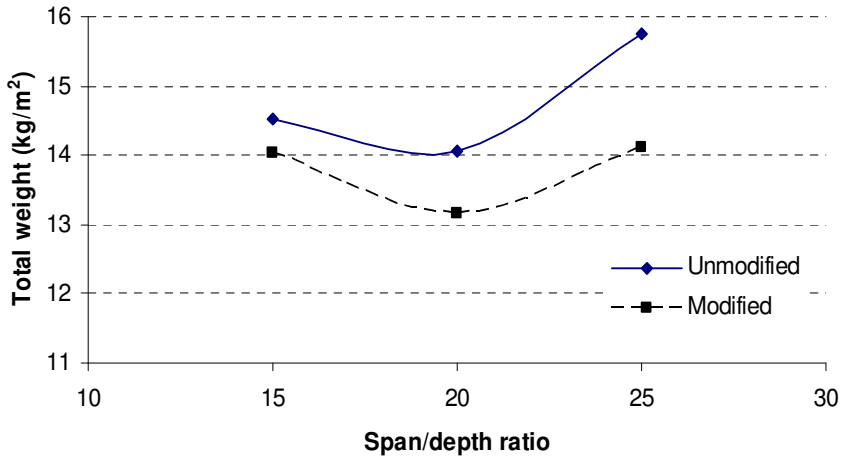

Fig. 5.23. Total weight (kg/m^2) of two-wing butterfly structures with unmodified arch and modified arch

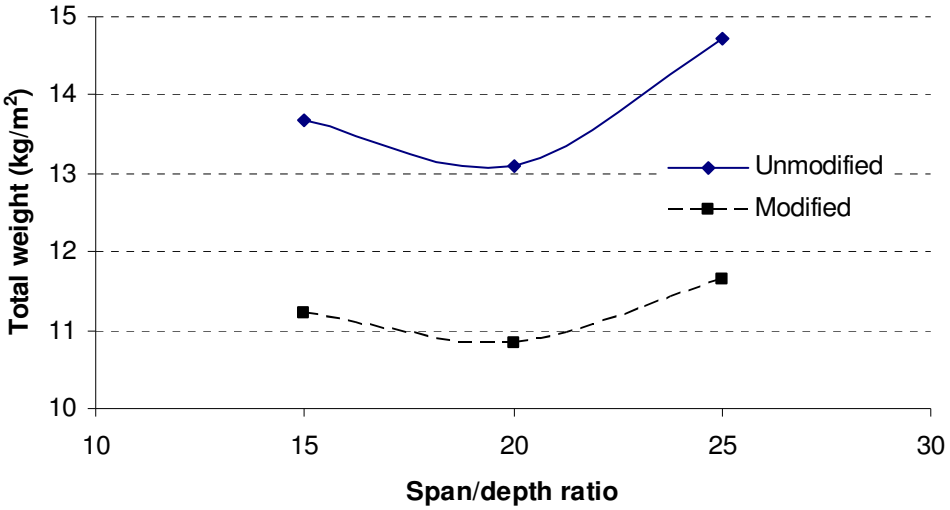

Fig. 5.24. Total weight (kg/m^2) of three-wing butterfly structures with unmodified arch and modified arch

The weight reduction is attributed to the replacing struts which can resist both tension and compression. Although the weight of these struts is higher than the weight of replaced cables, the flow of internal force induced in the modified arch is smoother resulting in smaller section sizes of other members and thus smaller total weight.

5.4. Summary

Chapter 5 presented the parametric studies, followed by the results and discussions of both DSTMS and Butterfly-wing structures. From the above discussions, it is concluded that the lightest weight of Umbrella and Cone-shaped DSTMS of 48m x 48m span are 18.81kg/m^2 and 17.71kg/m^2 which are equivalent to that of similar layout double layer space truss. The span/depth ratio and number of modules have different effects on the weights of web and chord components of DSTMS. Generally, the weight of chord to web ratio increases with the increase of span/depth ratio and decreases with the increase in number of modules. The optimum span/depth ratio and number of modules corresponding with the minimum

total design weight of DSTMS are 9 to 11 and 6 to 8 respectively. The deduced optimum depth/modular width ratio is found to be approximately 0.8.

For Butterfly-wing structures, the lowest weight of two-wing and three-wing butterfly structures of 30m arch's span are 14.06 and 13.1 respectively. The number of module and the arch-span/modular depth ratio of the deployable cable-strut arches have great influence on their design weight which is the dominant weight of butterfly-wing structures. The optimum arch-span/modular depth ratio and the optimum number of module of the arch corresponding with the minimum design weight of both two-wing and three-wing butterfly structures are found in ranges of 19 to 21 and 12 to 14 respectively. The deduced optimum gross height/average width ratio of module is about 0.58. By replacing the along-arch cables by struts, the results show that the weight two-wing and three-wing butterfly structures can be reduced about 10% and 20% respectively at the expense of longer erection time due to the assemblage of replacing struts.

CHAPTER 6

ROBUSTNESS OF STRUCTURES AGAINST HAZARDS

6.1. Introduction

Both Deployable strut-tensioned membrane structures (DSTMS) and Butterfly-wing structures have potential applications for large span structures, thus their robustness against progressive collapse must be considered. In these structures, membrane functions as structural component which contributes to the overall stability of the structures. On the other hand, the membrane is thin and thus vulnerable to damage. Therefore, it is important to ensure the safety of the supporting structure in the event of partial or total failure of membrane. There are several threats to membrane, in which, vandalism and fire are the most possible hazards. This chapter examines the robustness of DSTMS and Butterfly-wing structures against these two hazards.

In the vandalism scenario, membrane is considered to be totally damaged, and thus advanced analysis is performed to assess the robustness of DSTMS and Butterfly-wing structures subjected to total membrane removal. Dynamic impact due to the sudden loss of membrane tension is also taken into account in the robustness study.

In the fire scenario, the robustness of DSTMS and Butterfly-wing structures subjected to internal fire occurring at critical locations is assessed in accordance with relevant Codes, including BS 5950 : Part 8 (2003) and Eurocodes 1&3 : Part 1:2 (2001). The characteristics of membrane materials and the behaviour of membrane structures in fire are discussed and explained. The study also presents an approach for determining the

structural fire resistance of large space membrane structures based on their performance in real fire.

The aims of this chapter are to study the structural behaviour and to identify the critical factors influencing the robustness of DSTMS and Butterfly-wing structures in specific hazards. Thereby, the safety of the structures can be ensured with minimal cost needed against the hazards.

6.2. Parameters for investigating the robustness

6.2.1. Parameters of Deployable strut-tensioned membrane structures

The robustness of Umbrella DSTMS and Cone-shaped DSTMS will be investigated using the following parameters:

- Configuration: Flat roof Umbrella and Cone-shaped DSTMS (Figs. 5.1 & 5.2)
- Span: 48m x 48m
- Clear height of roof: 5.2m
- Inclination height/modular width: 0.2
- Span/depth ratio: 10
- Span/modular width ratio: 8
- Boundary condition: pin supported at 4 edges
- Material properties:
    - Strut elements
        - Young's modulus = 210 GPa
        - Yield strength = 275 MPa

- Cable elements
    - Young's modulus = 145 GPa
    - Breaking strength = 1089 MPa
- PVC coated membrane
    - Young's modulus = 420000 N/m
    - Tensile strength = 84000 N/m

The chosen inclination height/modular width ratio, span/depth ratio and span/modular width ratio are based on the optimum configuration derived in chapters 4 & 5. All structural elements sizes are kept the same as what were designed in chapter 5. Material properties, boundary conditions and loadings are unchanged.

6.2.2. Parameters of Butterfly-wing structures

The robustness of butterfly-wing structures will be investigated using the following parameters:

- Configuration: Two-wing and three-wing butterfly structures supported by deployable cable-strut arch (Fig. 5.18 & 5.19)
- Span: 30m
- Inclination angle of arch: 45°
- Rise/span ratio of arch: 0.5
- Arch-span/modular depth ratio: 20
- Number of module of arch: 12
- Boundary condition: hinge support for arches
- Material properties:

- Strut elements
    - Young's modulus = 210 GPa
    - Yield strength = 275 MPa
- Cable elements
    - Young's modulus = 145 GPa
    - Breaking strength = 1089 MPa
- PVC coated membrane
    - Young's modulus = 420000 N/m
    - Tensile strength = 84000 N/m

The chosen inclination angle, rise/span ratio, span/modular depth ratio and number of module of arch are based on the optimum configuration derived in chapters 4&5. All structural elements sizes are kept the same as what were designed in chapter 5. Material properties, boundary conditions and loadings are unchanged.

6.3. Robustness against vandalism

Membrane is susceptible to damage due to accidents or vandalism. In DSTMS and Butterfly-wing structures, membrane acts as a tension component contributing to the overall stability of the structures. Thus, it is necessary to assess the sufficiency of their structural redundancy to ensure that the removal and detensioning of the membrane do not cause the structures to collapse. In subsequent sections, behaviour of DSTMS and Butterfly-wing structures in the event of membrane failure will be investigated. Post collapse and dynamic analyses are performed to assess the robustness of the proposed structures in the scenario of total membrane damage due to vandalism.

6.3.1. Robustness of DSTMS against vandalism

The cable-strut skeleton of DSTMS is itself a determinate and stable structure. Membrane is a tension component to brace the struts the skeleton and help the structures achieve self-stress equilibrium. In DSTMS, membrane is assembled and tensioned from modules to modules. When a local damage happens, only the membrane area of modules related to the damage should be affected. Thus it is unlikely that the entire membrane area of the structure could be damaged suddenly. Therefore, in the robustness study of DSTMS, the membrane is assumed to be gradually damaged and detensioned until the skeleton structure is no longer prestressed and braced by the tensioned membrane. Progressive collapse analysis is performed to assess the robustness of DSTMS without membrane attached. The configurations of Umbrella and Cone-shaped DSTMS without membrane are illustrated in Fig. 6.1 and Fig. 6.2.

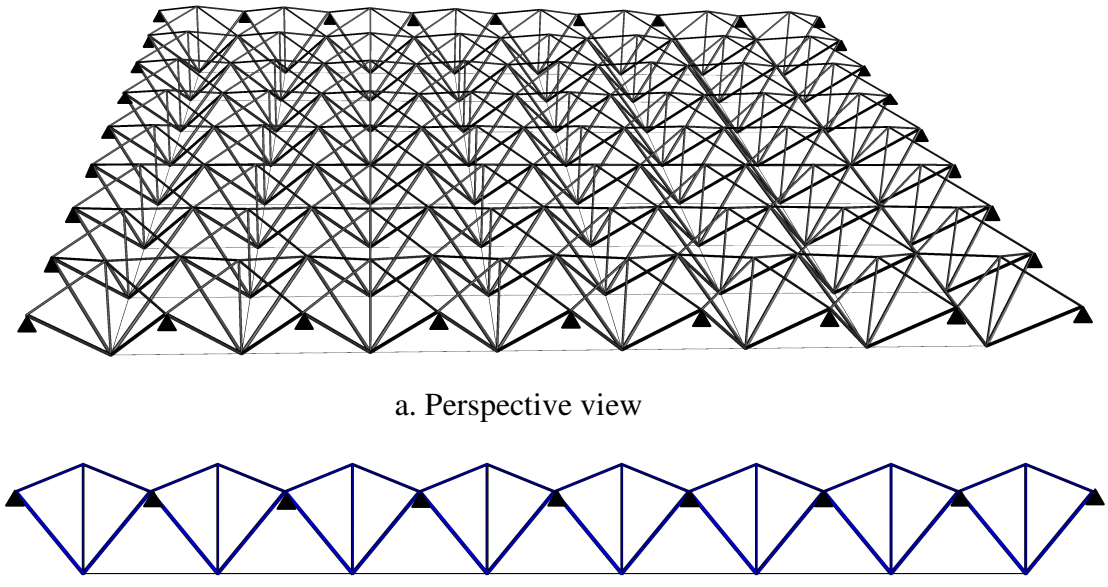

a. Perspective view

b. Front view

Fig. 6.1. Umbrella DSTMS with membrane removal

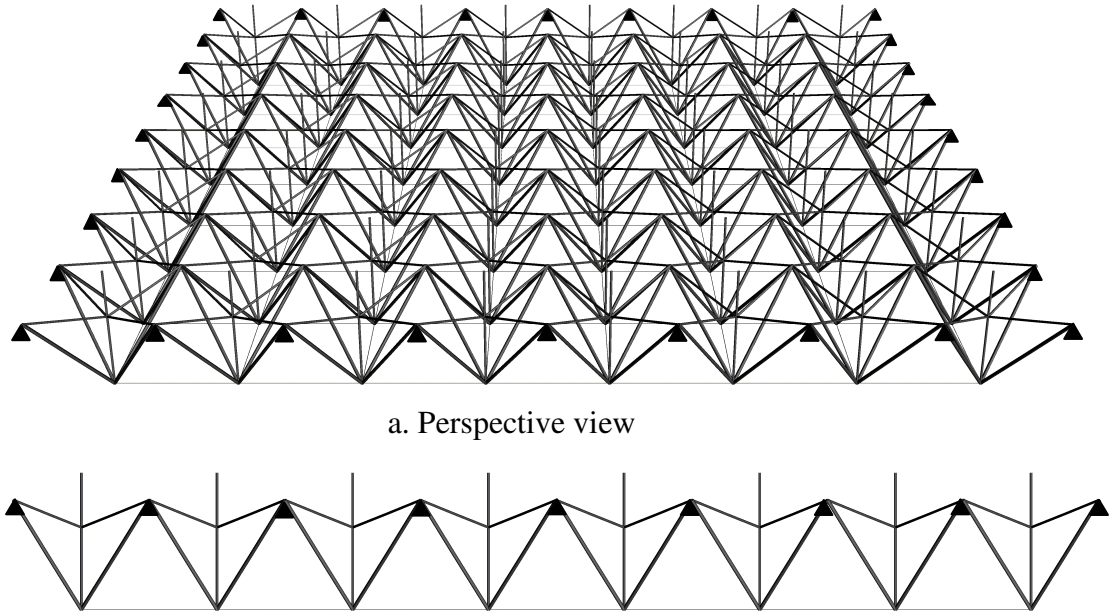

a. Perspective view

b. Front view

Fig. 6.2. Cone-shaped DSTMS with membrane removal

Owing to the complete removal of membrane, only gravity load combination is considered in the analysis. The wind load combination can be neglected since the wind force acting on the skeleton structure is negligible as compared to its self-weight. The designed gravity load combination of DSTMS in chapter 5 was (1.4 x self-weight + 1.6 x imposed load). Figures 6.3 & 6.4 show the mid-point vertical displacement against the load ratio of the Umbrella and Cone-shaped DSTMS with membrane removal. The load ratio is defined as the ratio of the applied loads to the design loads. The elastic utilization of structural members at ultimate load point of the structures is also given in Figs. 6.3 & 6.4.

From the elastic utilization of structural members shown in Figs. 6.3 & 6.4, it is observed that Umbrella DSTMS skeleton collapsed due to the failure of the corner struts while Cone-shaped DSTMS skeleton collapsed due to the failure of the center

bottom cables. This is because the behaviour of the structures is similar to that of a plate simply supported at four edges. The resultant force is a combination of elemental internal shear force and bending moment. The imposed load, which is applied at every bottom nodes, can be considered as uniform distributed load. Therefore the elemental internal shear force is largest at the edges, especially at the four corners where maximum shear forces of two perpendicular edges are overlapping. Thus, the struts at the four corners are subjected to high axial forces. On the other hand, the elemental bending moment is largest at the center, resulting in high tension force in bottom cables at the center of the structures.

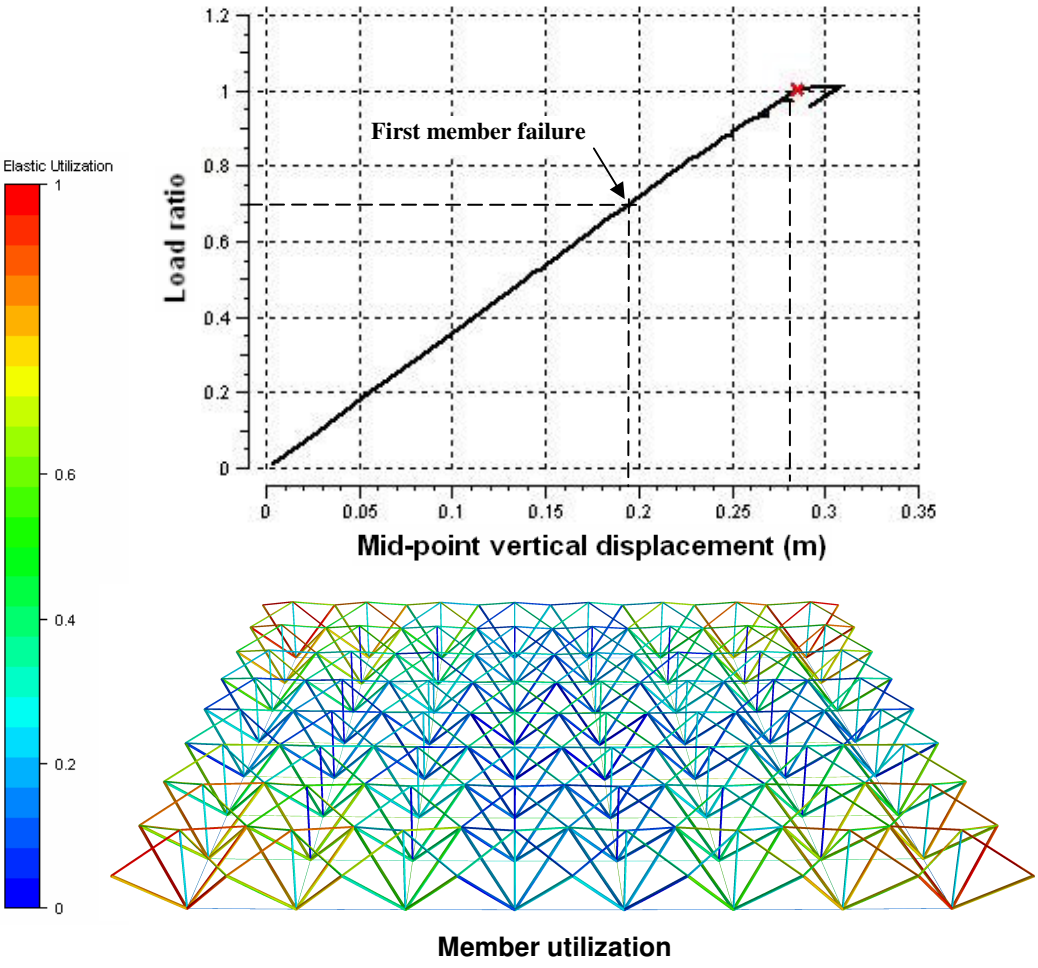

Fig. 6.3. Load-displacement curve and member utilization of Umbrella DSTMS with membrane removal

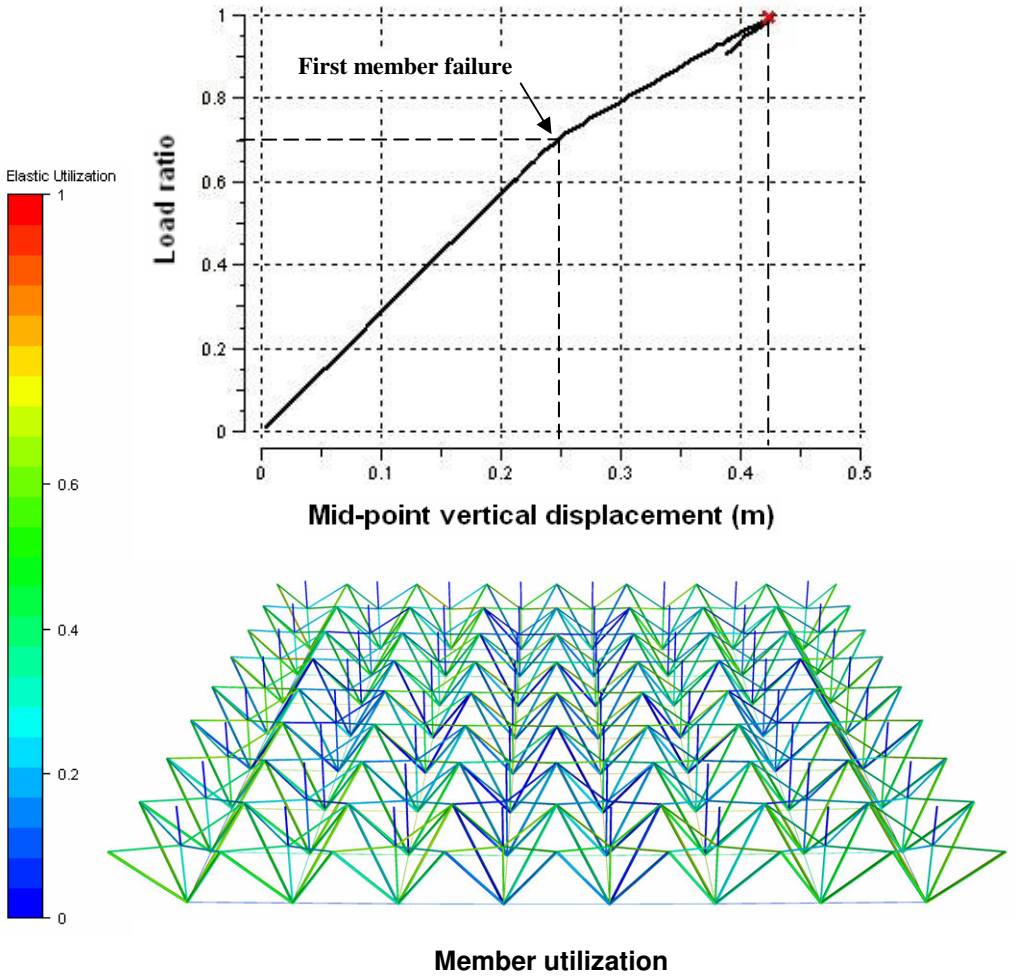

Fig. 6.4. Load-displacement curve and member utilization of Cone-shaped DSTMS with membrane removal

The load-displacement curves in Figs. 6.3 & 6.4 show that the collapse of both structures happened at load ratio of 1.0. It means that the ultimate load of DSTMS without membrane is equal to the design load of DSTMS. However, while both DSTMS were designed with first member failure at load ratio of 1.0 (see chapter 5), the first member failure of DSTMS without membrane happened at load ratio of 0.7 (see Figs. 6.3 & 6.4). In addition, the mid-point vertical displacements at load ratio of 1.0 (0.28m and 0.42m for Umbrella and Cone-shaped DSTMS with membrane removal respectively) were beyond the serviceability limit (span/200 = 0.24m), thus larger than those of DSTMS which were designed satisfactorily the serviceability limit.

The first member failure of DSTMS at higher applied load than that without membrane can be attributed to the effect of membrane prestress on the structural skeleton. The prestress in membrane also creates tension force in bottom cables, which may help to reduce vertical deflection of the structures.

Although DSTMS tend to be weaker in the event of membrane removal, it is necessary to note that the load factors should be scaled down due to the fact that structures are often not in full load conditions in the accidental scenario. In this study, the load factors are taken in accordance with EN 1990 Eurocode – Basis of structural design and Eurocode 1: Part 1.7 which are applicable for accidental limit state. Thus the accidental load combination will be: (1.0 x self-weight + 0.5 x imposed load). From the above results, the first member failure of both DSTMS with membrane removal happened at load ratio of 0.7, i.e. 0.7 x (1.4 x self-weight + 1.6 x imposed load) ≈ (1.0 x self-weight + 1.12 x imposed load). As such, there should be no member failure under the accidental load combination. Therefore, it can be concluded that the Umbrella and Cone-shaped DSTMS optimally designed in chapter 5 are safe in case the membrane is completely damaged in the accidental/vandalistic situation.

6.3.2. Robustness of Butterfly-wing structures against vandalism

Unlike DSTMS, the membrane of butterfly-wing structure is continuously spanning between the arches. Hence, it can be expected that the entire membrane area is damaged in a short period by tearing propagation due to vandalism/accident. Therefore, dynamic impact on the supporting arches due to the sudden loss of membrane tension forces must be considered.

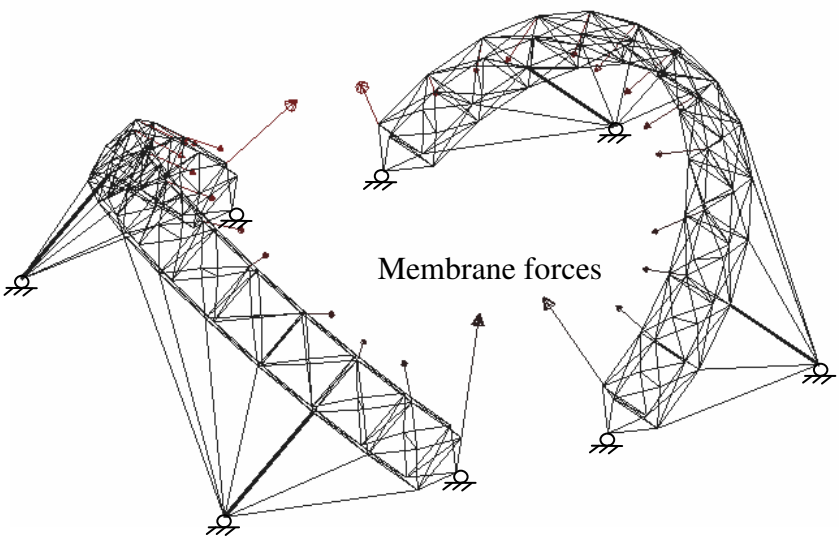

Fig. 6.5. Two-wing butterfly structure without membrane

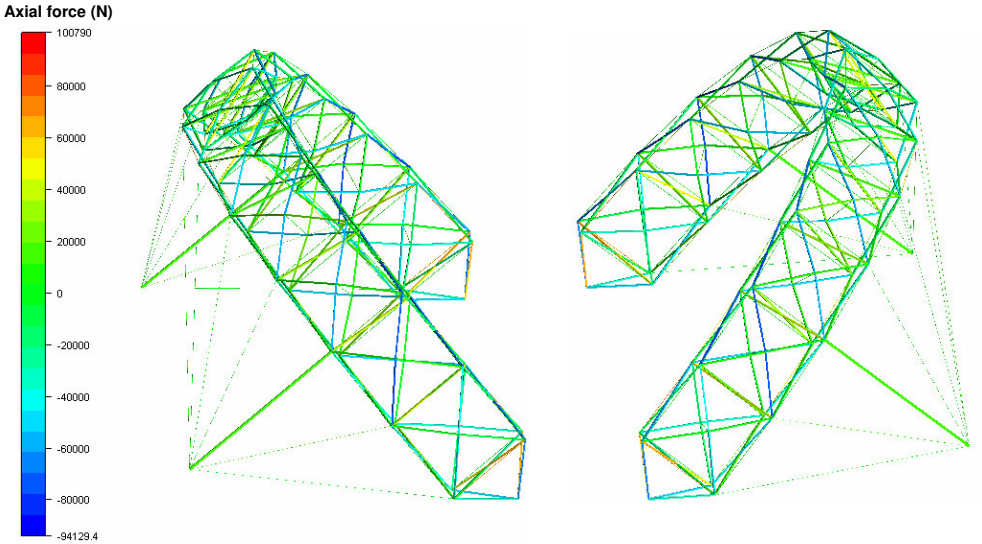

Fig. 6.6. Axial forces in members of Two-wing butterfly structure before membrane is damaged

The configurations of the two-wing & three-wing butterfly structures without membrane are illustrated in Figs. 6.5 & 6.7. As the membrane is totally damaged, each inclined arch is an individual structure and the safety struts prevents the collapse of the arches. Loading is taken in accordance with Eurocode 1: Part 1.7 and EN 1990 Eurocode applied for accidental limit state, therefore the design load combination is (1.0 x self-weight + 0.5 x wind load).

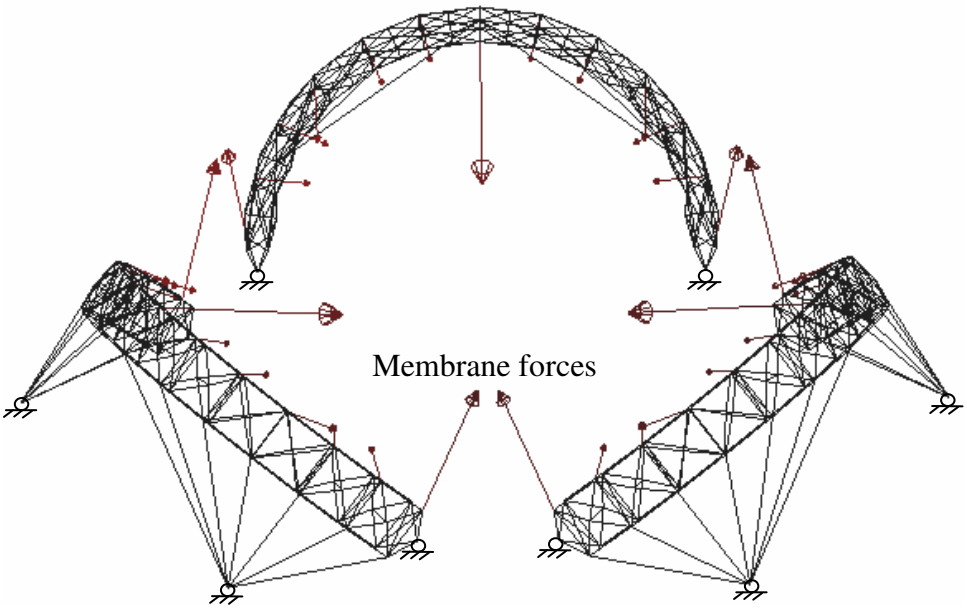

Fig. 6.7. Three-wing butterfly structure without membrane

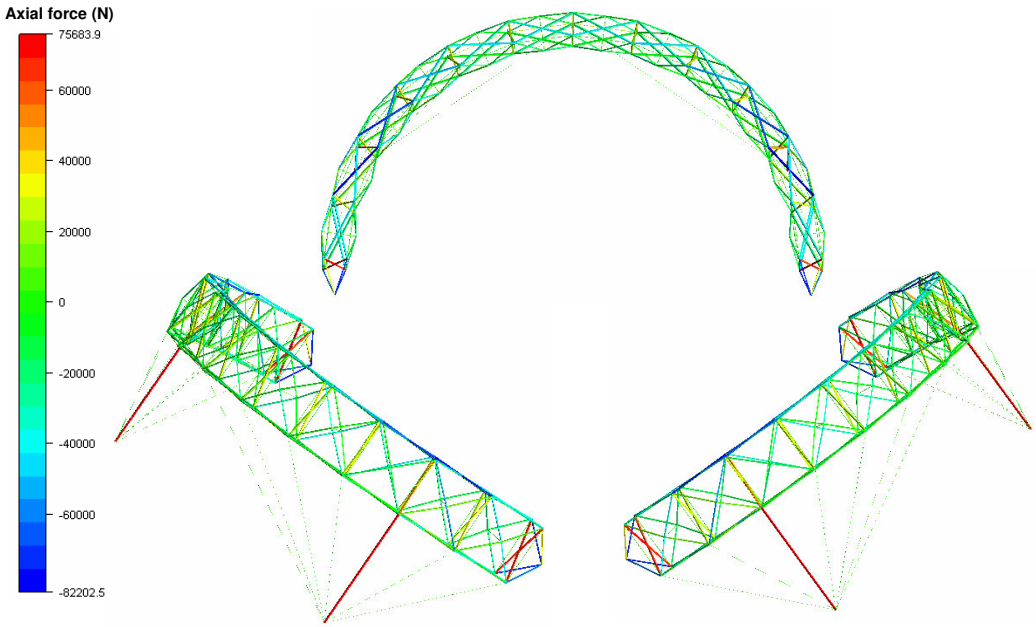

Fig. 6.8. Axial forces in members of Three-wing butterfly structures before membrane is damaged

The membrane forces acting on the arches before accident/vandalism are illustrated in Figs. 6.5 & 6.7 and tabulated in Appendix A of this thesis. Figures 6.6 & 6.8 show the axial forces in structural members before membrane is damaged. It can be seen that the anchor cables and safety struts were under tension due to the membrane forces. When

accident/vandalism happens, the membrane forces are assumed to be released linearly as shown in Fig. 6.9. In order to investigate the effect of dynamic impact on the arches, the loss duration (t_{loss}) of membrane forces in Butterfly-wing structures are reduced until the supporting arches collapse. Figures 6.10 – 6.15 show the time histories of the vertical displacement at mid-span of the arch and the axial force of the most critical member, which is the safety strut of the arch, for different t_{loss} of Two-wing and Three-wing butterfly structures. From the time history of displacement, it can be observed that the amplitude of vibration of the arch increase with the decrease of t_{loss}. This behaviour is expected since the smaller t_{loss} means the more sudden the loss of membrane forces, and thus the higher dynamic impact on the arch. At t_{loss} = 0.1s, the amplitude of vibration of the arch of Two-wing butterfly structure increased up to 270mm and the axial force in safety strut was inversed from 15kN in tension before accident to 70kN in compression (Fig. 6.12) which exceeds its buckling strength of 69kN. The failure of the safety strut resulted in the collapse of the arch since the safety strut is the structural component to keep the arch stable when the membrane is removed. Similarly, the arch of Three-wing butterfly structure collapsed at t_{loss} = 0.01s due to the failure of safety strut at compression force of 70kN (Fig. 6.15). The collapse of Three-wing butterfly structure at smaller t_{loss} can be explained by the more uniform membrane tension force acting along the arch, resulting in less extreme amplitude of vibration.

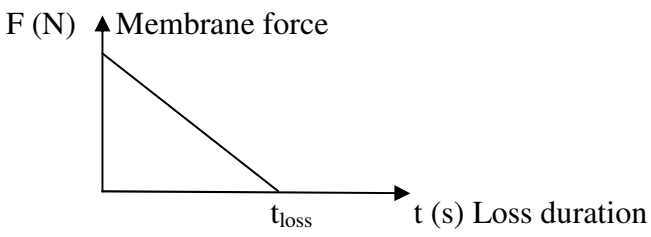

Fig. 6.9. Membrane forces vs. loss duration

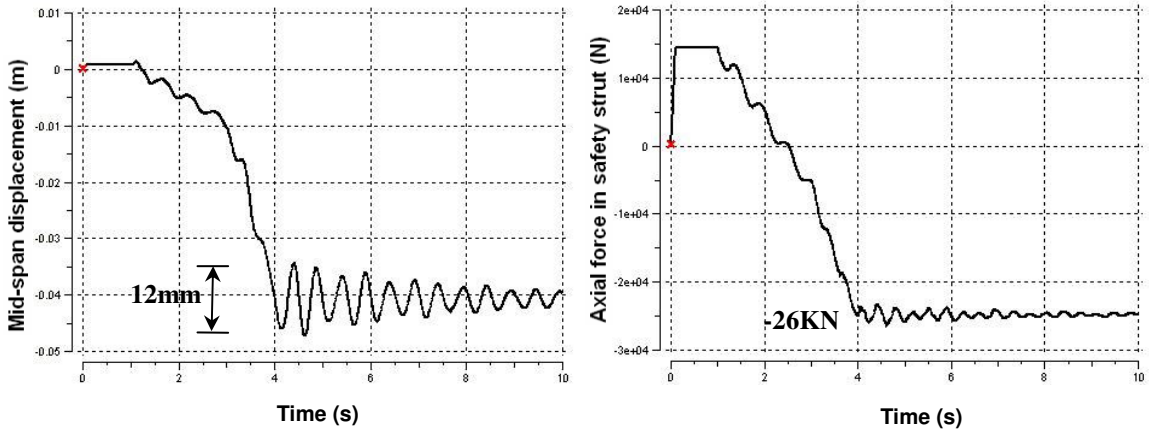

(a) (b)

Fig. 6.10. Time histories of (a) vertical displacement at arch's mid-span and (b) axial force in safety strut of Two-wing butterfly structure with t_{loss} = 3s

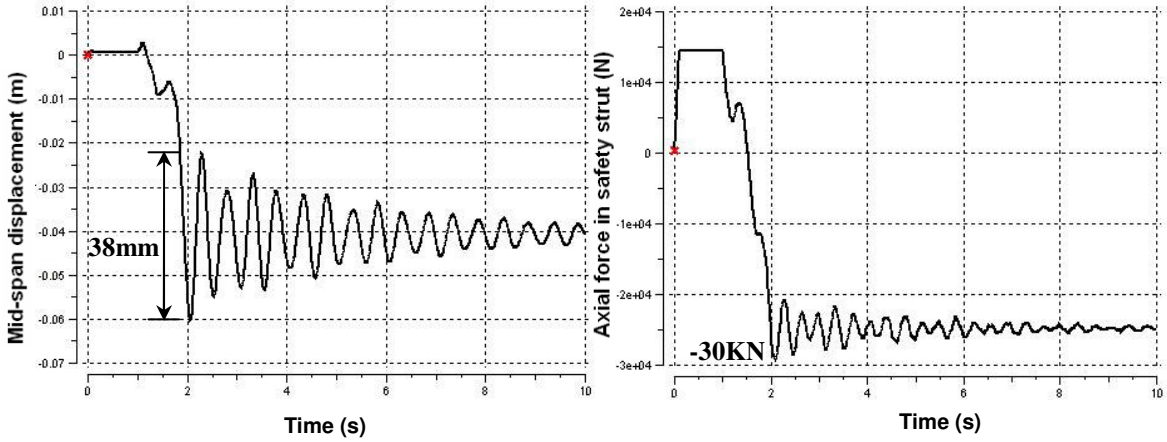

(a) (b)

Fig. 6.11. Time histories of (a) vertical displacement at arch's mid-span and (b) axial force in safety strut of Two-wing butterfly structure with t_{loss} = 1s

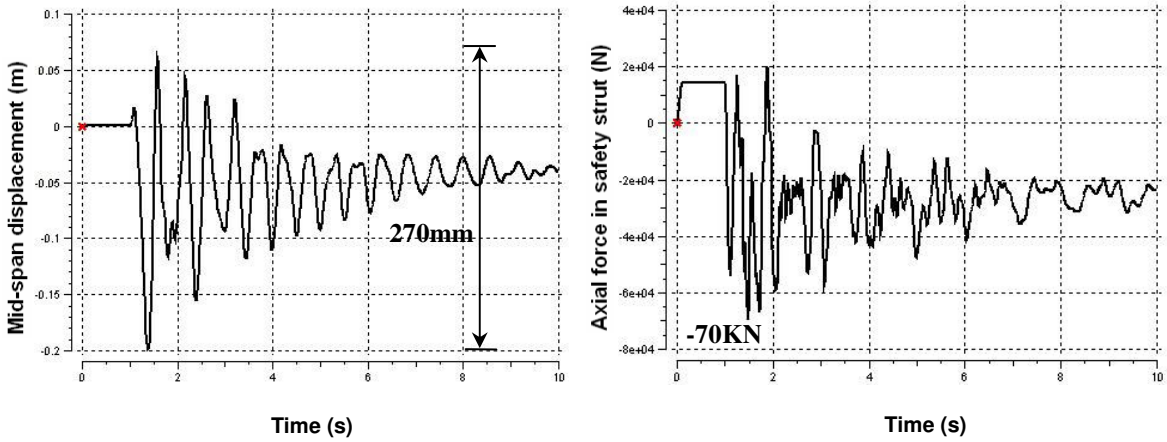

(a) (b)

Fig. 6.12. Time histories of (a) vertical displacement at arch's mid-span and (b) axial force in safety strut of Two-wing butterfly structure with t_{loss} = 0.1s

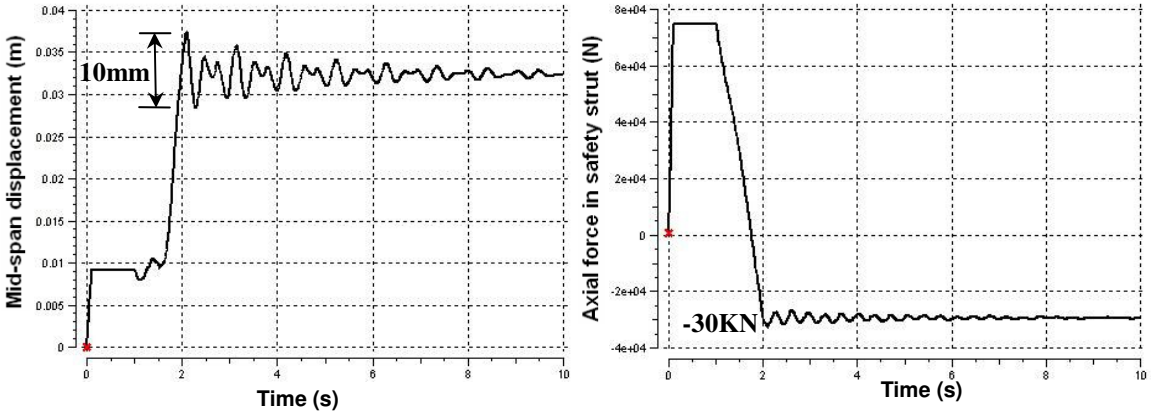

(a) (b)

Fig. 6.13. Time histories of (a) vertical displacement at arch's mid-span and (b) axial force in safety strut of Three-wing butterfly structure with t_{loss} = 1s

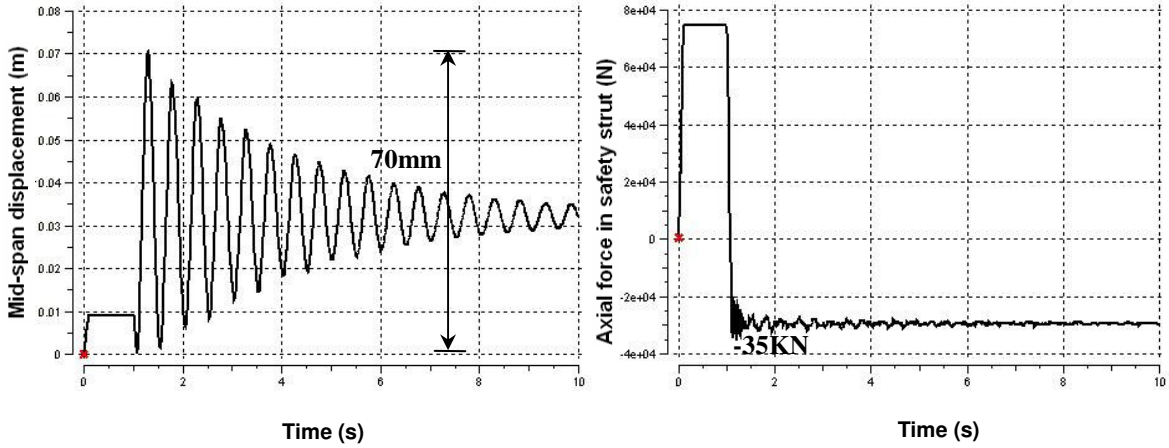

(a) (b)

Fig. 6.14. Time histories of (a) vertical displacement at arch's mid-span and (b) axial force in safety strut of Three-wing butterfly structure with t_{loss} = 0.1s

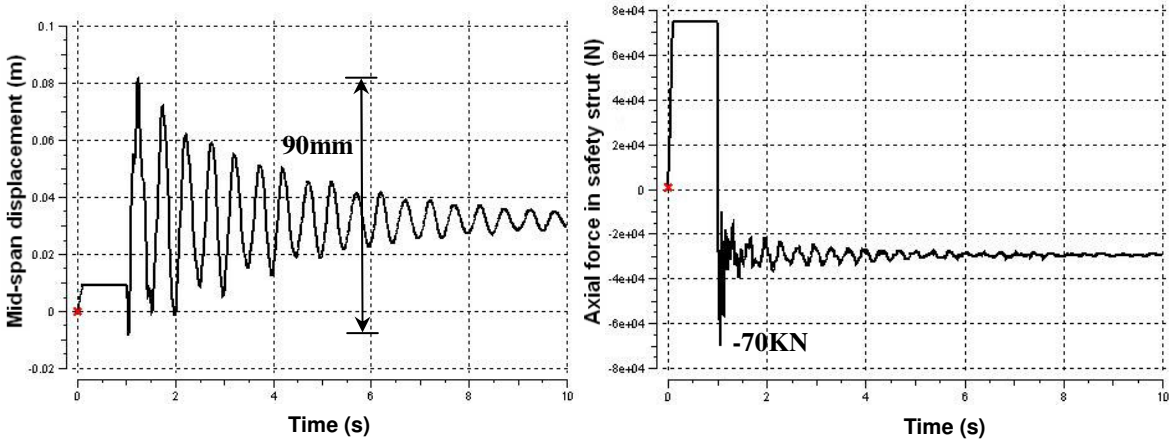

(a) (b)

Fig. 6.15. Time histories of (a) vertical displacement at arch's mid-span and (b) axial force in safety strut of Three-wing butterfly structure with t_{loss} = 0.01s

From the above results, it can be seen that the supporting arches of Two-wing and Three-wing butterfly structures can resist the dynamic impact induced by the sudden loss of membrane tension forces in the durations as short as 0.1s and 0.01s respectively. Although the sudden damage of membrane in Butterfly-wing structures is expected, it is unlikely that a total membrane area of over 1000m^2 can be damaged within 0.1s. Therefore it can be deduced that the supporting arches should not collapse and thus the Butterfly-wing structures optimally designed in chapter 5 are safe in the event of entire membrane suddenly damaged due to accident or vandalism. In general, the safety of Butterfly-wing structures in case of sudden loss of membrane can be ensured by designing the safety struts of adequate resistance.

6.4. Robustness against fire

Owing to the unique characteristics of membrane materials in fire, membrane structures such as DSTMS and Butterfly-wing structures tend to perform in a very different way as compared to traditional building structures during fire. They are often self-venting when exposed to fire. This is one of the useful characteristics of membrane structures because a highly ventilated space generally does not result in an intense fire which is clearly a benefit. Therefore, it is necessary to investigate the characteristics of membrane materials to consider the real behaviour of membrane structures in fire.

6.4.1. Fire characteristics of membrane materials

As mentioned in Chapter 5, the most common materials used for membrane structures are PVC coated polyester and PTFE coated fiberglass fabrics. Both PVC and PTFE

fabrics are made of polymer plastic which will not support combustion. For deployable membrane structures, PVC fabric is preferred than PTFE fabric due to its high flexibility. However, the fire characteristics of both fabrics will be presented in this chapter.

6.4.1.1. Fire characteristics of PVC coated polyester fabric

PVC coated polyester fabric can be described as a flame retardant material (Seaman, 1984). PVC fabric is actually a limited combustible material, which can ignite when introduced to persistent flaming but will be self-extinguishing upon removal of the heat source. It will not support combustion because a greater level of energy is required to degrade the material than that produced in the combustion process, thus such combustion will discontinue without added energy from the fire source. The material begins to degrade and melt at about 200-250°C and will be self-extinguishing when burned away from the fire source. This results in a hole created through the fabric panel. The size of the hole is in proportion to the size of the fire. However, before the PVC fabric is burned off, it ruptures at lower temperature as seams between the membrane panel slide apart at temperature above 100°C (Forster and Mollaert, 2004). Due to this self-extinguishing characteristic, conventional test methods for definition of combustibility as UBC Standard 4-1 or ASTM E136 are not intended to apply for PVC fabric. Flame spread tests such as ASTM E84 (formerly UBC 42-1) or BS7837 are the most appropriate to assess the actual performance of PVC fabric in real fire situation. Typical PVC fabric should pass the flame spread rating which do not support combustion, propagate flame or contribute fuel to fire and will immediate self-extinguish when a flame source is removed.

6.4.1.2. Fire characteristics of PTFE coated fiberglass fabric

PTFE coated fiberglass fabric is classified as non-combustible materials. It performs well when tested in accordance with almost standard prescribed fire tests such as ASTM E-136, ASTM E-108 and BS 476 Part 3, 5, 7. It can be heated up to temperature of 700-900°C without combustion. However, the seams of PTFE fabric fail at temperature of about 250°C. This results in local detensioning of the fabric which creates a hole in the membrane roof panel.

Apart from that, high level of toxicity may be generated if PTFE fabric is heated within a temperature of 450-700°C (Mick and Adam, 2003). However, this potential toxic hazard happens in very limited conditions. When temperature is out of the range 450-700°C or when the material is itself flaming or enveloped in a flame, toxicity will not occur.

6.4.2. Behaviour of membrane structures in fire

Unlike fire scenario in traditional building construction in which heat is building up in a confined space, the venting characteristic of membrane materials in fire leads to the distinguished performance of membrane structures during fire. Though it is dependant on the type of membrane materials, most membrane structures demonstrate similar behaviour when exposed to an internal fire.

The fire often starts burning locally in the enclosure. Hot smoke is produced and rises to the roof. The smoke becomes hotter so that the fabric membrane portion above or

adjacent to the fire location is heated up locally, causing the failure of seams connecting the membrane panels. The temperatures for seam failure of PVC and PTFE fabrics are 100°C and 250°C respectively. This results in the local retraction of unstressed fabric, creating a hole in the building roof through which the intense heat, smoke and harmful gas are discharged. While PTFE fabric is not combustible, PVC fabric may be involved locally in the fire but does not propagate to surrounding membrane surfaces that are not directly exposed to the fire. According to Mick & Adam (2003), this behaviour offers several advantages against traditional buildings as follows:

- The structure becomes self-venting at considerable low temperature (below 300°C), allowing smoke, harmful gas and intense heat to escape the enclosure thus reducing the exposure of structural members and building contents to fire. The greater the fire is, the larger the venting-hole is created. It is noted that gases produced in fire will remain in the buoyant gas layer and do not cause hazard until sufficient smoke and gas has been produced to fill the space. According to Buchanan (2001), only if the confined space is able to trap hot smoke so that the hot air temperature is heated up 600°C, the flashover will happen to cause hazard to structural members. With the creation of venting hole, at no time during the fire does the temperature reach a point that could cause damage to structural components. For steel material, it is demonstrated that strength reduction is negligible if temperature in steel is less than 550°C (EC 3, Part 1.2; BS 5950, Part 8).
- The self-venting behaviour of membrane structures also facilitates the evacuation in fire scenario. It helps to limit the accumulation of smoke in the occupied space, thus maintaining greater visibility of escape routes in the event

of fire. Toxic gases are also vented out through the hole without spreading into lower areas to harm occupants.

- The formation of venting hole in the roof allow the fire fighters to battle the fire without entering the building, thus preventing the possible danger happened to them.

The time to create venting hole in the structure depends not only on the type of membrane fabrics and but also on the height of the roof above the fire location. When the height of the space increases, the potential for self-venting reduces or requires relatively large time. However, the size of the smoke reservoir also increases so that the buoyant smoke will accumulates in the upper part of the enclosure, limiting the spread of toxic smoke into the lower occupied areas.

In the present study, the above described behaviour will be taken into account for determining the fire resistance of membrane structures.

6.4.3. Fire resistance of membrane structures

As membrane is damaged at low fire temperature, the fire resistance of membrane structures in this thesis, including DSTMS and Butterfly-wing structures, should be understood as the fire resistance of the steel supporting structure in fire. In practical fire engineering, fire resistance of steel structures is commonly determined through the fire resistance capacity of structural components which need to be larger than the required fire resistance period. The fire resistance period requirements are normally specified in the Codes for different types of structural components (e.g. Tables 9 & 10 of BS 5950: Part 8: 2003). The fire resistance capacity of structural components is

traditionally determined through experiment where standard components are subjected to ISO standard fire with definite loads implemented (Buchanan, 2002). According to this approach, the structural components of steel structures need to be protected in most cases with fire-proofing material to increase their fire resistance duration. Although the experiment-based traditional approach is simple for understanding and applying, it is not scientific. First, the temperature increase of an actual fire is usually different from that of standard fire, especially for the fire in large space membrane structures such as DSTMS and Butterfly-wing structures. In addition, the effect of load ratio, which is the ratio of the applied load in fire situation to the load bearing capacity of components at ambient temperature, is not taken into account.

In order to overcome the shortcoming of the experiment-based traditional approach, the performance-based approach (Meacham and Custer, 1995) may be employed. With this approach, the fire resistance of a steel structure is determined according to its performance in real fire. In the present study, a procedure for determining the fire resistance duration of large space membrane structures is proposed as shown in Fig. 6.16. In this procedure, the behaviour of large space membrane structures in fire is considered in selecting the natural fire model. The characteristics of the fire are considered in modelling the fire curve. The structural properties and configurations are considered in determining the temperature increase in structural components. The effect of load ratio is taken into account in determining the limiting temperatures of structural components. The thermal stress induced in structures is not yet captured in the procedure. However, its contribution is negligible to the load ratio. In the subsequent sections, this procedure will be illustrated step by step through determining the fire resistance capacity of DSTMS and Butterfly-wing structures.

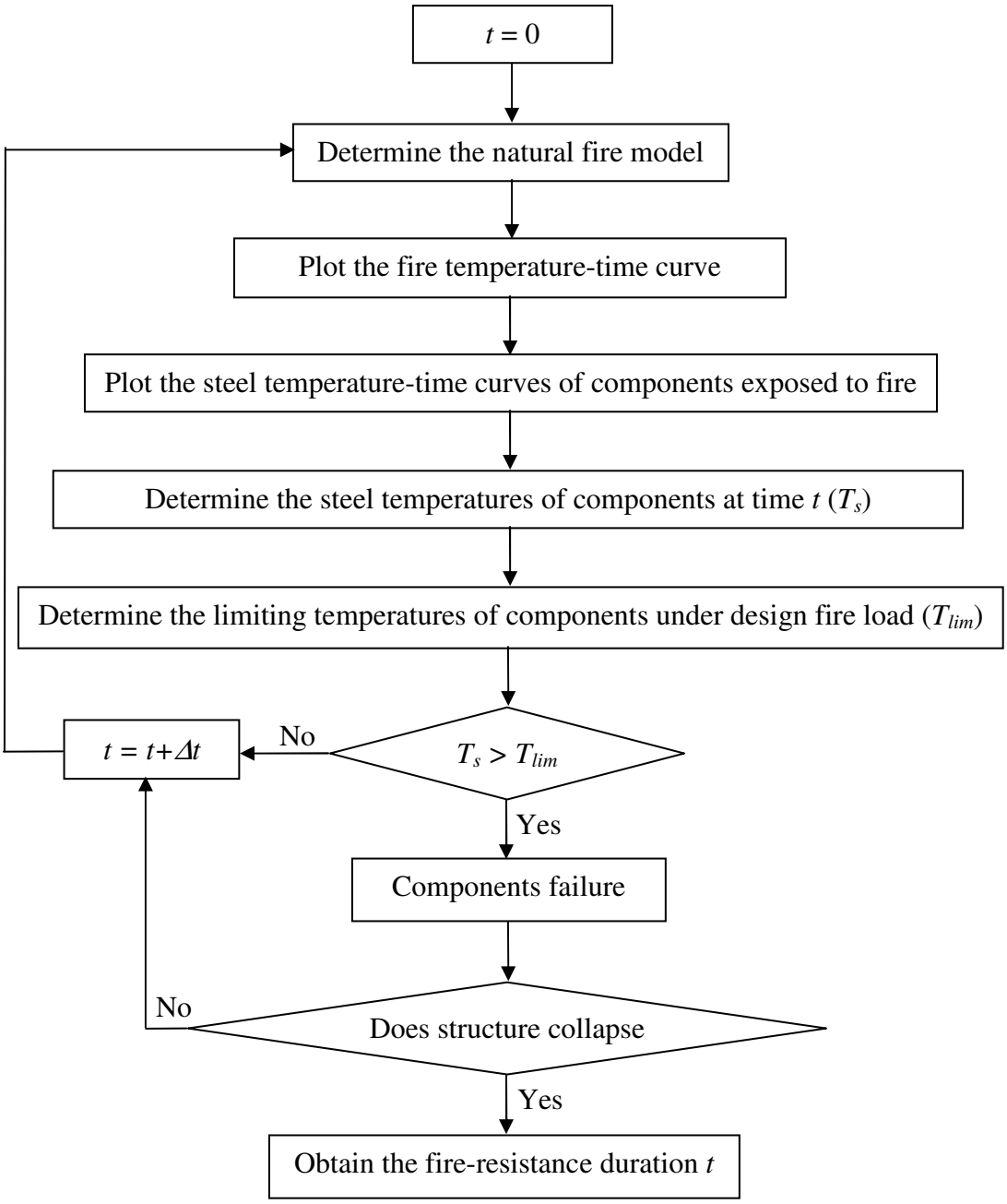

Fig. 6.16. Procedure for determining structural fire resistance

6.4.4. Natural fire model

In the reality, there are four stages which may be involved in fire development in an enclosure: ignition stage, fire growth stage, fully burning stage and decay stage (Fig. 6.17).

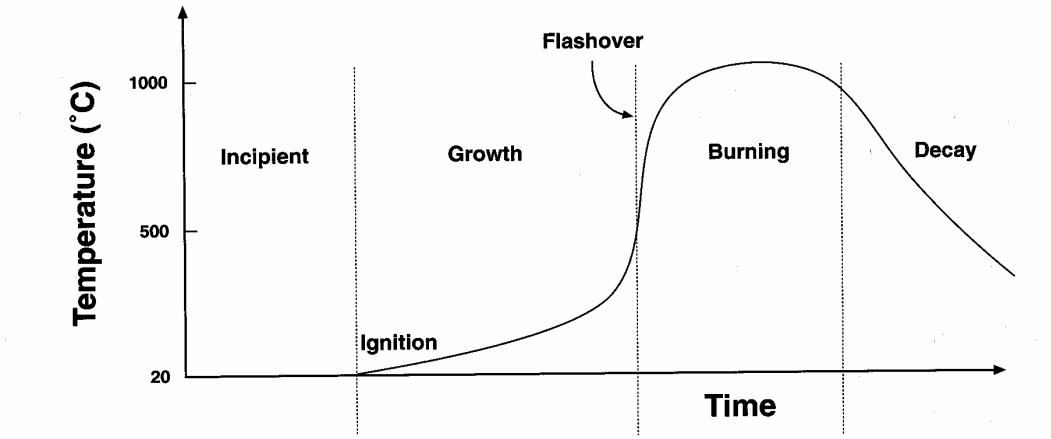

Fig. 6.17. Fire development in an enclosure (Wang, 2002)

- The fire incident starts from the ignition stage where the combustion materials placed near the ignition source catch fire. It causes smoke and heats up the surrounding environment.
- A local fire is burning in the growth stage. Hot smoke is produced and rises up to the ceiling. The smoke becomes hotter and the radiant heat from the smoke becomes more intense. The temperature inside the enclosure is typically below 500°C.
- Flashover is the transition from localized fire to a fully developed fire. Flashover happens when the following conditions are met: sufficient fuel and ventilation for fire to develop; the ceiling must be able to trap hot gases; radiant heat from the smoke to reach critical level to ignite all the combustible materials in the enclosure and cause them to burn; hot air temperature in the enclosure is about 600°C (Buchanan, 2002). In this stage, the entire enclosure is burning and the temperature may reach 1000°C, causing damage to almost all structural members exposed to fire.

- The fire starts to decay when about 70-80% of the fuel has been consumed. There is a transition from ventilation-controlled to fuel controlled fire and the fire continues until all fuel is consumed.

As described in section 6.4.1, either the PVC fabric is melt or the seam of PTEF fabric failed at temperature of about 250°C, creating venting hole in the roof. The venting hole prevents the happening of flashover and limits the propagation of the fire across the building as it would have occurred in a confined space. As a result, fire in membrane structures is usually limited to the second stage which is a typical local fire.

On the other hand, in large space building structures, it is hard for a fire to produce flashover which normally happen in building room less than 20mx20mx4m (Li, 2006). The fire will concentrate to a certain area and transport. The upper air-layer of the building is hot but the lower layer is still cool. Therefore, the temperature elevation of large space fire is slow and low, and thus large space fire is often restricted to a local fire.

Since DSTMS and Butterfly-wing structures are relevant to both membrane structures and large space enclosures, the fire in these structures is most likely to be localized. Thus, in this thesis, localized fire model defined in Eurocode 1: Part 1-2 (2001) is adopted for modelling the fire in DSTMS and Butterfly-wing structures. It is assumed that DSTMS are used for enclosing a workshop and Butterfly-wing structures are used for covering an amphitheatre. According to the architectural design and functions of these structures, the following assumptions are employed in determining the relevant design fire scenarios:

a. Large design fire sizes Q_{max} are assumed, which are 25MW for DSTMS and 10MW for Butterfly-wing structures. According to EC1: Part 1:2 (2001), the fire load density $q_{f,k}$ is taken as 500MJ/m^2 for workshop (DSTMS) and 300MJ/m^2 for amphitheatre (Butterfly-wing structures);
b. Room temperature is taken as 20°C and combustible materials are located on the floors;
c. The fire growth rate is assumed to be "fast" with time needed to reach a rate of heat release of 1MW t_α = 150s. The corresponding heat release rate per unit area RHR_f is taken as 500kW/m^2 and 250kW/m^2 for DSTMS and Butterfly-wing structures respectively (EC1:Part 1:2);
d. Conservatively assumed that automatic fire fighting systems will not decrease the heat release rate of the fire;

The corresponding fire area A_{fi} = Q_{max}/RHR_f, equivalent diameter of the fire $D_{fi} = \sqrt{\frac{4A_{fi}}{\pi}}$ and total energy contained in fuel in the fire area E_{fi} = $q_{f,k}\, A_{fi}$ are summarized in table 6.1.

Table 6.1. Characteristics of design fire scenarios

Type of structure	A_{fi} (m^2)	D_{fi} (m)	E_{fi} (MJ)
DSTMS	50	8	25000
Butterfly-wing structure	40	7.1	12000

According to EC1:Part 1.2 (Annex C), the temperature $T(z)$ along the vertical flame axis of a localized fire is determined as:

$$T(z) = 20 + 0.25(0.8Q)^{2/3}(z - z_0)^{-5/3} \qquad [°C] \qquad (6.1)$$

Where z is the height (m) along the flame axis (Figs. 6.19 & 6.21) and z_0 is the virtual origin of the axis given by:

$$z_0 = -1.02D_{fi} + 0.00524Q^{2/5} \quad \text{[m]} \tag{6.2}$$

and Q is the rate of heat release of the fire. Its growing phase is determined as

$$Q = 10^6 \left(\frac{t}{t_\alpha} \right)^2 \quad \text{[W]} \tag{6.3}$$

The growing phase is limited by a horizontal plateau corresponding to a value of Q_{max}. The horizontal plateau is limited by the decay phase, assumed to be a linear decrease, starting when 70% of the fire load has been consumed.

The time t_1 - growing phase, t_2 - plateau phase and t_3 - decay phase of the localized fire are determined as follows:

- The time t_1 to reach maximum heat release rate Q_{max} can be determined from Eq. 6.3: $t_1 = t_\alpha \sqrt{\frac{Q_{\max}}{10^6}} (s)$. The corresponding energy released in this growing phase is the area under the curve, which is 1/3 of the enclosing rectangle $E_1 = \frac{t_1 Q_{\max}}{3} (MJ)$
- The energy released in the decay phase $E_3 = 30\% E_{fi} (MJ)$ is the area of the enclosing triangle underneath. The time t_3 of this decay phase is given by $t_3 = \frac{E_3}{Q_{\max}/2} (s)$
- The energy released in the horizontal plateau $E_2 = E_{fi} - E_1 - E_3 (MJ)$ is the area of the enclosing rectangle underneath. The time t_2 of the horizontal plateau is given by $t_2 = \frac{E_2}{Q_{\max}} (s)$

The times t_1, t_2 and t_3 of DSTMS and Butterfly-wing structures are tabulated in Table 6.2. Their rate of heat release curves are plotted as shown in Fig. 6.18.

Table 6.2. Phase time of heat release rate

Type of structure	t_1 (s)	t_2 (s)	t_3 (s)
DSTMS	750	450	600
Butterfly-wing structure	474	682	720

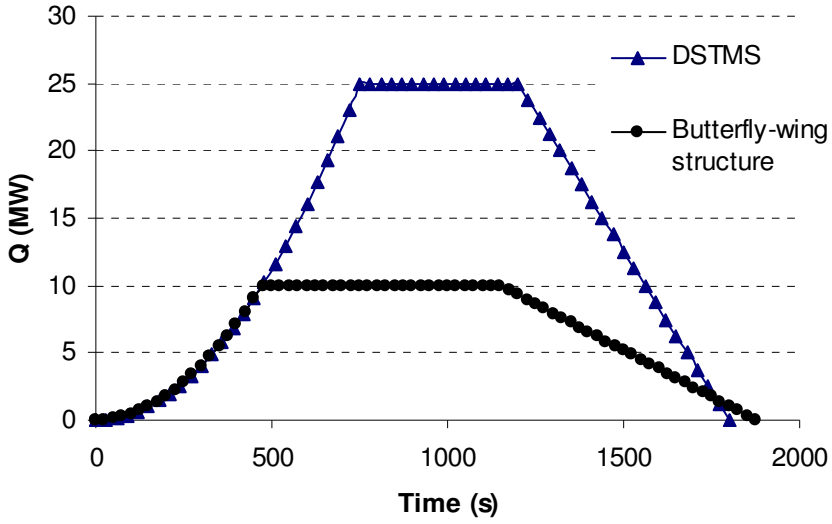

Fig. 6.18. Rate of heat release curves for different structures

The temperature of the localized fire defined in Eq. 6.1 is mainly dependant on the maximum heat release rate Q_{max} of the fire and the height (z) of the space. The fire temperature is directly proportional to the maximum heat release rate while inversely proportional to the height of the space. Obviously, the higher value of maximum heat release rate results in the higher heat of the fire. On the other hand, the higher the space means the longer the distance to the fire source, and thus the less thermal action of the fire to structural members.

Apart from that, the fire growth rate also affects the rate of heat release curve, and thus the fire temperature curve. The faster the growth rate, the longer the horizontal plateau phase (t_2) and thus the longer the period of maximum fire temperature. Since the temperatures of steel members exposed to fire increase slower than the fire temperature, the longer period of maximum fire temperature means the more available time for the temperatures of steel members to reach the ultimate fire temperature.

In the subsequent sections, critical fire locations and fire temperature-time curves of DSTMS and Butterfly-wing structures will be determined and presented.

6.4.4.1. Fire in Deployable strut-tensioned membrane structures

In DSTMS, the fire is assumed to happen at the corner and at the middle of the structures which are the most critical locations due to high resultant force. The critical fire locations are illustrated in Fig. 6.19. The surrounding support is assumed to be fully thermal insulation (e.g. concrete).

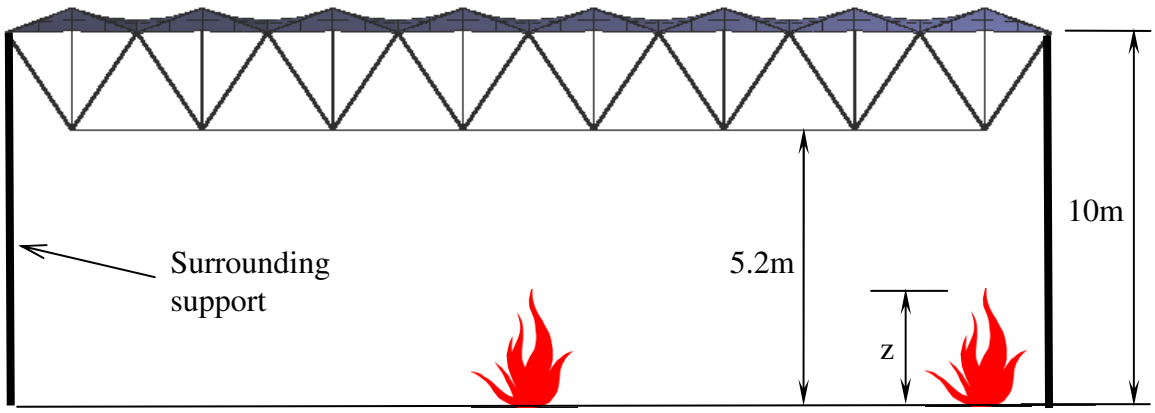

Fig. 6.19. Critical fire locations in DSTMS

In the present study, the clear height of both Umbrella and Cone-shaped DSTMS was chosen as 5.2m which is relative low for workshop. As the module depth = 1/10span = 4.8m, the height from the floor to membrane roof is 10m (see Fig. 6.19). The temperature-time curves of the fire at different height-levels of the structures are calculated based on Eq. 6.1 and plotted in Fig. 6.20. It can be seen that the fire temperature at membrane roof level (10m) is about 270°C. At this temperature, the PVC membrane will be burnt off and a venting hole will be created on the roof at the fire location.

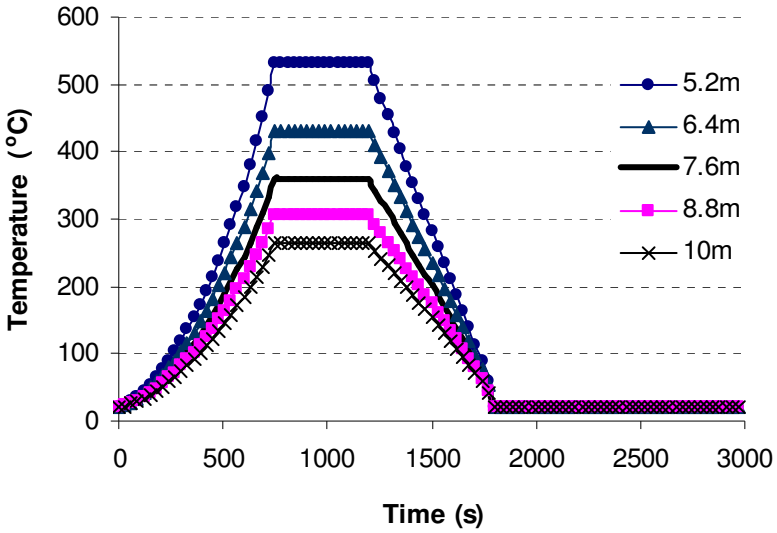

Fig. 6.20. Temperature-time curves at different height-levels of DSTMS

6.4.4.2. Fire in Butterfly-wing structures

In Butterfly-wing structures, the unfavourable fire location is at the support of the arch, where the structural members are closest to the fire source. However, there is a distance of 1.22m between the fire location and the support point (Fig. 6.21) due to a barrier which is designed to ensure the clearance height of 2m at the support location.

The barrier is assumed to be fully thermal insulation (e.g. concrete). The unfavourable fire location of Butterfly-wing structures is illustrated in Fig. 6.21.

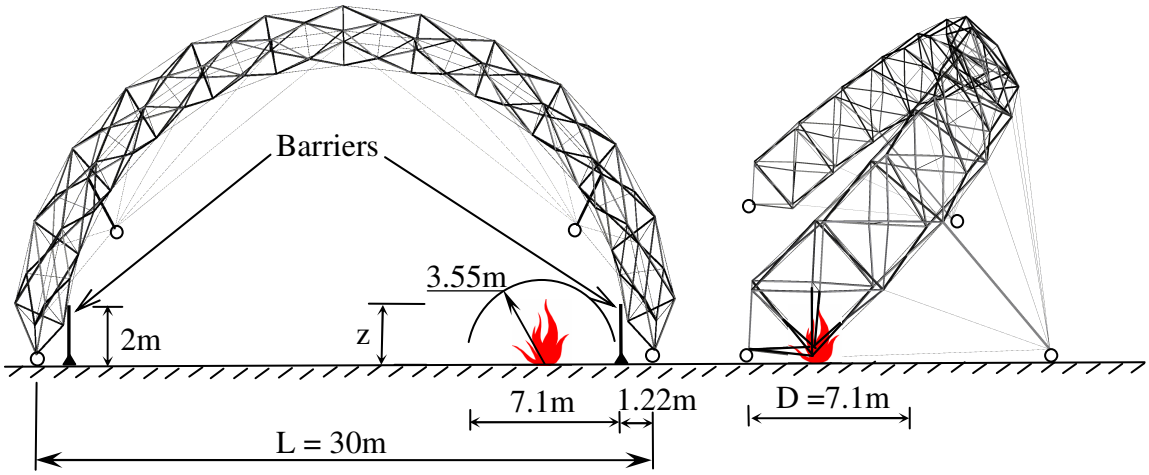

a. Front view b. Side view

Fig. 6.21. Unfavourable fire location in Butterfly-wing structures

The temperature-time curves of the fire at different height-levels of the structures are calculated based on Eq. 6.1 and plotted in Fig. 6.22. The closest distance from fire source to the membrane is 2.9m. It can be seen from Fig.6.22 that, at this level, the fire temperature is above 400°C which will burn off the PVC membrane. Although the membrane will be self-extinguished when burned away from the fire location, membrane damage due to tear propagation should be taken into account since the membrane span continuously between the arches. This critical scenario will be considered later when determining the fire resistance of Butterfly-wing structures.

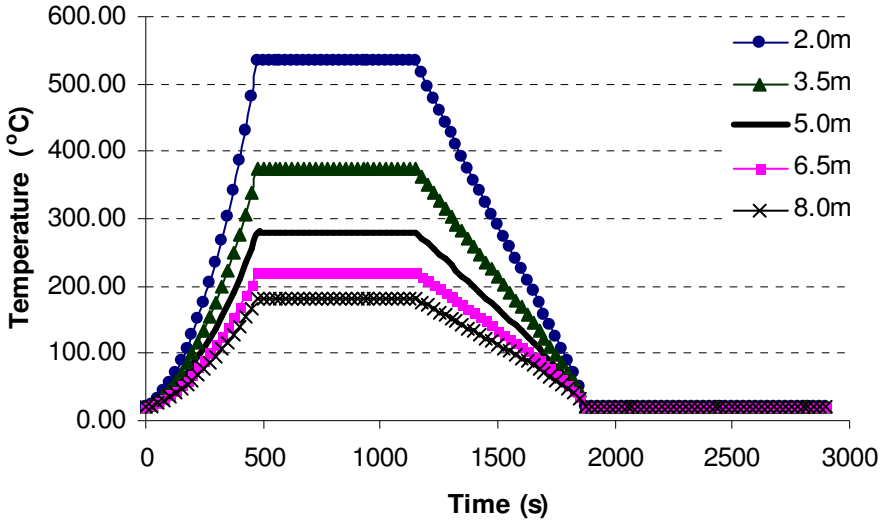

Fig. 6.22. Temperature-time curves at different height-levels of Butterfly-wing structures

6.4.5. Temperatures in steel members exposed to fire

The increase of temperature in an unprotected steel member can be calculated in accordance with EC3: Part 1-2:

$$\Delta T_s = \frac{h}{\rho C_s}\frac{A_m}{V}\left(T_{fi} - T_s\right)\Delta t \qquad [°C] \qquad (6.5)$$

where:

h is heat transfer coefficient per unit area, $h = h_r + h_c$ $\quad [W/m^2K]$

$h_r = \dfrac{\varepsilon_r \sigma\left[(273+T_{fi})^4 - (273+T_s)^4\right]}{(T_{fi} - T_s)}$ is the radiant heat transfer coefficient $[W/m^2K]$

h_c is the convective heat transfer, $h_c = 35\ W/m^2K$ for natural fire

ε_r = resultant emissivity = 0.7

σ = Stephan Boltzmann constant = 5.67 x 10^{-8} W/m^2K^4

A_m/V = section factor (m^{-1}) of the exposed steel member per unit length

T_{fi} = fire temperature (°C) at particular time t (sec), taken from Eq. 6.4.

T_S = steel temperature (°C), assumed to be uniform, at time t

The member temperatures of DSTMS and Butterfly-wing structures are calculated according to Eq. 6.5 using step by step procedure and presented in the subsequent sections.

6.4.5.1. Temperatures in steel members of DSTMS

Figures 6.23 & 6.24 show the temperature-time curves of the diagonal strut, top strut, vertical strut and bottom cable of Umbrella and Cone-shaped DSTMS which are nearest to the fire source. It can be observed that the temperature of top strut was lower than those of other members. This can be explained by the higher level in elevation of the top strut, which means the longer distance to the fire source and thus the less thermal action of the fire to the top strut. Apart from the distance to the fire source, the other factor affects the temperature of members is the section factor which is directly proportional to the temperature increase in member. This factor can be used to explain for the difference in temperature curves of the vertical strut, diagonal strut and horizontal cable although they have the same distance to the fire source.

The maximum member temperatures T_{max} of Umbrella and Cone-shaped DSTMS are summarized in tables 6.3 & 6.4. These temperatures will be compared with the limiting temperatures of corresponding members. Refer to Figs. 5.1 & 5.2 for the definition of diagonal strut, top strut, vertical strut and bottom cable.

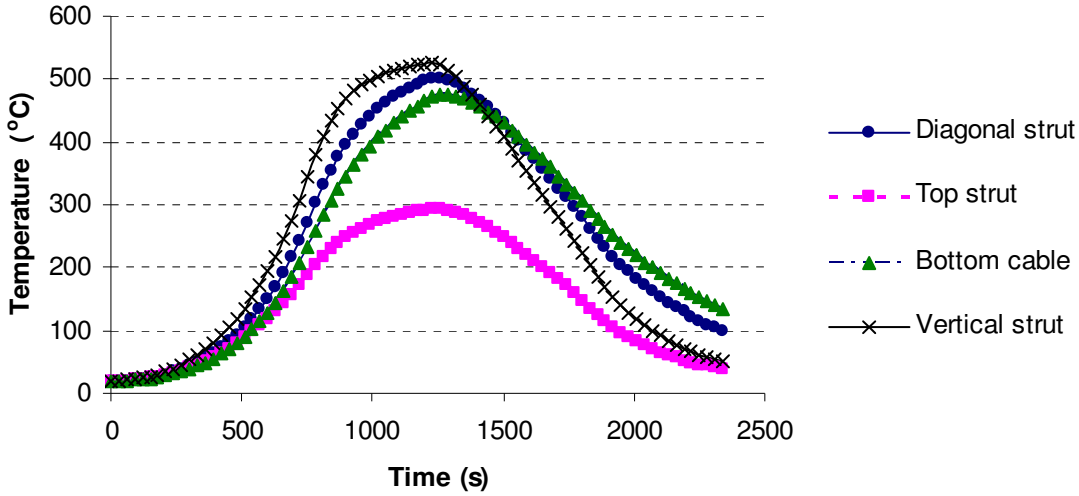

Fig. 6.23. Temperatures in steel members of Umbrella DSTMS exposed to fire

Table 6.3. Maximum member temperatures of Umbrella DSTMS

Type of member	Diagonal strut	Top strut	Vertical strut	Bottom cable
Section (*mm*)	O168.3x5	O114.3x3.2	O114.3x3.2	ϕ26
T_{max} (℃)	502	294	526	475

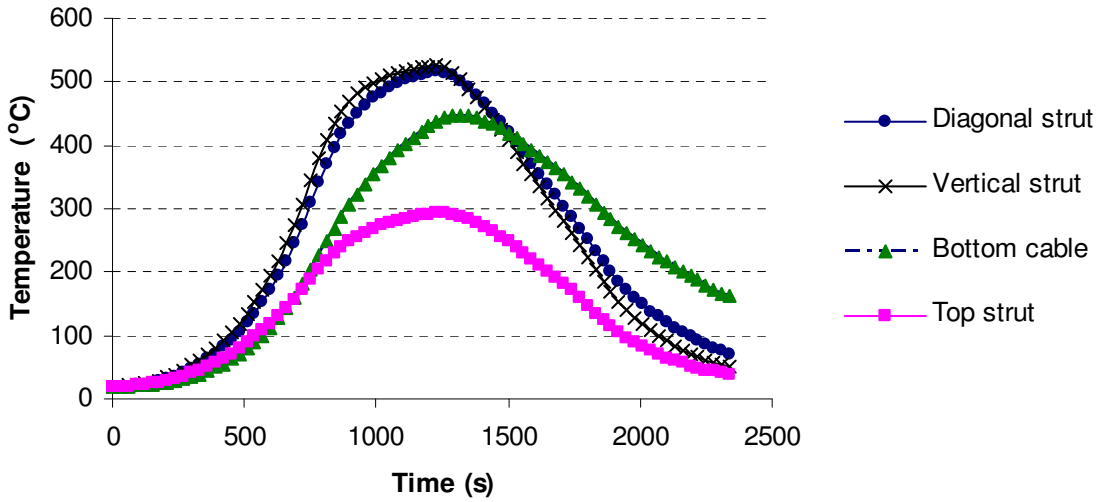

Fig. 6.24. Temperatures in steel members of Cone-shaped DSTMS exposed to fire

Table 6.4. Maximum member temperatures of Cone-shaped DSTMS

Type of member	Diagonal strut	Top strut	Vertical strut	Bottom cable
Section (*mm*)	O159x4	O108x3.2	O108x3.2	ϕ32
T_{max} (℃)	517	294	526	447

6.4.5.2. Temperatures in steel members of Butterfly-wing structures

Figures 6.25 & 6.26 show the temperature-time curves of the steel members of Two-wing and Three butterfly structures which are nearest to the fire source. The central cable and horizontal cable had the same temperature curve since they have the same section factor. Similarly, it can be observed that the temperature curves of scissor strut and pyramid strut seem coincided since the difference in their section factors is minor. The temperature curve of safety strut was lower than those of other members due to its longer distance to the fire source. The maximum member temperatures T_{max} of Two-wing and Three-wing butterfly structure are summarized in tables 6.5 & 6.6. Refer to Figs. 5.18 & 5.19 for the definition of scissor strut, pyramid strut, safety strut horizontal cable, central cable and anchor cable.

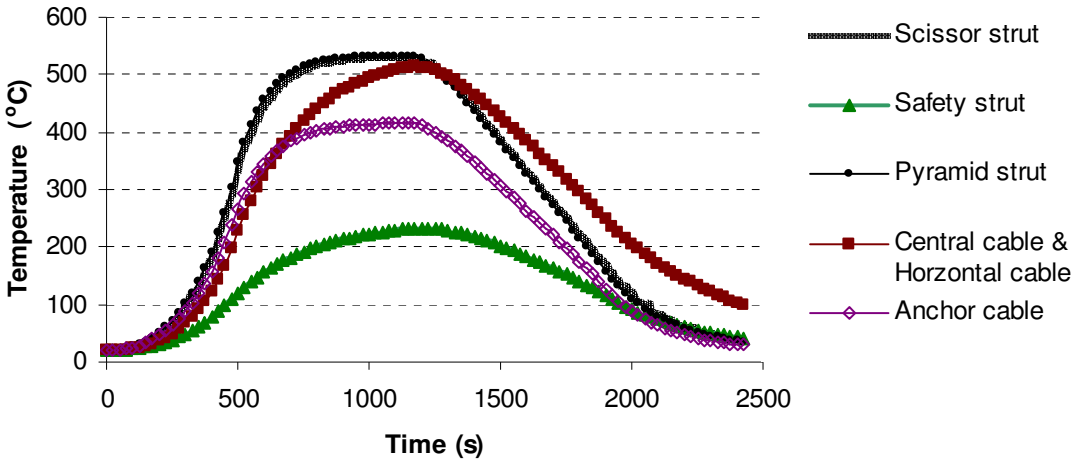

Fig. 6.25. Temperatures in steel members of two-wing butterfly structure exposed to fire

Table 6.5. Maximum member temperatures of Two-wing butterfly structure

Type of member	Scissor strut	Pyramid strut	Safety strut	Central cable	Horizontal cable	Anchor cable
Section (mm)	⌊80×3.6	⌊70×3.6	⌊100×5	ϕ26	ϕ26	ϕ12
T_{max} (℃)	533	533	233	513	513	415

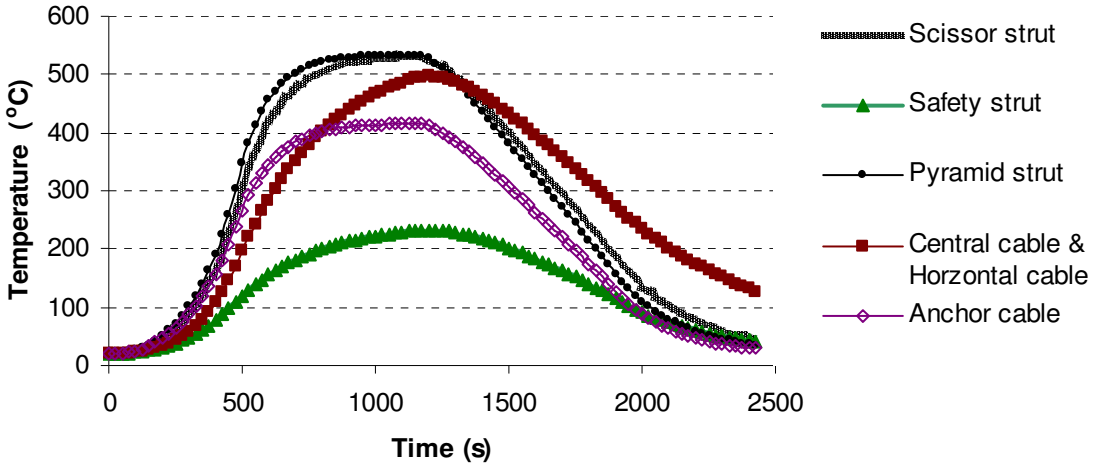

Fig. 6.26. Temperatures in steel members of three-wing butterfly structure exposed to fire

Table 6.6. Maximum member temperatures of Three-wing butterfly structure

Type of member	Scissor strut	Pyramid strut	Safety strut	Central cable	Horizontal cable	Anchor cable
Section (mm)	□100×4	□70×3.6	□100×5	ϕ32	ϕ32	ϕ12
T_{max} ($℃$)	531	533	233	496	496	415

6.4.6. Limiting temperatures of steel members exposed to fire

Since both DSTMS and Butterfly-wing structure were designed in accordance with BS 5950: Part 1 in chapter 5, accordingly in this study, the fire resistance of these structures will be determined by the limiting temperature method defined in BS 5950: Part 8 which is the Code of practice for fire resistance design. The limiting temperature T_{lim} of a structural steel member exposed to fire depends upon the load ratio of the member. Following are the load ratios for members in bending, in compression and in tension:

- Load ratio for members in bending:

$$R = \frac{M_f}{M_c} \qquad or \qquad R = \frac{mM_f}{M_b}$$

- Load ratio for members in compression:

$$R = \frac{F_f}{A_g p_c} + \frac{M_{fx}}{M_b} + \frac{M_{fy}}{p_y Z_y}$$

- Load ratio for members in tension:

$$R = \frac{F_f}{A_g p_y} + \frac{M_{fx}}{M_{cx}} + \frac{M_{fy}}{M_{cy}}$$

where

M_f is the applied moment at the fire limit state

M_b is the buckling resistance moment (lateral torisonal)

M_c is M_{cx} or M_{cy} as appropriate to the axis of bending, where they are the moment capacity of section about the major and minor axes in the absence of axial load

M is the equivalent uniform moment factor

A_g is the gross area

p_c is the compressive strength

p_y is the design strength of steel

F_f is the axial load at the fire limit state

M_{fx} is the maximum moment about the major axis at the fire limit state

M_{fy} is the maximum moment about the manor axis at the fire limit state

The limiting temperatures corresponding with the load ratio for members in bending, in compression and in tension are given in Table 8 of BS 5950: Part 8 (see Appendix B of this thesis). A structural steel member is considered as damaged when the temperature in that member T_s is higher than its limiting temperature T_{lim}. In the

subsequent section, limiting temperatures of structural members of DSTMS and Butterfly-wing structures will be determined and presented.

6.4.6.1. Limiting temperatures of steel members of DSTMS

The limiting temperatures of steel members of DSTMS are determined in two critical fire scenarios described in section 6.4.4.1: one at the corner of the structures where induced shear force is largest and another at the center of the structures where induced moment force is largest. Loading is taken in accordance with BS 5950: Part 8: 1990 applied for fire/accidental limit state:

- Load combination 1: 1.0 x self-weight + 0.8 x imposed load (where imposed load = 0.75kN/m^2, applied at all bottom nodes)
- Load combination 2: 1.0 x self-weight + 0.33 x wind uplift (where wind uplift pressure = 0.45kN/m^2)

a. Case 1 - Fire location at corner of structures

As mentioned in section 6.4.4.1, the membrane area above the fire source will be burnt off since the fire temperature at membrane roof level is higher than the melting temperature of the membrane material. All membrane parts involved in the fire range are assumed to be melt and detensioned, thus they will be removed as shown in Fig. 6.27 & 6.28. By determining the maximum member forces in the fire location, the load ratios and thus the limiting temperatures of steel members exposed to fire were determined and given in Tables 6.7 & 6.8. The positive and negative signs in front of the load ratio values denote the members in tension and compression respectively. The corresponding maximum member temperatures are also given for comparison.

Table 6.7. Critical temperatures of steel members exposed to fire at corner of Umbrella DSTMS

Type of member	Diagonal strut	Top strut	Vertical strut	Bottom cable
Section (*mm*)	O168.3x5	O114.3x3.2	O114.3x3.2	ϕ26
Length (*m*)	5.56	4.41	4.8	
R	(-) 0.5	(-) 0.66	(-) 0.51	(+) 0.12
T_{lim} (℃)	545	480	542	734
T_{max} (℃)	502	294	526	475

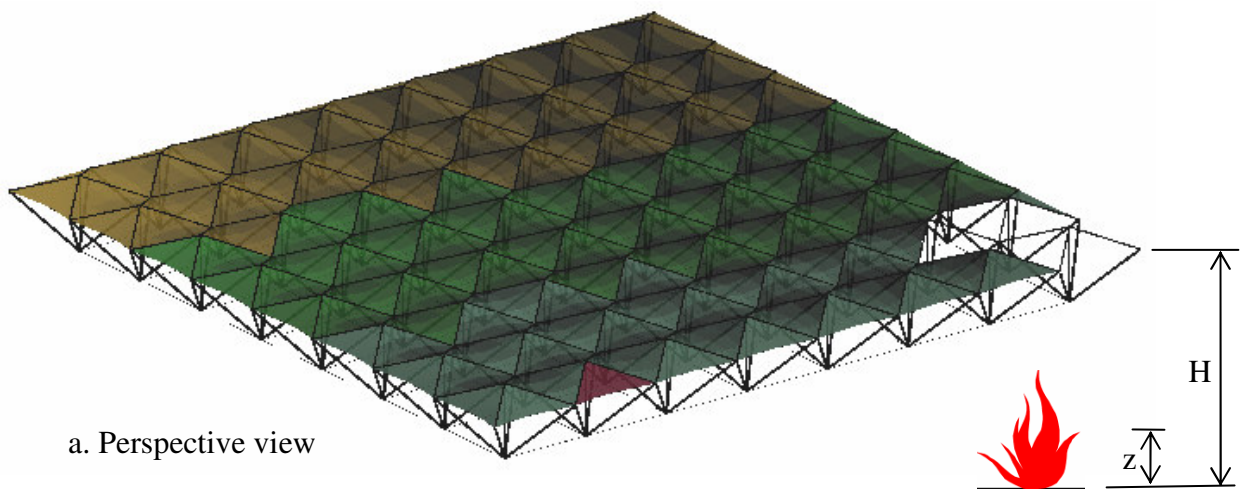

a. Perspective view

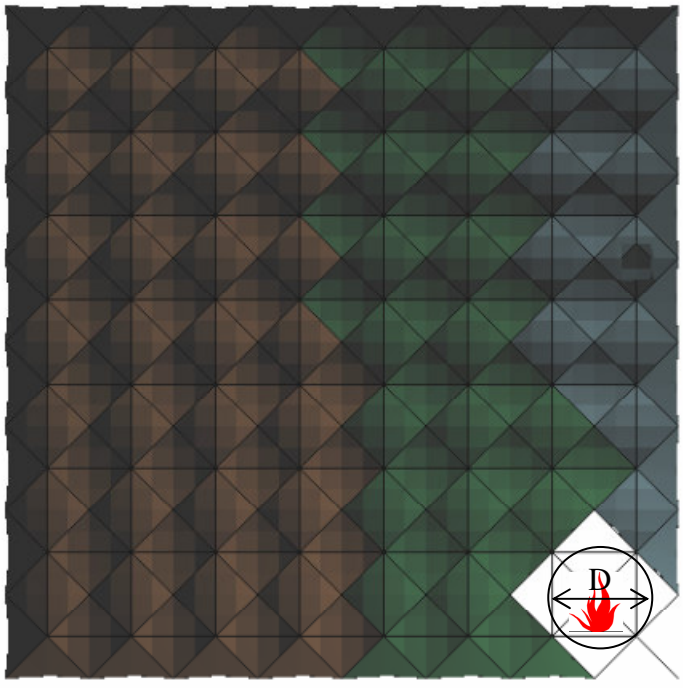

b. Plan view

Fig. 6.27. Fire location at corner of Umbrella DSTMS

Table 6.8. Critical temperatures of steel members exposed to fire at corner of Cone-shaped DSTMS

Type of member	Diagonal strut	Top strut	Vertical strut	Bottom cable
Section (*mm*)	O159x4	O108x3.2	O108x3.2	ϕ 32
Length (*m*)	6.41	4.41	3.6	
R	(-) 0.56	(-) 0.2	(+) 0.19	(+) 0.1
T_{lim} (℃)	524	635	696	745
T_{max} (℃)	517	294	526	447

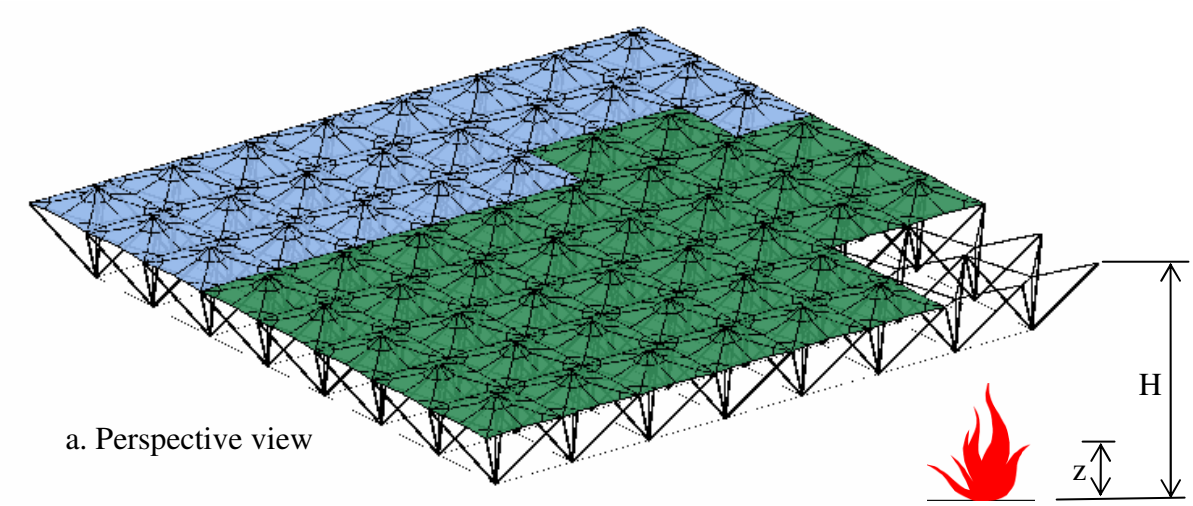

a. Perspective view

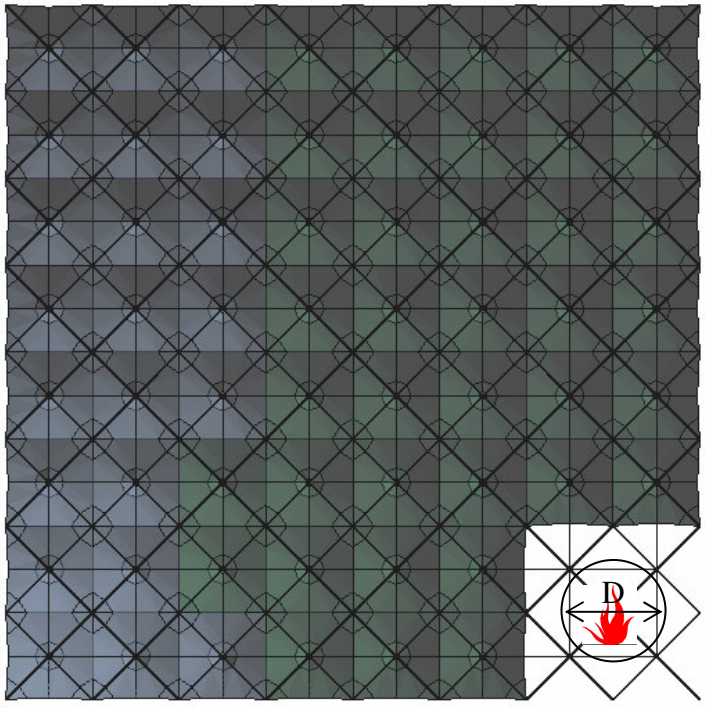

b. Plan view

Fig. 6.28. Fire location at corner of Cone-shaped DSTMS

b. Case 2 - Fire location at center of structures

Table 6.9. Critical temperatures of steel members exposed to fire at center of Umbrella DSTMS

Type of member	Diagonal strut	Top strut	Vertical strut	Bottom cable
Section (*mm*)	O168.3x5	O114.3x3.2	O114.3x3.2	ϕ26
Length (*m*)	5.56	4.41	4.8	
R	(-) 0.09	(-) 0.35	(-) 0.12	(+) 0.27
T_{lim} (℃)	635	613	635	652
T_{max} (℃)	502	294	526	475

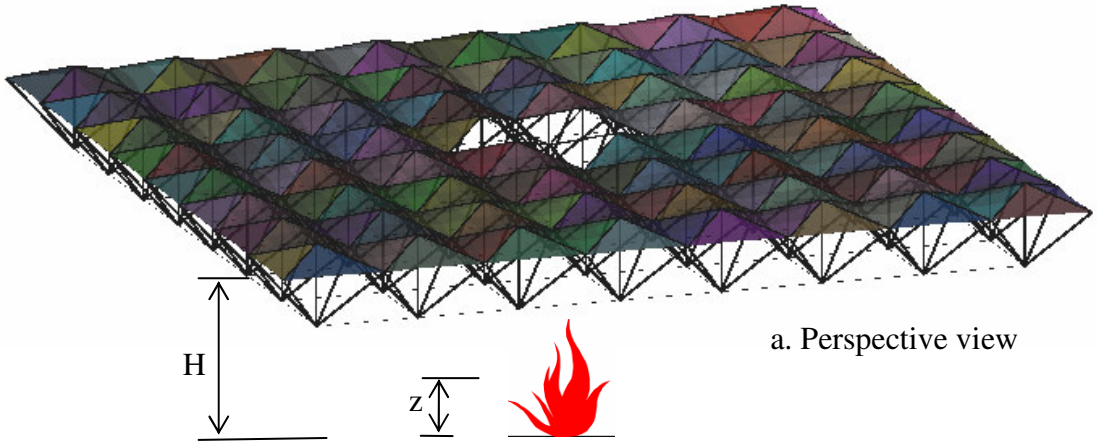

a. Perspective view

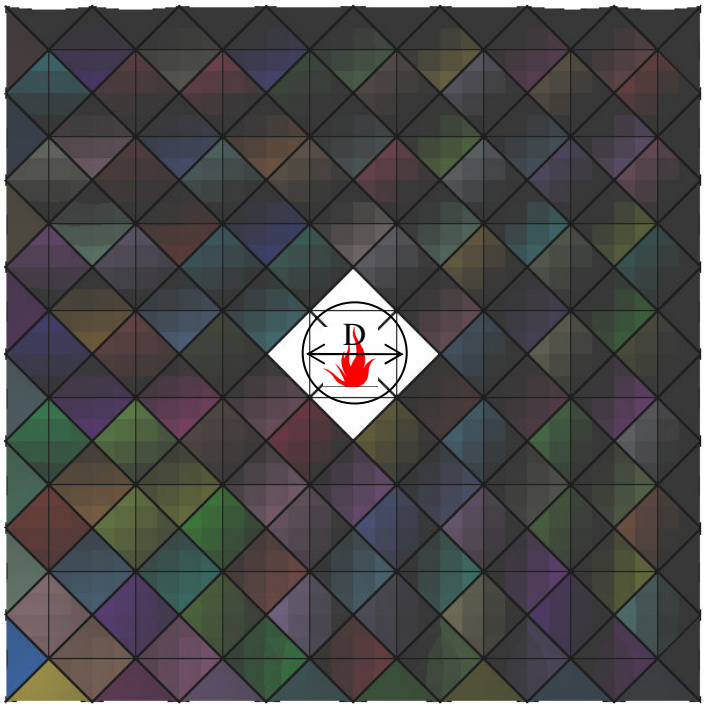

b. Plan view

Fig. 6.29. Fire location at center of Umbrella DSTMS

Table 6.10. Critical temperatures of steel members exposed to fire at center of Cone-shaped DSTMS

Type of member	Diagonal strut	Top strut	Vertical strut	Bottom cable
Section (*mm*)	O159x4	O108x3.2	O108x3.2	ϕ 32
Length (*m*)	6.41	4.41	3.6	
R	(+) 0.06	(-) 0.45	(-) 0.33	(+) 0.23
T_{lim} (℃)	967	636	685	741
T_{max} (℃)	517	294	526	447

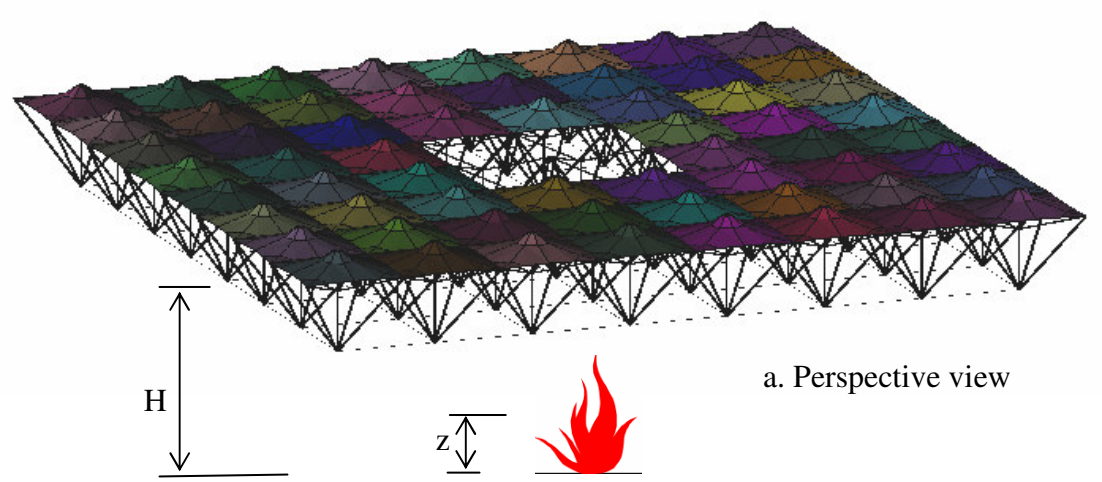

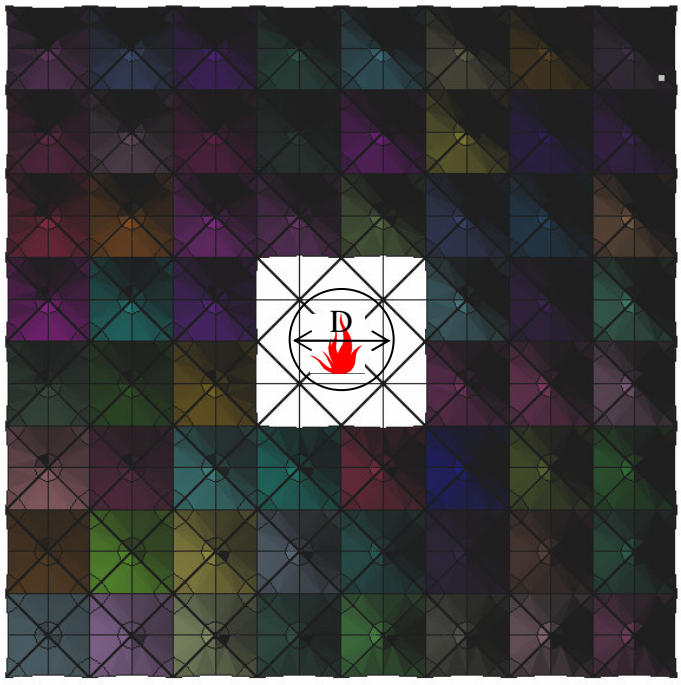

b. Plan view

Fig. 6.30. Fire location at center of Cone-shaped DSTMS

Similarly to the corner fire case, in the center fire case, the membrane parts at the center of the structures involved in the fire range are removed as shown in Figs. 6.29 & 6.30. The structures were analyzed with design loads in the fire situation to determine the member forces. With the maximum member forces in the fire location, the load ratios and thus the limiting temperatures of members exposed to fire were determined and the results are tabulated in tables 6.9 & 6.10. The corresponding maximum member temperatures are also given for comparison.

c. Discussion and conclusion

From the above results, it can be seen that all structural steel members of both DSTMS had the limiting temperatures larger than their maximum temperatures heated by the fire. It means that there is no member failure during the fire and thus the structures can fulfill any fire resistant duration requirement without fire protection. One possible reason is the limited temperature of the localized fire although the fire scenarios were designed in worst conditions such as high fire load, fast fire growth rate and critical fire locations. Another reason can be attributed to the structural configuration (structural height) which makes the distance far enough from structural members to the fire source. From the results, it can be concluded that the optimally designed DSTMS in chapter 5 are safe in the described fire scenario.

Apart from that, it can be observed that limiting temperatures of structural steel members in the corner fire case were lower than those in the center fire case. It means that the fire case at the corner of the structure was more critical than that at the center of the structure. This can be explained by the plate behaviour of DSTMS under gravity

load, in which the corners of the structures are subject to largest resultant forces, thus resulting in high load ratios in structural members. It is possible to conclude that the fire resistance duration of DSTMS can be increased if the fire is prevented from occurring at the corner of the structures.

In addition, it can be realized that the diagonal struts and vertical struts are the most critical members in the corner fire case since they had maximum member temperatures closest to their limiting temperatures. The reason is that they are both subjected to high load ratio and close distance to the fire source. This finding implies that fire resistance of DSTMS can be improved by providing fire protection to these critical members instead of protecting all structural members.

6.4.6.2. Limiting temperatures of steel members of Butterfly-wing structures

As mentioned in section 6.4.4.2, the membrane area closest to the fire source has a fire temperature above 400°C, thus it will be burnt off. There are two possible scenarios here. One can consider local damage of membrane at the fire location since the membrane is self-extinguishing once burnt away from the fire source. The other may take the tearing propagation in consideration since the membrane of butterfly-wing structures spans continuously between the arches, thus total membrane damage is expected. In the present study, the limiting temperatures of structural steel members of Butterfly-wing structures are determined in both scenarios.

a. Local membrane damage

Loading is taken in accordance with BS 5950: Part 8: 1990 applied for fire/accidental limit state:

- Load combination 1: 1.0 x self-weight + 0.33 x wind downward
- Load combination 2: 1.0 x self-weight + 0.33 x wind uplift

The values of wind downward and uplift pressures are the same as what was used in chapter 5. By determining the maximum member forces in the fire location, the load ratios and thus the limiting temperatures of structural steel members exposed to fire of two-wing and three-wing butterfly structures were found and summarized in tables 6.11 & 6.12. The positive and negative signs in front of the load ratio values denote the members in tension and compression respectively.

Table 6.11. Critical temperatures of steel members exposed to fire of Two-wing butterfly structure (in case of local membrane damage)

Type of member	Scissor strut	Pyramid strut	Safety strut	Central cable	Horizontal cable	Anchor cable
Section (*mm*)	□80×3.6	□70×3.6	□100×5	ϕ26	ϕ26	ϕ12
Length (*m*)	4.37	3.0	8.27			
R	(-) 0.42	(-) 0.32	(+) 0.01	(+) 0.03	(+) 0.13	(+) 0.08
T_{lim} (℃)	581	626	795	784	729	756
T_{max} (℃)	533	533	233	513	513	415

Table 6.12. Critical temperatures of steel members exposed to fire of Three-wing butterfly structure (in case of local membrane damage)

Type of member	Scissor strut	Pyramid strut	Safety strut	Central cable	Horizontal cable	Anchor cable
Section (*mm*)	□100×4	□70×3.6	□100×5	ϕ32	ϕ32	ϕ12
Length (*m*)	4.37	3.0	8.27			
R	(-) 0.4	(-) 0.41	(-) 0.12	(+) 0.03	(+) 0.22	(+) 0.2
T_{lim} (℃)	590	586	635	784	679	690
T_{max} (℃)	531	533	233	496	496	415

b. Total membrane damage

In the case of total membrane damage, the safety struts will prevent the collapse of the arches. The impact of the fire is unlikely to damage the whole membrane area in a short period, thus dynamic effect on the arch due to membrane damage can be neglected. By determining the maximum member forces in the fire location, the load ratios and thus the limiting temperatures of structural steel members exposed to fire of two-wing and three-wing butterfly structures were found and summarized in tables 6.13 & 6.14.

Table 6.13. Critical temperatures of steel members exposed to fire of Two-wing butterfly structure (in case membrane totally damaged)

Type of member	Scissor strut	Pyramid strut	Safety strut	Central cable	Horizontal cable	Anchor cable
Section (*mm*)	□80×3.6	□70×3.6	□100×5	ϕ26	ϕ26	ϕ12
Length (*m*)	4.37	3.0	8.27			
R	(-) 0.1	(-) 0.13	(-) 0.32	(+) 0.01	(+) 0.03	slackened
T_{lim} (℃)	635	635	626	795	784	
T_{max} (℃)	533	533	233	513	513	415

Table 6.14. Critical temperatures of steel members exposed to fire of Three-wing butterfly structure (in case membrane totally damaged)

Type of member	Scissor strut	Pyramid strut	Safety strut	Central cable	Horizontal cable	Anchor cable
Section (*mm*)	□100×4	□70×3.6	□100×5	ϕ32	ϕ32	ϕ12
Length (*m*)	4.37	3.0	8.27			
R	(-) 0.07	(-) 0.15	(-) 0.39	(+) 0.01	(+) 0.02	slackened
T_{lim} (℃)	635	635	595	795	789	
T_{max} (℃)	531	533	233	496	496	415

c. Discussion and conclusion

It can be seen from the above results that the limiting temperatures of structural steel members in local membrane damage case were lower than that in total membrane damage case. It can be explained by the higher member load ratios in the former due to wind force acting on membrane which no longer exists in the latter. In fact, when there is no membrane, the safety strut is the critical member and thus fire location near the safety strut's support may be more critical than that near the arch's support. However, if the fire is near the safety strut's support, the distance from the fire source to the membrane will be very large (over 10m), thus it will be unable to damage the membrane. Therefore, it can be concluded that it is not necessary to consider the scenario of total membrane damage in fire. On the other hand, the fire resistance duration of Butterfly-wing structures should be increased if fire is prevented from occurring near the arch's support.

Also from tables 6.11 – 6.14, it can be observed that limiting temperatures of structural steel members were larger than their maximum temperatures heated by the fire either in the case of local or total membrane damage. Similarly to DSTMS, the main reason is also due to the limited temperature of the localized fire which has no flashover stage. Another reason is attributed to the architectural function requiring a barrier at the support which prevents the fire from heating directly supporting struts at the ground level. It can be concluded from the results that the Butterfly-wing structures optimally designed in chapter 5 are safe in the described fire scenario. Apart from that, it can be realized from tables 11 & 12 of local membrane damage case that the scissor strut and pyramid strut had the highest maximum member temperatures and lowest limiting temperatures. This can be explained by the large section factors and high load ratios of

these members. Therefore, scissor strut and pyramid strut at the arch's support are the most critical members in fire. It can be deduced that the fire resistance of Butterfly-wing structures can be improved by protecting these critical members (including the supporting struts if barriers at arches' supports are not provided) instead of providing fire protection to all structural members.

6.4.7. Influence factors on fire resistance of membrane structures

The step-by-step procedure of the performance-based approach shown in Fig. 6.19 has been illustrated in determining the fire resistance of DSTMS and Butterfly-wing structures. This approach can ensure the fire safety of the structures without fire protection through considering their performance in real fire. According to this approach, the following factors have great influence on the capacity of fire resistance duration of large space membrane structures:

- Fire load: including the maximum heat release rate and the growth rate of the fire. While the maximum heat release rate is directly proportional to the temperature of the fire, the fire grow rate determine how fast the fire temperature and thus the structural member temperatures increase. Therefore, high maximum heat release rate and fast fire growth rate are the negative factors to the fire resistance capacity of the structures.
- Distance to the fire source: the temperatures of structural members are inversely proportional to their distance to the fire source. The larger the distance to fire source, the less thermal action of the fire to the structural members. Therefore, large distance to the fire source is a positive factor to the fire resistance capacity of the structures.

- Load ratio: structural members with high load ratio are subjected to low limiting temperatures in fire. Therefore, high load ratio in structural member is a negative factor to the fire resistance capacity of the structures.

Apart from the above factors, a less influence factor is the section factor which is proportional to the member temperature increase and thus negative to the fire resistance of the structural members. There are also other positive factors to the fire resistance capacity of the structures such as effective fire fighting and high structural redundancy.

By minimizing the negative factors and maximizing the positive factors, the fire resistance duration of large space membrane structures can be increased and the cost needed for the structures against fire can be saved.

6.5. Summary

Despite the high strength tensile performance, the membrane materials by their nature of small thickness are susceptible to vandalistic/accidental damage. Structural behaviour of DSTMS and Butterfly-wing structures was investigated in case of membrane failure. It was found that both DSTMS and Butterfly-wing structures are safe even in the event of complete damage of the membrane due to vandalism/accident. The safety of DSTMS without membrane is ensured by the self-stable supporting skeleton and while the safety of Butterfly-wing structures without membrane is ensured by the safety struts.

Another possible hazard to membrane structures is the fire scenario. Investigations on the characteristics of membrane materials and the behaviour of membrane structures in fire showed that fire occurring in the membrane structures was most likely to be localized. A procedure of performance-based approach was proposed for determining the structural fire resistance duration of large space membrane structures. This approach is used to ensure the fire safety of DSTMS and Butterfly-wing structures by considering their performance in real fire. Furthermore, this approach helps to identify the influence factors on the structural fire resistance, in which the major factors are the fire load, the distance to the fire source and the load ratio. By optimizing these factors, the cost needed for membrane structures against fire could be minimized.

CHAPTER 7

PROTOTYPES AND DESIGN GUIDELINES

7.1. Introduction

This chapter is aimed at illustrating the design concept and verifying the deployability of the proposed DSTMS and Butterfly-wing structures through physical prototypes. Scale prototypes are essential to develop hands-on experience on the shape and detail design so as to provide a better intuitive understanding about how to achieve the equilibrium membrane curvature form and how to make the structures deployable. In addition, through the prototypes, the interaction between the membrane and the deployable supporting structures can be illustrated. Experiments are carried out to verify the deployment and stowage efficiencies of these structures. The success of the prototype experiments demonstrates the feasibility of DSTMS and Butterfly-wing structures for implementation.

Another aim of this chapter is to provide design guidelines on how to implement, design, manufacture and deploy the DSTMS and Butterfly-wing structures for practical applications. The design guidelines cover a wide range of applications corresponding to different forms for these structures. It also provides the recommended structural parameters which are applicable for medium and large span applications for the preliminary design of these structures. In addition, it provides the detailed designs of joints, hinge connections, membrane connections and other related accessories to facilitate the manufacturing and installation of these structures. The deployment methods of these structures are also included in the design guideline.

7.2. Prototype investigation

As presented in chapter 2, a combination of computational modelling and physical modelling was employed in this thesis. Computational modelling is an economical method and thus was employed to illustrate the design concept and to generate various structural forms of DSTMS and Butterfly-wing structures as presented in chapter 3. In this chapter, physical modelling is conducted through building selective prototypes to verify the computational modelling results and to demonstrate the deployability of these structures. Apart from providing an intuitive understanding about the structures, physical prototypes develop the engineering sense of how the structures deploy and how to make them deployable.

7.2.1. Prototypes of DSTMS

Small scale models made of thin cloth and aluminum struts were built to investigate the membrane form and the deployment of DSTMS. Figure 7.1 shows the prototypes of a Cone-shaped DSTM module and four connected Umbrella DSTM modules.

(a) (b)

Fig. 7.1. Small scale models of (a) Cone-shaped DSTM and (b) Umbrella DSTM modules

As observed, the membrane surface of Cone-shaped DSTM module was in cone-like form while the membrane surface between the modules of Umbrella DSTMS was in saddle form. These membrane forms of DSTMS can be adjusted by changing the prestress in two principal curvatures of the surfaces (radial and circumferential curvatures of the cone in Cone-shaped DSTMS or concave and convex curvatures of the saddle in Umbrella DSTMS). The membrane prestress is controlled by the shape of the membrane patterns. By patterning the cloth into a series of strips matching with the form of the surface and cutting them smaller and differently in two directions, different prestresses and thus different membrane forms can be obtained.

Fig. 7.2. Prototype of curved form Umbrella DSTMS in deployed configuration

Apart from a flat form as illustrated in Fig. 7.1.b, a prototype of curved form Umbrella DSTMS was built as shown in Fig. 7.2. The prototype has two bays. Each bay consists of seven modules connected together. In the deployed configuration, the prototype covers an area of 1.3m x 3.1m and has a total weight of 4kg. In the folded configuration, it occupies an area of only about 0.1m x 0.3m (Fig. 7.3).

Fig. 7.3. Prototype of curved form Umbrella DSTMS in folded configuration

The curved form of the prototype was achieved by adjusting the grid size of bottom cables in the curved direction smaller than the size of the module. It was observed that when the structure was locked in the deployed configuration, it achieved the self-stress equilibrium state in which both membrane and bottom cables were in tension. The strut skeleton was braced and prestressed by the tensioned membrane. Therefore the stability of the strut skeleton was improved significantly as compared to that without membrane.

The following sections will discuss on how to make the prototype deployable through the design of the hub connecting the struts, and how to lock the deployment through the design of the telescopic vertical strut.

7.2.1.1. Hub design

Unlike the joints in space trusses which are rigid, the hubs connecting end nodes of struts in DSTMS are much more complicated. The basic requirement is that they must

be able to geometrically accommodate the large individual rotation of each connected strut. Furthermore, they must be designed so that they are able to accommodate all struts connected to them in a compact configuration. Last but not least, the number of hub types must be minimized to optimize the manufacturing cost.

Based on these requirements, a hub was designed so that only one type of hub needs for all top, middle and bottom joints of the prototype. Fig. 7.4 shows the geometry of the hub which was designed and manufactured by Deployable structures group in NUS. The hub design is relatively simple that allows four connected struts to rotate individually through the pin holes. Therefore they are reliable and easy to manufacture.

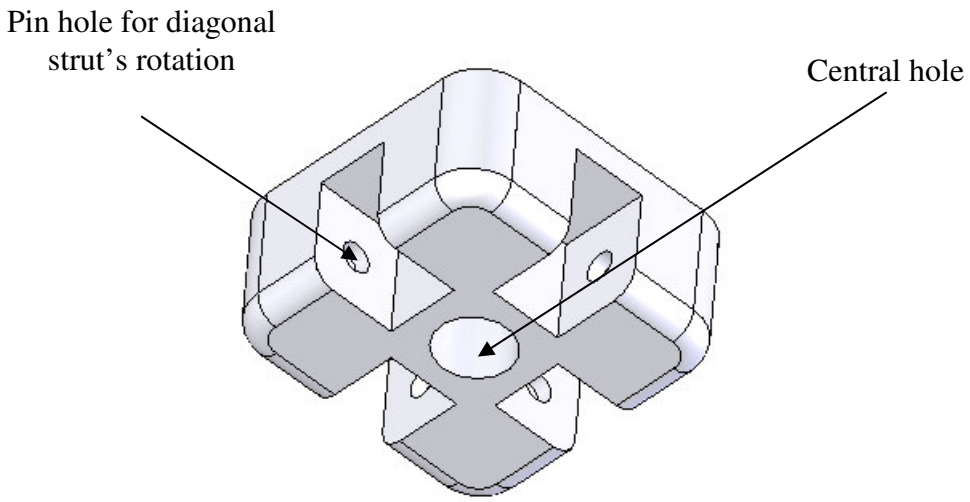

Fig. 7.4. Hub design

The middle joint comprises eight connected struts, thus it is formed by two hubs interconnected. A bolt is slotted into central hole of the two hubs and is tightened to clamp them together. Detail of middle joint design is illustrated in Fig. 7.5 below.

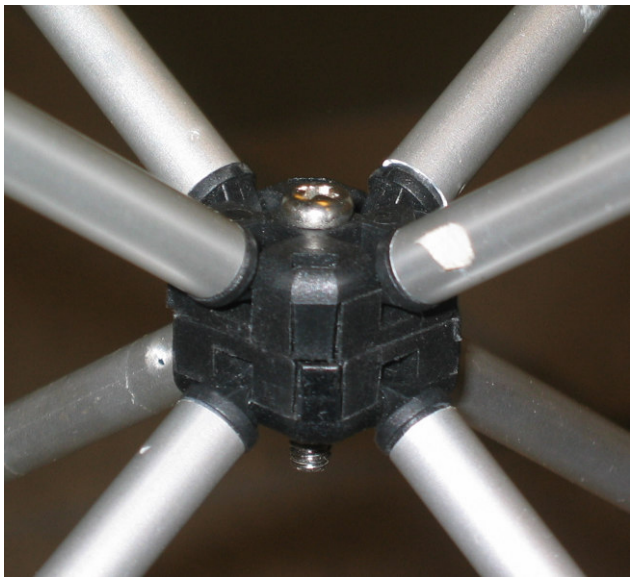

Fig. 7.5. Detail of middle joint

The top/bottom joint comprises one hub and one cable cap with cross-grooves for clamping top/bottom cable layers. The cable cap has a threaded hole at centre for connecting with the end of the vertical strut (see Fig. 7.6). The vertical strut's end is slotted into the central hole of the hub and then is bolted into the cable cap to clamp the hub in between.

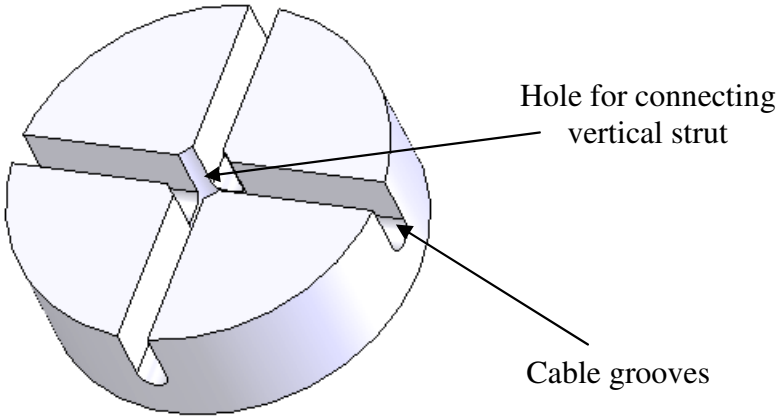

Fig.7.6. Cable cap

In the top joint, the fabric is clamped between the hub and the cable cap. Detail of top/bottom joint is shown in Fig. 7.7.

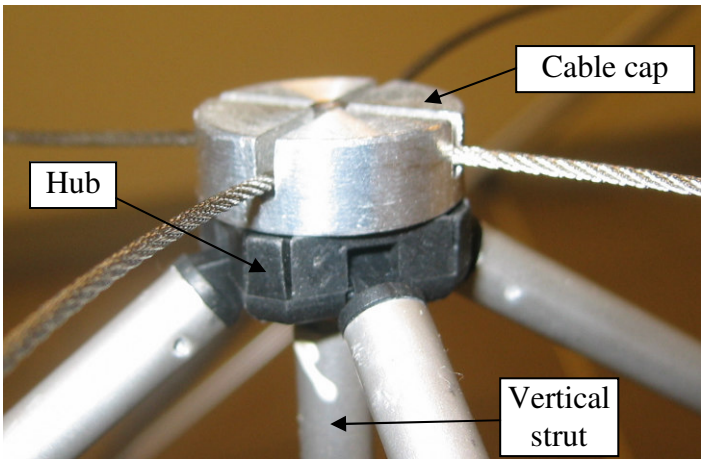

Fig. 7.7. Detail of top/bottom joint

For large scale prototypes, the hubs should be made of extruded aluminum to reduce the weight of the joints as well as the manufacturing cost. It makes the joint more compact and facilitates mass production. The extruded joint will be illustrated in section 7.3.3.1 of this chapter.

7.2.1.2. Telescopic vertical strut

The vertical strut was aimed at controlling and locking the deployment of the prototype. The vertical strut was designed as a telescope so that it is capable of lengthening or shortening to accommodate the change in geometry of the module (Fig. 7.8).

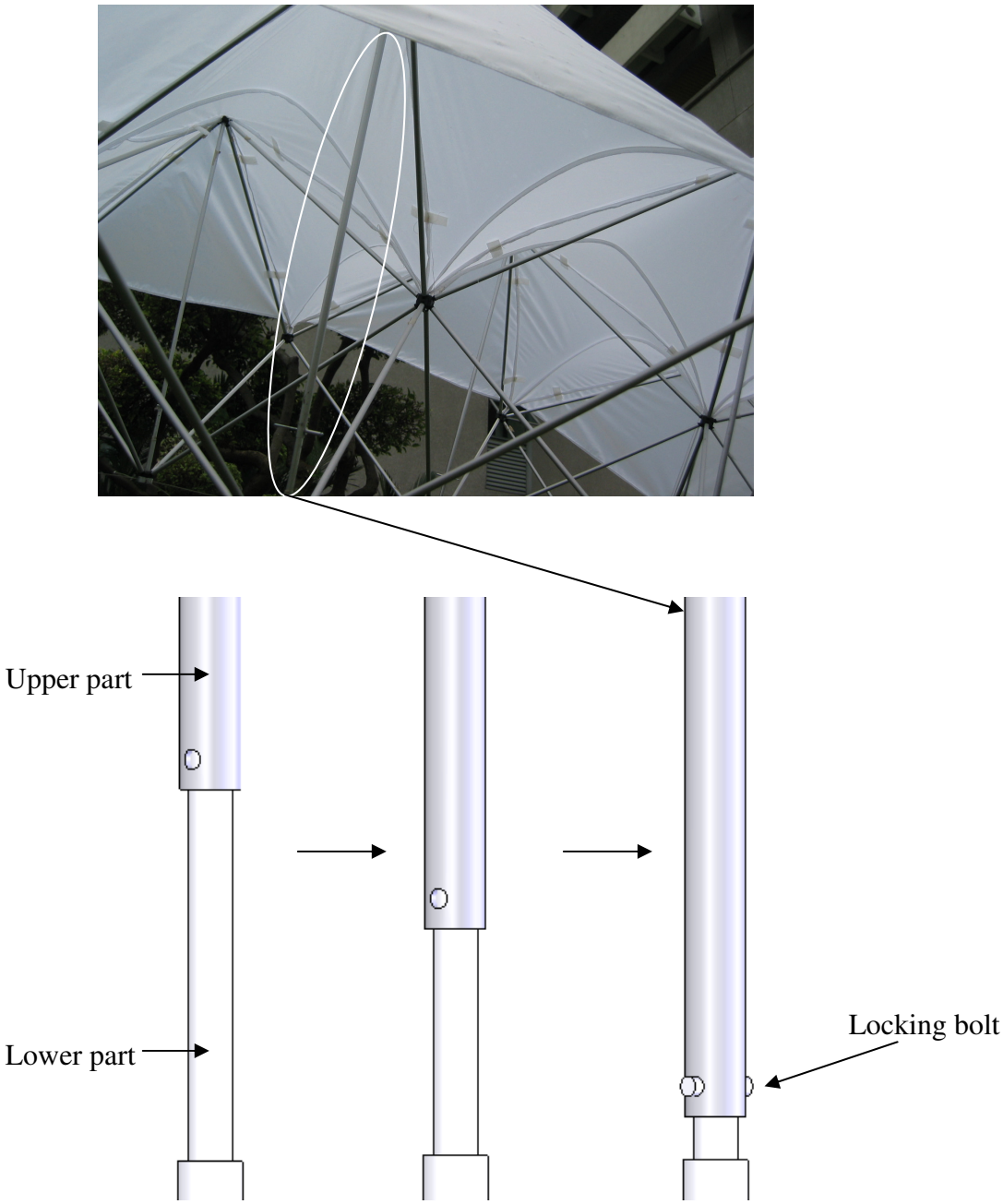

Fig. 7.8. Telescopic vertical strut of Umbrella DSTMS model

The vertical strut consists of upper and lower parts. The upper part allows the lower part to slot inside it. The two parts are therefore can slide within each other to shorten or lengthen the vertical strut. The two ends of the vertical strut are threaded so that they can be bolted to the cable caps of top/bottom joints as described previously. When

the structure is in deployed configuration, a bolt is slotted through the corresponding holes on the upper and lower parts to provide translational restraint to the vertical strut. The translational restraint of the vertical strut is the deployment locking of structure, which prevents the structure from deploying further or collapsing back.

Telescopic vertical strut was chosen for small scale prototypes in order to improve the stability of the prototype during deployment. For large scale structures, it may not be suitable and will be replaced by cantilever vertical strut which will be designed in section 7.3.3.1.

7.2.1.3. Deployment verification

Figures 7.9 – 7.14 show the deployment of the prototype of a curved form Umbrella DSTMS. The prototype was deployed efficiently by two persons within a minute. It was found that the self-weight of the structure facilitated the deployment process and the deployment of the strut skeleton helped to open and tension the membrane. During the deployment, the bottom cables might jam if they were not stowed properly. This problem could be avoided by grouping the bottom cables carefully in right position.

Fig. 7.9. Compact folded configuration

Fig. 7.10. Start to deploy

Fig. 7.11. Deploying – Step 1

Fig. 7.12. Deploying – Step 2

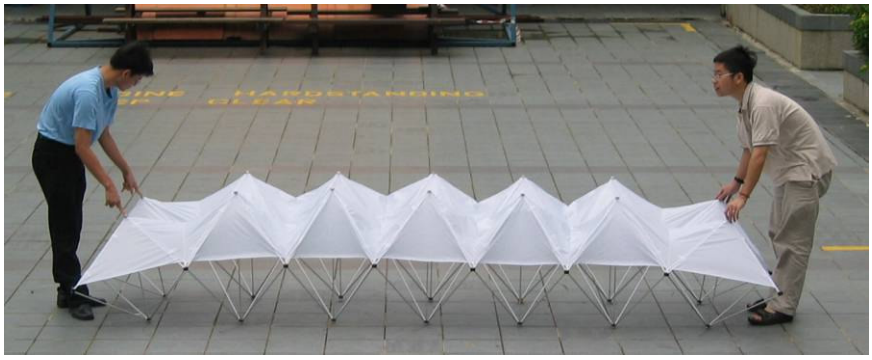

Fig. 7.13. Deploying – Step 3

Fig. 7.14. Final configuration after locking

The deployment test has demonstrated successfully the structural concept and the deployability of DSTMS.

7.2.2. Prototypes of Butterfly-wing structures

Figure 7.15 shows the small scale prototype of two-wing butterfly structure. The plastic arches were able to rotate about the supports and kept stable in inclination position by the thin cloth membrane and the anchor cables. The tension in the cables, and thus the prestress in the membrane were controlled by the bolts at the anchor points. In final configuration, the whole structure was in self-stress equilibrium and the membrane had a typical saddle form.

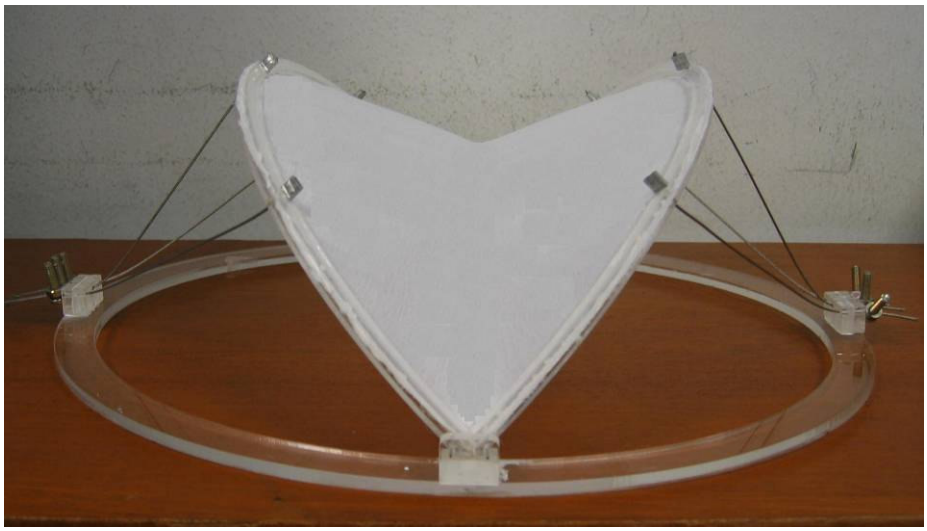

Fig. 7.15. Scale prototype of two-wing butterfly structure

Figures 7.16 to 7.20 show the configuration and deployment process of the scale prototype of a multiple two-wing butterfly structure which was made of stocking and foam. The prototype could be deployed either from one end (in this case) or both ends. Initially, all arches were raised up and kept vertically by temporary struts at two ends. One end was fixed while the others were able to slide along the ground beam. The membrane in the middle was opened up and tensioned. When the arches were in final position, they were fixed to the ground beam. The two end arches were rotated outward and then tensioned against the anchor points by anchor cables.

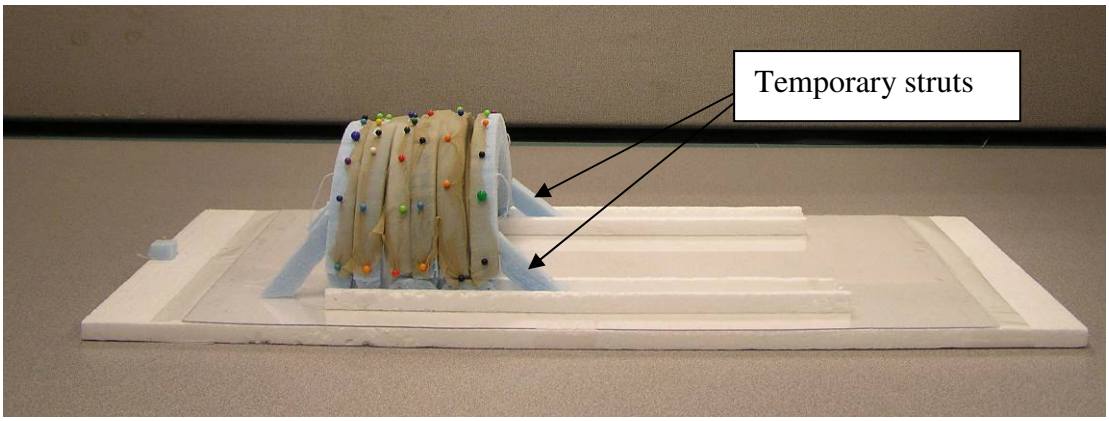

Fig. 7.16. Arches are raised up and kept vertically

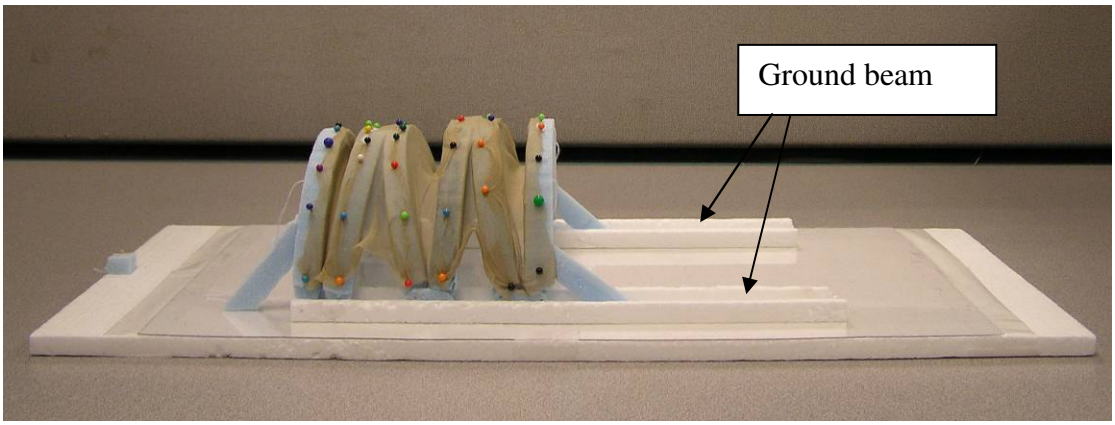

Fig. 7.17. Start to deploy

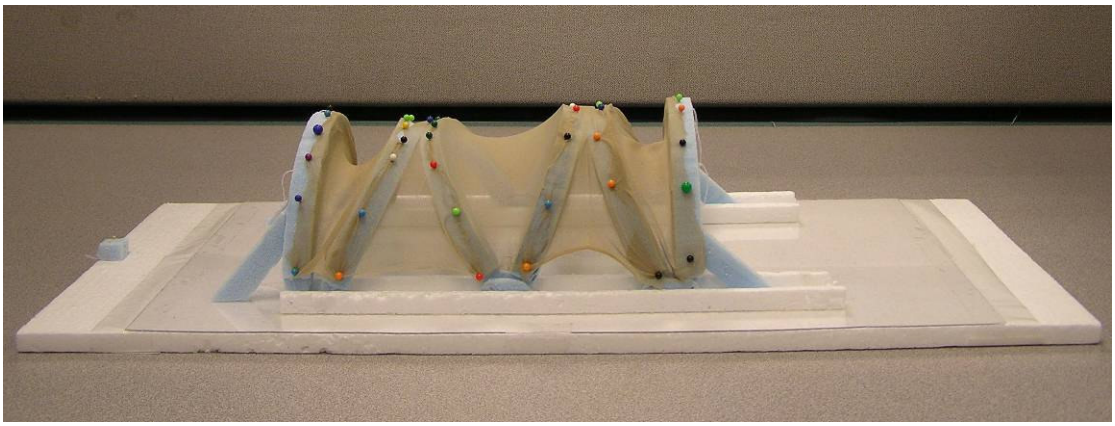

Fig. 7.18. Arches slide along ground beam

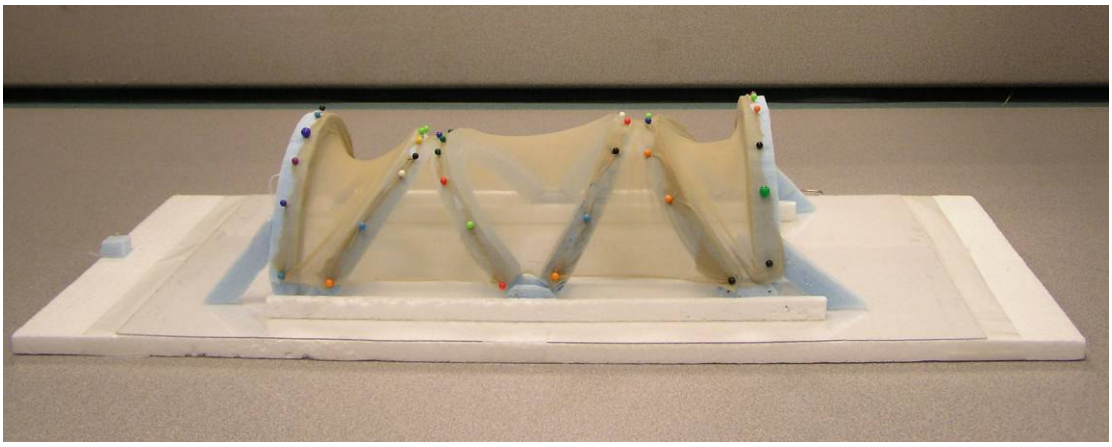

Fig. 7.19. Arches are fixed to ground beam at final position

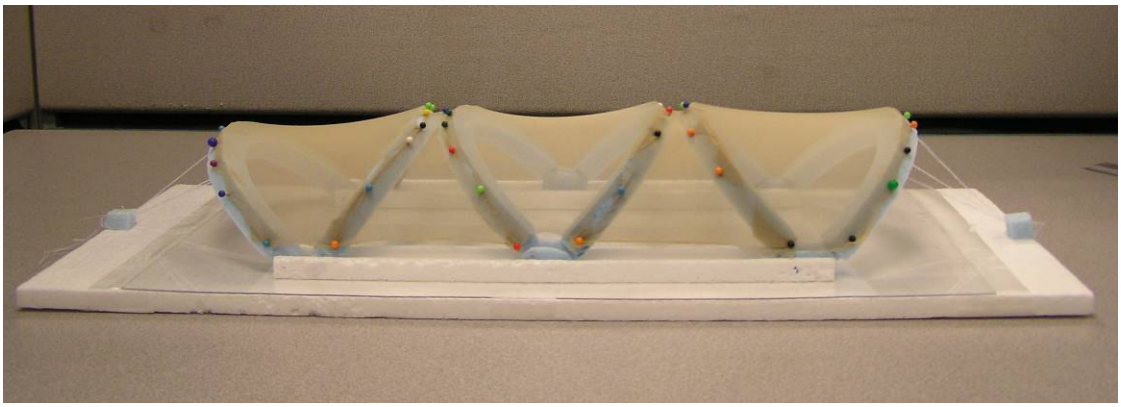

Fig. 7.20. Final configuration

In the final configuration, the structure was in self-stress equilibrium and the membrane was in a series of saddle form as shown in chapter 3.

7.3. Design guidelines

7.3.1. Application overview

Both DSTMS and Butterfly-wing structures are aimed at space enclosures. Since they are deployable for fast-track erection and foldable for relocation, they are most suitable for emergency or military applications which often need to be rapidly erected on site and relocated to places of demand.

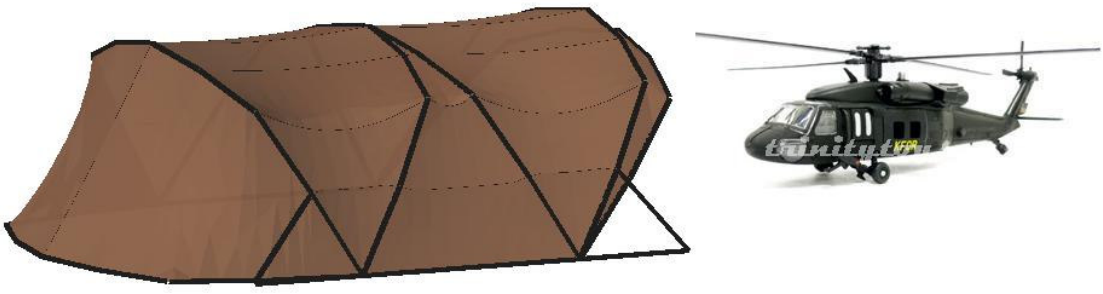

Fig. 7.21. Multiple two-wing butterfly structure for deployable helicopter shelter

One application of the proposed systems is for deployable shelters. Figure 7.21 shows a multiple two-wing butterfly structure employed as a military helicopter shelter. The entrances at the two ends of the shelter can be designed with fold-up doors. The span of helicopter shelter is in range of 15m – 20m, therefore rigid arch made of hollow section is advisable. The arch should be segmented for the ease of transportation. The details of segmented arch and guide-track ground beam will be presented in section 7.3.3.2 of this chapter.

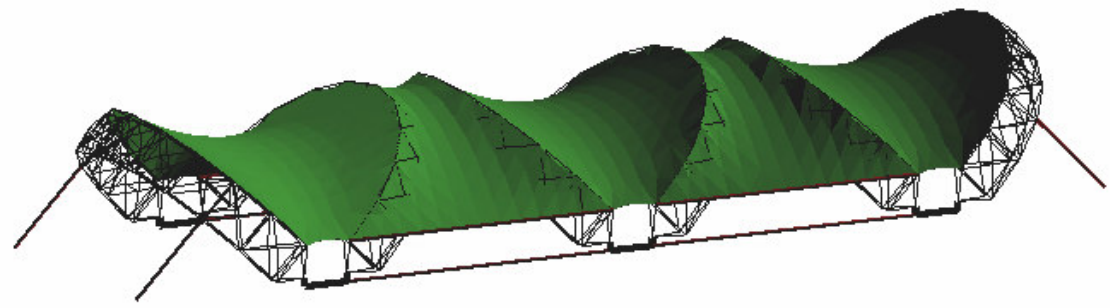

Fig. 7.22. Multiple two-wing butterfly structure using deployable cable-strut arch

For deployable shelter of larger span (over 20m), rigid arch of multiple two-wing butterfly structure can be replaced by the deployable cable-strut arch (described in section 3.2.6) as illustrated in Fig. 7.22. The joint design to allow for the deployment of the arch will be discussed in section 7.3.3.3 of this chapter. This form is also suitable for emergency relief such as hospitality pavilions or refugee tents.

On the other hand, DSTMS in the form of barrel vault shown in Fig. 7.23 are also able to provide large span deployable shelter for accommodating fighting aircrafts.

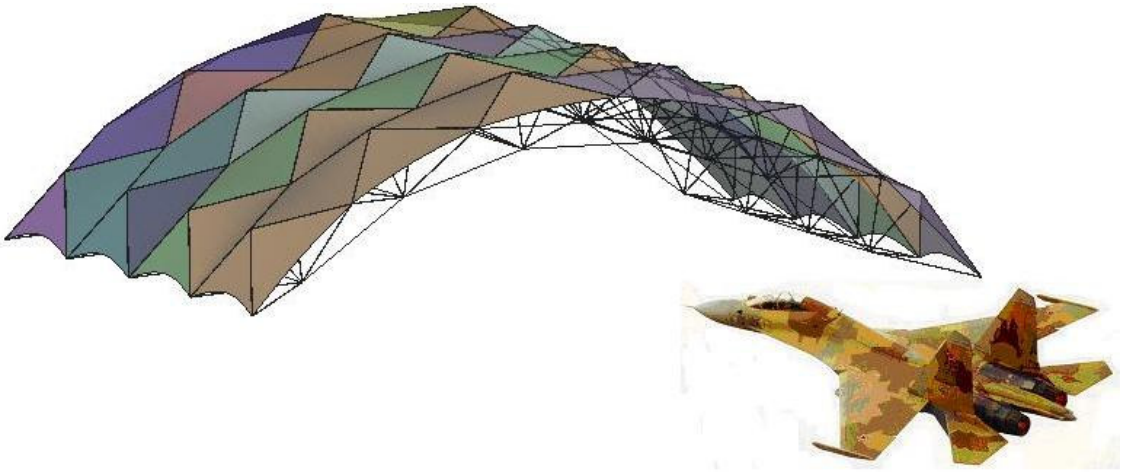

Fig. 7.23. Umbrella DSTMS for military aircraft shelter

Besides deployable shelter, DSTMS can be used for the roof system of aircraft hangar to accommodate large wing-span plane as well as to perform maintenance services as shown in Fig. 7.24.

Fig. 7.24. Umbrella DSTMS for roof system of aircraft hangar

Apart from military purpose, DSTMS and Butterfly-wing structures are also applicable for sport facilities such as tennis court, swimming pool etc. Figure 7.25 shows a DSTMS used for swimming pool roof system. The roof system is not only capable of

rapid construction due to its deployability but it is also weather adaptive which is attributed to its foldability. In the rain or snow season, the roof is deployed in place to prevent the rain or snow fall while in the sunny season, it is stowed back to allow the sunshine to reach the swimming pool.

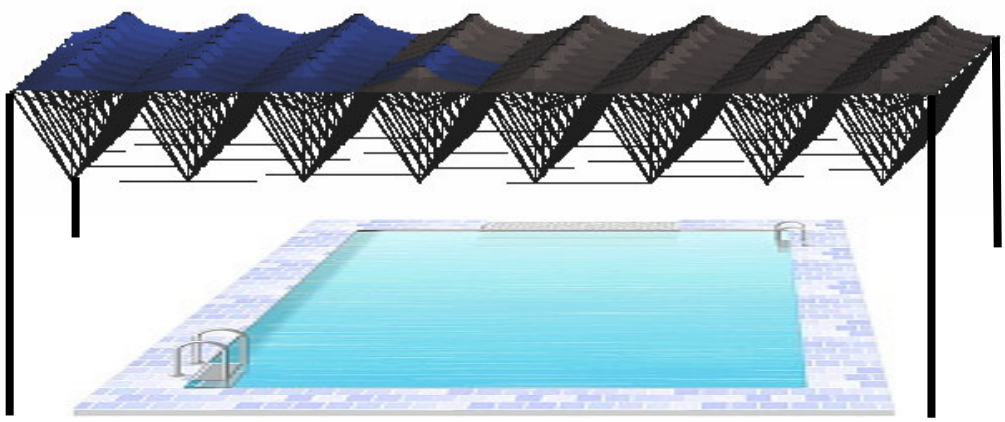

Fig. 7.25. Cone-shaped DSTMS for roof system of swimming pool

In addition, Butterfly-wing structures are suitable for applications which require rapid construction as well as attractive appearance like exhibitions, amphitheatres, etc. The eye-catching curvature of membrane surface creates the striking appearance of the structures. Figure 7.26 shows a two-wing butterfly structure (supported by the deployable cable-strut arch) which is used to cover an amphitheatre. The deployable cable-strut arch is employed to allow for larger enclosure. The grand stands are arranged at the two wings while the stage is arranged at the center of the structure. Similar arrangement can be applied for three-wing and four-wing butterfly structures which can accommodate more audiences.

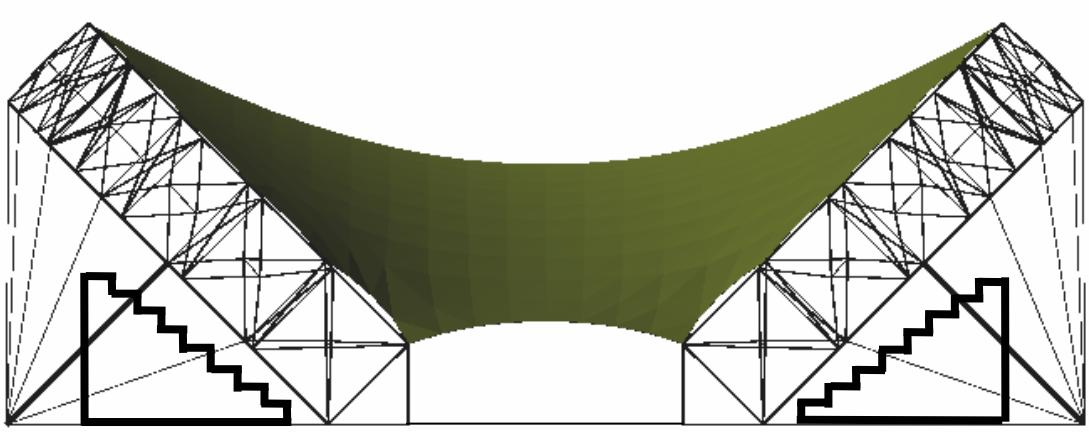

Fig. 7.26. Two-wing butterfly structure (using deployable arch) for covering amphitheatre

The application range of DSTMS and Butterfly-wing structures is still open but not restricted to the above space enclosures. By using triangular or pentagonal simplex, DSTMS can be applied for other applications apart from flat roof and barrel vault, such as dome, etc. On the other hand, by assembling either identical or different single butterfly-wing forms, multiple butterfly-wing structures (e.g. multiple three-wing and four-wing as described in sections 3.2.5 and 3.2.6) are able to enclose applications of any shape and size.

7.3.2. Recommended structural parameters for preliminary design

It is worth noting that the structural design of DSTMS, and other space structures in general, depends on a series of input structural parameters such as structural configuration, structural span, support condition, loading condition, etc. This section aimed at providing the recommended structural parameters and member sizes for the preliminary design of DSTMS and Butterfly-wing structures subjected to conditions.

7.3.2.1. Preliminary design of DSTMS

Table 7.1 may serve as the preliminary design table which is applicable for DSTMS of following parameters:

- Configuration: Flat roof Umbrella and Cone-shaped DSTMS
- Structural span: 48m x 48m square grid
- Support condition: pin-supported at four edges
- Materials: Steel grade S275 and PVC fabric, prestress level of 2kN/m
- Loading condition: Imposed gravity load of 0.75kN/m^2 and wind uplift of 0.45kN/m^2

Table 7.1. Recommended structural parameters and member sizes for preliminary design of DSTMS

DSTMS	Structural parameters (m)			Structural member sizes (mm)			
	Structural depth	Modular width	Inclination height	Top strut	Diagonal strut	Vertical strut	Bottom cable
Umbrella	6	4.8	0.96	O114.3x3.2	O168.3x5	O114.3x3.2	ϕ26
Cone-shaped	6	4.8	0.96	O108x3.2	O159x4	O108x3.2	ϕ32

(Refer to Figs. 5.1 & 5.2 for the definitions of structural depth H, inclination height h, modular width W, top strut, diagonal strut, vertical strut and bottom cable)

For structural spans other than 48m x 48m, the following design parameters may be used for the preliminary design of DSTMS

- Inclination height/modular width = 0.2
- Span/depth ratio = 9 – 11
- Span/modular width ratio = 6 – 8

The design algorithm presented in chapter 5 then can be used for sizing the structural members of DSTMS.

7.3.2.2. Preliminary design of Butterfly-wing structures

Table 7.2 and table 7.3 may serve as the preliminary design tables which are applicable for Butterfly-wing structures of following parameters:

- Configuration: Two-wing and three-wing using deployable cable-strut arch
- Arch span: 30m
- Support condition: hinge support at arches' feet
- Materials: Steel grade S275 and PVC fabric, prestress level of 1.5kN/m
- Loading condition: wind uplift of 0.45kN/m^2 and wind downward of 0.1kN/m^2

Table 7.2. Recommended structural parameters for preliminary design of Butterfly-wing structures

Butterfly-wing structures	Structural parameters of deployable arch (m)				
	Inclination angle (degree)	Arch rise	Modular depth	Modular average width	Modular crossed-width
Two-wing	45	15	1.5	4.113	4.109
Three-wing	45	15	1.5	4.113	4.109

(Refer to Figs. 4.7, 5.18 & 5.19 for the definitions of inclination angle α, arch rise H, modular depth h, average width $W=1/2(W_u+W_l)$ and crossed-width W_c)

Table 7.3. Recommended member sizes for preliminary design of Butterfly-wing structures

Butterfly-wing structures	Structural member sizes (mm)						
	Pyramid strut	Scissor strut	Supporting strut	Safety strut	Horizontal cable	Central cable	Anchor cable
Two-wing	⌊70×3.6	⌊80×3.6	⌊70×3.6	⌊100×5	ϕ26	ϕ26	ϕ12
Three-wing	⌊70×3.6	⌊100×4	⌊70×3.6	⌊100×5	ϕ32	ϕ32	ϕ12

(Refer to Figs. 5.18 & 5.19 for the definitions of pyramid strut, scissor strut, supporting strut, safety strut, horizontal cable, central cable and anchor cable)

If modified deployable cable-strut arch (mentioned in section 5.3.5.2 of chapter 5) is used, the recommended member sizes for preliminary design of Butterfly-wing structures are given in table 7.4.

Table 7.4. Recommended member sizes for preliminary design of Butterfly-wing structures with modified deployable arch

Butterfly-wing structures	Structural member sizes (mm)							
	Pyramid strut	Scissor strut	Supporting strut	Safety strut	Middle strut	Horizontal cable	Central cable	Anchor cable
Two-wing	⌊60×3.2	⌊80×3	⌊65×3	⌊100×5	⌊85×3	ϕ14	ϕ14	ϕ12
Three-wing	⌊60×3	⌊80×4	⌊70×3.6	⌊100×5	⌊90×3.6	ϕ12	ϕ12	ϕ12

For arch spans other than 30m, the following design parameters may be used for the preliminary design of Butterfly-wing structures:

- Inclination angle of the arch = 45° – 60°
- Rise/span ratio of the arch = 0.375 – 0.5
- Arch-span/modular depth ratio = 19 – 21
- Number of module of the arch = 12 – 14

The design algorithm presented in chapter 5 then can be used for sizing the structural members of DSTMS.

7.3.3. Joint and accessories designs

This section provides the detailed designs of joint and accessories for the manufacturing of large scale structures. The solutions for membrane connections are also given.

7.3.3.1. Joint design of DSTMS

As mentioned earlier, aluminum extrusion is the economical option for manufacturing a large quantity of DSTMS joints.

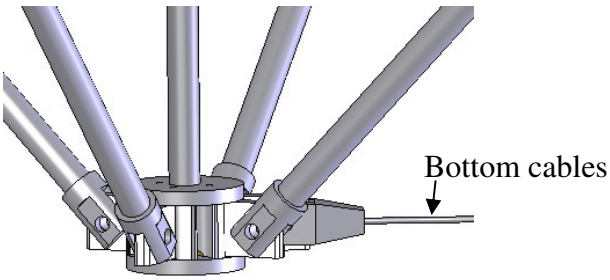

(a) Bottom joint

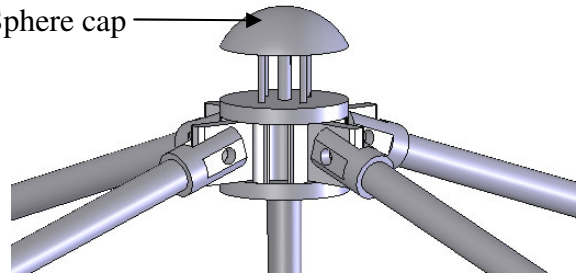

(b) Top joint

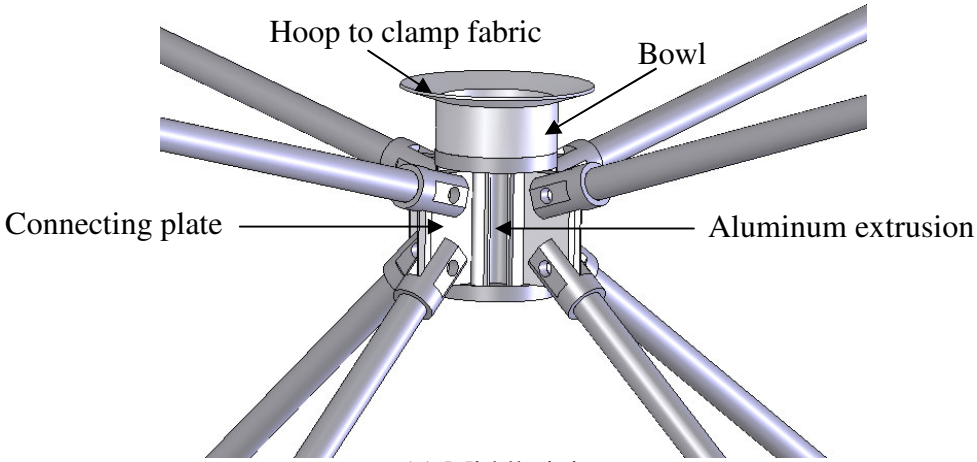

(c) Middle joint

Fig. 7.27. Aluminum extruded joints for Umbrella DSTMS

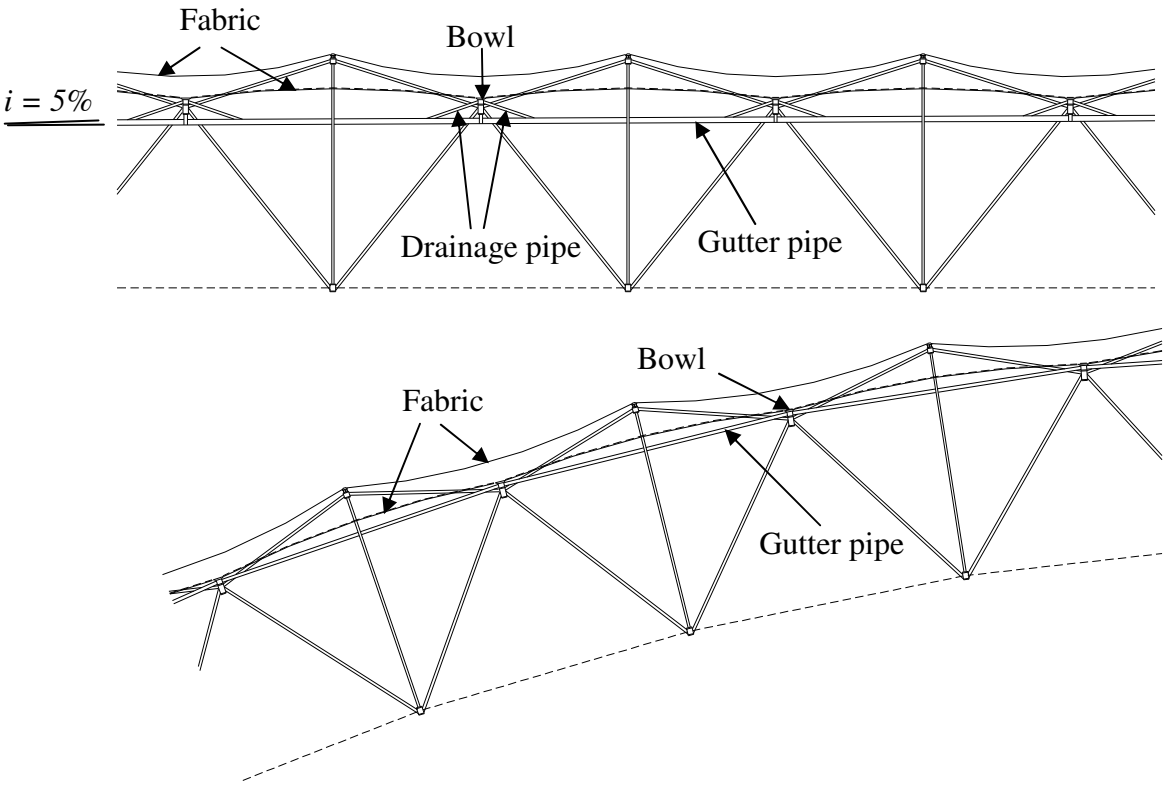

Fig. 7.28. Drainage solutions for flat and curved Umbrella DSTMS

Figure 7.27 shows the aluminum extruded joint designs for Umbrella DSTMS. The joints were made of aluminum extrusion body with grooves for plates connecting struts slotted into it. The top joint was designed with a sphere cap for membrane fabric placed over on it (Fig. 7.29). The middle joint was designed with a bowl for clamping the fabric membrane and for collecting rain water.

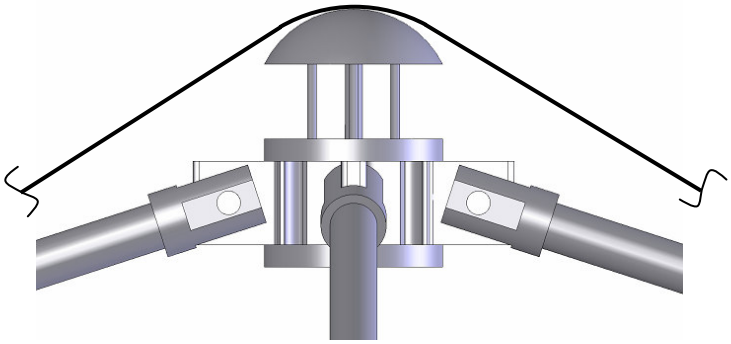

Fig. 7.29. Fabric placed over top joint

Figure 7.30 shows the detailed design of the bowl. The fabric was clamped at the hoop of the bowl by aluminum channel. Drainage holes were designed at the bottom of the bowl for connecting the piles of drainage system.

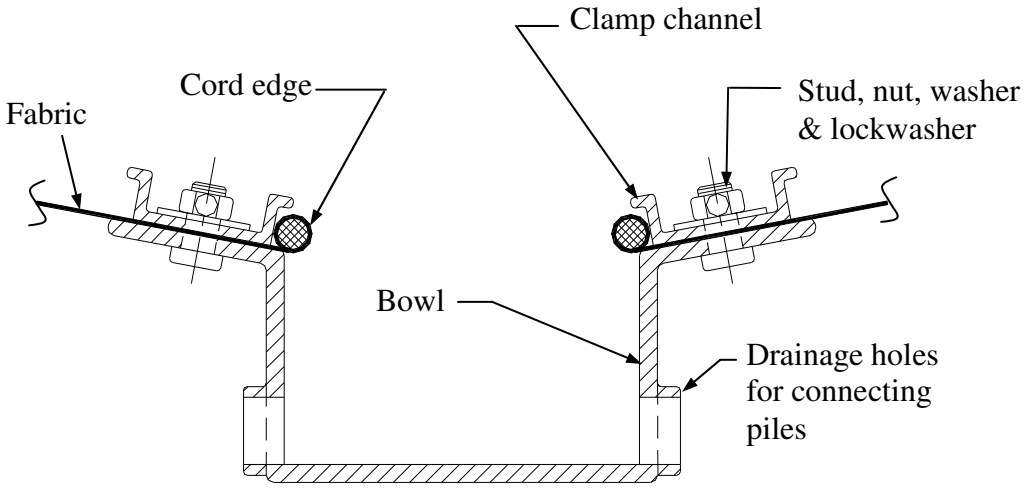

Fig. 7.30. Bowl design of Umbrella DSTMS

Figure 7.28 shows how the drainage and gutter piles were arranged in flat and curved DSTMS. In flat DSTMS, the bowl was connected to the gutter piles through the drainage piles. The gutter piles was hanged beneath the middle joints and designed with 5% slope to drain out the rain water to the downspouts at two edges of the roof and then to the ground. In curved DSTMS, the bowl was connected directly to the gutter piles. Rain water collected at the bowl will be drained out through the gutter piles toward the two edges due to the inherent curvature of the roof.

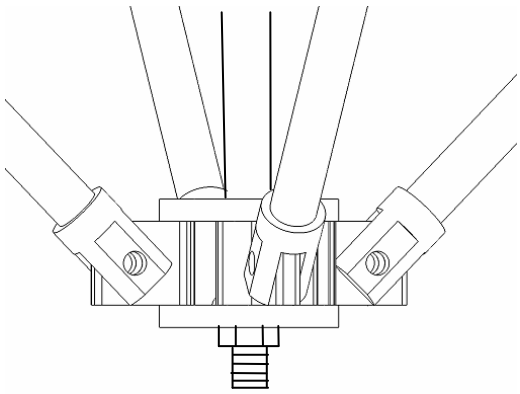

Fig. 7.31. Locking bolt of vertical strut

As mentioned earlier, telescopic vertical strut is not suitable for large scale structures. Here the vertical strut was designed as a cantilever with one end was fixed to the top joint and another end could be slotted and bolted to the bottom joint as shown in Fig. 7.31. This bolt connection is used to shorten the vertical strut to achieve the final configuration as well as the self-stress equilibrium of the structure.

7.3.3.2. Segmented arch design of Butterfly-wing structures

For arch span of less than 20m, rigid arch made of steel/aluminum tube is an economical option for Butterfly-wing structure. The arch was segmented for the ease

of transportation. Figure 7.32 & 7.33 show how two segments were connected through fin plates and bolt connections. The fabric membrane was attached to the arch through the rope track bolted to the bracket which was welded along the arch (Fig. 7.33).

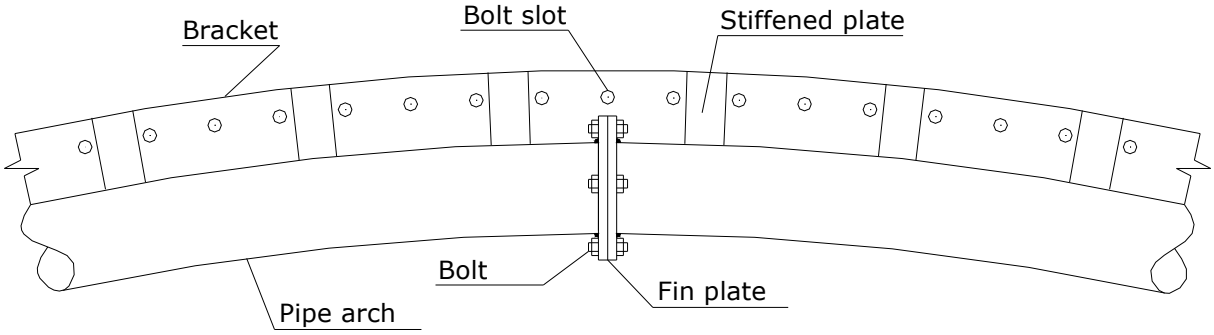

Fig. 7.32. Segmented arch

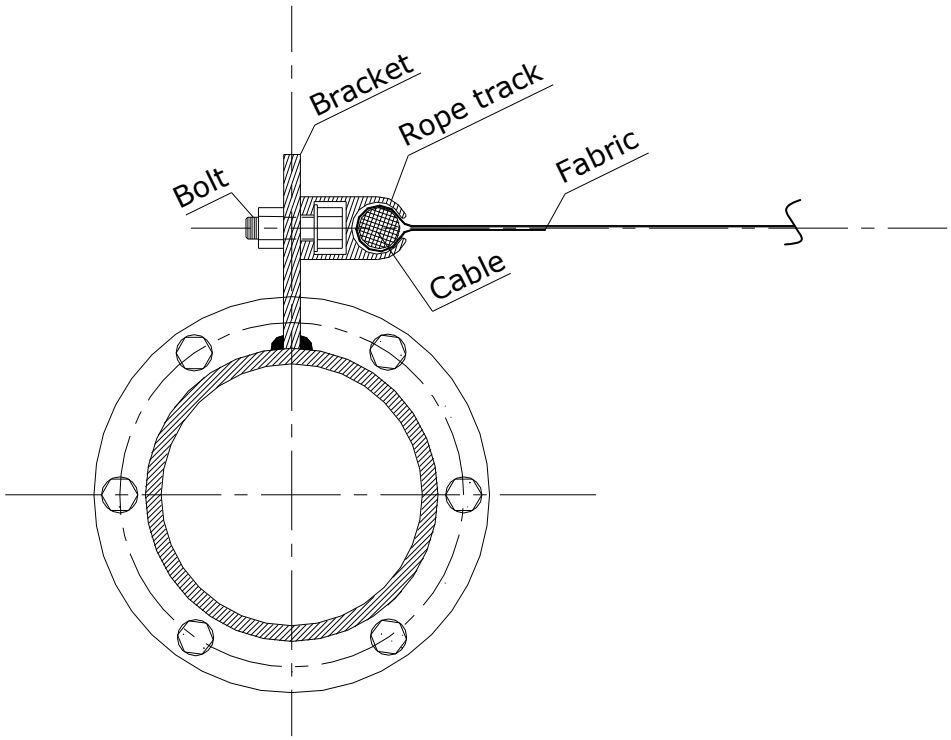

Fig. 7.33. Membrane connected to the arch through bracket

Alternatively, the rope track could be bolted directly to the arch as shown in Figs. 7.34. This can avoid the torsion induced by the eccentricity of the membrane connection as in the case of using bracket. However, the fin plate needs an opening for the rope track going through (Fig. 7.34).

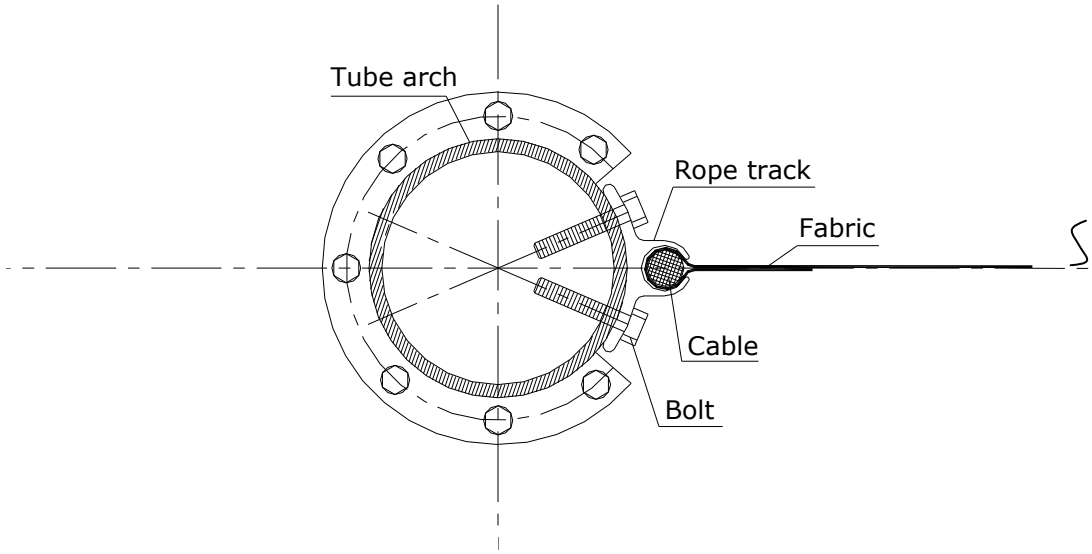

Fig. 7.34. Membrane connected concentrically to the arch

7.3.3.3. Hinge connection and ground beam designs of Multiple butterfly-wing membrane structure

The deployment of Multiple butterfly-wing structures is attributed to the hinge connecting the arches' peaks and the ground beam acting as the guide-track. For the ease of the hinge design and membrane connection design, square tube was chosen for the rigid arch as shown in Fig. 7.35.

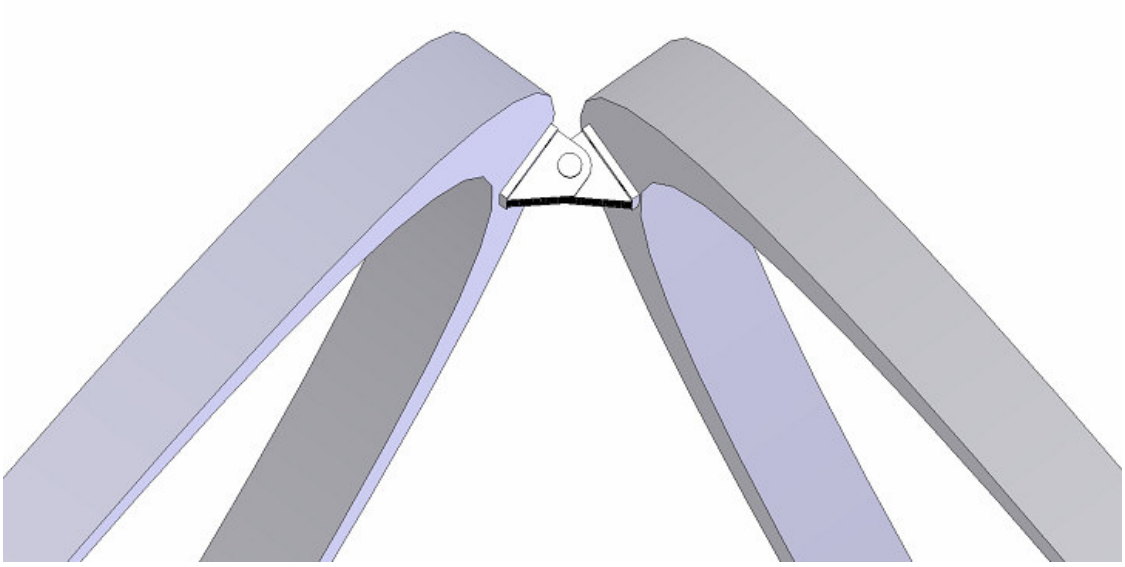

Fig. 7.35. Arches connected at their peaks by hinge connection

Figure 7.36 shows the design of the hinge which consists of two parts connected by a pin. Each part of the hinge was designed with a series of alternate parallel ribs which help to enhance the stiffness of the hinge. The cylindrical pin slotted between the two parts allows the smooth rotation of the hinge. There were four holes drilled on each part of the hinge for bolting the hinge to the arches.

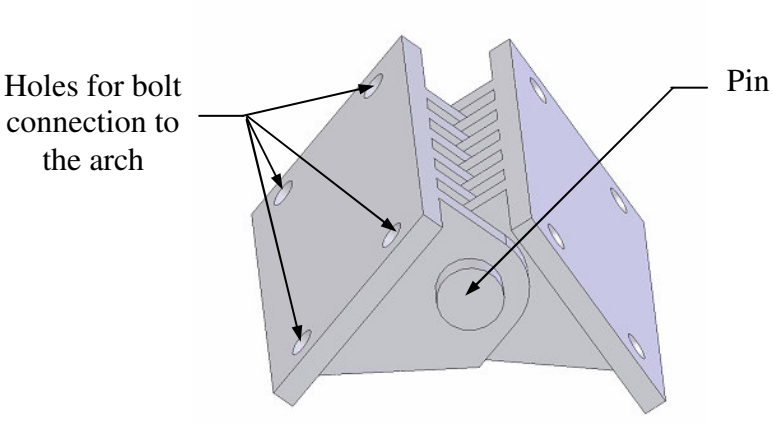

Fig. 7.36. Hinge connection design

Figure 7.37 shows how the fabric membrane was attached to the square tube arches. The fabric roped edge was compressed between the gaskets by the clamp bar. The bearing of the roped edge against the clamp bar provides the fixity of the fabric membrane to the rigid arch. The clamp bar was continuous, rounded and padded to securely clamp the fabric edge and uniformly transfer the fabric membrane stress without developing stress concentration.

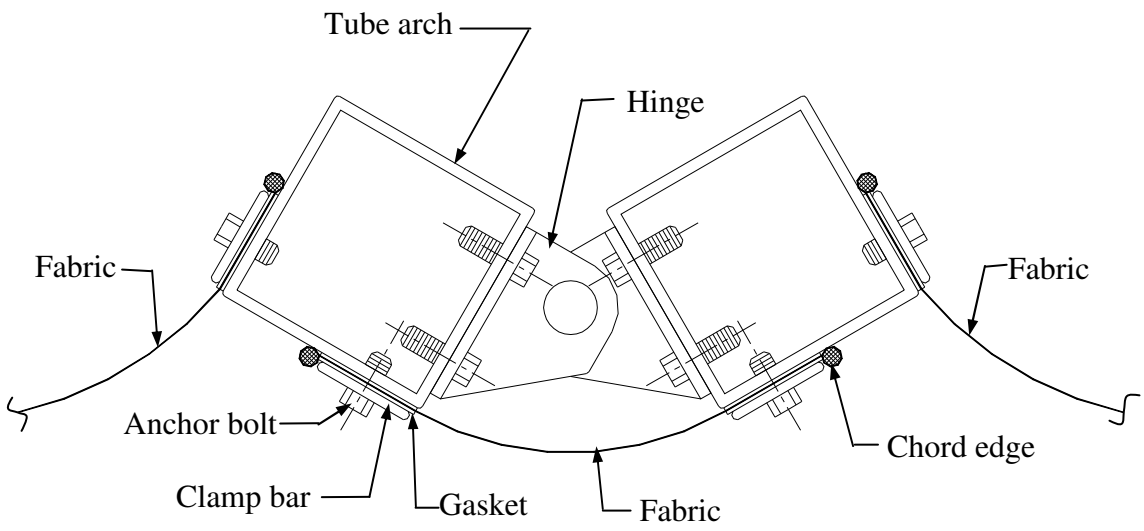

Fig. 7.37. Membrane connection to the square tube arch

Another component contributing to the deployment of the Multiple butterfly-wing structures is the ground beam. Apart from the function of anchoring the structures to the foundation, the ground beam acts as a guide track for the arches sliding along during the deployment.

Figure 7.38 shows how the trolley and ground beam were designed to enable the sliding of the arches in Multiple butterfly-wing structures. The arches were pin-connected to the C-channel trolley and thus they were able to rotate about the pin bolt.

The trolley was fitted inside the C-channel ground beam. The sliding of the trolley was facilitated by the rollers beneath. When the structure is fully deployed, the trolley can be locked in position by slotting bolts through the corresponding holes on the trolley and the ground beam. Alternatively, the trolley can be locked by putting stoppers at its two ends.

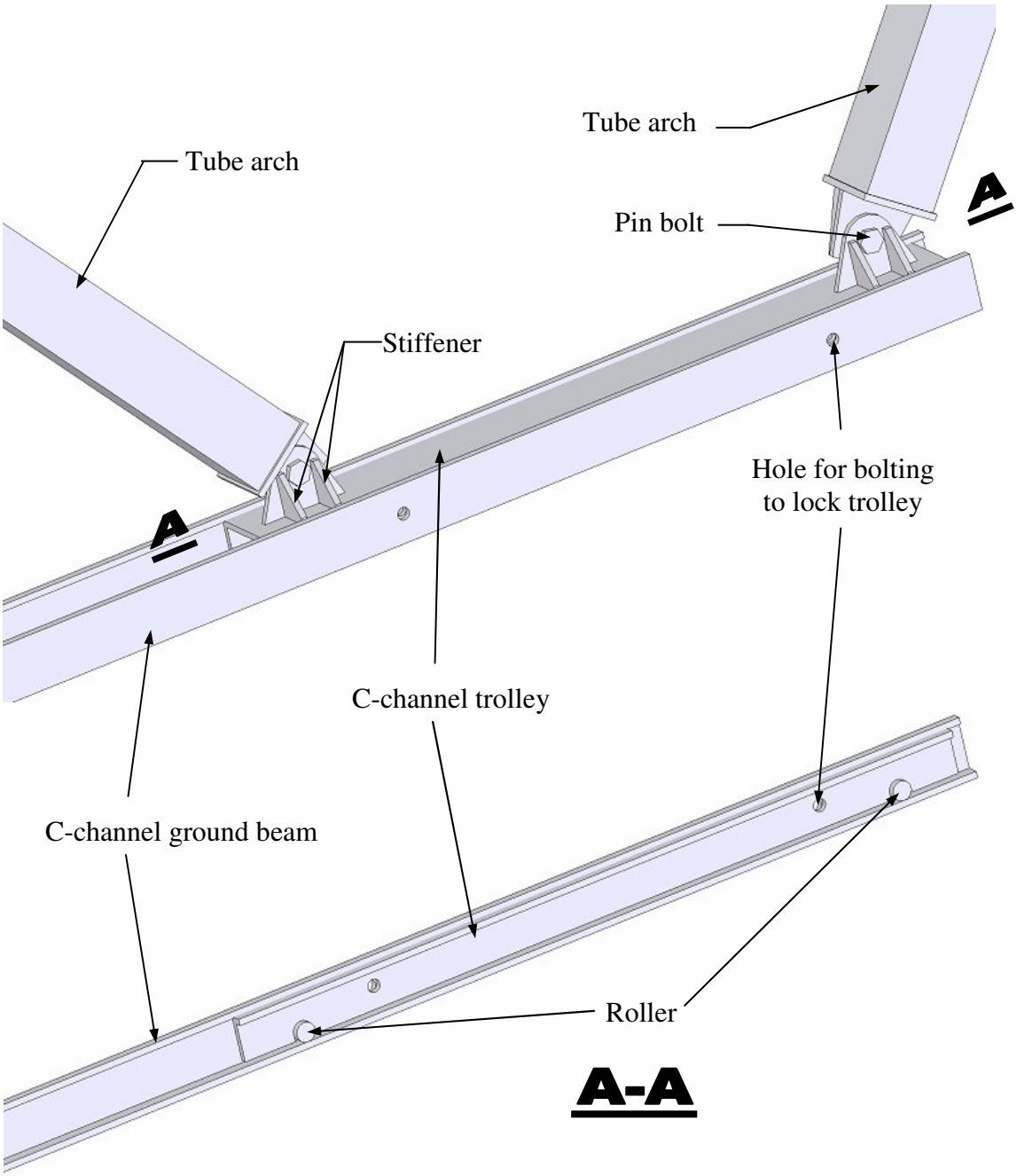

Fig. 7.38. Arches sliding along ground beam

7.3.3.4. Joint and membrane connection designs of deployable cable-strut arch

This section is aimed at detailing the joint and membrane connection for the deployable cable-strut arch of Butterfly-wing structures. As mentioned in chapter 5, all struts of the deployable arch were made of square hollow sections. Therefore, the joint was made of square tube accordingly. There are two types of joints which are the top/bottom joint and the middle joint. The top/bottom joint is the concentric joint while the middle joint is the eccentric joint. Figure 7.39 shows the design of top and middle joints designed by Vu (2007) and the corresponding full scale prototypes of the joints. The joints were welded from the tubes of the same size for the ease of manufacturing process. The prototypes demonstrated that these joint concepts were workable.

The membrane was connected to the upper middle joints of the deployable arch (see Figs. 5.18 & 5.19). Basically, there are two types of membrane connections which are those along the edges and those at the corners of the membrane. The designs of these two membrane connection types are shown in Fig. 7.40. Both connections were designed with the turn-buckles to tolerate the unexpected deviation during the installation and the loss of membrane prestress during the lifetime of the structures.

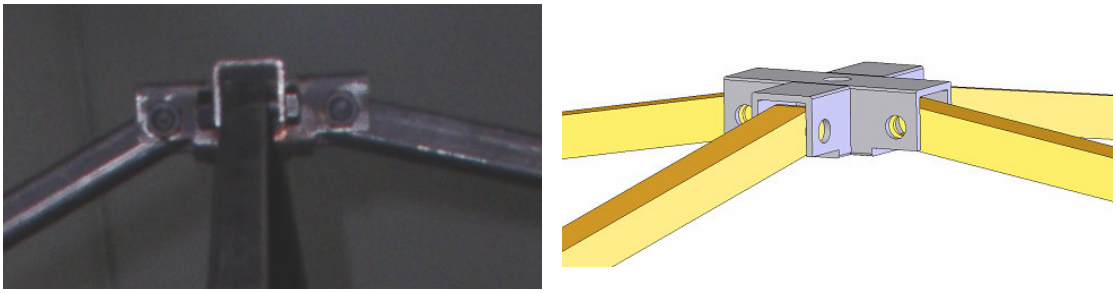

a. Top/bottom joint

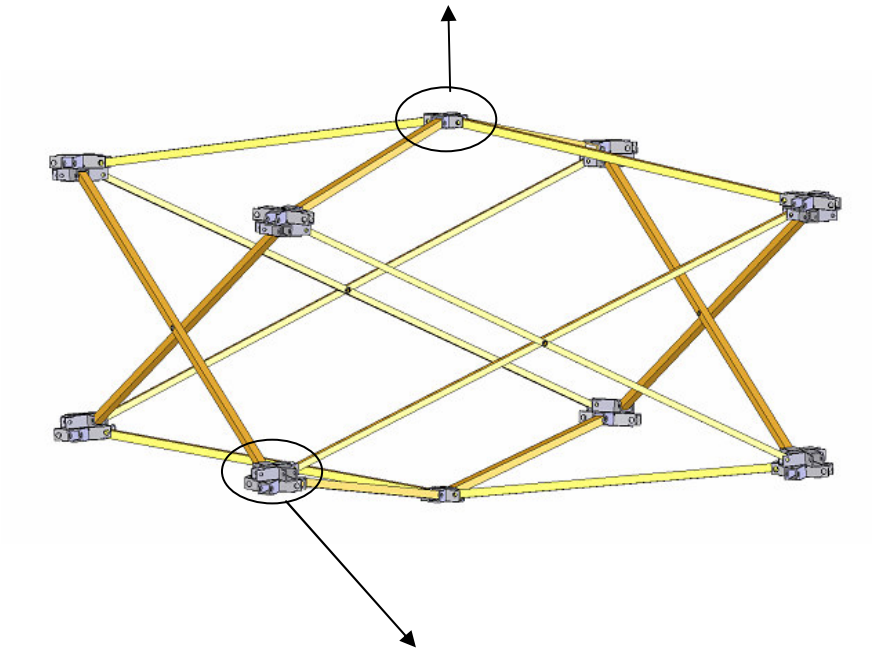

b. Middle joint

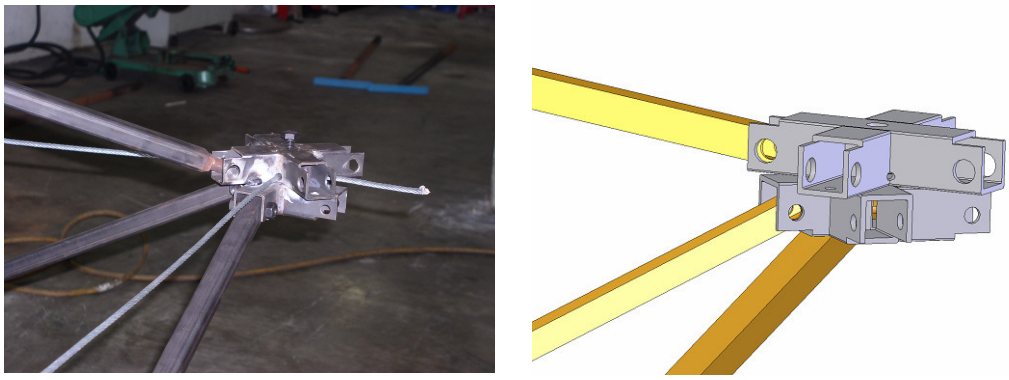

Fig. 7.39. Joint design and full scale prototypes (Vu, 2007)

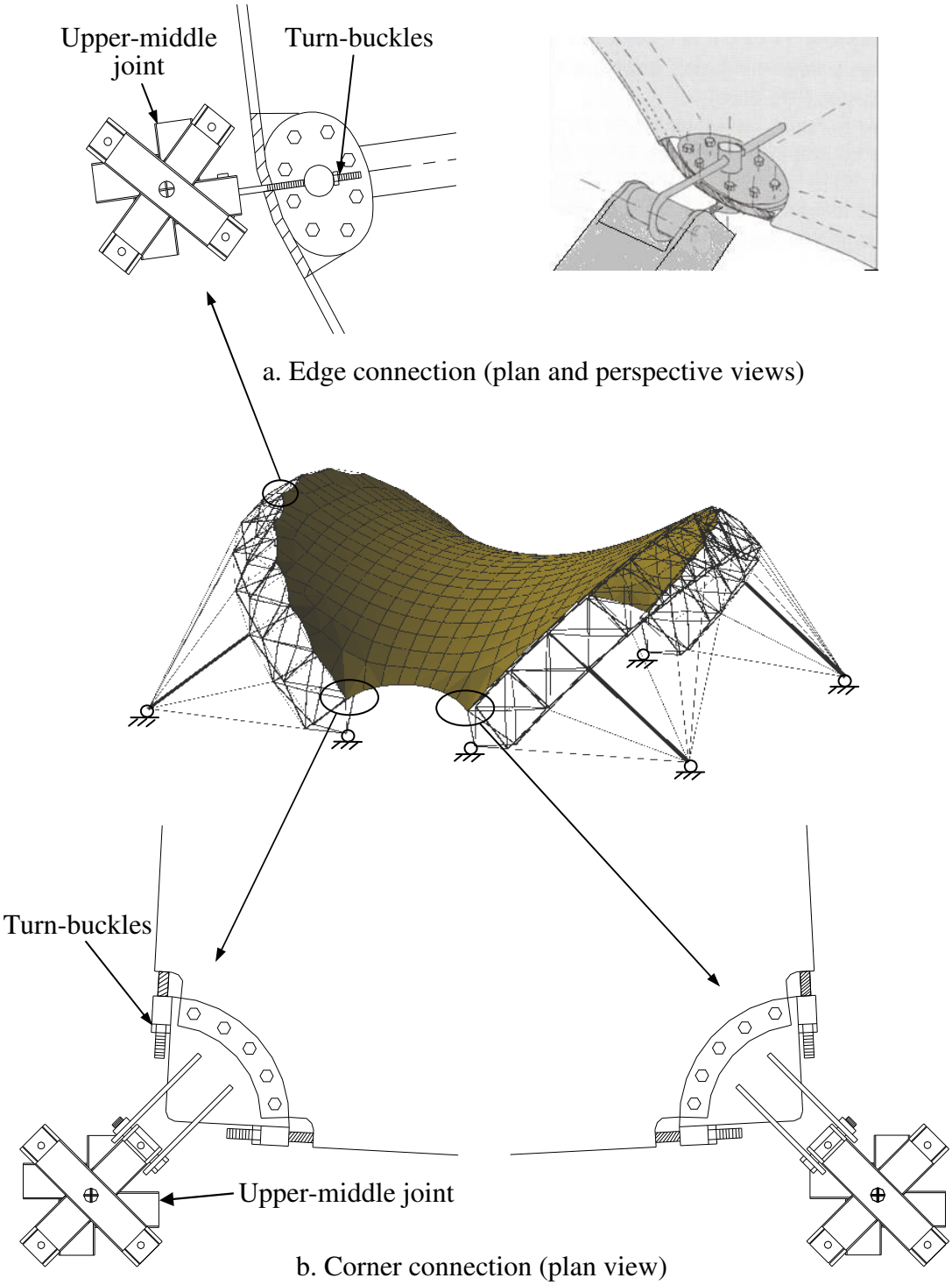

Fig. 7.40. Membrane connections to the deployable arch

7.3.4. Deployment methods

7.3.4.1. Deployment method for DSTMS

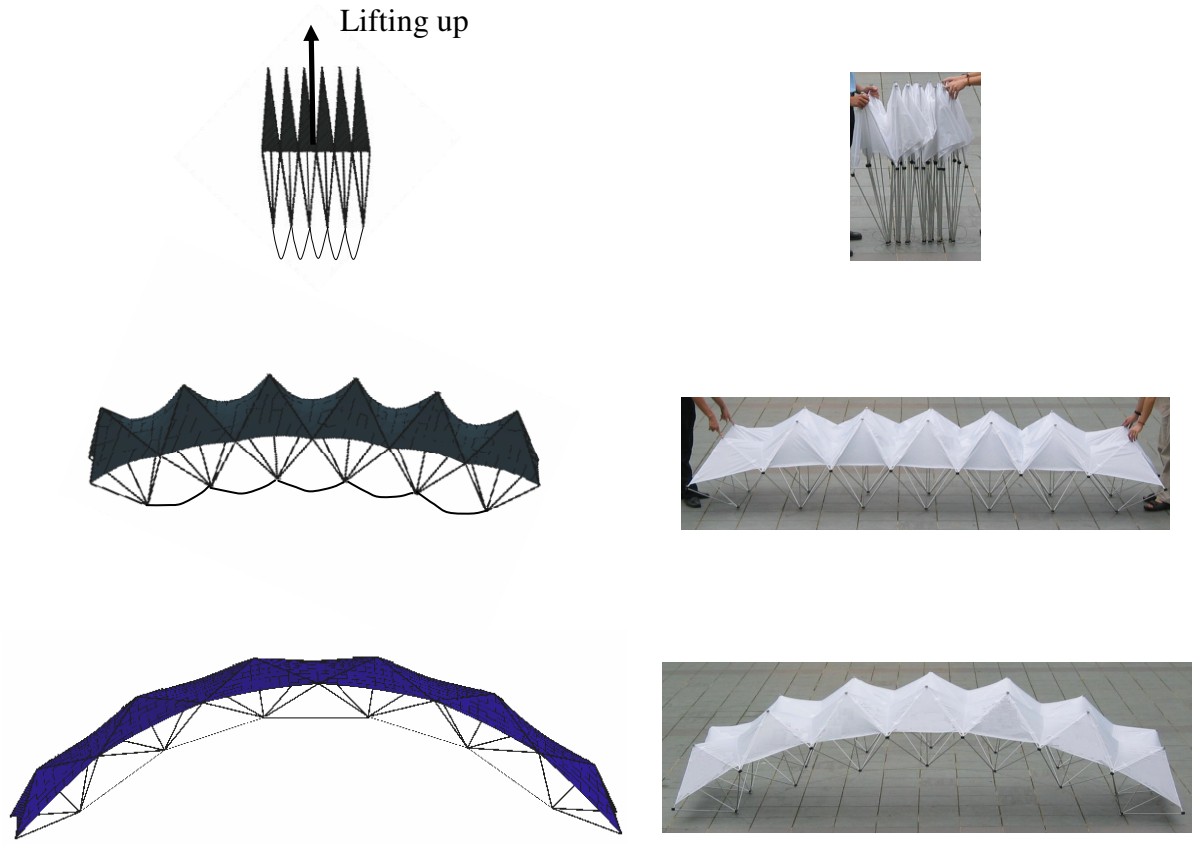

Fig. 7.41. Deployment of Umbrella DSTMS by self-weight

DSTMS can be deployed by using lifting equipment. The structure is lifted up and deployed under its self-weight. Depending on the size of the structures and the capacity of lifting equipment, the structure can be wholly or partially deployed. Figure 7.41 show how to deploy a DSTMS by lifting up. Before deploying, the structure is tied in a bundle and lifted up at its center gradually. During the lifting process, the ties are loosened to allow the structure to deploy under its self-weight until the membrane is fully open and subject to tension which prevents further deployment of the structure. The vertical strut is then bolted to the bottom joint and is shortened by tightening the

bolt to further deploy the structure until its final configuration. The structure is now stable in its self-stress equilibrium state and can be placed to the final position (see Fig. 7.42 for illustration).

Fig. 7.42. Moving DSTMS prototype in self-stress equilibrium state

7.3.4.2. Deployment method for Butterfly-wing structures using deployable arch

Each deployable arch is deployed individually before the deployment of the structure is carried out. Deployment of the arch can be performed in the same way as that of DSTMS above. Alternatively, the arch can be deployed on the ground without the need of lifting equipment as shown in Fig. 7.43. The arch in a bundle was lied down on its side and pulled out at two ends to open up. Figure 7.45 illustrate the deployment process of the full scale prototype of the arch carried out by Deployable structures group in NUS. This deployment method was found to be simple and easy to control. Lifting equipment is only needed in the deployment of the whole structure when all arches are required to be raised up vertically.

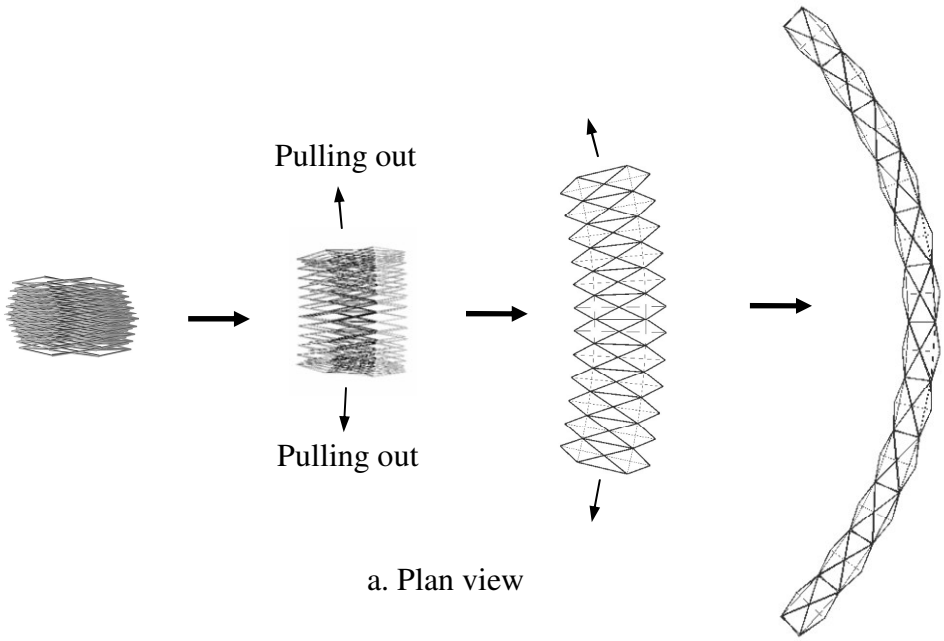

a. Plan view

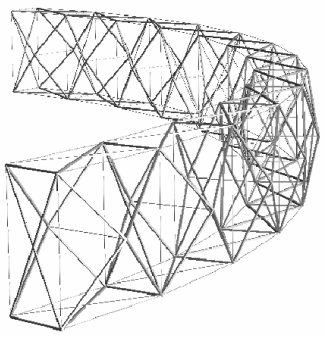

b. Perspective view

Fig. 7.43. Arch deployed horizontally on the ground

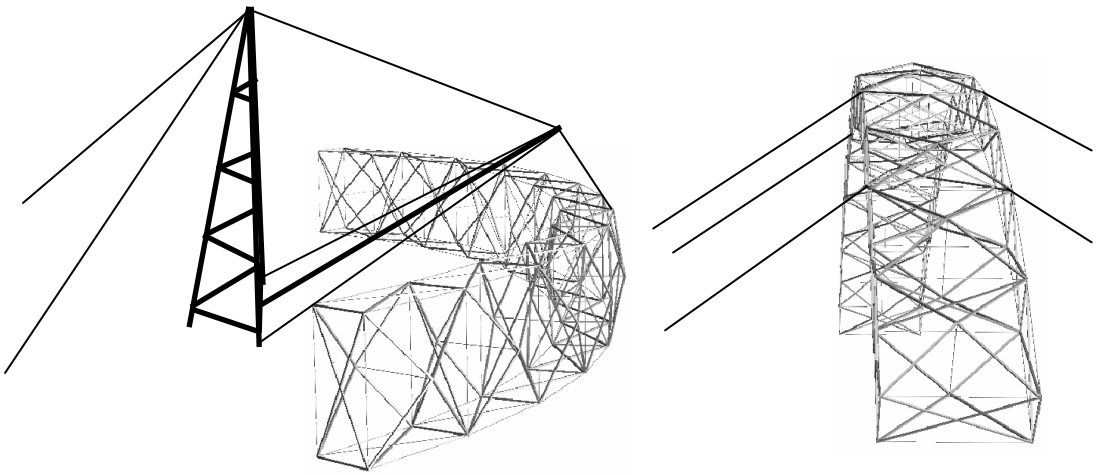

Fig. 7.44. Arch raised up by erection tower

Fig. 7.45. Full scale prototype deployed horizontally on the ground

The arch can be raised up without the need of crane. Figure 7.44 shows how to raise up the arch by using the erection tower. This method was used to raise up the space truss arch of up to 10 tons of the B-2 shelter system (American Spaceframe Fabricators, Inc.). The erection tower was designed in tripod shape with a system of pulleys and winches to control the raising up of the arch. Once the arch stands up vertically, it is anchored down with cables for stability. Membrane is then attached to the arch. Deployment of single butterfly-wing structures can be simply done by letting the arches rotate outward gradually under the control of anchor cable system and the erection tower.

For multiple butterfly-wing structures, the peaks of adjacent arches need to be hinge connected together before the deployment can proceed. The boundary arches are kept vertically by temporary struts. During the deployment process, the boundary arches are slide outward by pushing the trolley while still being kept vertically. The whole structure is therefore slide along the ground beam as a kinematic chain. The directions of the ground beam for different types of multiple butterfly-wing structure are shown in table 3.1 of chapter 3. At the final position, the trolleys at arches' feet are fixed to the ground beam and the boundary arches are rotated outward by anchor cable system. Figure 7.46 illustrates the deployment process of multiple two-wing butterfly structure using deployable arch.

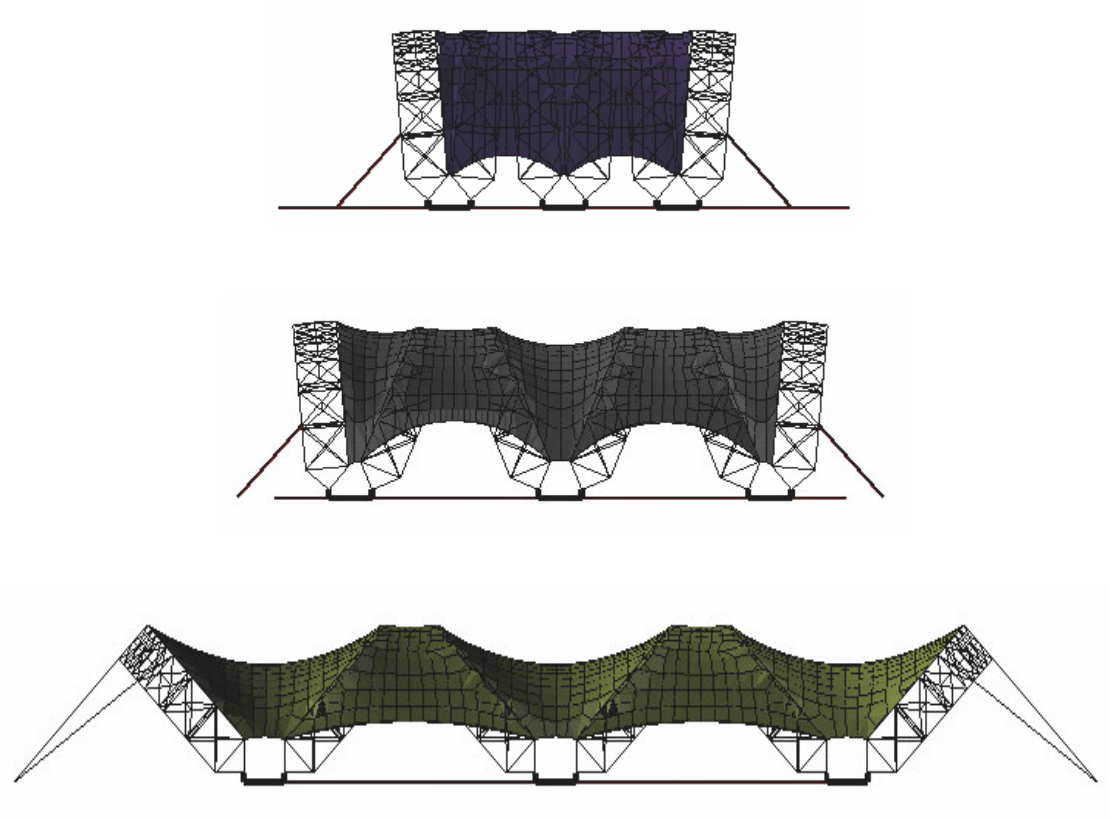

Fig. 7.46. Arches sliding along ground beam during deployment process

7.4. Summary

The design concept and the deployability of DSTMS and Butterfly-wing structures were verified through physical prototypes. It was confirmed that the deployment mechanisms of these structures were workable. In addition, it was found that the attached membrane could be opened up and tensioned during the deployment while the tensioned membrane helped the structures achieve self-stress equilibrium in final configuration.

A design guideline was developed for DSTMS and Butterfly-wing structures. It provided the recommended structural parameters and member sizes for preliminary design of these structures. Detailed designs of joints and related accessories of these structures were proposed and developed to facilitate the manufacturing and installation. The design guideline also covered the instruction of deployment methods for each group of structures. Several applications corresponding with different forms of DSTMS and Butterfly-wing structures were proposed for either military or civilian purposes.

CHAPTER 8

CONCLUSIONS AND RECOMMENDATIONS FOR FUTURE RESEARCH

8.1. Conclusions

This thesis proposed two novel deployable membrane systems, the so-called Deployable strut-tensioned membrane structures (DSTMS) and Butterfly-wing structures, which addressed the demands of modern construction: easy transportation, rapid erection, cost effectiveness, high structural efficiency and high versatility. The concept, analysis procedure and detail design are provided for practical implementation of these structures.

The conceptual and generative designs presented in chapter 3 showed that various deployable forms of DSTMS and Butterfly-wing structures for space enclosure are possible. Different deployable forms of DSTMS were generated from various DSTM simplexes, and furthermore, by assembling the simplexes in different grid configurations. Two novel DSTM simplexes of high structural and deployment efficiencies, namely Umbrella and Cone-shaped simplexes, were proposed and developed. These DSTM simplexes have several possible configurations such as triangular, square or pentagonal simplexes. However, only square simplex was explored comprehensively in this thesis since it has high efficiency in arranging grid layout and joint design/manufacture. The DSTMS grid layout could be arranged in square or diagonal pattern and could be in the form of flat roof or barrel vault. Apart from DSTMS, many attractive forms of Butterfly-wing structures were created by

making use of the inclined arches and arranging them in different configurations. Three butterfly-wing structures, which have two wings, three wings and four wings corresponding with the number of the arches used in the structures, were proposed for space enclosure. Structures with a larger number of wings were not considered because the larger number of wings might result in fairly low profile in elevation and flat surface at center of the structures. Apart from single butterfly-wing structures, generative design showed that various deployable forms of multiple butterfly-wing structures can be generated by assembling these single butterfly-wing structures in reciprocal manner. The high versatility of DSTMS and Butterfly-wing structures provides clients, architects and engineers with various options for a space enclosure.

The concept of integrating the tensioned membrane into the deployable supporting structures was implemented in DSTMS and Butterfly-wing structures. The numerical and physical studies showed that, in the deployed configuration, the tensioned membrane helped the structures achieve self-stress equilibrium state. In DSTMS, the tensioned membrane provided restraint to the strut skeleton and resulted in self-stress equilibrium among the tension force in the membrane, the self-weight of the strut skeleton and the tension force in the bottom cables. In Butterfly-wing structures, the tensioned membrane provided restraint to the compression arches and resulted in self-stress equilibrium among the tension force in the membrane, the self-weight of the arch and the tension force in anchor cables. The restraint and self-stress equilibrium effects of membrane on the structures suggest that the membrane could enhance the structural stability of DSTMS and Butterfly-wing structures. It was also demonstrated in chapter 6 that DSTMS without membrane were subjected to premature local failure and larger displacement.

The morphology study of DSTMS and Butterfly-wing structures showed that they possessed effective anticlastic surfaces which were necessary for the tensioned membrane to resist external loads. While the Umbrella and Cone-shaped DSTMS had the membrane surfaces in typical saddle and cone-shaped forms, different Butterfly-wing structures resulted in different saddle forms. These anticlastic surfaces of DSTMS and Butterfly-wing structures were verified by computational and physical modellings. Apart from that, shape effect studies were carried out to determine the optimum membrane surface curvatures which result in minimum membrane stress of DSTMS and Butterfly-wing structures (chapter 4). The findings suggest that DSTMS has optimum membrane surface curvature when the inclination height/modular width ratio is 0.2 while Butterfly-wing structures has optimum membrane surface curvature when the inclination angle and the rise/span ratio of the arch are in range of 45° to 60° and 0.375 to 0.5 respectively.

A series of parametric studies were carried out to provide the optimum design parameters which result in minimum weight of DSTMS and Butterfly-wing structures (chapter 5). As the studies were aimed at the design of large and medium span structures, DSTMS of 48mx48m span and Butterfly-wing structures of 30m deployable arch span were chosen as the case studies. The results showed that the span/depth and span/modular width ratios had significant influence on the weight of DSTMS. For Butterfly-wing structures, the number of module and the arch-span/modular depth ratio had significant influence on the weight of the arch and thus the weight of the structures. The findings suggest that the optimum span/depth and span/modular width ratios for minimum design weight of DSTMS are 9 to 11 and 6 to 8 respectively. On the other hand, the number of module of 12 to 14 and the

span/depth ratio of 19 to 21 are recommended for the deployable cable-strut arch to achieve the minimum design weight of Butterfly-wing structures. The minimum design weight of Umbrella and Cone-shaped DSTMS were 18.81 kg/m^2 and 17.71 kg/^{2} respectively, which are comparable with the self-weight of similar layout double-layer space trusses of equivalent loading conditions (Makowski 1981). This indicates that the DSTMS possess a high structural efficiency which overcomes the main drawback of low stiffness of existing deployable space frames.

The robustness of DSTMS and Buttterfly-wing structures against hazards was investigated in chapter 6 with two possible hazards to membrane which are vandalism and fire. On the one hand, it was found that the optimally designed DSTMS and Butterfly-wing structures were safe even in the event of complete membrane damage due to vandalism. The safety of DSTMS without membrane is ensured by the self-stable supporting skeleton and while the safety of Butterfly-wing structures without membrane is ensured by the safety struts. On the other hand, a procedure of performance-based approach was proposed for determining the fire resistance of large space membrane structures through considering their performance in real fire. This approach could ensure the safety of the optimally designed DSTMS and Butterfly-wing structures in fire without the need of costly fire protection. Furthermore, this approach identified the influence factors on the structural fire resistance which could be optimized to minimize the cost needed for membrane structures against fire.

The detailed solutions to joints, membrane connections and related accessories of DSTMS and Butterfly-wing structures were developed in chapter 7. Reduced scale prototypes were built to verify their conceptual design and deployability. It was found

that they could be stowed back into a compact bundle and deployed rapidly for space enclosure with proper pin-joint design. The high stowage/deployment efficiencies result in saving the transportation cost and the construction time of these structures.

8.2. Recommendations for future research

As DSTMS and Butterfly-wing structures are proposed for the first time, they can be explored comprehensively further. Some recommendations for future researches are as follows

1. DSTM simplexes should not be limited to Umbrella and Cone-shaped simplexes. Further morphology studies need to be carried out to find out other possible DSTM simplexes which may have higher deployment or structural efficiency. In addition, other configurations apart from square DSTM simplex, such as triangular and pentagonal simplexes, should be studied further to widen the application range of the structures, such as dome, etc.
2. The parametric studies carried out in chapter 5 need to be extended to different structural spans and configurations to confirm the results of optimum design parameters of DSTMS and Butterfly-wing structures. Apart from that, the parametric studies should be carried out on other forms such as barrel vault DSTMS and multiple Butterfly-wing structures to determine the optimum design parameters for these structures.
3. Experiments should be carried out on full scale prototypes for verifying the numerical results as well as the constructability of DSTMS and Butterfly-wing structures. By performing loading tests, the structural behaviour and efficiency of these structures could be examined. Apart from that, through building and erecting

full scale prototypes, the design guideline of these structures could be improved and completed.

4. Advanced analysis should be developed to study the progressive collapse of DSTMS and Butterfly-wing structures in fire. The thermal expansion of steel members should be integrated in the advanced analysis to take the effect of thermal forces on load ratios of the members into account. Thereby the fire resistance of the structures should be determined more accurately.

REFERENCES

AISI (1973), Manual for Applications of Steel Cable for Buildings.

American Spaceframe Fabricators, Inc, website: www.asfi.net

Arup (2003), National productivity and quality specifications, Briefing presentation to SIA

Arygis J. H., and Scharpf D.W. (1972), "Large deflection analysis of prestressed networks", Proceeding ASCE, Journal of the Structureal Division, ST3, p.633-654.

ASTM E84 (2007), American Standard Test Methods for Surface Burning Characteristics of Building Materials.

ASTM E108 (2007), American Standard Test Methods for Fire Tests of Roof Coverings.

ASTM E136 (2004), American Standard Test Methods for Behaviour of Materials in a Vertical Tube Furnace at 750ºC.

Atake, K. (2000), "ATAKE's structure – new variation of the scissors technique", MARAS III, WIT Press, USA, 143-154.

Barnes, M.R. (1988), "Form-finding and analysis of prestressed nets and membranes", Computer and Structures, Vol. 30, No. 3, p.685-695.

Barnes, M.R. (1994), "Form and stress engineering of tension structures", Structural Engineering Review Vol. 6, No. 3-4, p.175-202.

Bathe, K. J. (1996), "Finite element procedures in Engineering analysis", Printice Hall, Englewood Cliffs, New Jersey, USA.

Berger H. (1996), "Light Structures, Structures of Light, The Art and Engineering of Tensile Architecture", Birkhouser Verlag, Basel.

Bouderbala, M. and Motro, R. (1998), "Folding tensegrity systems", IUTAM-IASS, Solid mechanics and its applications, Vol.80, Cambridge, UK.

Brian, F. (1994), "Cable and membrane roofs – A historical survey", Structural Engineering Review Vol. 6, No. 3-4, p.145-174.

British Standard Institute, BS 476 (1970), Fire test on building materials and structures, BSI 1970.

British Standard Institute, BS 5950 : Part 1 (2000), Code of practice for design: Rolled and welded sections, BSI 2000.

British Standard Institute, BS 5950 : Part 8 (2003), Code of practice for fire resistant design, BSI 2003

British Standard Institute, BS 6399 : Part 2 (1995), Code of practice for wind loads, BSI 1995.

British Standard Institute, BS 7837 (1996), Specification for flammability performance for textiles used in the construction of marquees and similar textile structures, BVI 1996.

Buchanan A.H. (2002), "Structural design for fire safety", John Willey & Sons Ltd.

Day, A. S. (1965), "An introduction to Dynamic Relaxation", The Engineer, UK, 219-221.

Day A. S. (1978), "A general computer technique for form finding for tension structures", IASS Conference, Shell and Spatial Structures, the Development of Form, Morgantown, USA.

D'Anza, G. (2002), "Forten2000: a system for Tensile Structures, Design and Manufacturing", Baku Group DT.

Edmund C.C.C., Extreme wind characteristics over Singapore – an area in the equatorial belt (1999), Journal of Wind Engineering and Industrial Aerodynamics, Volume 83, Issue 1-3, p.61-69.

Escrig, F., Sanchez, J. and Valcarel, J.P. (1996), "Expandable arches", MARAS II, Computational Mechanics Publication, UK, p.123-131.

Escrig F. (1985), "Expandable space structures", International Journal of Space Structures, Vol. 1, , No. 2, p.79-91.

European Committee for Standardization, CEN EN 1990, Eurocode: Basis of structural design, CEN 2001

European Committee for Standardization, CEN EN 1991, Eurocode 1: Action on structures, Part 1-2: General actions Actions on structures exposed to fire, CEN 2001.

European Committee for Standardization, CEN EN 1991, Eurocode 3: Action on structures, Part 1-2: General rules Structural fire design, CEN 2001.

European Committee for Standardization, CEN EN 1991, Eurocode 1: Action on structures, Part 1-7: General actions – Accidental actions, BSI 2006.

Fibertech Co., PO Box 11844 Al-Jubail 31691 KSA

Forster B. and Mollaert M. (2004), "European Design Guide for Tensile Surface Structures", Tensinet.

Fuller, R. Buckminster (1962), "Tensile-Integrity Structures", U.S. Patent No. 3,063,521.

Gantes, C. (2001), "Deployable Structures: Analysis and Design", WIT Press, USA.

Gerardo C. and Levy M.P. (1992), "Proceedings of the Eighth Conference of Computing in Civil Engineering and Geographic Information Systems Symposium, ASCE, June 7-9 1992.

Gough M. (1998), "In the laboratory of constructivism: Karl Ioganson's cold structures", October, No. 84, MIT Press, p.90-117.

Grundig L., Moncrieff E., Singer P. and Strobel D. (2000), "A history of the principal developments and applications of the Force Density Method in Germany 1970-1999", Proceeding IASS-IACM 2000, Fourth International Colloquium on Computational of Shell and Spatial Structures, June 2000, Chania-Crete, Greece.

Gulvanessian H. (2001), EN 1990 Eurocode – Basis of structural design, Proceedings of ICE, Civil Engineering 144, p.8-13, Nov 2001.

Hanaor A., (1993), "Double-layer tensegrity grids as deployable structures", International Journal of Space Structures, Vo. 8, No. 1&2, p.135-145.

Hanaor A. and Levy R. (2001)., "Evaluation of Deployable Structures for Space Enclosures", International Journal of Space Structures, Vol. 16, No. 4.

Hernandez C.H. (1996), New ideas on deployable structures, MARAS II, Computational Mechanics Publications, UK, p.63-72.

Huntington, C.G., (2004), "Tensioned fabric roof", ASCE Press, USA.

IL5 (1973), "Convertible roofs", Institute of Light Weight Structure, University of Stuttgart.

Ishii, K. (1995), "Membrane structures in Japan", SPS Publishing Company, Tokyo, 1995.

Ishii, K. (2000), "Structural Design of Retractable Roof Structures", WIT Press, USA.

Jacob S. (2003), Le Grande Arche de la Defense, Urban Design Politics.

Kent E.M. (1992), "Kinematic Periodic Structures (KPS)", Innovative Large Span Structures, Concept, Design, Construction, Proceedings IASS-CSCE International Congress, University of Waterloo, Ontario, Canada, Canadian Society of Civil Engineers, Montreal, p.485-496.

Kroplin B. and Wagner R. (1995), "Pneumatic Tube-Structures, Some Examples", IASS Bullentine, Vol. 36, No. 2, August 1995, p.67-72.

Lee, B.H., (2001). "Analysis, design and implementation of cable-strut structures", MEng thesis, National University of Singapore, Singapore.

Leonard, J.W., (1988). "Tension structures: behaviour and analysis", McGraw-Hill, Inc.

Leonhardt F. and Schlaich J. (1972), "Structural design of roofs over the sports arenas for the 1972 Olympic Games: Some problems of prestressed cable net structures", The structural engineer, 50, No.3, p.113-119.

Lewis W. J. (2003), "Tension structures – Form and behaviour", Thomas Telford Publishing, UK.

Li, J. J. and Chan, S. L. (2004), "An integrated analysis of membrane structures with flexible supporting frames", Finite Elements in Analysis and Design 40, p.529-540.

Liew, J.Y.R., Lee, B.H. and Wang B.B. (2002), "Innovative use of star prism (SP) and Di-Pyramid (DP) for spatial structures". Journal of Constructional Steel Research, Vol. 59, No.3, p.335–57.

Liew, J.Y.R. and Lee, B.H. (2003), "Experimental study on reciprocal prism (RP) grid for space structures", Journal of Construction Steel Research, (59), Elsevier Press, 1363-1384.

Linkwitz, K. and Schek, H.-J., (1971), `Einige Bemerkungen zur Berechnung von vorgespannten Seilnetzkonstruktionen,´ *Ingenieur-Archiv* 40, p.145-158.

Makowski, Z.S. (1981), "Analysis, design and construction of double-layer grids", Applied Science Published, London.

Meacham, B. J. and Custer, R.L.P (1995), "Performance based fire safety engineering: An introduction of basis concepts", Journal of fire protection engineering, SFPE, Boston, MA. 7:2, p.35-54.

Mick, G. and Adam, M. (2003), "Design of light weight structures during fire", Unpublished research report, Institution of Structural Engineers, UK.

Mollaert, M. (1996), "Retractable membrane roofs", MARAS II, Computational Mechanics Publication, UK, p.407-417.

Motro, R. and Bouderbala, M. (1996), "Mobile tensegrity systems", MARAS II, Computational Mechanics Publication, UK, p.103-112.

Motro R. (2003), "Tensegrity – Structural system for the Future", Kogan Page Science Published, UK & USA.

Otto, F. (1969), "Tensile Structures", Vol.2, MIT Press, Cambridge, UK.

Pellegrino, S. and You, Z. (1996), "New solution for foldable roof structures", MARAS II, Computational Mechanics Publication, UK, p.35-44.

Pinero, E.P. (1961), "A reticular movable theatre", The Architects' Journal, Vol.134, 299.

Pinero E. P. (1962), "Expandable framing", Progressive Architecture, 12, p.154-155.

Pugh, A. (1976), "An Introduction to Tensegrity", Berkeley, California, University of California Press.

Riches, C.G. and Gosling, P.D. (1998), "Pneumatic Structures: A Review of concepts, Applications and Analytical Methods", Lightweight Structures in Architecture Engineering and Construction, Proc. LSA98, Hough R. and Melchers R., eds, LSA A, Sydney, V2, p.883-894.

Rubb bulding, www.rubb.com

Sanchez, C.L. (1996), "Geometric models for expandable structures", MARAS II, Computational Mechanics Publication, UK, p.93-102.

Sastre R. (1996), "Expandable arches", MARAS II, Computational Mechanics Publications, UK, p.123-134.

Scheck, H. J., (1973). "The Force Density Method for Form Finding and Computation of General Networks". Computer Methods in Applied Mechanics and Engineering.

Seaman R.N. and Venkataraman B., (1976). "Utilization of Vinyl Coated Synthetic Fabrics in Industrial Applications". Journal of Coated Fabrics Vol.5.

Seaman R.N. (1984), "Fire performance history of flame retardant membrane structures", International Symposium on Architectural Fabric Structures: The Design Process, p.201-204.

Shaeffer, R.E. (1995), "Tensioned fabric structures: a practical introduction", American Society of Civil Engineers, Task Committee of Tensioned Fabric Structures.

Shelter systems, USA. Website: http://www.shelter-systems.com/

Southwell R.V. (1946), "Relaxation methods in theoretical physics", Oxford University Press.

Sprung Instant Structure, USA. Website: http://www.sprung.com/

Tabarrok B. and Qin Z. (1991), "Nonlinear analysis of tension structures", Computer and Structures, Vol. 45, No 5/6, p.973-984

UBC 4-1 (1997), Uniform Building Code: Proscenium Fire Safety Curtains.

Vu K.K., Liew J.Y.R., and Anandasivam K. (2006), "Deployable Tension-Strut Structures: from concept to implementation", Journal of Constructional Steel Research, Vol. 62, Issue 3, p. 195-209.

Vu K.K. (2007), “Deployable tension strut structures: Concept, structural behaviour and implementation”, PhD thesis, National university of Singapore.

Walter B. (1986), “Air structures – Early development and Outlook”, Proceedings of the First International Conference on Lightweight Structures in Architecture, Sydney, 1986, p.554.

Wang B.B. (2004), “Free-standing Tension Structures”, Spon Press, New York, USA.

Wang B.B. (1998), “Cable-strut systems: Part II – Tensegrity”, Journal of Constructional Steel Research, Vol. 45, No. 3, p.281-289.

Wang B.B. (1998), “Cable-strut systems: Part II – Cable-strut”, Journal of Constructional Steel Research, Vol. 45, No. 3, p.291-299.

Zienkiewicz, O.C. and Taylor, R.L. (2000), “The Finite Element Method”, Butterworth Heinemann.

Appendix A

Membrane forces acting on an arch of Butterfly-wing structure

Node	Two-wing structure			Three-wing structure		
	F_x (N)	F_y (N)	F_z (N)	F_x (N)	F_y (N)	F_z (N)
1	4.2E+04	-2.9E+04	6.0E+04	4.3E+04	1.6E+04	1.1E+05
2	4.8E+03	-3.2E+04	1.2E+04	2.4E+04	-4.1E+04	3.7E+03
3	1.6E+04	-1.7E+04	-7.2E+03	2.9E+04	-3.0E+04	-7.2E+03
4	1.6E+04	-9.3E+03	-8.2E+03	4.3E+04	-4.0E+02	-2.4E+04
5	1.4E+04	1.0E+04	-9.3E+03	2.8E+04	8.4E+03	-1.4E+04
6	3.7E+03	-1.5E+04	1.5E+02	1.6E+04	4.0E+03	-5.6E+03
7	6.8E+03	7.1E+00	-3.8E+03	1.3E+04	2.3E+01	-3.8E+03
8	3.7E+03	1.5E+04	1.6E+02	1.6E+04	-4.0E+03	-5.6E+03
9	1.4E+04	-1.0E+04	-9.3E+03	2.8E+04	-8.4E+03	-1.4E+04
10	1.6E+04	9.3E+03	-8.2E+03	4.3E+04	-4.0E+02	-2.4E+04
11	1.6E+04	1.7E+04	-7.2E+03	2.9E+04	3.0E+04	-7.2E+03
12	4.8E+03	3.2E+04	1.2E+04	2.4E+04	4.1E+04	3.7E+03
13	4.2E+04	2.9E+04	6.0E+04	4.3E+04	-1.6E+04	1.1E+05

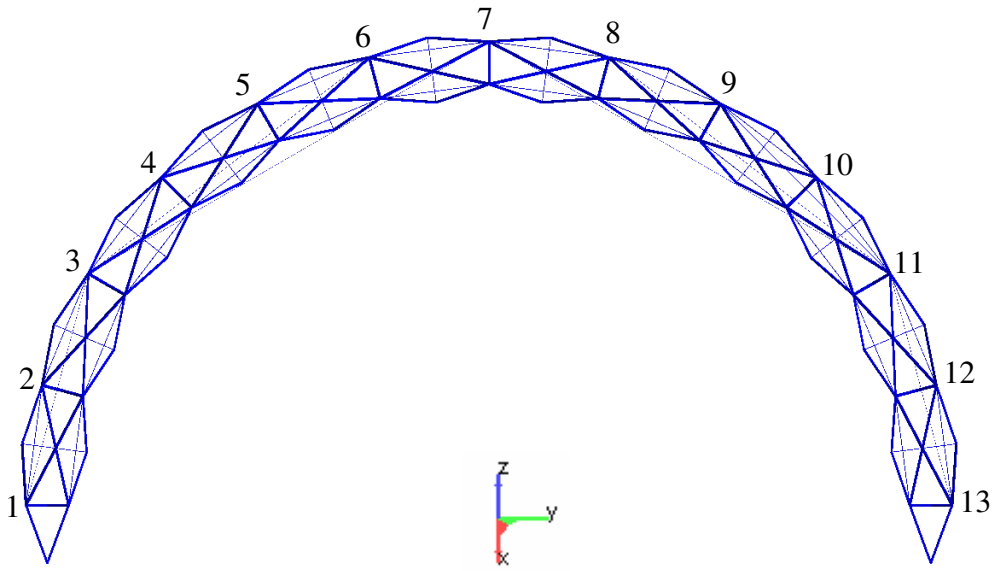

Fig. A1. Positions of nodal membrane forces acting on the arch

Appendix B

BS 5950 : Part 8 : 1990 – Code of practice for fire resistant design

Table 8 — Limiting temperatures for the design of protected and unprotected hot finished members

Description of member	Limiting temperature at a load ratio of:						
	0.7	0.6	0.5	0.4	0.3	0.2	0.1
	°C	°C	°C	°C	°C	°C	°C
Members in compression, for a slenderness λ[a]:							
≤ 70	510	540	580	615	655	710	800
> 70 but ≤ 180	460	510	545	590	635	635	635
Non-composite members in bending supporting concrete slabs or composite slabs:							
unprotected members, or protected members							
complying with item a) or b) of 6.3	590	620	650	680	725	780	880
other protected members	540	585	625	655	700	745	800
Composite members in bending supporting concrete slabs or composite slabs:							
unprotected members, or protected members complying with item a) or b) of 6.3							
i) 100 % degree of shear connection	550	580	610	645	685	740	840
ii) 40 % degree of shear connection	575	600	635	665	700	760	865
other protected members							
i) 100 % degree of shear connection	495	530	570	610	650	705	785
ii) 40 % degree of shear connection	530	560	595	630	675	725	795
Members in bending not supporting concrete slabs:							
unprotected members, or protected members							
complying with item a) or b) of 6.3	520	555	585	620	660	715	810
other protected members	460	510	545	590	635	690	770
Members in tension: all cases	460	510	545	590	635	690	770

NOTE For beams supporting a composite slab the limiting temperatures only apply when the voids between the top of the beam and underside of the steel deck are filled with non-combustible void fillers. For guidance on limiting temperatures when void fillers are not used, see [2].

[a] λ is the slenderness, i.e. the effective length divided by the radius of gyration.

LIST OF PUBLICATIONS

ARTICLE IN JOURNAL

INTERNATIONAL REFEREED

PUBLISHED

1. Liew J.Y.R. and Tran T.C., "Novel deployable strut-tensioned membrane structures", *Journal of International Associations of Shell and Spatial Structures*, Vol. 47, No. 1 (2006), p.17-30, (Spain).

2. Tran T.C. and Liew J.Y.R., "Butterfly structure for spatial enclosures", *Journal of International Associations of Shell and Spatial Structures*, Vol. 47, No. 3 (2006), p.291-302 (Spain).

ACCEPTED FOR PUBLICATION

3. Tran T.C., Liew J.Y.R, "Structural efficiency of deployable strut-tensioned membrane structures", *Advanced Steel Construction*, (2007) (Hong Kong).

SUBMITTED

4. Tran T.C., Liew J.Y.R, "Rapidly erectable membrane structures for spatial enclosure", *International Journal of Steel Structures,* (Submitted, 2007) (Korea).

CONFERENCE PAPER

LOCAL/REGIONAL

ORAL PRESENTATION

PUBLISHED

1. Tran T.C., Liew J.Y.R., "Effect of support flexibility on tensioned fabric structures", *Proceedings of the 17th KKCNN Symposium on Civil Engineering,* p.303-308, 13-15 Dec 2004, Thailand.

2. Tran T.C., Liew J.Y.R, "Butterfly structure: A conceptual design", *Proceedings of the 18th KKCNN Symposium on Civil Engineering*, p.695-700, 18-20 Dec 2005, Kaohsiung, Taiwan.

3. Tran T.C., Liew J.Y.R., "Development of butterfly-wing membrane structure for space enclosure", *Proceedings of the 19th KKCNN Symposium on Civil Engineering,* p.261-264, 10-12 Dec 2006, Kyoto, Japan.

INTERNATIONAL

ORAL PRESENTATION

PUBLISHED

4. Tran T.C., J. Y. R. Liew, K. Anandasivam, "An investigation on the deployability of tensioned membrane structures", *Proceedings of the International Symposium on Shell and Spatial Structures: Theory, technique, valuation and maintenance (IASS2005)*, p.635-642, 6-9 Sep 2005, Bucharest, Romania.

5. Tran T. C., Liew J.Y.R, "Structural efficiency of deployable strut-tensioned membrane structures", *Proceedings of the 8th International Conference on Steel Space Composite Structures,* p.135-143, 15-17 May 2006, Kuala Lumpur, Malaysia.

6. Tran T.C., Liew J.Y.R, "Development of a new deployable shelter", *Proceedings of the Adaptable 2006 Conference*, Vol. 2, p.7-141 to 7-145, 3-5 Jul 2006, Eindhoven, the Netherlands.

7. K.K. Vu, Tran T.C., Liew J.Y.R, K. Anandasivam, "Deployable strut-tensioned structures: Design guidelines", *Proceedings of the Adaptable 2006 Conference*, Vol. 2, p.7-136 to 7-140, 3-5 Jul 2006, Eindhoven, the Netherlands.

8. Tran T.C., Liew J.Y.R, "Deployable butterfly-wing structure for space enclosure", *Proceedings of the International Symposium on Shell and Spatial Structures: Theory, technique, valuation and maintenance (IASS2006)*, p.236-238, 16-19 Oct 2005, Beijing, China.

9. Tran T.C., Liew J.Y.R, "Rapidly erectable membrane structures for spatial enclosure", *Proceedings of the 4th International Symposium of Steel Structures*, Vol.3, p.1028-1033, 16-17 Nov 2006, Korea.

PUBLIC SEMINAR

Tran T.C., *Tensioned fabric structure and its novelty for Deployable stressed membrane structure*, Annual seminar of Structural Steel Research Group, 13 Mar 2004 Department of Civil Engineering, National University of Singapore, Singapore.

Tran T.C., *Novel deployable membrane system for spatial structures*, Annual seminar of Structural Steel Research Group, 1 Apr 2005, Department of Civil Engineering, National University of Singapore, Singapore.

Tran T.C., *Innovation in deployable membrane structures*, Annual seminar of Structural Steel Research Group, 31 Mar 2006, Department of Civil Engineering, National University of Singapore, Singapore.

Tran T.C., *Advance in deployable membrane structures*, Annual seminar of Structural Steel Research Group, 1 Mar 2007, Department of Civil Engineering, National University of Singapore, Singapore.